



**VNiVERSiDAD
D SALAMANCA**

CAMPUS DE EXCELENCIA INTERNACIONAL

MECANISMOS DE REGULACIÓN DE LA GLUCOLISIS EN NEURONAS Y SU FUNCIÓN EN SUPERVIVENCIA CELULAR

PATRICIA RODRÍGUEZ RODRÍGUEZ

Salamanca, 2013

Directores:

Prof. Dr. D. Juan Pedro Bolaños Hernández

Prof^a. Dra. D^a. Ángeles Almeida Parra

Juan Pedro Bolaños Hernández, Catedrático de Bioquímica y Biología Molecular de la Universidad de Salamanca, y Ángeles Almeida Parra, Investigadora del Instituto de Investigación Biomédica de Salamanca y Profesora Asociada del Departamento de Bioquímica y Biología Molecular de la Universidad de Salamanca.

AUTORIZAN:

La presentación de la Tesis Doctoral titulada **“Mecanismos de regulación de la glucólisis en neuronas y su función en supervivencia celular”**, que ha sido realizada bajo su dirección por la Licenciada en Farmacia y Bioquímica Dña. Patricia Rodríguez Rodríguez, en el Departamento de Bioquímica y Biología Molecular y en el Instituto de Biología Funcional y Genómica, de la Universidad de Salamanca. En nuestra opinión, reúne todos los requisitos científicos y formales para ser defendida y optar al Título de *Doctor Europaeus*.

Salamanca, a 17 de Junio de 2013



Fdo.: Juan Pedro Bolaños Hernández

Fdo.: Ángeles Almeida Parra

INDEX

1. INTRODUCTION.....	1
1. GLUCOSE METABOLISM IN THE CENTRAL NERVOUS SYSTEM.....	3
1.1. GLUCOSE TRANSPORTERS	4
1.2. GLUCOSE METABOLIC PATHWAYS	5
1.3. LACTATE CONSUMPTION IN NEURONS AND THE ASTROCYTE-NEURON LACTATE SHUTTLE HYPOTHESIS.....	15
1.4. REACTIVE OXYGEN SPECIES (ROS) GENERATION AND DETOXIFICATION	17
2. GLUTAMATERGIC NEUROTRANSMISSION	20
2.1. GLUTAMATE	20
2.2. GLUTAMATE RECEPTORS	20
2.3. GLUTAMATE TRANSPORTERS.....	23
2.4. GLUCOSE METABOLISM IN GLUTAMATERGIC NEUROTRANSMISSION	24
2.5. EXCITOTOXICITY	26
2. HYPOTHESIS AND OBJECTIVES	31
3. MATERIALS AND METHODS	35
1. PLASMID CONSTRUCTIONS, AMPLIFICATION AND PURIFICATION	37
1.1. pEGFP-C1-TIGAR PLASMID CONSTRUCTION	37
1.2. G6PD, PFKFB3 and mutPFKFB3 PLASMID CONSTRUCTIONS.....	38
1.3. BACTERIAL TRANSFORMATION AND PLASMIDS PURIFICATION	39
2. “SMALL INTERFERING RNA” (SIRNA) DESIGN.....	39
3. ANIMALS.	40
4. CELL CULTURE	41
4.1. CORTICAL NEURONS IN PRIMARY CULTURE.....	41
4.2. ASTROCYTES IN PRIMARY CULTURE	42
4.3. HEK-293T	42
5. CELL TREATMENTS.....	43
5.1 CELL TRANSFECTIONS	43
5.2 NMDA RECEPTORS STIMULATION	43
5.3 INHIBITION OF PPP ACTIVITY AND MITOCHONDRIAL PYRUVATE UPTAKE.....	44
6. DETERMINATION OF Ca²⁺ UPTAKE	44
7. ELECTROPHORESIS AND PROTEIN IMMUNODETECTION (WESTERN BLOT)	45

8. PROTEIN IMMUNOPRECIPITATION	46
9. REVERSE TRANSCRIPTION-PCR (RT-PCR)	47
10. FLOW CYTOMETRIC ANALYSIS OF APOPTOTIC CELL DEATH	48
11. DETECTION OF REACTIVE OXYGEN SPECIES (ROS)	49
12. DETERMINATION OF METABOLITES	49
12.1. D-GLUCOSE	49
12.2. L-LACTATE	50
12.3. GLUCOSE-6-PHOSPHATE (G6P).....	50
12.4. GLUTATHIONE	51
12.5. FRUCTOSE-2,6-BISPHOSPHATE.....	52
13. PGI ACTIVITY DETERMINATION	53
14. PFK-1 ACTIVITY DETERMINATION	53
15. GLYCOLYTIC FLUX ASSESMENT	54
16. PENTOSE-PHOSPHATE PATHWAY (PPP) FLUX MEASUREMENTS	55
17. IMMUNOCYTOCHEMISTRY	59
18. CONFOCAL MICROSCOPY OF TRANSFECTED CELLS	59
19. STATISTICAL ANALYSIS	59
4. RESULTS	61
1. GLYCOLYTIC FLUX INCREASES BY INHIBITING PENTOSE-PHOSPHATE PATHWAY (PPP) OR MITOCHONDRIAL PYRUVATE UPTAKE IN NEURONS	63
2. THE RATE OF GLUCOSE OXIDIZED THROUGH THE PPP IS INHIBITED BY DHEA AND NOT BY HCN	64
3. PHOSPHOGLUCOSE ISOMERASE (PGI) IS A HIGHLY ACTIVE ENZYME IN NEURONS	66
4. KNOCK-DOWN OF PGI INCREASES PPP ACTIVITY	67
5. EFFECT OF DHEA AND HCN ON GLUCOSE-6-PHOSPHATE CONCENTRATION	69
6. EFFECT OF DHEA AND HCN ON EXTRACELLULAR AND INTRACELLULAR LACTATE CONCENTRATIONS	69
7. CORTICAL PRIMARY NEURONS RESPOND TO GLUTAMATE RECEPTORS ACTIVATION BY INCREASING INTRACELLULAR Ca²⁺ LEVELS	71
8. NMDAR STIMULATION PROMOTES PROTEIN STABILIZATION OF THE GLYCOLYTIC-PROMOTING ENZYME PFKFB3 IN NEURONS	73

9. NMDAR STIMULATION DOES NOT ALTER THE PFKFB3 mRNA LEVELS IN NEURONS.	74
10. NMDAR STIMULATION TRIGGERS NUCLEUS-TO-CYTOSOL PFKFB3 TRANSLOCATION.....	75
11. NMDAR STIMULATION INCREASES THE RATE OF GLYCOLYSIS AND DECREASES THE RATE OF PPP THROUGH PFKFB3.....	78
12. NMDAR STIMULATION LEADS TO IMPAIRMENT OF GLUTATHIONE REGENERATION THAT IS MEDIATED BY PFKFB3 STABILIZATION.	80
13. THE PPP TO GLYCOLYSIS SHIFT CAUSED BY NMDAR STIMULATION TRIGGERS OXIDATIVE STRESS.....	81
14. NMDAR ACTIVATION TRIGGERS APOPTOTIC DEATH BY SWITCHING PPP TO GLYCOLYSIS.....	83
15. EXPRESSION OF A MUTANT FORM OF PFKFB3 INSENSITIVE TO APC/C-Cdh1 MIMICS NMDAR AT CAUSING OXIDATIVE STRESS AND NEURONAL DEATH.....	84
16. THE FRUCTOSE-2,6-BISPHOSPHATASE TIGAR PROTEIN IS EXPRESSED IN NEURONS.....	85
17. ASSESSMENT OF APOPTOSIS AND SUPEROXIDE LEVELS IN PRIMARY NEURONS FROM TIGAR KNOCKOUT MICE.....	86
18. OVER-EXPRESSION OF THE FULL-LENGTH TIGAR cDNA DECREASES FRUCTOSE-2,6-BISPHOSPHATE CONCENTRATION	87
19. TIGAR PREVENTS PFKFB3-INDUCED INCREASE IN MITOCHONDRIAL SUPEROXIDE AND NEURONAL DEATH.....	88
20. KNOCKDOWN OF TIGAR IS NOT SUFFICIENT TO INCREASE THE RATE OF GLYCOLYSIS IN PRIMARY NEURONS	89
21. KNOCKDOWN OF TIGAR INCREASES APOPTOTIC NEURONAL DEATH WITHOUT INCREASING SUPEROXIDE	90
22. CONFOCAL ANALYSIS REVEALS NUCLEAR LOCALIZATION OF TIGAR IN NEURONS, BUT NOT IN ASTROCYTES	91
5. DISCUSSION.....	93
1. GLYCOLYSIS AND PPP ARE DYNAMIC PROCESSES IN INTACT NEURONS	95
2. GLYCOLYSIS AND PPP CAN BE MODULATED BY ENDOGENOUS STIMULI WITH PATHOPHYSIOLOGICAL CONSEQUENCES	98
3. TIGAR: A NEW PLAYER IN NEURONAL GLUCOSE METABOLISM AND BEYOND.....	99
6. CONCLUSIONS AND FUTURE PERSPECTIVES.....	101

7. RESÚMEN EN ESPAÑOL	105
INTRODUCCIÓN	107
1. Metabolismo glucídico en el cerebro.	107
2. Neurotransmisión glutamatérgica y excitotoxicidad.	109
HIPÓTESIS Y OBJETIVOS	110
RESULTADOS Y DISCUSIÓN	111
1. La actividad glucolítica en neuronas aumenta tanto al inhibir la vía de las pentosas fosfato como la captación mitocondrial de piruvato.	111
2. La velocidad de oxidación de glucosa por la PPP se inhibe con DHEA.	112
3. La fosfoglucoasa isomerasa (PGI) presenta una actividad elevada en neuronas.	113
4. El silenciamiento de la PGI conlleva un incremento en la actividad de la PPP.	114
5. Efecto de DHEA e HCN sobre la concentración de G6P.	115
6. Las neuronas corticales en cultivo primario responden a la activación de los receptores de glutamato incrementando los niveles de Ca^{2+} intracelular.	116
7. La activación de receptores NMDA promueve la estabilización de la enzima pro-glucolítica PFKFB3 en neuronas.	117
8. La estimulación de receptores NMDA produce la translocación del núcleo al citosol de la PFKFB3.	119
9. La estabilización de PFKFB3 mediada por receptores NMDA aumenta la actividad glucolítica y disminuye la de PPP.	121
10. La estimulación de receptores NMDA produce un defecto en la regeneración de glutatión mediada por la estabilización de PFKFB3.	123
11. La desviación del metabolismo de la glucosa de la PPP a glucolisis como consecuencia de la estimulación de receptores NMDA produce estrés oxidativo.	124
12. La activación de receptores NMDA induce muerte neuronal por apoptosis como consecuencia de la desviación del metabolismo glucídico de la PPP a glucolisis.	126
13. La expresión de una forma mutada de PFKFB3 no detectable por APC/C-Cdh1 produce un efecto similar a la activación de receptores NMDA.	127
14. La proteína TIGAR, con función fructosa-2,6-bisfosfatasa, se encuentra expresada en neuronas.	129
15. Determinación de apoptosis y niveles de superóxido en neuronas procedentes de ratones KO de TIGAR.	129
16. TIGAR previene el incremento en superóxido mitocondrial y en apoptosis mediado por PFKFB3.	130
17. El silenciamiento de TIGAR no es suficiente para incrementar la velocidad glucolítica en neuronas primarias.	131

18. El silenciamiento de TIGAR en neuronas incrementa la muerte por apoptosis sin afectar a los niveles de superóxido.....	132
19. TIGAR presenta una localización nuclear en neuronas	133
CONCLUSIONES.....	135
8. REFERENCES.....	137

ABBREVIATIONS

AD: Alzheimer's disease

ADP: Adenosine diphosphate

AMP: Adenosine monophosphate

AMPA: 2-amino-3-(3-hydroxy-5-methyl-isoxazol-4-yl)propanoic acid

APC/C: Anaphase-promoting complex/cyclosome

ATP: Adenosine triphosphate

BCA: Bicinchoninic acid (assay)

BSA: Bovine serum albumin

cDNA: Complementary DNA

Cdk 5: Cyclin-dependent kinase 5

CMV: Cytomegalovirus

DAPI: 4,6-diamidine-2-phenylindol chloridrate

DMEM: Dulbecco's modified eagle medium

DMSO: Dimethyl sulfoxide

DNA: Deoxyribonucleic acid

dNTPs: Deoxyribonucleotides

EDTA: Ethylenediamine tetraacetic acid

eGFP: Enhanced green fluorescent protein

EGTA: Ethylene glycol tetraacetic acid

E4P: Erythrose-4-phosphate

F2,6P₂: Fructose-2,6-bisphosphate

F1,6P₂: Fructose-1,6-bisphosphate

G6P: Glucose-6-phosphate

G6PD: Glucose-6-phosphate dehydrogenase

GAP: Glyceraldehyde-3-phosphate

GAPDH: Glyceraldehyde-3-phosphate dehydrogenase

GPx: Glutathione peroxidase

GRx: Glutathione reductase

GSH: Reduced glutathione, γ -L-glutamyl-L-cysteinyl-glycine

GSR: Glutathione reductase

GSSG: Glutathione disulfide, oxidized glutathione

GSx: Total glutathione

HEPES: 4-(2-hydroxyethyl)-1-piperazineethanesulfonic acid

ABBREVIATIONS

H₂O₂: Hydrogen peroxide

HK: Hexokinase

HIF1: Hypoxia inducible factor 1

K_m: Michaelis-Menten constant

LDH: Lactate dehydrogenase

MPEP: 2-methyl-6-(phenylethynyl)pyridine

MPTP: 1-methyl-4-phenyl-1,2,3,6-tetrahydropyridine

mRNA: Messenger RNA

NAD⁺: Nicotinamide adenine dinucleotide (oxidized). **NADH(H⁺)**: reduced form

NADP⁺: Nicotinamide adenine dinucleotide phosphate (oxidized). **NADPH(H⁺)**: reduced form

NO: Nitric oxide

NOS: Nitric oxide synthase

NMDA: N-methyl-D-aspartate

O²⁻: Superoxide anion

OH[·]: Hydroxyl radical

ONOO⁻: Peroxynitrite

PB: Phosphate buffer

PBS: Phosphate buffered saline

PCR: Polymerase chain reaction

PD: Parkinson's disease

PEP: Phosphoenol pyruvate

PFK-1: 6-Phosphofructo-1-kinase

PFK-2: Phosphofructo kinase 2

PFKFB: 6-phosphofructo-2-kinase/fructose-2,6-bisphosphatase

PFKFB3: 6-phosphofructo-2-kinase/fructose-2,6-bisphosphatase-3

PGI: Phosphoglucose isomerase

PKA: Protein kinase A

PKC: Protein Kinase C

PPP: Pentose-phosphate-pathway

ROS: Reactive oxygen species

R5P: Ribose-5-phosphate

Ru5P: Ribulose-5-phosphate

S.E.M.: Standard error of the mean

SDS: Sodium dodecyl sulfate

SDS-PAGE: Sodium dodecyl sulfate-polyacrylamide gel electrophoresis

siRNA: Small interfering RNA

SOD: Superoxide dismutase

S7P: Sedoheptulose-7-phosphate

TIGAR: TP53-induced glycolysis and apoptosis regulator

TCA: Tricarboxylic acid cycle

X5P: Xilulose-5-phosphate

6-NBDG: 6-(N-(7-nitrobenz-2-oxa-1,3-diazol-4-yl) amino)-2-deoxyglucose

1,3-bPG: 1,3-Bisphosphoglycerate

3-PG: 3-Phosphoglycerate

2-PG: 2-Phosphoglycerate



1. INTRODUCTION

1. GLUCOSE METABOLISM IN THE CENTRAL NERVOUS SYSTEM

The brain only represents ~2% of the total body weight but it accounts for more than a 20% of the body consumption of O₂ and glucose (Sokoloff *et al.* 1950). Whilst the adult brain in mammals is highly dependent on glucose as an energetic substrate, ketone bodies (3-hydroxybutyrate and acetoacetate) can be considered an alternative brain fuel during early postnatal life. Thus, ketone bodies synthesis by astrocytes plays an essential role in neuronal survival in pathological conditions where glucose delivery to the brain is decreased, (Guzman & Blazquez 2004, Blazquez *et al.* 1999). Despite glucose may be used for oxidative metabolism to produce ATP, it is also important as a source of carbons for fatty acid, cholesterol, neurotransmitters, aminoacids, glycerol-3-phosphate and, in astrocytes, glycogen synthesis (Cataldo & Broadwell 1986). Most part of the energy generated by glucose metabolism is thought to be used to fulfill the energetic needs for neurotransmission (Attwell & Laughlin 2001, Ames 2000).

A correct glucose brain metabolism is essential for survival, and there have been a large number of reports documenting alterations in glucose metabolism in patients with neurodegenerative diseases. Decreased cerebral glucose metabolism ascribed to diminished glucose transport and reduced glucose phosphorylation has been described in patients with Alzheimer's disease (AD) (Piert *et al.* 1996). In addition, several studies have documented "diabetes like" alterations in AD patients, including metabolic alterations associated to insulin resistance that can contribute to the development of AD (Mosconi *et al.* 2008, Cunnane *et al.* 2011, Carvalho *et al.* 2012, Schioth *et al.* 2012). Brain hypometabolism has also been suggested in the etiology of Huntington's disease, as glucose consumption is reduced in the presymptomatic stages of the disease (Ciarmiello *et al.* 2006). Studies of Parkinson's disease (PD) patients have also provided evidence for alterations similar to those in AD that include abnormal glucose tolerance and increased insulin resistance (Aviles-Olmos *et al.* 2013).

1.1. GLUCOSE TRANSPORTERS

Cells take up glucose by transporters located in the plasma membrane. There are two different classes of glucose transporters with different kinetic properties: GLUT (GLUT1-GLUT12) that are sodium-independent, and SGLT (SGLT1-SGLT6) that are sodium-dependent (see Table 1). Cells express different transporters depending on their specific metabolic requirements (Shah *et al.* 2012). The main isoforms expressed in brain cells are GLUT1, GLUT3 and GLUT5 (See table 1). GLUT3 is present predominantly in neurons and GLUT5 is specific of microglia. GLUT1, which is detected in the blood-brain barrier and astrocytes, is the only vehicle responsible for the transport of glucose into the brain. A defect in glucose transport into the brain, known as GLUT1 deficiency syndrome, leads to neurological disorders associated with epilepsy and delays in mental and motor development in children (Klepper & Voit 2002).

TRANSPORTER	EXPRESSION IN BRAIN	SUBSTRATES/TRANSPORTS
GLUT 1	Brain endothelial and epithelial-like brain barriers, glial cells.	Glucose, galactose, mannose, glucosamine, ascorbic acid
GLUT 2	Astrocytes	Mannose, galactose, fructose, glucose, glucosamine
GLUT 3	Neurons, brain endothelial cells	Glucose, galactose, mannose, xylose, dehydroascorbic acid
GLUT 4	Hippocampal and cerebellar neurons	Glucose, dehydroascorbic acid, glucosamine
GLUT 5	Brain microglia	Fructose, Glucose
GLUT 6	Brain	Glucose
GLUT 8	Neurons	Glucose
SGLT 1	Cortical, pyramidal and purkinje neuronal cells	>Glucose, ≥ galactose
SGLT2	Brain	Glucose, galactose
SGLT3	Brain	Glucose, Na ⁺ (H ⁺)
SGLT4	Brain	Glucose, mannose, fructose
SGLT6	Neurons	Myo-inositol, glucose

Table 1: Glucose transporters in brain. Adapted from Shah *et al* 2012.

When glucose enters the cell it is phosphorylated by hexokinase; the resulting product, glucose-6-phosphate (G6P), is retained in the cytoplasm to be metabolized by the pentose phosphate pathway (PPP), glycolysis (Wamelink *et al.* 2008), or be stored as glycogen.

1.2. GLUCOSE METABOLIC PATHWAYS

1.2.1. GLYCOGEN IN THE BRAIN

Astrocytes are the only cells in the nervous system able to storage glycogen under non-pathologic conditions (Wiesinger *et al.* 1997), where it functions as a transient glucose reservoir under resting conditions (Watanabe & Passonneau 1973). Neurons express the enzyme responsible for glycogen synthesis, glycogen synthase, but under normal conditions they keep the machinery for glycogen synthesis inactive by maintaining glycogen synthase phosphorylated (inactive). In addition, neurons degrade both glycogen synthase and protein targeting glycogen (PTG), a regulatory subunit of protein phosphatase 1 that activates, through dephosphorylation, glycogen synthase (Vilchez *et al.* 2007). When glycogen synthase is dephosphorylated (thus activated), it leads to glycogen accumulation and triggers apoptotic neuronal death, a phenomenon that is characteristic of a form of progressive myoclonus epilepsy, Lafora disease (Vilchez *et al.* 2007, Collins *et al.* 1968).

Glycogenolysis is induced when there is a deficit of glucose supply to the brain (Choi *et al.* 2003). Actually, astrocyte glycogen is critical for maintaining synaptic activity and for neuronal survival during hypoglycemia (Swanson & Choi 1993, Suh *et al.* 2007). Neuronal synaptic activity in normal condition also stimulates glycogen degradation by astrocytes (Swanson *et al.* 1992) and its glycolytically conversion in lactate (Dringen *et al.* 1993). Lactate is then released and transported to neurons that can use it as an energetic substrate.

1.2.2. GLYCOLYSIS

Glycolysis transforms glucose into pyruvate in 10 enzymatic reactions. Besides 2 mols of pyruvate, 2 mols of ATP, 2 mols of NADH(H⁺), 2 H⁺ and 2 of H₂O are produced per mol of glucose (Nelson & Cox 2001). Three enzymes are key regulatory points in this pathway as they catalyze irreversible reactions that generate intermediates arriving from other metabolic pathways (Nelson & Cox 2001). These three enzymes are hexokinase, 6-phosphofructo-1-kinase (PFK-1) and pyruvate kinase (see figure 1).

Hexokinase is expressed under four different isoenzymes (HKI-IV) (Wilson 2003). The most abundant isoenzyme in brain is HKI and is physically associated (70-90%) with the outer mitochondrial membrane. Release of HKI from mitochondria causes a severe decrease in its activity (Rose & Warms 1967) that, in neurons, triggers oxidative damage (Saraiva *et al.* 2010). Besides preventing neuronal oxidative damage, mitochondrial-bound HKI is neuroprotective, maintains adequate glutathione levels and induces neurite outgrowth (Wang *et al.* 2008). HKII also associates with mitochondria, where it promotes neuronal survival; its overexpression is sufficient to protect against rotenone (a mitochondrial complex I inhibitor)-induced cell death (Gimenez-Cassina *et al.* 2009). In astrocytes HKI is also associated with mitochondria but inhibition of gap junctions upregulates and stimulates the translocation of HKI from mitochondria to microtubules at the same time that promotes GLUT1 translocation to the plasma membrane, inducing a significant expression of HKII and GLUT3, which are normally not present in astrocytes (Sanchez-Alvarez *et al.* 2004).

Glycolytic rate in neurons is much lower than in astrocytes (Herrero-Mendez *et al.* 2009), an observation that is accompanied by a lower rate of the oxidation of glucose through the tricarboxylic acid cycle (TCA) in neurons (Garcia-Nogales *et al.* 2003). However glycolytic activity in neurons is essential for fast axonal transport of vesicles to nerve terminals, as it provides the ATP necessary for this process (Zala *et al.* 2013). Glucose in astrocytes is predominantly used in the glycolytic pathway, which appears to be predominantly “anaerobic” (Leo *et al.* 1993) i.e., that converts glucose into lactate, which can be used as a fuel by neurons.

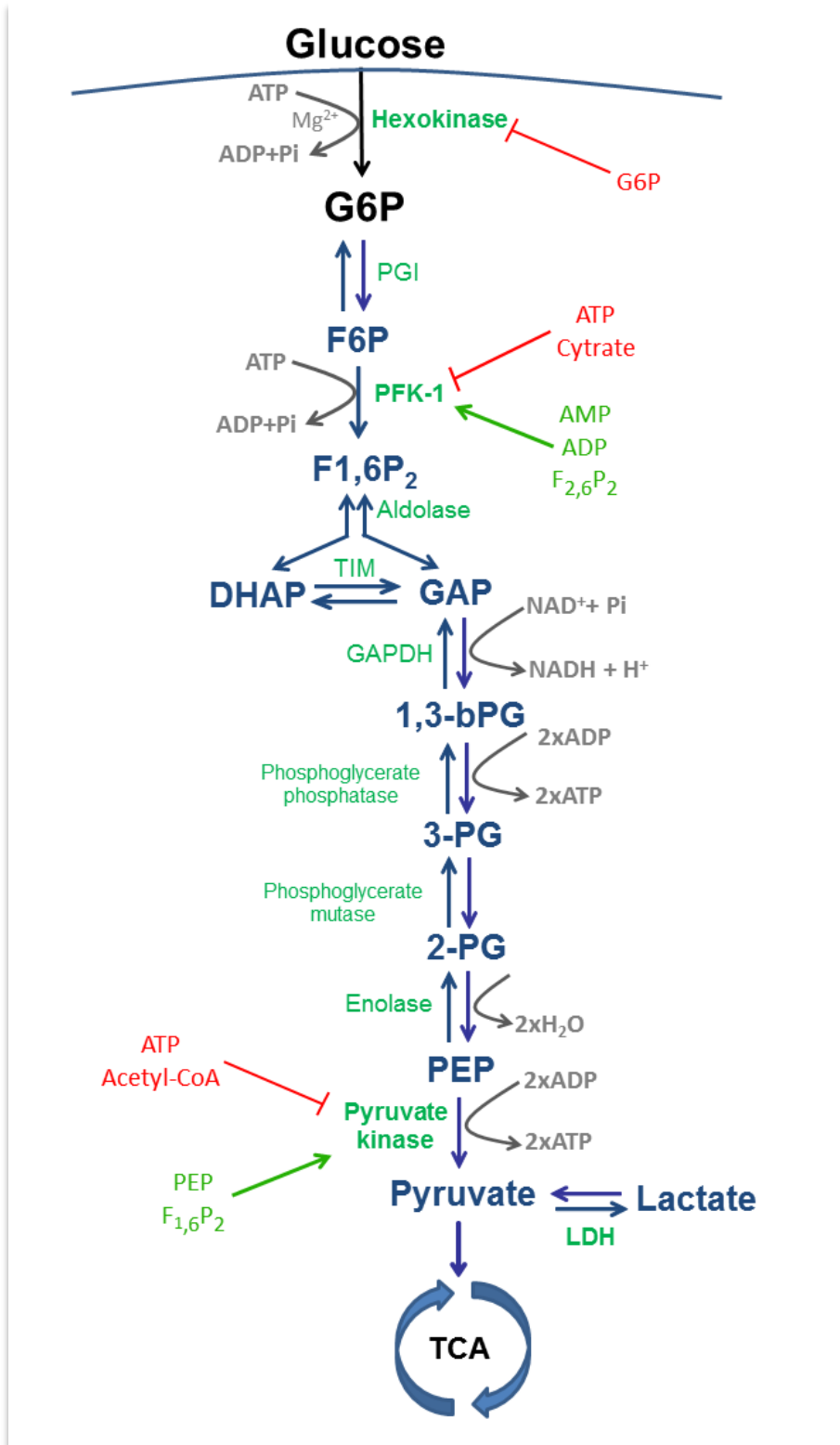


Figure 1: Schematic representation of the glycolytic pathway. Abbreviations used: G6P: Glucose 6 phosphate; PGI: Phosphoglucose isomerase; F6P: Fructose-6-phosphate; F1,6P₂: Fructose-1,6-bisphosphate; TIM: Triose-phosphate isomerase; DHAP: Dihydroxyacetone phosphate; GAP: Glyceraldehyde-3-phosphate; GAPDH: Glyceraldehyde-3-phosphate dehydrogenase; F2,6P₂: Fructose-2,6-bisphosphate; 1,3-bPG: 1,3-Bisphosphoglycerate; 3-PG: 3-Phosphoglycerate; 2-PG: 2-Phosphoglycerate; LDH: Lactate dehydrogenase; PEP: Phosphoenolpyruvate; PFK-1: 6-Phosphofructo-1-kinase. Allosteric inhibitors of the enzymes are indicated in red, and allosteric activators in green. Stoichiometry has been omitted for clarity.

PFK-1 regulation by fructose-2,6-bisphosphate

6-Phosphofructo-1-kinase (PFK-1) is a master regulator of glycolysis (Hue & Rider 1987, Van Schaftingen *et al.* 1982, Uyeda 1979). It is a tetramer that is composed of different combinations of 3 different subunits: L-type (liver), M-type (muscle) and P-type (platelets), each with different kinetic properties although all of them requiring the presence of fructose-2,6-bisphosphate (F2,6P₂) for full activity. In the brain, the three subunits are expressed, although M-type is the most abundant (Dunaway *et al.* 1988, Almeida *et al.* 2004).

PFK-1 catalyzes the phosphorylation of fructose-6-phosphate (F6P) into fructose-1,6-bisphosphate (F1,6P₂). PFK-1 is regulated by different negative (ATP and citrate) and positive (AMP, ADP and F2,6P₂) allosteric effectors; its main positive allosteric effector is F2,6P₂.

Two enzymes are responsible for the synthesis and degradation of F2,6P₂, namely 6-phosphofructo-2-kinase/fructose-2,6-bisphosphatase (PFKFB) and TP53-induced glycolysis and apoptosis regulator (TIGAR). In view of the relevance of these enzymes in the context of this thesis, we will describe them in separate sections.

PFKFB

PFKFB is a bifunctional enzyme that presents a kinase domain which synthesizes F_{2,6}P₂ and a bisphosphatase domain, which dephosphorylates it to obtain fructose-6-phosphate (see Figure 2).

PFKFB activity is regulated by citrate and phosphoenol pyruvate (PEP), that are potent allosteric inhibitors of the enzyme (Van Schaftingen *et al.* 1982). Glucagon inhibits the kinase activity of the hepatic (PFKFB1) enzyme by activating protein kinase A (Payne *et al.* 2005). On the other hand, phosphate is a cofactor for PFKFB and its presence increases the V_{max} of the enzyme and decreases the K_m for F6P (Laloux *et al.* 1985).

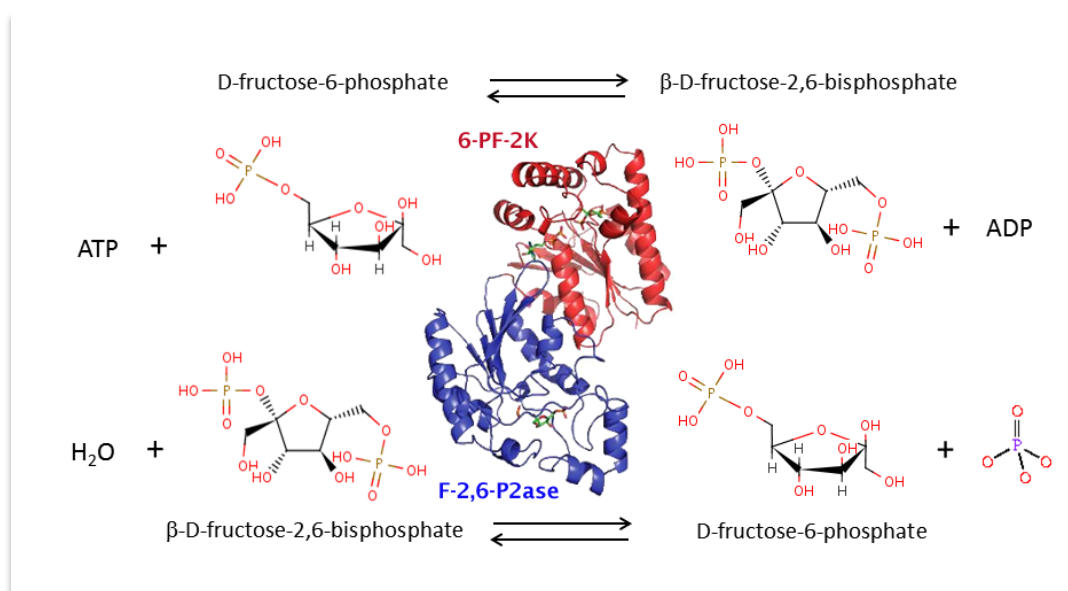


Figure 2: PFKFB is a bifunctional enzyme. PFKFB kinase domain (red) synthesizes fructose-2,6-bisphosphate from fructose-6-phosphate at the expense of 1 ATP molecule. PFKFB bisphosphatase domain (blue) dephosphorylates fructose-2,6-bisphosphate and produces fructose-6-phosphate.

PFKFB is expressed by 4 different genes yielding 4 different isoforms (PFKFB1-4), which have different kinetic properties and tissue-expression pattern according to the specific needs. PFKFB1 is expressed in liver and muscle, PFKFB2 in heart, kidney and pancreatic islets, PFKFB3 in placenta, cancer cell lines, monocytes and Kupffer cells and PFKFB4 in testicles (Bartrons & Caro 2007). PFKFB3 is the

INTRODUCTION

most abundant PFKFB isoform in brain (Okar *et al.* 2001, Herrero-Mendez *et al.* 2009).

There are different alternative splicing variants of PFKFB3 depending on the species. In humans, ubiquitous PFK-2 (uPFK-2) is the most abundant isoform in the brain, placenta and breast cancer cells, and its ortholog in the rat is the RB2K6 alternative variant (Watanabe & Furuya 1999).

PFKFB3 presents the highest kinase-to-bisphosphatase activity (~700:1) (Ventura *et al.* 1991). Thus, expression of its full-length cDNA yields a protein that is almost a kinase, i.e. F_{2,6}P₂-synthetizing, hence glycolytic-promoting enzyme.

PFKFB3 is phosphorylated by PKA and PKC on Ser⁴⁶¹ without affecting K_m for F6P or ATP and neither its bisphosphatase activity (Tominaga *et al.* 1997). When, under hypoxic conditions, the ratio AMP:ATP increases, AMP-activated protein kinase (AMPK) is activated and phosphorylates PFKFB3 on Ser⁴⁶¹, activating it and causing an increase in F_{2,6}P₂ levels that stimulates glycolysis and cytosolic ATP production (Marsin *et al.* 2002). PFKFB3 can also be phosphorylated at Ser⁴⁶¹ by MK2 (MAPK-activated protein Kinase-2), leading to an increase in its activity (Novellademunt *et al.* 2013, Bolanos 2013).

PFKFB3 promoter has elements that can be activated upon binding of the hypoxia inducible factor 1 (HIF-1). Thus, under hypoxic conditions, *PFKFB3* is transcriptionally upregulated and this is accompanied by an increase in glycolytic flux and ATP levels (Minchenko *et al.* 2002, Obach *et al.* 2004). *PFKFB3* promoter also presents a serum response element that is activated upon serum response factor binding in a p38αMAPK-MK2 pathway-dependent process (Novellademunt *et al.* 2013, Bolanos 2013). *PFKFB3* expression can also be induced in response to progestins (Novellademunt *et al.* 2012) or insulin (Riera *et al.* 2002) in cancer cells and pro-inflammatory molecules such as interleukine-6 (Ando *et al.* 2010) and adenosine (Ruiz-Garcia *et al.* 2011).

PFKFB3 shows another regulatory mechanism that accounts for the low levels of this protein in neurons. PFKFB3 is the only PFKFB isoform that presents a Lys-Glu-Asn (KEN) box in its sequence. This motif is a recognition site for Cdh1, an adaptor protein for the E3 ubiquitin ligase anaphase-promoting complex/cyclosome

(APC/C) that ubiquitinates target proteins to be degraded by the proteasome (see section 2.5.4). Unlike astrocytes, APC/C-Cdh1 is very active in neurons and maintains PFKFB3 protein levels very low; this accounts for the differential regulation of glycolysis in neurons and astrocytes. Thus, during inhibition of mitochondrial respiration, astrocytes maintain their ATP levels, while in neurons ATP concentration decreases progressively and is accompanied by a decrease in the mitochondrial membrane potential ($\Delta\psi_m$) that finally triggers apoptotic cell death (Bolanos *et al.* 1994, Almeida *et al.* 2001). The study of the mechanism revealed that inhibition of respiration caused an increase in AMP levels in astrocytes that lead to AMPK phosphorylation that, in turn, activated PFKFB (Almeida *et al.* 2004). The low levels of PFKFB3 in neurons explains why these cells are unable to upregulate glycolysis upon mitochondrial damage (Herrero-Mendez *et al.* 2009). In fact, overexpression of PFKFB3 in neurons is sufficient to stimulate glycolysis and maintain $\Delta\psi_m$ during inhibition of mitochondrial respiration (Herrero-Mendez *et al.* 2009). However, this effect is transient, because the increase in glycolysis triggered by PFKFB3 overexpression is accompanied by a decrease in the utilization of glucose through the PPP. Consequently, decrease in the regeneration of reduced glutathione triggers oxidative stress leading to neuronal death (Herrero-Mendez *et al.* 2009) (see Figure 7).

TIGAR

The protein structure of TIGAR (TP53-induced glycolysis and apoptosis regulator) is very similar to the fructose-2,6-bisphosphatase domain of PFKFB (see Figure 3) and, like PFKFB, it regulates F_{2,6P₂} levels (Li & Jogl 2009) by degrading it, thus, inhibiting glycolysis and promoting PPP. This causes a decrease in intracellular reactive oxygen species (ROS) and limits apoptosis and autophagy in cancer cells (Bensaad *et al.* 2006, 2009).

Besides its function as a bisphosphatase TIGAR translocates to the mitochondria

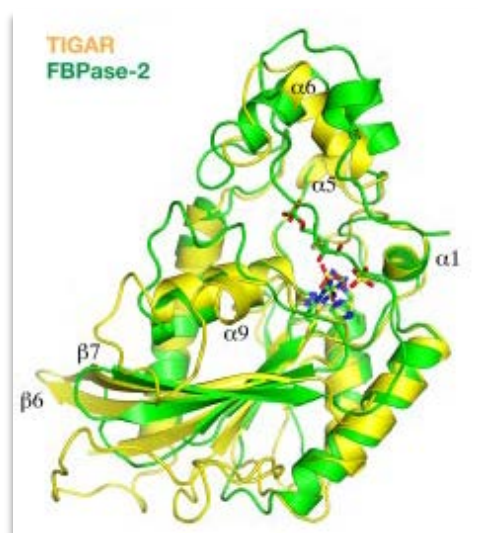


Figure 3: Superposition of TIGAR (yellow) and FBPase-2 (green) structures. Obtained from Li *et al.*, 2009.

under hypoxic conditions by forming a complex with hexokinase-II. This triggers an increase in hexokinase activity that leads to increased glycolysis, helping to maintain the mitochondrial membrane potential and limiting mitochondrial ROS (Cheung *et al.* 2012). TIGAR also plays a role in regulating cell cycle by mediating de-phosphorylation of retinoblastoma and stabilization of RB-E2F1 complex thus delaying the entry of cells in S phase of the cell cycle (Madan *et al.* 2012).

Despite its intriguing effects over cell cycle and metabolism in cancer cells, to our knowledge, nothing is known about TIGAR expression and function in brain.

Metabolism of pyruvate

Pyruvate, the pyruvate kinase (PK) product, is the last metabolite of glycolysis. Neurons can obtain most of it from lactate, which, according to the astrocyte-neuron lactate shuttle hypothesis, would be provided by astrocytes (Pellerin *et al.* 2007). There are three PK isoenzymes, namely class L (liver), class A (adipose tissue, kidney) and class M, that is present in muscle and brain (Carbonell *et al.* 1973, Farrar & Farrar 1995). In the cytosol, pyruvate can be reduced to lactate by a reaction catalyzed by lactate dehydrogenase (LDH), or transformed into alanine in a transamination reaction catalyzed by alanine aminotransferase. In the mitochondrial matrix, pyruvate can also be converted into acetyl-CoA or oxaloacetate in the reactions catalyzed by the pyruvate dehydrogenase complex or pyruvate carboxylase, respectively (see figure 4).

Within the brain, pyruvate carboxylase is exclusively present in astrocytes (Yu *et al.* 1983). Neurons, however, show a pyruvate dehydrogenase (PDH) complex activity higher than astrocytes (Halim *et al.* 2010). This high PDH activity is important in cholinergic neurons, which require additional amounts of acetyl-CoA for acetylcholine synthesis (Szutowicz *et al.* 2013).

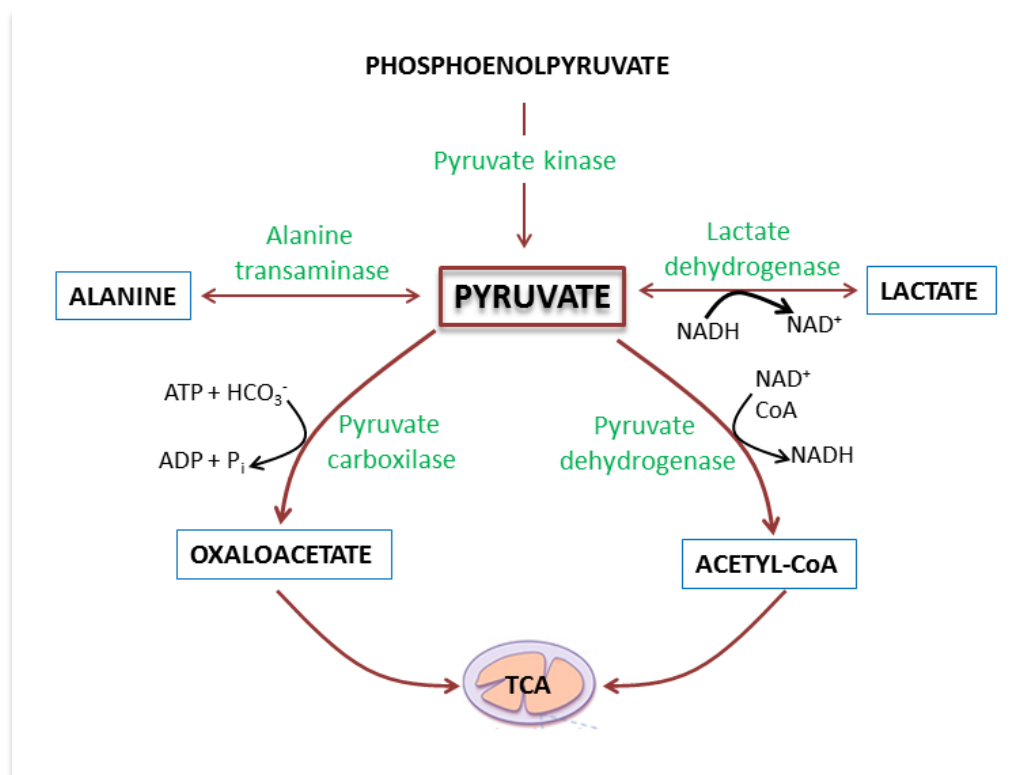


Figure 4: Schematic representation of pyruvate fates in the cell.

1.2.3. PENTOSE-PHOSPHATE PATHWAY

Besides glycolysis, PPP is the main glucose utilization pathway. PPP can be divided into an oxidative phase and a non-oxidative phase. In the oxidative phase, G6P is oxidized into ribulose-5-phosphate (Ru5P), a process that generates 2 mols of NADPH(H⁺) per mol of G6P (Wamelink *et al.* 2008). In the non-oxidative phase, Ru5P produces ribose-5-phosphate and xylulose-5-phosphate, that can later be transformed in the glycolytic intermediates glyceraldehyde-3-phosphate and fructose-6-phosphate (Baquer *et al.* 1988).

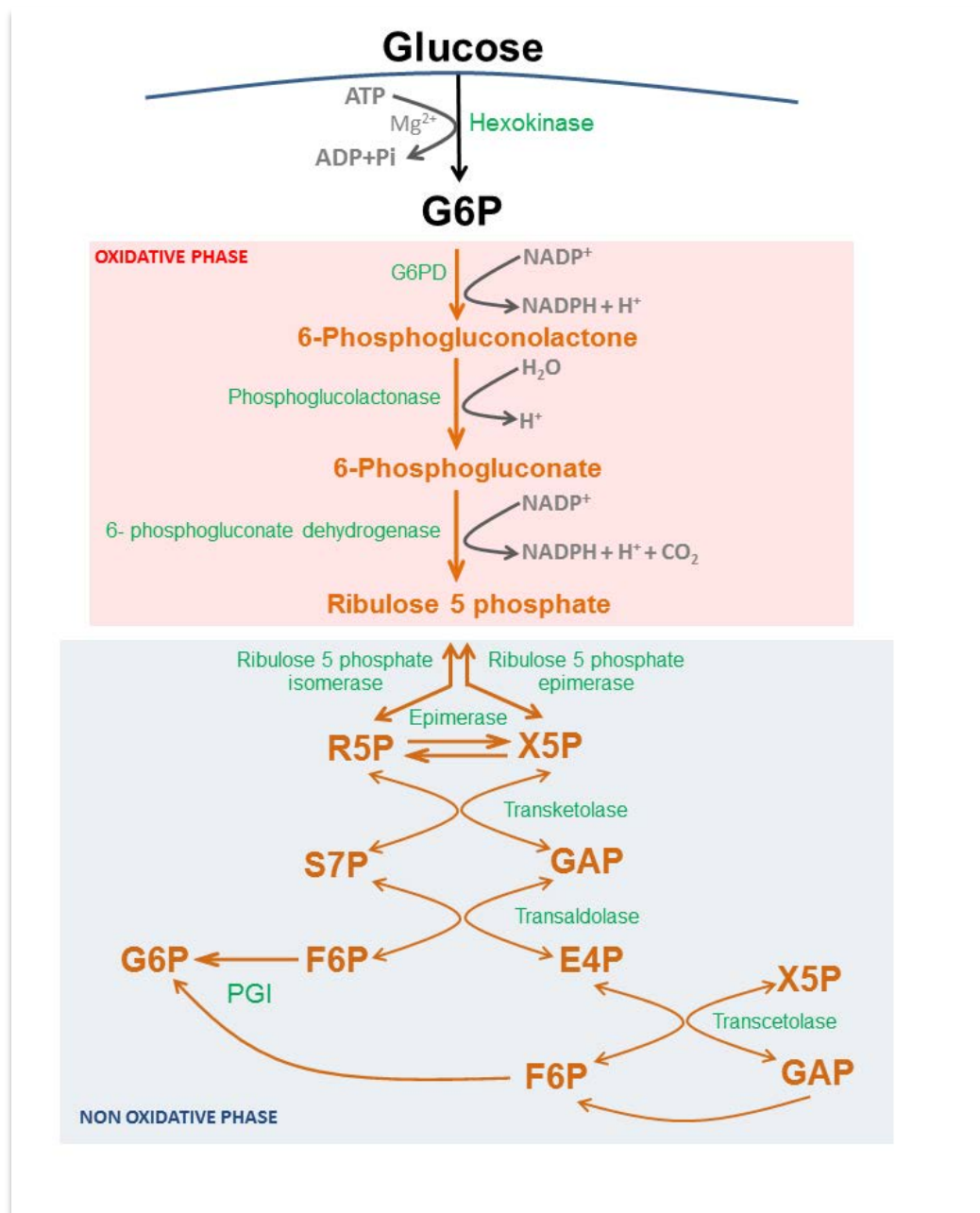


Figure 5: Pentose-phosphate pathway. Abbreviations used: G6P: Glucose-6- phosphate; G6PD: Glucose- 6- phosphate dehydrogenase; E4P: Erythrose-4-phosphate; F6P: Fructose-6-phosphate; GAP: Glyceraldehyde-3-phosphate; PGI: Phosphoglucose isomerase; R5P: Ribose-5- phosphate; S7P: Sedoheptulose-7-phosphate; X5P: Xilulose-5- phosphate.

The rate-limiting enzyme of PPP is glucose-6-phosphate dehydrogenase (G6PD). G6PD activity is different between neuronal types, and is essential for generating NADPH(H⁺) (Biagiotti *et al.* 2003). PPP activity in resting conditions, as well as the increase in its activity that takes place during activation, is higher in astrocytes than

in neurons. However, neurons actively metabolize glucose by the PPP, and has been shown to be essential for neuronal survival (Delgado-Esteban *et al.* 2000, Herrero-Mendez *et al.* 2009). Moreover, H₂O₂ increases PPP activity (Ben-Yoseph *et al.* 1994), and peroxynitrite (ONOO⁻), a strong oxidant derived from nitric oxide, triggers an increase in PPP activity and NADPH(H⁺) levels in neurons by activating G6PD and thus protecting these cells against nitrosative stress (Garcia-Nogales *et al.* 2003).

1.3. LACTATE CONSUMPTION IN NEURONS AND THE ASTROCYTE-NEURON LACTATE SHUTTLE HYPOTHESIS.

Glucose has been largely recognized as an essential substrate for brain cells (Sokoloff 1992) but, besides the classical view of glucose as the only substrate for oxidative metabolism in neurons, in the last few years several evidences have shown that lactate can also be oxidized by these cells (Bouzier-Sore *et al.* 2003, Zielke *et al.* 2007). Indeed, several works have reported that in resting conditions lactate is the preferential substrate for neurons (Bouzier-Sore *et al.* 2003, Boumezbeur *et al.* 2010). This is consistent with the astrocyte-neuron lactate shuttle hypothesis (ANLSH). According to this hypothesis, astrocytes would take up glucose from the blood circulation, transform it into lactate, and supply the latter to neurons through the monocarboxylate transporters (MCTs), thus providing neurons a substrate for energy production (Pellerin *et al.* 2007).

The use of lactate by neurons is supported by the fact that neurons and astrocytes express different isoforms of lactate dehydrogenase (LDH), the enzyme responsible for the conversion of lactate into pyruvate. Neurons express preferentially LDH1, which is associated with a higher pyruvate-producing capacity, while astrocytes express the LDH5 isoform, which is associated with tissues that do not consume, but produce, high amounts of lactate (Pellerin *et al.* 1998). Moreover, under resting conditions, astrocytes release ~85% of the glucose they consume as lactate. In addition, astrocytes and neurons also differ in the expression of monocarboxylate transporters (MCTs): astrocytes predominantly express MCT1 and MCT4, which are responsible for lactate efflux, whereas neurons express MCT2, specialized in lactate influx (Pierre & Pellerin 2005) (see figure 6). All these data support the ANLSH, at least in resting conditions; however,

how neuronal metabolism is modified during neurotransmission, as well as the preferred substrate in these conditions, still remains elusive.

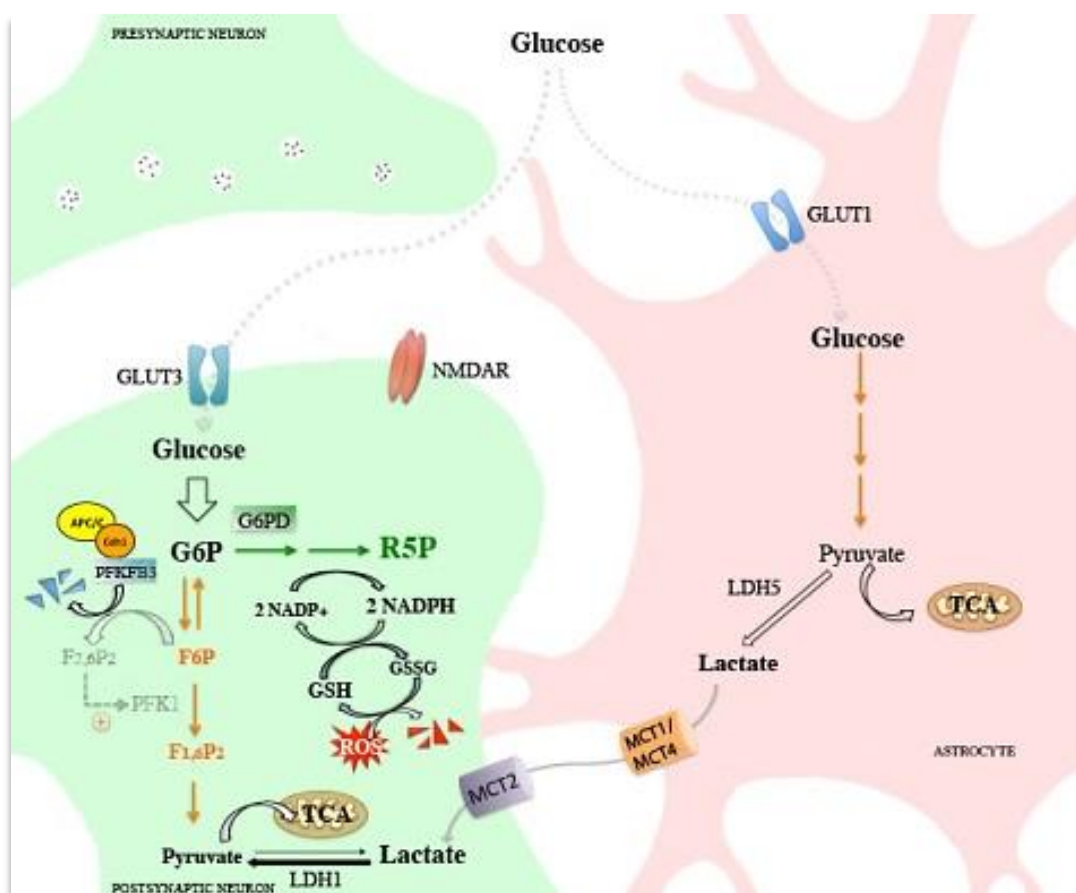


Figure 6: Astrocyte-neuron interaction in energy metabolism. Under resting conditions, glucose can be actively used through the PPP in neurons due to the low activity of PFKFB3, which is continuously degraded by APC/C-Cdh1. Neurons can thus efficiently produce NADPH(H^+), necessary for antioxidant glutathione regeneration from its disulfide form (GSSG). Astrocytes take up glucose, a part of which is transformed into pyruvate and used to fuel the TCA cycle, whereas the rest is transformed into lactate, exported to the synaptic cleft, and used as an energy fuel by neurons; in this process, the cellular distribution of the monocarboxylate carriers (MCT1/MCT4 and MCT2) and lactate dehydrogenase (LDH1 and LDH5) isoforms is critical. Accordingly, neurons can meet their energy requirements without compromising the redox detoxification system.

1.4. REACTIVE OXYGEN SPECIES (ROS) GENERATION AND DETOXIFICATION

1.4.1 ROS GENERATION

Reactive oxygen species (ROS) are produced physiologically. The main source of ROS is the mitochondrial electron transport chain. The leading ROS are superoxide anion ($O_2^{\cdot-}$), hydrogen peroxide (H_2O_2) and hydroxyl radical ($\cdot OH$). ROS can physiologically regulate protein function and gene expression, as well as cell proliferation and differentiation (Halliwell 2011, Rebrin & Sohal 2008).

$O_2^{\cdot-}$ is generated by the donation of a single electron to O_2 (Murphy 2009), largely at complexes I and III of the mitochondrial respiratory chain. However, it can also be generated by the action of enzymes such as xanthine oxidase, NADPH(H^+) oxidase, cyclooxygenase or lipoxygenase. $O_2^{\cdot-}$ can be transformed into H_2O_2 in a reaction catalyzed by superoxide dismutase (SOD), or reduce Fe^{3+} to Fe^{2+} by the Haber-Weis reaction. Fe^{2+} can be re-oxidized to Fe^{3+} by the Fenton reaction, leading to the formation of $O_2^{\cdot-}$ from H_2O_2 (Temple *et al.* 2005). Apart from the reaction catalyzed by SOD, H_2O_2 can be generated by the action of other enzymes, such as monoamine oxidase (MAO) in the catabolism of dopamine. Besides ROS, nitrogen oxidative species, such as peroxynitrite ($ONOO^-$), can be spontaneously formed by the reaction of $O_2^{\cdot-}$ with nitric oxide (see figure 7).

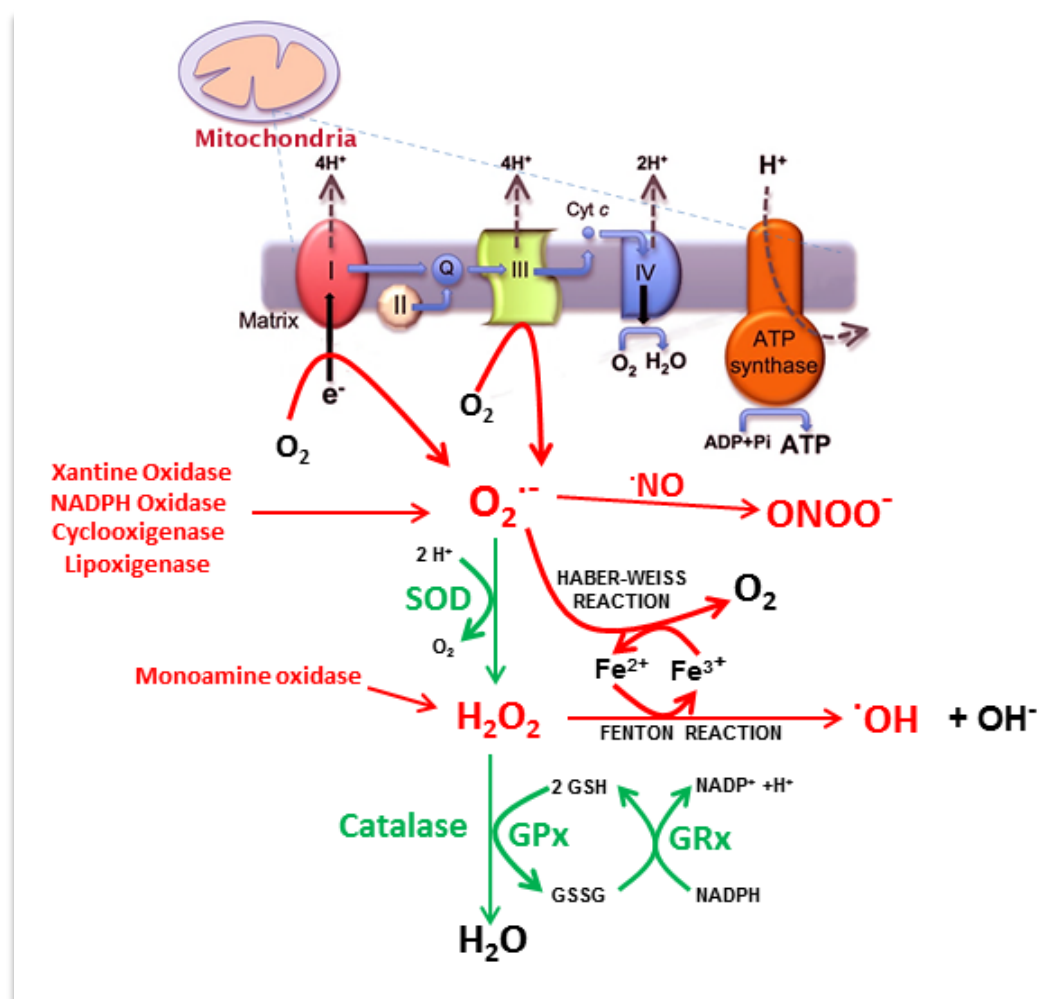


Figure 7: ROS generation and detoxification systems in the cell. Abbreviations used: SOD: superoxide dismutase; GPx: Glutathione peroxidase; GRx: glutathione reductase; GSH: Glutathione; GSSG: oxidized glutathione; $O_2^{\cdot-}$: superoxide anion; $ONOO^-$: peroxynitrite; $\cdot OH$: hydroxyl radical; H_2O_2 : hydrogen peroxide; $\cdot NO$: nitric oxide. ROS generation systems are indicated in red, and ROS detoxification systems in green.

1.4.2 ROS DETOXIFICATION SYSTEMS

Cells have many antioxidant systems to counteract the actions of ROS. These systems include compounds such as ascorbate or vitamin E, which directly trap radicals acting as scavengers, and enzymatic systems (see below). Ascorbate is especially abundant in the central nervous system (CNS). Its concentration is regulated homeostatically between the intracellular and extracellular compartments, and is especially abundant in neurons (Shimizu *et al.* 1960). Vitamin E is present in two-fold higher levels in astrocytes when compared with neurons, and protects astrocytes against mitochondrial oxidative damage (Heales

et al. 1994). SOD converts $O_2^{\cdot -}$ into H_2O_2 and is expressed under two different intracellular isoforms: manganese superoxide dismutase (MnSOD), that detoxifies cells from superoxide released into the mitochondrial matrix, and copper/zinc superoxide dismutase (Cu/ZnSOD), that detoxifies cytosolic superoxide. There is also an extracellular form of SOD (SOD3) that detoxifies extracellular $O_2^{\cdot -}$. Another form of H_2O_2 -detoxifying system is catalase, which is placed in peroxisomes.

Besides these, there are additional ROS detoxifying systems using thiols as cofactors. Glutathione (γ -L-glutamyl-L-cysteinyl-glycine, GSH) is the most abundant small thiol (0.5-10 nmol/l) in animal cells and tissues, and plays an essential role in protecting against oxidative and nitrosative stress. It is synthesized *de novo* in the cytosol by two ATP-dependent consecutive reactions, catalyzed by glutamate-cysteine ligase and glutathione synthetase. Most part of GSH synthesis in the brain takes place in astrocytes that liberate it to the extracellular space (Hirrlinger *et al.* 2002). GSH is then transformed into cysteinyl-glycine (Cys-gly), that is hydrolyzed by aminopeptidase, generating cysteine and glycine that are taken up by neurons, which use them as precursors for GSH biosynthesis (Dringen *et al.* 2001). Despite GSH biosynthesis is exclusively cytosolic, GSH enters mitochondria through carriers located in the inner mitochondrial membrane, and accounts for a 10-15% of the total cellular GSH (Mari *et al.* 2009).

Glutathione exerts its antioxidant function as an electron donor for peroxides detoxification in reactions catalyzed by glutathione peroxidases (GPxs1-4), which reduce H_2O_2 to H_2O , hence oxidizing reduced glutathione (GSH) to its disulfide (oxidized) form (GSSG). GPx4 is exclusively located in the mitochondria and has an important role in reducing lipid peroxides (Flohe *et al.* 1971). An important system for H_2O_2 detoxification are peroxiredoxins (Prxs), that are located both in mitochondria and cytosol and require reduced thioredoxin to be re-generated. Glutathione can also spontaneously react with different free radicals, such as superoxide, hydroxyl radical and nitric oxide, also generating GSSG (Dringen 2000). GSH can be regenerated from GSSG by reducing GSSG in a NADPH(H^+)-dependent reaction catalyzed by glutathione reductases (GRxs), that are present in cytosol and mitochondria (Flohe *et al.* 2011). Thus, as we will discuss below, NADPH(H^+) generated in the PPP is essential for glutathione regeneration, an essential system for neuronal survival (Herrero-Mendez *et al.* 2009).

2. GLUTAMATERGIC NEUROTRANSMISSION

2.1. GLUTAMATE

Glutamate is the major excitatory neurotransmitter in the mammalian brain and is implied in information processing and synaptic plasticity. Compared to other neurotransmitters, the levels of glutamate are extremely high in the mammalian central nervous system, approaching 5–10 mmol/kg (Butcher & Hamberger 1987); these levels are ~1000-fold higher than those of many other important neurotransmitters, such as dopamine, norepinephrine, and serotonin. Its concentration in the synaptic cleft in resting conditions remains low (~0.6 μM). However, during synaptic transmission glutamate is released from the presynaptic neuron in a short period of time (1-2 ms), reaching concentrations higher than 100 μM . These concentrations are restored back to normal levels by the high affinity glutamate transporters located in pre and post-synaptic neurons, as well as in the adjacent glial cells.

2.2. GLUTAMATE RECEPTORS

The excitatory effects of glutamate are exerted via the activation of three major types of ionotropic receptors (AMPA, KAINATE and NMDA) and several classes of metabotropic receptors linked to G-proteins (Dong *et al.* 2009).

2.2.1. METABOTROPIC GLUTAMATE RECEPTORS

Metabotropic glutamate receptors are G-protein-coupled receptors. They are classified into 8 subtypes (mGLU1 to mGLU8) that are divided into three groups based on their G-protein coupling, molecular structure, amino acid sequence homology and pharmacological profile.

Group-I includes mGlu1 and mGlu5; they are coupled to phospholipase C (Tanabe *et al.* 1992, Joly *et al.* 1995). Activation of these receptors generates inositol-1,4,5-trisphosphate (InsP3) and diacylglycerol (DAG); InsP3 releases Ca^{2+} from the endoplasmic reticulum and together with DAG activates protein kinase C (PKC) respectively. In general, mGlu1 and mGlu5 receptors increase neuronal excitability,

so they have been studied as targets to prevent glutamate-mediated neurodegeneration. (+)-2-Methyl-4-carboxyphenylglycine, a potent and selective antagonist of mGlu1, is neuroprotective in models of excitotoxic death (Bruno *et al.* 1999). 2-Methyl-6-(phenylethynyl)-pyridine (MPEP), an inhibitor of mGluR5 receptors, also prevents degeneration in the 1-methyl-4-phenyl-1,2,3,6-tetrahydropyridine (MPTP) mouse model of PD, as it prevents the function of these receptors in facilitating NMDA receptors activation (Hsieh *et al.* 2012).

Group-II and Group-III are preferentially localized in the preterminal region of axons; they are negatively coupled to adenylate cyclase. Group-II includes mGlu2 and mGlu3 (Emile *et al.* 1996); their activation attenuates glutamate release (Mateo & Porter 2007, Grueter & Winder 2005). Group III mGluRs (GluR4, GluR6, GluR7, GluR8) also function to restrain glutamate or GABA release from axon terminals, preventing over activation of postsynaptic NMDA receptors (Vera & Tapia 2012). Actually, endogenous glutamate activates these receptors and protects against excitotoxicity (Vera & Tapia 2012). Moreover, a specific agonist of mGLUR8 has been shown to reverse motor deficits in prolonged models of PD (Johnson *et al.* 2013).

2.2.2. IONOTROPIC GLUTAMATE RECEPTORS

Ionotropic receptors activated by glutamate are the *N*-methyl-*D*-aspartic acid (NMDA), α -amino-3-hydroxy-5-methylisoxazole-4-propionate (AMPA) and kainic acid (KA) receptors.

-AMPA and kainate receptors

AMPA receptors (AMPA receptors) and kainate receptors are tetrameric cationic channels permeable to Na^+ and Ca^{2+} . AMPARS are composed by GluA1-A4 subunits that mediate fast excitatory synaptic transmission in the mammalian central nervous system (Heine *et al.* 2008). Kainate receptors are composed by five different subunits GLUK1, GLUK2, GLUK5, GLUK6 and GLUK7, and they can be presynaptically placed, where they modulate glutamate release (Chittajallu *et al.* 1996) or postsynaptically, where they can mediate excitatory neurotransmission (Vignes & Collingridge 1997).

-NMDA receptors

NMDA receptors (NMDAR) are cationic channels permeable to Na^+ , K^+ , and Ca^{2+} that mediate many neuronal functions including plasticity, synapsis consolidation during neuronal differentiation, long term potentiation (LTP), regeneration and survival (McDonald & Johnston 1990, Castellano *et al.* 2001, Cheng & Ip 2003). NMDARs need two different agonists bound simultaneously to open the channel pore: glutamate and glycine (Paoletti & Neyton 2007). The NMDAR channel pore is blocked in a voltage dependent manner by Mg^{2+} .

NMDARs work as a heterotetramer that contains two NR1 subunits that are essential for the functionality of the receptor. They contain a glycine-binding site and two NR2 (NR2A-NR2D) subunits that contain the glutamate-binding site. The most widely expressed NMDARs contain the obligate subunit NR1 plus either NR2B or NR2A or a mixture of the two, but NR3 subunits can also substitute NR2 in the receptors, making Ca^{2+} permeability to decrease (Matsuda *et al.* 2003).

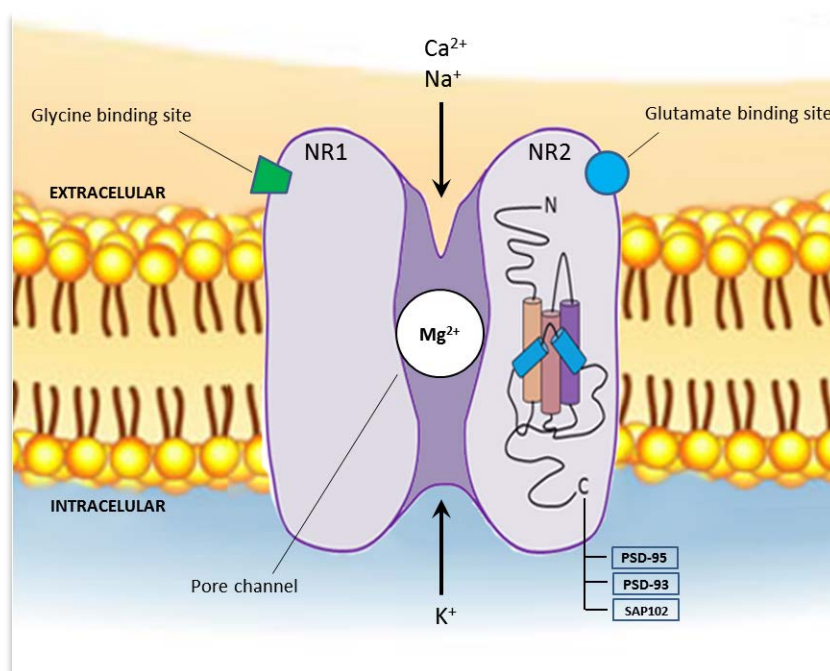


Figure 8. Schematic representation of NMDAR structure. NR1 and NR1 subunits are represented, as well as MAGUKs proteins to which NR2 subunit binds in its intracellular domain (PSD-95, SAP-102, PSD-93). NMDAR present a glycine binding site in its NR1 subunit and a glutamate binding site in NR2. The channel pore is blocked by Mg^{2+}

In synapses, NMDAR is bound to a multiproteic complex with the carboxyl end of NR1 and NR2 subunits (Collins *et al.* 2006). This complex facilitates localization of the receptor in specific areas, such as the postsynaptic density, where it allows the coupling with a wide variety of signal transduction cytosolic molecules (Waxman & Lynch 2005). Carboxyl end of NR2 binds MAGUKs proteins (membrane associated guanylate cyclases), such as PSD-95, SAP-102 and PSD-93. These proteins allow others to be located nearby the receptors in such a way that they can be more efficiently activated by Ca^{2+} , that is the case of nNOS (neuronal nitric oxide synthase) (Aarts *et al.* 2002).

There is a large body of evidence supporting the hypothesis that synaptic NMDARs activate neuroprotective and trophic pathways, whereas the extrasynaptic ones are responsible for excitotoxicity (Kaufman *et al.* 2012, Hardingham *et al.* 2002, Hardingham & Bading 2010, Puddifoot *et al.* 2012). Synaptic NMDAR activation induces CREB (cAMP response element binding protein) activity and BDNF (brain derived neurotrophic factor), triggering anti-apoptotic signals, while activating the extrasynaptic ones has the opposite effects (Hardingham *et al.* 2002). However, recent publications have questioned this statement by demonstrating that prolonged synaptic NMDAR activation triggers excitotoxic cell death (Wroge *et al.* 2012).

Regardless their location, there is much evidence of a differential function of NMDAR depending on their subunit composition, as they have different effects on cytosolic calcium accumulation, mitochondrial morphology and MAPK signaling, in which NR2B would preferentially trigger neuronal death signals (Choo *et al.* 2012, Paul & Connor 2010).

2.3. GLUTAMATE TRANSPORTERS

There is no evidence for extracellular metabolism of glutamate. This excitatory amino acid is cleared from the extracellular space by a family of Na^{+} -dependent 'high-affinity' transporters. Glutamate transporters are termed GLAST (EAAT1), GLT I (EAAT2), EAAC (EAAT3), EAAT4, and EAAT5 (Kanai & Hediger 1992, Pines *et al.* 1992). EAAC and EAAT5 are found exclusively in neurons, whereas GLAST and GLTI, the major contributors to glutamate uptake, are glia-specific

transporters, posing astrocytes responsible for a major part of glutamate uptake and metabolism in the brain (Rothstein *et al.* 1996).

2.4. GLUCOSE METABOLISM IN GLUTAMATERGIC NEUROTRANSMISSION

There is increasing evidence pointing out that glutamatergic stimulation has critical consequences on neuronal metabolism. As mentioned before, metabolic homeostasis is essential for the maintenance of neuronal redox status and survival. Thus, metabolic modifications may have great implications in the pathophysiology of neurodegenerative diseases, in which excitotoxic mechanisms have been described.

2.4.1. GLUTAMATERGIC NEUROTRANSMISSION STIMULATES LACTATE RELEASE BY ASTROCYTES

During glutamatergic neurotransmission, astrocytes remove excess glutamate from the synaptic cleft (Rothstein *et al.* 1996). Glutamate is taken up by astrocytes through glutamate transporters, which are Na⁺-dependent. The subsequent increase in intracellular Na⁺ activates the Na⁺/K⁺ ATPase activity, hence decreasing the ATP:ADP ratio, which promotes astrocytic glycolysis (Pellerin & Magistretti 1994). At the same time, glucose transport in astrocytes is enhanced by stimulating GLUT1 transporter in a Na⁺-Ca²⁺ dependent manner (Loaiza *et al.* 2003, Chuquet *et al.* 2010, Porrás *et al.* 2008). This up regulation of glycolysis is translated in an increase of lactate production by astrocytes and, according to the ANLSH, neurons would take it up and transform it into pyruvate for use as an energy source (Pellerin & Magistretti 1994).

2.4.2. GLUCOSE UPTAKE BY NEURONS DURING NMDAR ACTIVATION

How glucose uptake by neurons is affected by neurotransmission is yet a controversial issue. Real-time confocal microscopy studies tracing 6-[N-(7-nitrobenz-2-oxa-1,3-diazol-4-yl)amino]-6-deoxyglucose (6-NBDG), a non metabolizable glucose analog fluorescence probe, indicated that glutamate inhibits glucose transport in cultured hippocampal neurons (Porrás *et al.* 2004). In contrast, an increased glucose uptake has been observed by tracing 2-deoxy- [1-

^3H]glucose-6-phosphate accumulation in cerebellar neurons in culture subjected to NMDAR stimulation (Bak *et al.* 2009). These results have been reproduced in cortical neurons tracing 6-NBDG (Ferreira *et al.* 2011). Moreover, the increase in nitric oxide levels that occur after stimulation of NMDAR in primary cultured cortical and hippocampal neurons triggers an increase in GLUT3 surface expression that is accompanied by an increase in glucose uptake (Ferreira *et al.* 2011), confirming the importance of rapid GLUT3 externalization in energy metabolism and cytoprotection (Cidad *et al.* 2004). Although it is important to notice that all these studies are performed in neurons in culture, where the possible influence of astrocytes is neglected, there is *in vivo* evidence also supporting these findings. Thus, by rat whisker stimulation and imaging of 6-NBDG trafficking by two-photon microscopy, during activation of the somatosensory cortex there is an increase in glucose uptake both in neurons and astrocytes, although the increase observed in astrocytes is much higher (Chuquet *et al.* 2010). Accordingly, despite there is still some controversy, it seems clear that glutamatergic neurotransmission is accompanied by an increase in glucose uptake by both neurons and astrocytes; however, the metabolic fate of glucose in each cell type, which does not have to be necessarily identical remains unclear.

2.4.3. NMDAR STIMULATION ALTERS ENERGY METABOLISM IN NEURONS

Another question that still remains elusive is how neuronal metabolism is modified during neurotransmission and the preferential substrate used for meeting the ATP needs during this process. Two-photon fluorescence imaging of NADH(H^+) on hippocampal slides showed evidence of a two-phase metabolic response in which neurons exert an early increase in oxidative metabolism followed by activation of astrocytic glycolysis (Kasischke *et al.* 2004). Interestingly, it is known that extracellular lactate levels modulate astrocytic glycolysis (Sotelo-Hitschfeld *et al.* 2012), suggesting the existence of a negative feedback regulatory mechanism of glucose consumption by astrocytes that may be important for glucose redistribution to brain areas or cells where it is needed.

Tracing the fate of [1- ^{13}C] or [3- ^{13}C]glucose and lactate in astrocytic and neuronal cultures showed that, in resting conditions, neurons use lactate preferentially over glucose for oxidative metabolism, while astrocytes prefer glucose (Bouzier-Sore *et*

al. 2006, Bak *et al.* 2006). Interestingly, stimulation of NMDAR in glutamatergic neurons in primary culture increases glucose oxidative metabolism, as assessed by registering the fate of [1,2-¹³C]acetyl-CoA derived from either [U-¹³C]glucose or [U-¹³C] lactate, a measure of the TCA cycle activity (Bak *et al.* 2006, 2009). Furthermore, glucose resulted to be necessary for maintaining neurotransmitter homeostasis (Bak *et al.* 2006). This increase in glucose oxidative metabolism by the TCA in neurons was dependent on the increase in intracellular Ca²⁺ levels that takes place after NMDARs stimulation (Bak *et al.* 2009, 2012), but the molecular mechanisms underlying this process still remain elusive.

2.5. EXCITOTOXICITY

Excitotoxicity is a pathologic process that triggers cell death and occurs when NMDAR are over activated. It is related with the pathogenesis of many neurodegenerative diseases, like Huntington, AD, PD or Amyotrophic Lateral Sclerosis. The mechanisms downstream NMDAR over activation are multiple and complex and, despite they have been widely investigated, they are not yet fully understood.

2.5.1. EXCITOTOXICITY TRIGGERS Ca²⁺ OVERLOAD AND CALPAINS ACTIVATION

The Ca²⁺ overload that takes place after NMDARs stimulation plays a critical role in the excitotoxic process. Choi, by changing the extracellular ionic environment of cortical neurons in primary culture and exposing them to glutamate, described a Ca²⁺-dependent component in excitotoxicity, and concluded that at low glutamate exposures, Ca²⁺ plays a critical role in neuronal death (Choi 1987). He also suggested the influence of NMDAR over-activation in this process (Choi 1987).

Apart from the initial increase in cytosolic Ca²⁺ after NMDAR stimulation, there is a so called delayed calcium deregulation that persists after glutamate removal, which triggers other effects, such as activation of calpains, a family of Ca²⁺-dependent cysteine proteases (Brustovetsky *et al.* 2010). Calpains process the full-length isoform of tropomyosin-related kinase B (TrkB-FL), a receptor for neurotrophins like brain-derived neurotrophic factor (BDNF). This leads to the formation of a truncated protein that lacks the tyrosine-kinase domain (TrkB-T1) (Vidaurre *et al.*

2012). This TrkB-FL / TrkB-T1 imbalance is associated with a rat model of focal cerebral ischemia, which presents high TrkB-T1 levels and reduction of TrkB-FL upon NMDARs overstimulation (Vidaurre *et al.* 2012). Calpains also trigger the proteolytic cleavage of the Na⁺/Ca²⁺ exchanger (NCX), the major plasma membrane Ca²⁺ extruding system; this impairs calcium homeostasis and leads to neuronal death (Bano *et al.* 2005, Brustovetsky *et al.* 2010). This effect can be enhanced by a reversal of the NCX that takes place during stimulation of AMPAR and that leads to an increase in intracellular Ca²⁺ and activation of calpains (Araujo *et al.* 2007).

2.5.2. MITOCHONDRIAL DYSFUNCTION AND EXCITOTOXICITY

Mitochondria contribute to prevent excessive cytosolic Ca²⁺ levels by taking up cytosolic Ca²⁺ through uniporters located in their inner membrane (Gunter & Gunter 1994, White & Reynolds 1997, Gunter & Gunter 2001). However, during the excitotoxic process, the increase in Ca²⁺ cause mitochondrial overload and triggers an activation of the permeability transition pore (PTP), that leads to inner mitochondrial membrane depolarization and inhibition of ATP synthesis (Wang *et al.* 1994, Khodorov *et al.* 1996). Inhibition of the oxidative phosphorylation and loss of the mitochondrial membrane potential finally lead to increased ROS and cytochrome c release, playing a key role in glutamatergic excitotoxicity (Urushitani *et al.* 2001, Luetjens *et al.* 2000).

Excitotoxicity and oxidative stress also alter mitochondrial fission and fusion, leading to fragmented mitochondria, an effect that has been observed in many neurodegenerative diseases (Knott *et al.* 2008, Nguyen *et al.* 2011). Moreover, mutations in optic atrophy type 1 (OPA1), a dynamin-related GTPase that is essential for mitochondrial fusion, also trigger NMDAR upregulation, leading to the excitotoxic process (Nguyen *et al.* 2011).

2.5.3. OXIDATIVE AND NITROSATIVE STRESS

Oxidative and nitrosative stress takes place when ROS and NOS overload the antioxidant defenses of the cell. In excitotoxic processes, when increased mitochondrial Ca^{2+} uncouples the mitochondrial electron transport chain and collapses the mitochondrial membrane potential, free electrons are accumulated in the mitochondria, and can react with molecular oxygen, producing superoxide anion ($\text{O}_2^{\cdot-}$). Besides this, nNOS is localized close to NMDAR by an interaction with PSD95. Thus, nNOS is more easily activated by Ca^{2+} entry through NMDAR. Excessive production of nitric oxide ($\cdot\text{NO}$) when NMDAR are over-activated is toxic and can react with other ROS, such as $\text{O}_2^{\cdot-}$ to produce ONOO^- .

All these processes lead to oxidative stress that triggers oxidation of proteins (particularly aromatic or cysteine residues), nucleic acids and lipids (Poyton *et al.* , Temple *et al.* 2005), leading to protein malfunction. Mitochondria are the main source of ROS in the cell and thus are more sensitive to oxidative damage, such as oxidation of Fe-S clusters of proteins, including some respiratory chain complexes and aconitase, mitochondrial DNA mutations (Fukui & Moraes 2008, Hekimi *et al.* 2011) or lipid peroxidation. All these modifications and alterations can finally trigger a massive damage that activates macro-autophagy and cell death processes (Brand 2011). Specifically, peroxidation of cardiolipin, a mitochondria-specific phospholipid, leads to mitochondrial membrane permeabilization, release of pro-apoptotic factors, finally leading to cell death (Samhan-Arias *et al.* 2011).

2.5.4. EXCITOTOXIC ACTIVATION OF NMDAR TRIGGERS Cdh1 HYPERPHOSPHORILATION AND APC/C INACTIVATION

The anaphase-promoting complex/cyclosome (APC/C) is an E3 ubiquitin ligase that regulates cell cycle progression (Thornton & Toczyski 2006) by targeting cell cycle proteins for degradation by the proteasome. To be active, APC/C needs to be bound to the co-activator proteins, Cdc20 or Cdh1, which participate in substrate recognition (Visintin *et al.* 1997) by detecting degradation motifs in the target proteins, predominantly the destruction (D) box (RxxLxxxxN) and the KEN box (KENxxxN) (Barford 2011). During early mitosis APC/C is activated by Cdc20, whereas in late mitosis it binds Cdh1 and controls mitotic exit and G1 maintenance. Besides cell cycle progression regulation, it has been shown that glutamate over-

activation of NMDAR triggers Cdh1 phosphorylation leading to its inactivation, by Cdk5. Cdk5 is activated when it binds p25, the proteolytic product of p35 (Lee *et al.* 2000). Upon glutamate NMDAR stimulation, as we have mentioned before, there is a Ca^{2+} overload that leads to calpain activation (Brustovetsky *et al.* 2010). Calpains transform p35 in p25, thus activating Cdk5 (Lee *et al.* 2000). Cdk5 phosphorylates Cdh1 and sequesters it in the cytosol, thus inhibiting APC-Cdh1 activity leading to the accumulation of its substrates (Jaquenoud *et al.* 2002, Maestre *et al.* 2008)

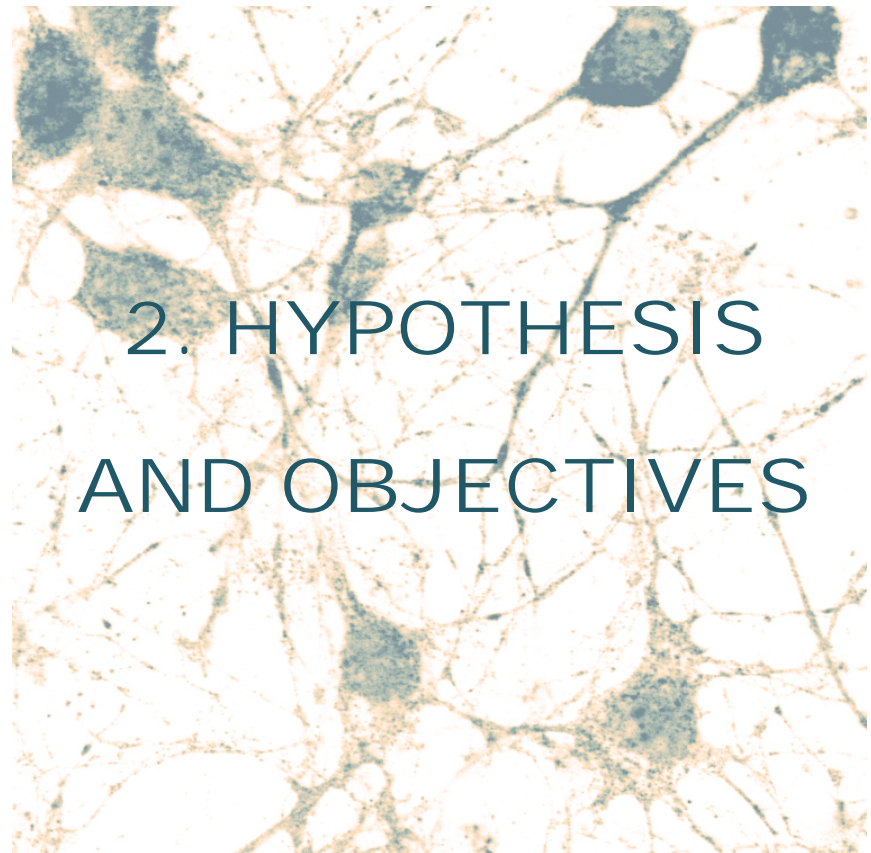
Inactivation of the APC/C-Cdh1 complex leads to cyclin B1, a well-known substrate of this complex, accumulation, which triggers neuronal apoptotic death (Maestre *et al.* 2008). Interestingly, cyclin B1 accumulates in degenerating brain areas in AD disease and stroke, that are pathologic conditions that have been widely associated with an excitotoxic neuronal death (Vincent *et al.* 1997, Wen *et al.* 2004)

2.5.5. OVERVIEW ON THE RELATIONSHIP BETWEEN EXCITOTOXICITY AND NEURODEGENERATIVE DISEASES

Many evidences in animal models and humans suggest the implication of excitotoxicity in the development of neurodegenerative diseases. Early alterations in the glutamatergic system have been described in Huntington's disease, including decreased glutamate uptake by astrocytes due to decreased levels of GLAST and GLT-1 glutamate transporters (Lievens *et al.* 2001, Estrada-Sanchez *et al.* 2009), increased responses to NMDA and decreased Mg^{2+} sensitivity (Starling *et al.* 2005), as well as changes in NMDAR subunits composition. The dopaminergic neurons that degenerate in PD are also vulnerable to excitotoxicity, and group III metabotropic glutamate receptors agonists have been proved to improve akinesia in mice models of the disease (Broadstock *et al.* 2012). Amyotrophic lateral sclerosis (ALS) is characterized by the degeneration of motor neurons; several data from ALS patients and Cu/Zn-SOD mutant mice, that are a well-known animal model of the disease, have associated the development of this disease with impaired Ca^{2+} homeostasis, oxidative stress and mitochondrial dysfunction (Kruman *et al.* 1999) as well as defects in glutamate transport due to loss in glutamate transporter GLT-1 (Rothstein *et al.* 1995, Howland *et al.* 2002). AD is characterized by the presence of amyloid β deposits that can enhance

INTRODUCTION

NMDA excitotoxicity by impairing glutamate transporters and calcium regulation (Mattson *et al.* 1992). There are several reports indicating that targets against different aspects related to the excitotoxic process could be effective in AD treatment, like Ca^{2+} blocking agents (Weiss *et al.* 1994, Le *et al.* 1995) and glutamate receptors antagonist. Actually, memantine is the only drug proved to be effective for clinical treatment of AD so far. It blocks opened channels associated with ionotropic glutamate receptors and its off-rate is fast so it does not accumulate and interfere with normal glutamatergic transmission (Lipton 2004, Glodzik *et al.* 2008).



2. HYPOTHESIS AND OBJECTIVES

HYPOTHESIS AND OBJECTIVES

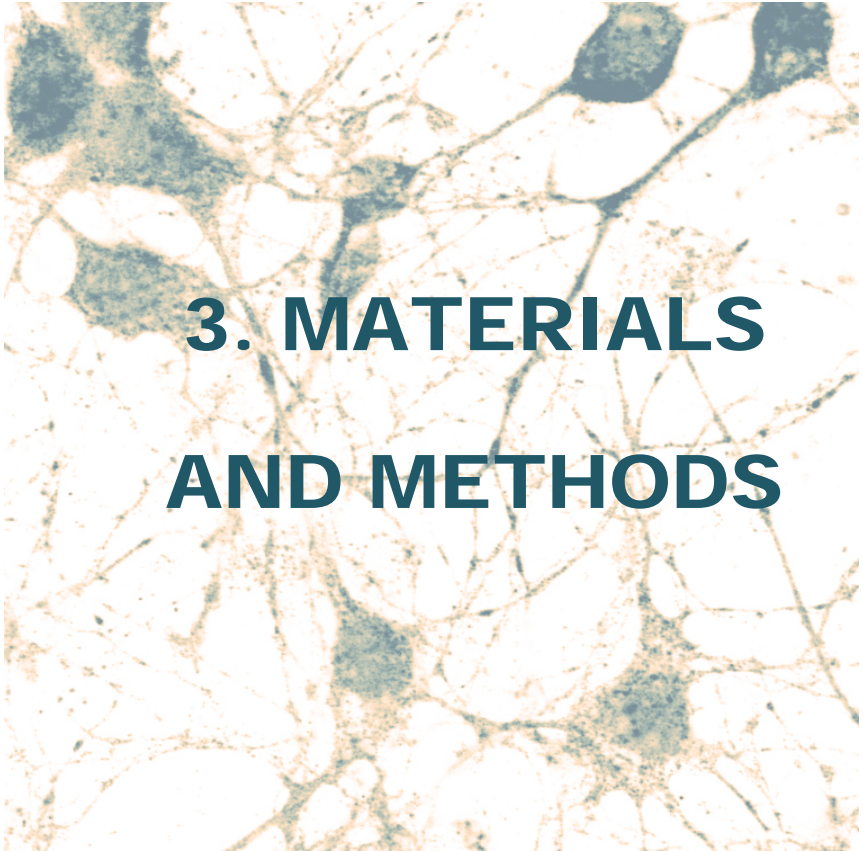
1. Hypothesis

In view of the previously described premises, we hypothesize that glucose should be preferentially metabolized through the PPP in neurons in order to generate NADPH(H⁺) for regenerating glutathione. However, to date no unambiguous method to address this issue is available. Moreover, NMDAR activation leads to APC/C-Cdh1 complex inactivation, and we believe that this should trigger stabilization of PFKFB3. Under these circumstances, there would be a metabolic change leading to decreased glucose oxidation through the PPP thus contributing to the oxidative stress and neuronal death observed in excitotoxicity. Finally, the fructose-2,6-bisphosphatase novel protein TIGAR occurrence in neurons –and possible function therein– is unknown, but it might play key role(s) in neuronal metabolism and/or survival yet to be characterized.

2. Objectives

With the aim to address the above-mentioned hypotheses, we planned to elucidate the following objectives:

- 1- To design and establish a suitable method to accurately determine the glycolytic and PPP fluxes in attached intact neurons in primary culture.
- 2- To attempt to quantify the relative contributions of glycolysis and PPP to the overall glucose metabolism of neurons.
- 3- To ascertain whether excess neurotransmission, as induced by over-activation of glutamate receptors, triggers PFKFB3 stabilization and changes in glucose metabolism, redox status or survival in neurons.
- 4- To investigate whether TIGAR is expressed in brain cells and, and in such a case, whether it plays any role in the regulation of neuronal glucose metabolism and/or survival.

A microscopic image of plant tissue, likely a cross-section of a stem or root, showing a network of cells and vascular bundles. The cells are stained, with some appearing dark green and others lighter. The text "3. MATERIALS AND METHODS" is overlaid in the center of the image.

3. MATERIALS AND METHODS

1. PLASMID CONSTRUCTIONS, AMPLIFICATION AND PURIFICATION

1.1. pEGFP-C1-TIGAR PLASMID CONSTRUCTION

Human TIGAR full length cDNA (812 bp, NM_020375) was obtained by PCR using, as template, a pcDNA 3.1+ plasmid where it was initially cloned (generous gift from Prof. R. Bartrons, University of Barcelona) using the oligonucleotides detailed in table 1; these were designed targeting the 5' and 3' extremes of TIGAR cDNA flanked by the restriction sequences of HindIII in 5'-end and of EcoRI in 3'-end.

OLIGONUCLEOTIDE	SEQUENCE 5' → 3'	Tm
Forward + HindIII restriction site	5'-CCCAAGTTGGGCGCTCGCTTCGCTCTGACTGTTGTC-3'	81.9°C
Reverse + EcoRI restriction site	5'-GGAATTCCTTAGCGAGTTTCAGTCAGTCCATT-3'	67.2°C

Table 1: Oligonucleotides employed in the PCR to obtain TIGAR cDNA. An additional sequence for HindIII and EcoRI was added in 5' and 3' oligonucleotides respectively (blue).

PCR conditions were 10 min at 95 °C, 35 cycles of 30 seconds at 95 °C, 30 seconds at 60 °C and 1.5 minutes at 72 °C. Final extension was carried out for 10 min at 72 °C.

The PCR product and the pEGFP-C1 plasmid (4.7 kb, Clontech) were then digested for 1 hour with *EcoRI* and *HindIII* enzymes in order to generate cohesive extremes that would further facilitate ligation and insertion. Digestion products were finally incubated with T4 ligase for 30-45 minutes at room temperature, obtaining the vector named pEGFP C1-TIGAR shown in figure 1. The success of the ligation was checked by restriction analysis and western blot (obtaining a band at 57 KDa, corresponding to GFP (25 KDa) plus TIGAR (32 KDa) molecular weights).

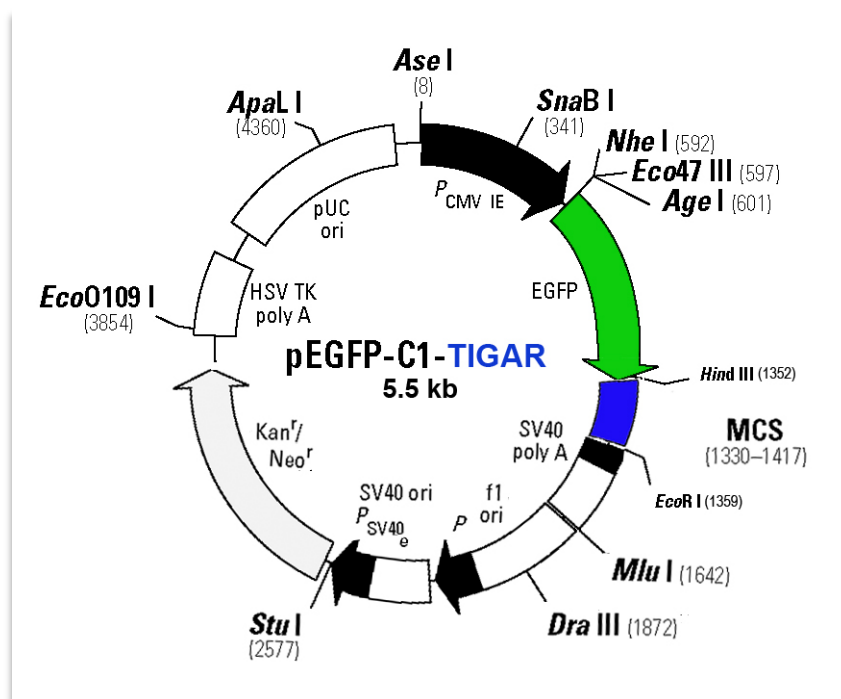


Figure 1: pEGFP-C1 vector with human TIGAR cDNA (blue) inserted between HindIII and EcoRI restriction sites in the MCS.

pEGFPC1-TIGAR vector expresses green fluorescent protein (GFP) fused at TIGAR C-terminus. This allows the identification of transfected cells and subcellular localization by fluorescence microscopy and flow cytometry.

1.2. G6PD, PFKFB3 and mutPFKFB3 PLASMID CONSTRUCTIONS

The complete cDNA that codifies for rat G6PD was inserted in the *EcoRI* site of the expression vector pEGFP (Clontech) and sequenced (Sequencing service, University of Salamanca) to confirm the correct insertion in reading phase with GFP (Garcia-Nogales *et al.* 2003).

Rat PFKFB3 full-length cDNA (splice variant K6; 1563 bp; accession number BAA21754) was obtained, by reverse-transcriptase polymerase chain reaction (RT-PCR), previously at our laboratory. PFKFB3 cDNA was fused, at its 5'-terminus, with the full-length cDNA encoding GFP in the pEGFPC1 vector. In order to obtain the mutPFKFB3 construction, GFP-PFKFB3 cDNA fusion construct was subjected to site-directed mutagenesis of its

KEN-box to AAA using the QuikChange XL site-directed mutagenesis kit (Stratagene, La Jolla, CA, USA) (Herrero-Mendez *et al.* 2009).

1.3. BACTERIAL TRANSFORMATION AND PLASMIDS PURIFICATION

E. coli competent cells, strain DH-5 α , were used for all bacterial transformations. Bacteria culture mediums (LB, LB-agar and 2 x YT) were prepared with bactotripton, yeast extract and agar from DIFCO Laboratories (Detroit, Michigan, USA).

Extraction and purification of the plasmids after the amplification in bacteria was performed using the Wizard plus Midipreps system (Promega, Madison, Wisconsin, USA). To isolate and purify the cDNA from agarose gels, a commercial kit from Gibco BRL (Life Technologies Inc., Barcelona, Spain) was used. UV light is mutagenic, thus, to avoid UV light exposure of the gel bands, each sample was loaded in duplicate. Only one of the bands was exposed to UV in order to detect it and cDNA was purified from the other band.

2. “SMALL INTERFERING RNA” (SIRNA) DESIGN

siRNA against PGI was obtained from Dharmacon Research Inc. (Lafayette, Colorado, USA). The oligonucleotides employed were designed according to the rational design criteria of Reynolds (2004) and Ui-Tei (2004), with the software available at Dharmacon's webpage.

Specificity of these sequences was confirmed by BLAST against the complete genome of *Rattus norvegicus*, *Mus musculus* and *Homo sapiens*. siRNA sequences used for knockdown experiments are detailed in table 2 (only forward oligonucleotides are shown).

PROTEIN	ACCESSION NUMBER	SEQUENCE	POSITION
PFKFB3	NM_057135	5'-AAAGCCTCGCATCAACAGC-3'	1908-1926
TIGAR	NM_177003	5'-GCGCGGAAAGGATTTCTTT-3'	475-493
PGI	NM_207192	5'-CCTTACCAGACGTAGTGTT-3'	1248-1266
Luciferase		5'- CTGACGCGGAATACTTCGA-3'	

Table 2. Sequences used for the siRNA knockdown experiments.

Cells were transfected at 3 days in culture and all siRNA were used at 100 nM, with the exception of TIGAR siRNA that resulted to be effective at 20 nM. Experiments were performed at day 6, i.e. 72 hours post transfection, as this is was the incubation period at which the highest knock down efficiency was obtained.

3. ANIMALS.

Albine Wistar rats and C57BL/6J mice were bred and provided by the Animal Experimentation Service of the University of Salamanca. We also performed primary cultures from TIGAR KO mice (Cheung *et al.* 2013) from the animal facility of “The Beatson Institute for Cancer Research” (Glasgow, UK). The animals were bred in cages and a light-dark cycle was maintained for 12 hours. Humidity was between 45% and 65% and temperature between 20°C and 25°C. Animals were fed *ad libitum* with a standard solid diet (17 % proteins, 3 % lipids, 58.7 % glucidic component, 4.3 % cellulose, 5 % minerals and 12 % humidity) and they had free access to the water all the time.

Gestational stage was controlled by limiting the cohabitation of virgin rats with males to one night. At 9:00 hours of the following day, rats that had the presence of spermatozoids in the vaginal smear accompanied by epithelial cells from the vagina (that are characteristic of a fertile day of the estrus) were isolated. Under these conditions, gestational period of the rat is assumed to be 21.7 days.

All animal handlings and procedures are in agreement with the current regulation from the European commission 18.06.2007 (2007/526/CE) and Spanish legislation (RD 1201/2005) related to accommodation and experimental animals care. All the protocols performed in this Thesis were approved by Bioethics Committee of the University of Salamanca.

4. CELL CULTURE

4.1. CORTICAL NEURONS IN PRIMARY CULTURE

Cortical neurons in primary culture were prepared from fetal embryos of 16 days (E16) rats or mice according to standard procedure (Almeida *et al.* 1998). In brief, pregnant rats or mice were sacrificed in a CO₂ atmosphere and the embryos were removed by hysterectomy. Embryos were transferred to a laminar flux cabin (TC48, Gelaire Flow Laboratories, McLean, Virginia, USA) in order to maintain the sterile conditions of the culture. Cranium and cerebral hemispheres were removed using scissors, forceps and 70% ethanol-impregnated handkerchiefs. The brain tissue was then placed in a polystyrene Petri plate containing the disintegration solution (116 mM NaCl, 5.4 mM KCl, 1.01 mM NaH₂PO₄, 1.5 mM MgSO₄, 26 mM NaHCO₃, 4 mM glucose, 10 mg/ml phenol red, 0.3 % w/v albumin and 20 µg/ml DNase type I pH 7.2) and very smoothly chopped with a scalpel. After this, it was placed in a 50 ml tube (BD, Falcon, Bedford, Massachusetts, USA) and left for 4 minutes for decantation. The pellet was re-suspended in trypsinization solution (disintegration solution supplemented with 0.025 % w/v, trypsin) and incubated at 37 °C for 15 minutes in a thermostatic bath. Trypsinization was stopped by adding fetal calf serum (FCS; Roche Diagnostics, Heidelberg, Germany) at a final concentration of 10 %, v/v, and the tissue was centrifuged at 500 x g during 5 minutes (Beckman Instruments, Palo Alto, California, USA).

The pellet was re-suspended in 12 ml of disintegration solution and triturated with a silicon-coated Pasteur pipette for 9 strokes. After letting the cellular solution stand for 4 minutes, the supernatant containing the dissociated cells was carefully removed and placed in a fresh 50 ml tube. This process was repeated once more in order to increase yield. The supernatants were then centrifuged at 500 x g for 5 minutes. The cellular sediment was re-suspended, first, in 1ml DMEM (Dulbecco's Modified Eagle Medium; Sigma-Aldrich Chemical Co., Barcelona, Spain), followed by another 19 ml DMEM. 10 µl of the cellular suspension was diluted four times and mixed with an equal volume of trypan blue 0.4 % (Sigma-Aldrich) for alive cellular counting using a Neubauer chamber (Zeiss, Oberkochen, Germany) and a phase contrast microscope (CK30 model, Olympus, Japan).

The cell suspension was diluted in culture medium (DMEM supplemented with 10% v/v FCS plus penicillin (100 U/ml), streptomycin (100 µg/ml) and amphotericin B (0.25 µg/ml,

from Sigma- Aldrich) at a final density of 10^6 cells/ml and seeded at 250.000 cells/cm² in plastic culture plates (Nunc; Roskilde, Denmark), previously coated with poly-D-lysine (10 µg/ml; Sigma-Aldrich). Plates were placed in a thermostated cell-culture incubator at 37°C (Thermo Forma 310, Thermo-Fisher Scientific, Ohio, USA) and 5% CO₂ atmosphere.

After 2 days in culture, medium was removed and replaced by DMEM supplemented with 5% v/v horse serum (Sigma-Aldrich) and 20 mM glucose (Sigma-Aldrich). At 4 days in culture 10 µM cytosine arabinoside (Sigma-Aldrich) was added to prevent non neuronal cells proliferation. Cells were used for the experiments at 6-7 days in culture. Under these conditions, neuronal cultures showed 97-99 % purity as assessed by immunoreaction with the neuronal marker Map-2 (Almeida *et al.* 2005).

4.2. ASTROCYTES IN PRIMARY CULTURE

Astrocytes in primary culture were obtained from rat pups from 0 to 24 hours of age (Almeida *et al.* 1998). Animals were cleaned with 70% ethanol, decapitated and the whole brain was removed under a laminar flux cabin. Cerebellum and olfactory bulb were removed using forceps and cerebral hemispheres were cleaned from meninges and blood vessels. The tissue was then placed in a Petri dish with the disintegration solution. Cellular suspension was obtained as previously described for neurons.

Cellular suspension was seeded at 250,000 cells/cm² in DMEM supplemented with 10%, v/v, FCS in 175 cm² culture flasks (BD, Falcon). Cells were incubated in a thermostatic cell-culture incubator at 37 °C and 5% CO₂ atmosphere. Culture medium was renewed twice per week. After 2 weeks, the culture had an approximate purity of 90-95%, as assessed by immunoreaction with the antibody against GFAP (Glial Fibrillary Acidic Protein; Sigma-Aldrich).

4.3. HEK-293T

The cell line obtained from human embryo kidney 293T (HEK293T) was maintained in DMEM supplemented with 10% v/v FCS. 24 hours before the experiment cells were seeded, at 100,000 cells/cm², in plates previously coated with 10 µg/ml of Poly-D-Lysine (Sigma-Aldrich).

5. CELL TREATMENTS

5.1 CELL TRANSFECTIONS

Cell transfections were performed at day 3 in culture with the cationic reagent Lipofectamine 2000™ or Lipofectamine LTX with Plus Reagent™ (Invitrogen, Madrid), following manufacturer's instructions. The conditions for transfection optimal efficiency were assessed by quantifying the number of GFP⁺ cells by fluorescence microscopy. Lipofectamine LTX with Plus Reagent™ resulted to be more effective than Lipofectamine 2000; thus, we decided to use the former for transfections.

Transfection of cells with plasmid vectors was carried out using a final concentration of 1.6 µg/ml of DNA. In some experiments, we used 0.16 µg/ml of DNA to reduce the amount of protein synthesized (Almeida *et al.* 2010). In these cases, the final DNA concentration was also 1.6 µg/ml, which was achieved with the empty DNA vector. The correct translation of the DNA plasmids was assessed by western blot, 24 hours after transfection.

5.2 NMDA RECEPTORS STIMULATION

Neurons at 6 days *in vitro* were incubated with 100 µM glutamate (plus 10 µM glycine) or 100 µM NMDA (plus 10 µM glycine) in buffered Hanks' solution (134.2 mM NaCl, 5.26 mM KCl, 0.43 mM KH₂PO₄, 4 mM NaHCO₃, 0.33 mM Na₂HPO₄ 2H₂O, 20 mM HEPES, 4 mM CaCl₂ 2H₂O, 5.5 mM glucose, pH 7.4), for 15 min. Where indicated, incubations were performed in the presence of 10 µM MK-801 (Sigma), a highly selective non-competitive NMDA receptor antagonist, which was added 5 minutes before incubation with glutamate or NMDA. After 15 minutes, Hank's media was removed and replaced by culture medium (DMEM; 5% v/v HS, 20 mM glucose), and neurons were further incubated for the indicated time periods.

5.3 INHIBITION OF PPP ACTIVITY AND MITOCHONDRIAL PYRUVATE UPTAKE.

To inhibit PPP activity, we used dehydroepiandrosterone (DHEA), a potent noncompetitive inhibitor of glucose-6-phosphate dehydrogenase (G6PD), the rate limiting enzyme of the PPP. DHEA (Sigma D-5297) was dissolved in ethanol at 1 mM and used at a final concentration of 1 μ M (Filomeni *et al.* 2011, Frolova *et al.* 2011). Controls received the same volume of the vehicle.

To inhibit mitochondrial pyruvate uptake, we used α -ciano-3-hydroxycinnamate (HCN) (Sigma C-2020), which was dissolved in H₂O at 50 mM and used at a final concentration of 0.1 mM, a concentration that specifically inhibits mitochondrial -not plasma membrane- pyruvate transport (Alvarez *et al.* 2003).

6. DETERMINATION OF Ca²⁺ UPTAKE

To estimate the intracellular Ca²⁺ dependent changes by NMDAR stimulation in cortical neurons in primary culture, we used the fluorescent probe Fura-2 (acetoxymethyl-derivative; Life Technologies, Eugene, OR, USA). Fura-2 is a UV-excitable fluorescent calcium indicator. Upon calcium binding with Fura-2, the maximum fluorescence excitation shifts from 363 nm (Ca²⁺-free) to 335 nm (Ca²⁺-saturated), while the maximum fluorescence emission remains unchanged at ~510 nm.

Neurons seeded in 96-well plates (Nunc) were, at 6 days, incubated with Fura-2 (2 mM; dissolved in dimethyl sulphoxide (DMSO)) for 40 min in DMEM at 37 °C. Cells were then washed and further incubated with standard buffer (140 mM NaCl, 2.5 mM KCl, 15 mM Tris-HCl, 5 mM D-glucose, 1.2 mM Na₂HPO₄, 1 mM MgSO₄ and 1 mM CaCl₂, pH 7.4) for 30 min at 37 °C. Finally, the standard buffer was removed and experimental buffer (140 mM NaCl, 2.5 mM KCl, 15 mM Tris-HCl, 5 mM D-glucose, 1.2 mM Na₂HPO₄ and 2 mM CaCl₂, pH 7.4), either in the absence or in the presence of MK801 (10 μ M), was added.

Fluorescence emissions at 510 nm, after excitations at 335 and 363 nm, respectively, were recorded at 1 second intervals in a Varioskan Flash (Thermo Fischer, Vantaa, Finland) spectrofluorometer at 32 °C. After approximately 10 seconds, glutamate (100 μ M) or NMDA (100 μ M) (plus 10 μ M glycine) was injected, and emissions were further recorded for 50 more seconds. Ca²⁺-dependent fluorescence changes were estimated by

representing the ratio of fluorescence emitted at 510 nm obtained after excitation at 335 nm divided by that at 363 nm (F335/F363). Background subtraction was accomplished from emission values obtained in Fura-2-lacking (DMSO-containing) neurons. In preliminary experiments, the Ca²⁺ specificity of the measurements was tested in Ca²⁺-free experimental buffer containing 1 mM ethylene glycol tetraacetic acid (EGTA), which fully prevented the changes in 510 nm emissions.

7. ELECTROPHORESIS AND PROTEIN IMMUNODETECTION (WESTERN BLOT)

To obtain total cell protein extracts, cells were washed with PBS and lysed in RIPA buffer (1% sodium dodecylsulphate, 10 mM ethylene diamine tetraacetic acid (EDTA), 1 % v/v Triton Tx-100, 150 mM NaCl, 10 mM Na₂HPO₄, pH 7.0), supplemented with phosphatase (1 mM Na₃VO₄, 50 mM NaF) and protease (100 µM phenylmethylsulfonyl fluoride (PMSF), 50 µg/ml aprotinin, 50 µg/ml leupeptin, 50 µg/ml pepstatin, 50 µg/ml anti-papain, 50 µg/ml amastatin, 50 µg/ml bestatin and 50 µg/ml soybean trypsin inhibitor) cocktail inhibitors, and boiled for 5 min. Extracts were then centrifuged at 13,000 x g for 10 minutes and the supernatant transferred to a new tube. Protein concentration was determined using the commercially available BCA protein assay kit (Pierce, Rockwell, Illinois, USA).

Aliquots of the cell extracts and a molecular weight marker (PageRuler™ Plus Prestained Protein Ladder, Thermo Scientific) were loaded in a sodium dodecyl sulfate (SDS) polyacrylamide gel (acrylamide/bisacrylamide 29/1; BioRad Laboratories S.A., Alcobendas, Madrid) and subjected to vertical electrophoresis (MiniProtean, Bio-Rad, Hercules, CA, USA). Proteins were transferred to nitrocellulose membranes (Hybond®, Amersham Biosciences), blocked with 5% w/v low-fat milk in TTBS (20 mM Tris, 500 mM NaCl and 0,1 % v/v Tween 20, pH 7.5) for 1 hour at room temperature, and incubated with the desired primary antibody (see table 3) over night at 4 °C. GAPDH was used as loading control.

The following day, membranes were washed 3 times with TTBS and incubated with the secondary antibody, conjugated with the horseradish peroxidase (HRP), in 2% w/v bovine serum albumin (BSA) in TTBS for 1 hour at room temperature.

Signal was detected with the enhanced chemiluminescence kit (Pierce, Thermo Scientific, Waltham, MA, USA) by exposing membranes on a Kodak XAR-5 film (Sigma-Aldrich). For quantification, auto radiographies were scanned and the bands were analyzed using image treatment software (NIH Image, Wayne Rasband, National Institutes of Health, Bethesda, Maryland, USA). Values were expressed as the target protein/ GAPDH band intensities ratio.

PROTEIN	PRIMARY ANTIBODY	DILUTION	SECONDARY ANTIBODY	DILUTION
PFKFB3	Novus Biologicals (H00005209-M08)	1/1000	Mouse Anti-IgG Bio-Rad	1/10000
TIGAR	Lifespan Biosciences (LB-B462)	1/1000	Rabbit Anti-IgG Bio-Rad	1/10000
PGI	PGI Santa Cruz Biotechnology (sc-30392)	1/500	Goat Anti- IgG Santa Cruz Biotechnology	1/10000
GAPDH	Life technologies (Cat# 4300)	1/40000	Mouse Anti-IgG Bio-Rad	1/10000
G6PD	Sigma (A9521)	1/500	Rabbit Anti-IgG Bio-Rad	1/10000
GFP	Abcam (ab290)	1/2000	Rabbit Anti-IgG Bio-Rad	1/10000
Cdh1	Dr. J. Gannon	1/20	Mouse Anti-IgG Bio-Rad	1/10000
Phosphoserine	Invitrogen (61-8100)	1/500	Rabbit Anti-IgG Bio-Rad	1/10000

Table 3. Antibodies used for western blot immunodetection.

8. PROTEIN IMMUNOPRECIPITATION.

To obtain total cell protein extracts, cells were washed with PBS and lysed in RIPA buffer (1% sodium dodecylsulphate, 10 mM ethylene diamine tetraacetic acid (EDTA), 1 % v/v Triton Tx-100, 150 mM NaCl, 10 mM Na₂HPO₄, pH 7.0), supplemented with phosphatase

(1 mM Na₃VO₄, 50 mM NaF) and protease (100 µM phenylmethylsulfonyl fluoride (PMSF), 50 µg/ml aprotinine, 50 µg/ml leupeptine, 50 µg/ml pepstatin, 50 µg/ml anti-papain, 50 µg/ml amastatin, 50 µg/ml bestatin and 50 µg/ml soybean trypsin inhibitor) cocktail inhibitors, and boiled for 5 min. Extracts were then centrifuged at 13,000 x g for 10 minutes and the supernatant transferred to a new tube. Protein concentration was determined using the commercially available BCA protein assay kit (Pierce, Rockwell, Illinois, USA).

50 µg of proteins were diluted in a final volume of 200 µl RIPA and incubated with anti-Cdh1 antibody at 1/10 dilution over night at 4 °C. The following day, 15 µl of sepharose A (0.12 g/ml; GE Healthcare) were added to each sample, and incubated for 1 hour at 4 °C. The samples were then centrifuged (1 min, 4000 rpm) and washed 3 times with RIPA. Pellet was re-suspended in loading buffer and subjected to the same protocol as a normal western blot.

9. REVERSE TRANSCRIPTION-PCR (RT-PCR).

Total RNA was purified from neurons using a commercially available kit (Sigma, Saint Louis, MO, USA). PFKFB3 mRNA expression was analyzed in a 4.5% agarose (Nusieve) gel electrophoresis after RT-PCR using the oligonucleotides detailed in table 4.

OLIGONUCLEOTIDE	SEQUENCE 5' → 3'	Tm
PFKFB3 forward	5'-CCAGCCTCTTGACCCTGATAAATG-3'	57.8°C
PFKFB3 reverse	5'-TCCACACGCGGAGGTCCTTCAGAT-3'	64.6°C
GAPDH forward	5'-CTGGCGTCTTCACCACCAT-3'	53.0°C
GAPDH reverse	5'-AGGGGCCATCCACAGTCTT-3'	53.1°C

Table 4. Oligonucleotides employed in PFKFB3 RT-PCR.

Reverse transcription was performed at 48 °C for 50 min, and PCR conditions were 10 min at 95 °C, 35 cycles of 1 min at 95 °C, 1 min at 58 °C and 30 s at 68 °C. Final extension was carried out for 10 min at 72 °C. In no case was a band detected by PCR without reverse transcriptase.

10. FLOW CYTOMETRIC ANALYSIS OF APOPTOTIC CELL DEATH

Allophycocyanin (APC Ex/Em 650/660 nm) conjugated annexin-V and 7-aminoactinomycin D (7-AAD) (Becton Dickinson Biosciences, San Jose, CA, USA) were used to quantitatively determine the percentage of apoptotic neurons by flow cytometry. In apoptotic cells, the membrane phospholipid phosphatidylserine (PS) is translocated from the inner to the outer leaflet of the plasma membrane. Annexin V is a protein that has a high affinity for PS and binds cells with exposed PS. 7-AAD is a nucleic acid dye that is used as an indicator of necrotic cells.

After transfection, cells were carefully detached from the plate with EDTA tetrasodium 1 mM and incubated with annexin V- APC and 7-AAD in binding buffer (0.1 M Hepes, 1.4 M NaCl, 25 mM CaCl₂) following the manufacturer's instructions. After 15 minutes of incubation, GFP, annexin V-APC and 7-AAD signals were detected in channels FL1, FL4 and FL3 respectively in a FACScalibur (BD, Biosciences) flux cytometer and analyzed using CellQuest™ PRO and Paint-A-Gate™ PRO (BD Biosciences) software. Only annexin V-APC-stained cells that were 7-AAD-negative were considered apoptotic.

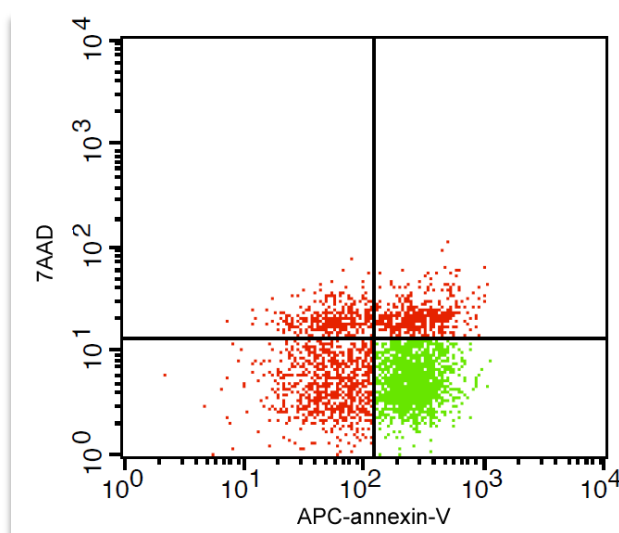


Figure 2: Total cell population stained with 7AAD and APC-annexin acquired in the cytometer. Only annexin V-APC-stained cells that were 7-AAD-negative were considered apoptotic (green).

11. DETECTION OF REACTIVE OXYGEN SPECIES (ROS)

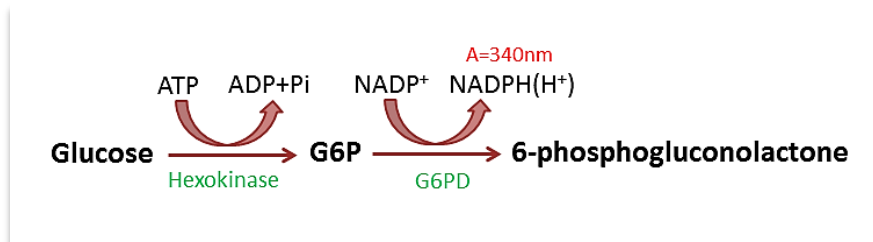
ROS detection was performed using MitoSox-RedTM (Invitrogen), a fluorogenic marker that selectively binds superoxide anion in live cells mitochondria, exhibiting red fluorescence when oxidized.

Neurons were incubated with 2 μM MitoSox-RedTM in DMEM for 30 min, washed with PBS and carefully detached from the plate with 1 mM EDTA tetrasodium. MitoSox-RedTM fluorescence was then assessed by flow cytometry in a FACScalibur flux cytometer and analyzed using CellQuestTM PRO and Paint-A-GateTM PRO (BD Biosciences) software.

12. DETERMINATION OF METABOLITES

12.1. D-GLUCOSE

D-Glucose in the buffer used for PPP and glycolytic flux determination was measured spectrophotometrically reading the increase in NADPH(H⁺) absorbance at 340 nm produced in two consecutive reactions, catalyzed by hexokinase and glucose-6-phosphate dehydrogenase (G6PD) (Roche diagnostics Corporation, Mannheim, Germany) after 10 minutes incubation (Bergmeyer *et al.* 1974).



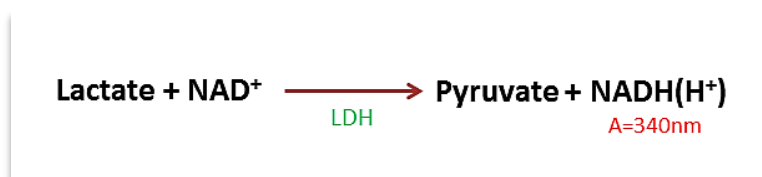
Reaction buffer was: 2 U/ml Hexokinase, 1 U/ml G6PD, 0.38 mM ATP, 0.38 mM NADP⁺, 3.8 mM MgCl₂ and 38.5 mM Tris-HCl pH 8

12.2. L-LACTATE

L-Lactate was measured spectrophotometrically according to the method of Gutmann and Wahlefeld (1974). The increase in the absorbance of NADH(H⁺) produced in the reaction catalyzed by lactate dehydrogenase (LDH, Roche) was measured in a Varioskan Flash (Thermo Fischer, Vantaa, Finland) spectrofluorometer at 340 nm after 1 hour incubation.

To assess extracellular lactate concentration, an aliquot of the cell culture or experimental buffer was obtained after 1.5 h of incubation with the cells. To assess intracellular lactate concentration, neurons were lysed in 0.6 M NaOH and the resulting extract de-proteinized with the same volume of 1% w/v ZnSO₄.

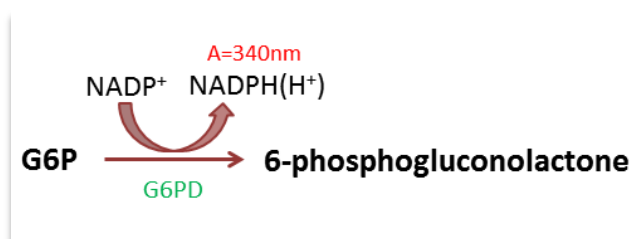
The reaction buffer was 250 mM glycine, 500 mM hydrazine, 1 mM EDTA, 1 mM NAD⁺, 22.5 U/ml LDH (pH 9.5).



12.3. GLUCOSE-6-PHOSPHATE (G6P)

G6P was measured spectrophotometrically by determining the increase in NADPH(H⁺) absorbance at 340 nm produced in the reaction catalyzed by G6PD. Neurons were lysed in 0.6 M NaOH and the resulting extract de-proteinized with the same volume of 1% w/v ZnSO₄.

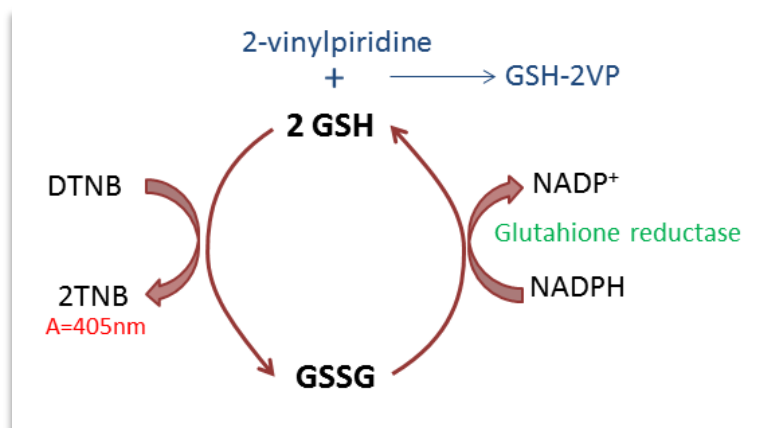
The reaction buffer consisted of 0.2 M triethanolamine, 5 mM MgCl₂, 0.2 mM NADP⁺, 0.17 U/ml G6PD, pH 7.6.



12.4. GLUTATHIONE

The method is based on GSH oxidation at the expense of DTNB (5,5'-ditio-bis-acid 2-nitrobenzoic) (Sigma-Aldrich), that is reduced to TNB ($\lambda_{\max}= 405 \text{ nm}$). The just-formed GSSG is then re-generated to GSH at the expenses of NADPH(H^+) and glutathione reductase. This is, therefore, a cyclic reaction which speed is directly dependent on the amount of total glutathione (GSx).

Cells were washed with ice-cold PBS, lysed in 1 ml of 1% (w/v) sulfosalicylic acid (SSA, Sigma) per 10^6 cells and centrifuged at $13,000 \times g$ for 5 minutes. The supernatants were then placed in a fresh tube in order to determine total glutathione content. An equal volume of 0.1 M NaOH was added to the same amount of cells to assess protein concentration. The quantification of GSx was made by extrapolating the sample slope values to the standard curve (0-50 μM GSSG in 1% w/v SSA). Samples were registered for a 10 minutes (20 iterations) period at 405 nm.

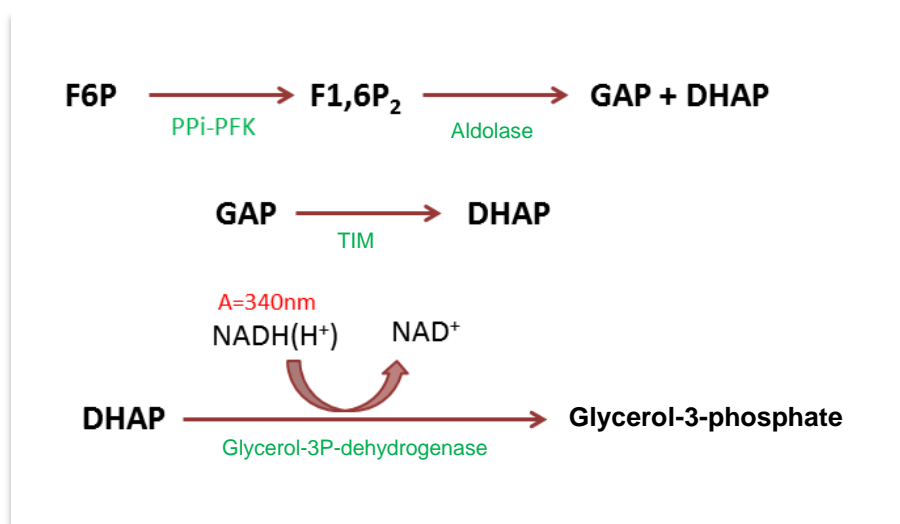


To determine oxidized glutathione (GSSG), samples or GSSG standards were incubated with 2-vinylpyridine plus 0.2 mM Tris for 1h at 4 °C. This reaction protects the sulfhydryl group of GSH by forming a thioether. Thus, GSH does not react in the determination assay, and only GSSG is measured in these samples. Absorbance was recorded at 405 nm for a 10 minutes (20 iterations) period in a Varioskan Flash (Thermo Fischer, Vantaa, Finland) spectrofluorometer. The sample slope values were extrapolated to the standard curve (0-5 μM GSSG in 1% w/v SSA). Finally, reduced glutathione concentration (GSH) was calculated from the formula $\text{GSx}=\text{GSH}+2\text{GSSG}$, according to Tietze (1969).

The reaction buffer consisted of 0.4 mM NADPH(H⁺) (Sigma-Aldrich), 1 mM EDTA, 0.3 mM DTNB, 0.1 M sodium phosphate buffer pH 7.5 and 1U/ml glutathione reductase (Sigma-Aldrich).

12.5. FRUCTOSE-2,6-BISPHOSPHATE

F2,6P₂ concentration was determined spectrophotometrically according to the method described by Van Schaftingen (1982). The method consists of measuring the decrease of NAD⁺ absorbance at 340 nm every 10 minutes in four consecutive reactions, the first catalyzed by the phosphofructokinase-pyrophosphate (PPi-PFK; Sigma-Aldrich), the second catalyzed by aldolase, the third by TIM and the last one catalyzed by glycerol-3-phosphate dehydrogenase.



Cells were smoothly detached from the plates with 1 mM EDTA tetra-Na⁺ and centrifuged at 500 x g for 5 minutes. The pellet was then lysate with 0.1 N and centrifuged at 4 °C (20,000 x g, 20 minutes). An aliquot of the homogenate was used for protein determination; the rest was heated at 80 °C during 5 minutes and centrifuged again (20,000 x g, 20 minutes). The supernatant was then used for F2,6P₂ determination.

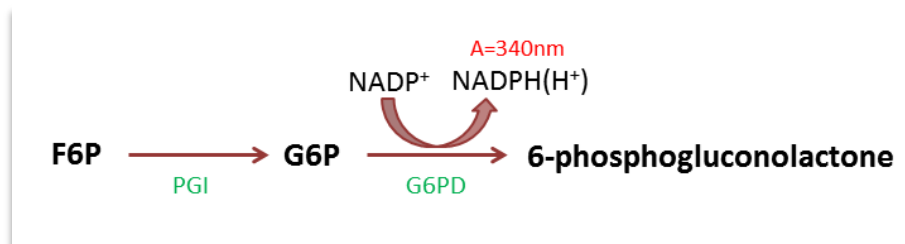
The reaction buffer consisted of: 0.1 M Tris-HCl, 5 mM MgCl₂, 2 mM F6P, 0.3 mM NADH(H⁺), 0.45 U/ml aldolase, 5 U/ml TIM, 1.7 U/ml glycerol-3-phosphate dehydrogenase, 0.01 U/ml PPi-PFK (pH 8).

13. PGI ACTIVITY DETERMINATION

PGI activity was determined spectrophotometrically by determining the increase in NADPH(H⁺) absorbance at 340 nm every 30 seconds for 5 minutes in total. Cells were detached with PBS and centrifuged at 500 x g 5min. They were then re-suspended in lysis buffer (100 mM Tris-HCl, 7 mM MgCl₂; pH 7.6), lysated with 3 cycles of freeze/thawing, centrifuged at 12,000 x g for 5 minutes more and the supernatant stored at -80 °C for PGI determination.

The reaction buffer consisted of 100 mM Tris-HCl, 7 mM MgCl₂, 0.8 mM NADP⁺, 0.5 U G6PD, 4 mM F6P.

Before adding F6P, the samples and the rest of the components of the buffer were incubated in order to let the G6P present in the sample consume.

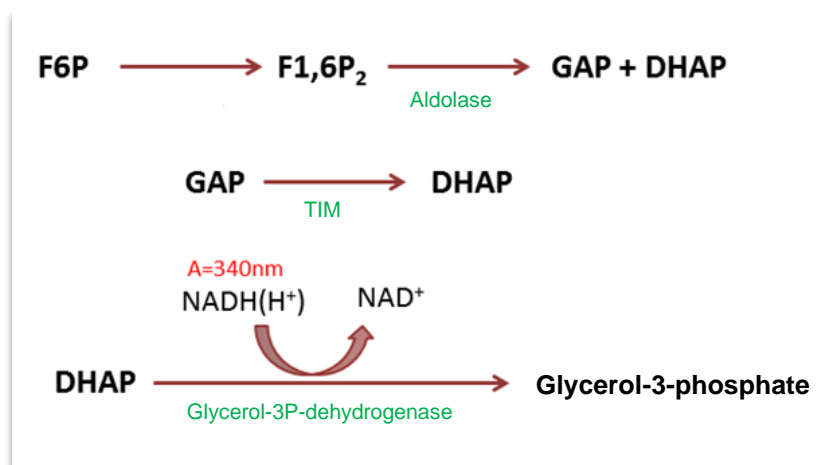


14. PFK-1 ACTIVITY DETERMINATION

PFK-1 activity was determined spectrophotometrically by determining the decrease of NADH(H⁺) absorbance at 340 nm every 10 seconds for at least 3 minutes in four consecutive reactions, the first catalyzed by the phosphofructokinase present in the sample, the second catalyzed by aldolase, the third by TIM and the last one catalyzed by the glycerol-3-phosphate dehydrogenase.

Cells were detached from the plate with PBS and centrifuged at 500 x g 5min. They were then re-suspended in storage buffer (20 mM KHPO₄, 0.1 mM EDTA 20% glycerol; 10 mM DTT, 0.1 mM PMSF, pH 7.4), lysed with 3 cycles of freeze/thawing, centrifuged at 12,000 x g for 5 minutes more and the supernatant stored at -80 °C for PFK-1 determination.

The reaction buffer consisted of: 0.1 mM fructose-6-phosphate, 50 mM imidazole, 1 mM MgCl_2 , 0.1 mM $\text{NADH}(\text{H}^+)$, 1 mM ATP, 1 μM fructose-2,6-bisphosphate, 0.45 U/ml aldolase, 5 U/ml TIM, 1.7 U/ml glycerol-3-phosphate dehydrogenase (pH 7.4).



15. GLYCOLYTIC FLUX ASSESSMENT

The glycolytic flux was determined in attached cells by determining the production of $^3\text{H}_2\text{O}$ from D-[3- ^3H]glucose in the reaction catalyzed by aldolase. To do so, cells were seeded at 250,000 cells/cm² in the bottom of 25 cm² flasks. At day 6 in culture, medium was replaced by a Krebs-Elliott buffer (11 mM Na_2HPO_4 , 122 mM NaCl , 3.1 mM KCl , 0.4 mM KH_2PO_4 , 1.2 mM MgSO_4 , 1.3 mM CaCl_2 ; pH 7.4) supplemented with 5 mM D-glucose and in the presence of 5 $\mu\text{Ci/ml}$ of D-[3- ^3H]glucose. Before sealing the flask with a rubber cap, a 1.5-ml Eppendorf tube containing 1 ml of water (for $^3\text{H}_2\text{O}$ trapping) was fixed inside the flask by holding it from the flask tab using a rib (see figure 3). In order to ensure an adequate O_2 supply throughout incubation period, the atmosphere of the flasks was gassed with an $\text{O}_2:\text{CO}_2$ (95:1) mixture for 20 seconds, before the flasks were sealed. In preliminary experiments (not shown), we observed that $^3\text{H}_2\text{O}$ release was linear with time up to 90 minutes, thus, flasks were incubated in a thermostatic orbital shaker for 90 minutes. After the incubation period, reaction was stopped by adding 0.2 ml of 20% w/v perchloric acid and flasks were incubated for another 96 hours to allow equilibration of $^3\text{H}_2\text{O}$. Results were expressed as nmol of D-[3- ^3H]glucose turned into $^3\text{H}_2\text{O}$ per minute and per mg protein.

The efficiency of $^3\text{H}_2\text{O}$ trapping in the eppendorf tube was determined to be a 28%. To do so, known μCi of $^3\text{H}_2\text{O}$ were added to the experimental buffer in the bottom of the flask. Samples were then incubated for 90 minutes and further left stabilizing for 96 hours after perchloric acid addition. Total μCi in the eppendorf tube were then measured for calculating the percentage of $^3\text{H}_2\text{O}$ trapped, which was taken in account for the calculations.

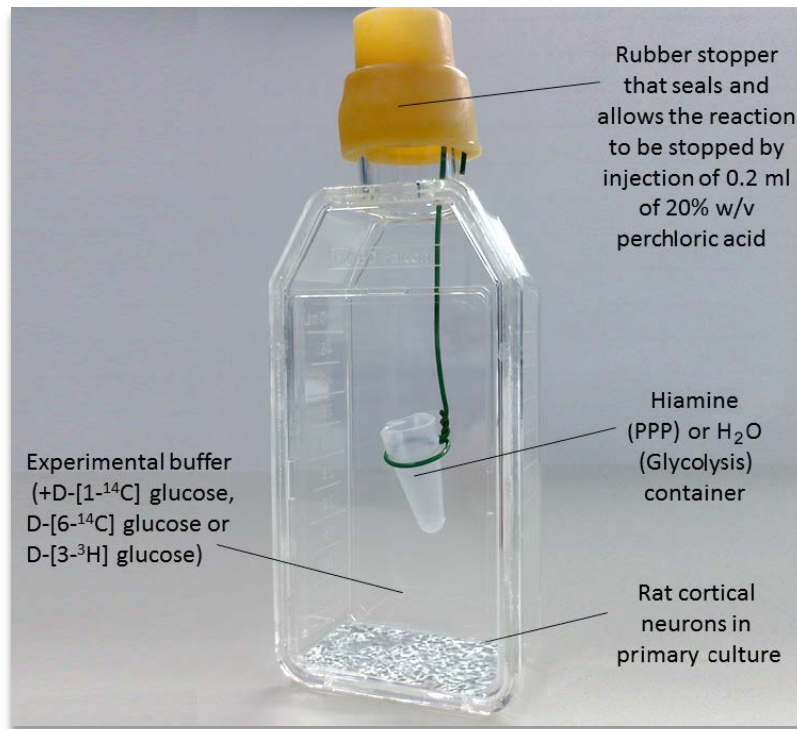


Figure3. Schematic representation of the method for PPP and glycolytic flux determination in attached cells. Cells were seeded at $250,000/\text{cm}^2$ on the bottom of the flask. At day 6 in culture the medium was removed and replaced by experimental buffer plus D-[3- ^3H]glucose for glycolytic measurements or D-[1- ^{14}C]glucose or D-[6- ^{14}C] for PPP measurements. Hiamine (PPP) or H_2O (glycolysis) was added in the central well. The flask was then supplied with a $\text{O}_2:\text{CO}_2$ (95:1) mixture and sealed with a rubber stopper. After 90 minutes the reaction was stopped by injecting 0.2 ml of 20% w/v perchloric acid.

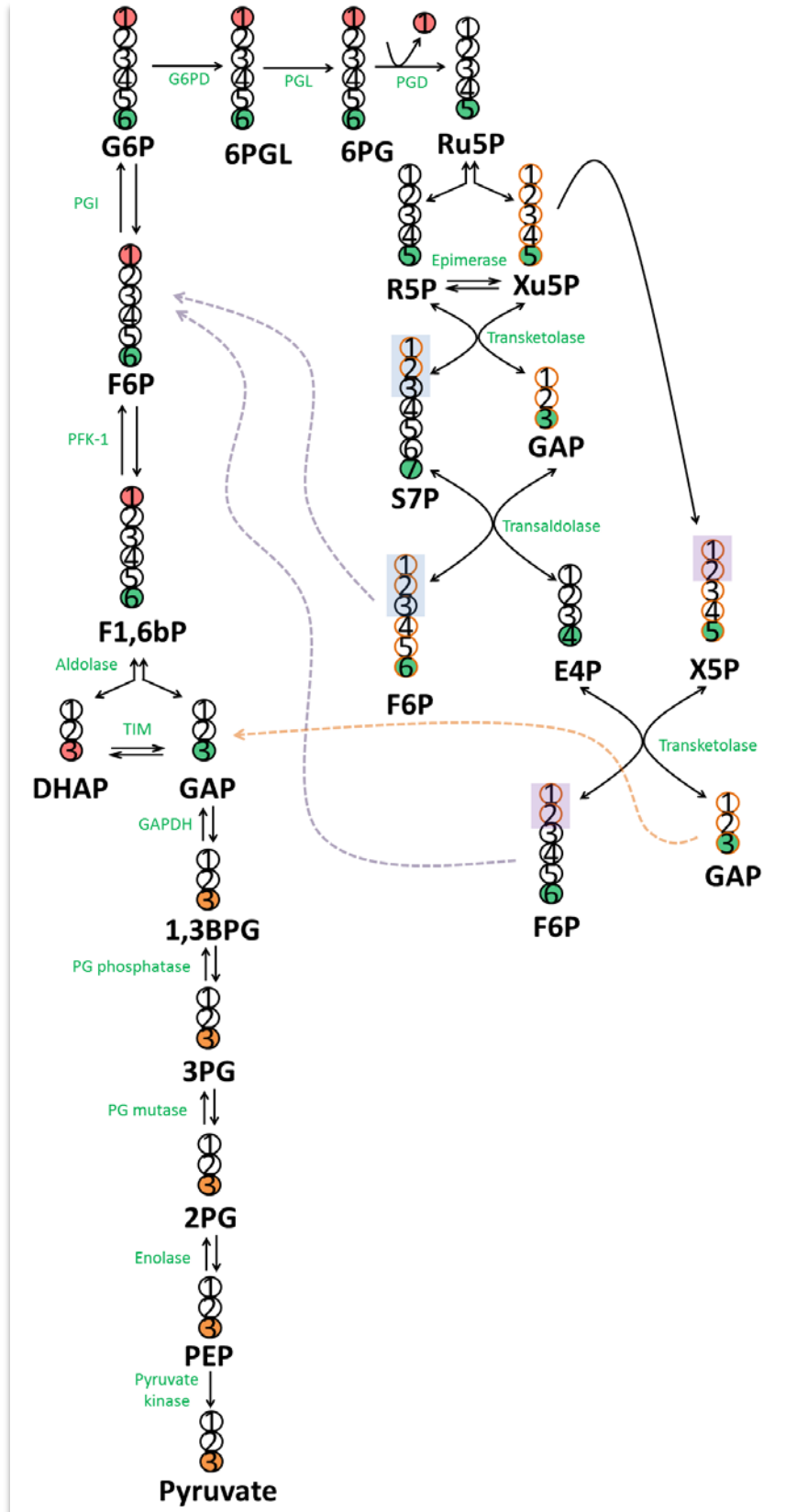
16. PENTOSE-PHOSPHATE PATHWAY (PPP) FLUX MEASUREMENTS

The PPP was measured in attached cells by determining the difference of $^{14}\text{CO}_2$ produced from D-[1- ^{14}C]glucose, metabolized both in the tricarboxylic acid cycle and 6-phosphogluconate dehydrogenase reaction in the PPP and the $^{14}\text{CO}_2$ produced from D-[6- ^{14}C]glucose, metabolized only in the tricarboxylic acid cycle, in the reactions catalyzed

MATERIALS AND METHODS

by isocitrate dehydrogenase and α -ketoglutarate dehydrogenase (see figure 4). To do so, cells were seeded at 250,000 cells/cm² in the bottom of 25 cm² flasks. At day 6 in culture, medium was replaced by a Krebs–Elliott buffer (11 mM Na₂HPO₄, 122 mM NaCl, 3.1 mM KCl, 0.4 mM KH₂PO₄, 1.2 mM MgSO₄, 1.3 mM CaCl₂; pH 7.4) supplemented with 5 mM D-glucose and in the presence of 0.5 μ Ci/ml of either D-[1-¹⁴C]glucose or D-[6-¹⁴C]glucose. Before sealing the flask with a rubber cap, a 1.5-ml Eppendorf tube containing 0.8 ml of benzetonium hydroxyde (Sigma-Aldrich) for ¹⁴CO₂ trapping was fixed inside the flask by holding it from the flask tab using a rib (see figure 3). In order to ensure an adequate O₂ supply throughout incubation period, the atmosphere of the flasks was gassed with an O₂:CO₂ (95:1) mixture for 20 seconds, before the flasks were sealed. In preliminary experiments (not shown), we observed that ¹⁴CO₂ release was linear with time up to 90 minutes, thus, flasks were incubated in a thermostatic orbital shaker for 90 minutes. After the incubation period, reaction was stopped by adding 0.2 ml of 20% w/v perchloric acid and flasks were incubated for another 90 minutes to allow ¹⁴CO₂ trapping by the benzetonium hydroxide. Results were expressed as nmol of glucose turned into ¹⁴CO₂ per minute and per mg protein.

The efficiency of ¹⁴CO₂ trapping by the benzetonium hydroxide was determined to be a 75%. To do so, known μ Ci of NaH¹⁴CO₃ were added to the experimental buffer in the bottom of the flask. Samples were then incubated for 90 minutes and further left stabilizing for 90 minutes more after perchloric acid addition. Total μ Ci in the eppendorf tube were then measured for calculating the percentage of ¹⁴CO₂ trapped, which was taken in account for the calculations.



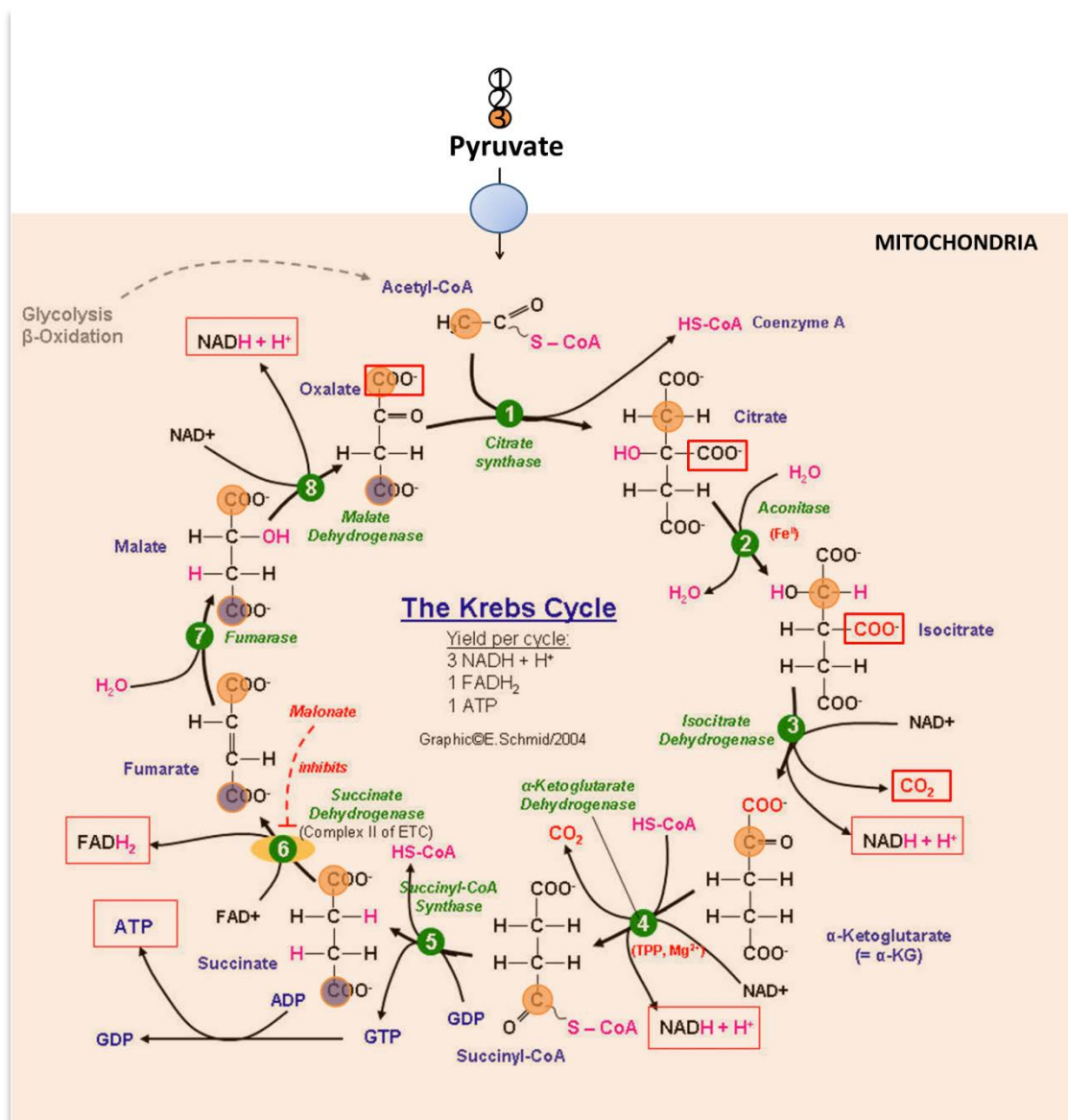


Figure 4. Schematic representations of the fate of the radiolabeled carbons used for the PPP flux assessment. D-[1-¹⁴C] glucose is decarboxylated in the reaction catalyzed by 6-phosphogluconate dehydrogenase. D-[6-¹⁴C] glucose that enters PPP is transformed back into GAP or F6P in the non-oxidative branch of PPP. D-[6-¹⁴C] glucose and D-[1-¹⁴C] glucose can also enter glycolysis. After their transformation in DHAP and GAP they are indistinguishable and will be further decarboxylated in the different turns of the TCA in the reactions catalyzed by isocitrate dehydrogenase and α -ketoglutarate dehydrogenase.

17. IMMUNOCYTOCHEMISTRY

Neurons were grown on glass coverslips. At day 6 in culture they were fixed with 4% paraformaldehyde (v/v) in PBS for 20 min and washed with phosphate buffered saline (PBS, 136 mM NaCl, 2.7 mM KCl, 7.8 mM Na₂HPO₄ 2H₂O, 1.7 mM KH₂PO₄ pH 7.4). They were then incubated in 5% goat serum, 1% BSA PBS-Tx 0.2% for 1h at room temperature. Afterwards they were incubated with the TIGAR primary antibody in 2% goat serum, 1% BSA, PBS-Tx 0.2% overnight at 4°C. The following day they were washed with PBS-Tx 0.2% and incubated with the secondary antibody (rabbit anti IgG (H+L) conjugated with Alexa 488, Molecular Probes, Invitrogen, Ref A11008 at 1/500 dilution) and the nuclear marker either DAPI (Sigma, Ref D9542, 1/1000) or TOPRO-3 (Invitrogen, Ref T3605, 1/1000) in 2% goat serum, 1% BSA, PBS-Tx 0.2% for 1 hour at room temperature. Glass coverslips were then placed on a glass slide using SlowFade® (Molecular Probes, Oregon, USA) in order to avoid fluorescence loss. Confocal microscopy images were obtained using a Leica SP5 microscope (DMI-6000B model; Leica Microsystems GmbH, Wetzlar, Germany) and processed with photoshop cs5 software.

18. CONFOCAL MICROSCOPY OF TRANSFECTED CELLS.

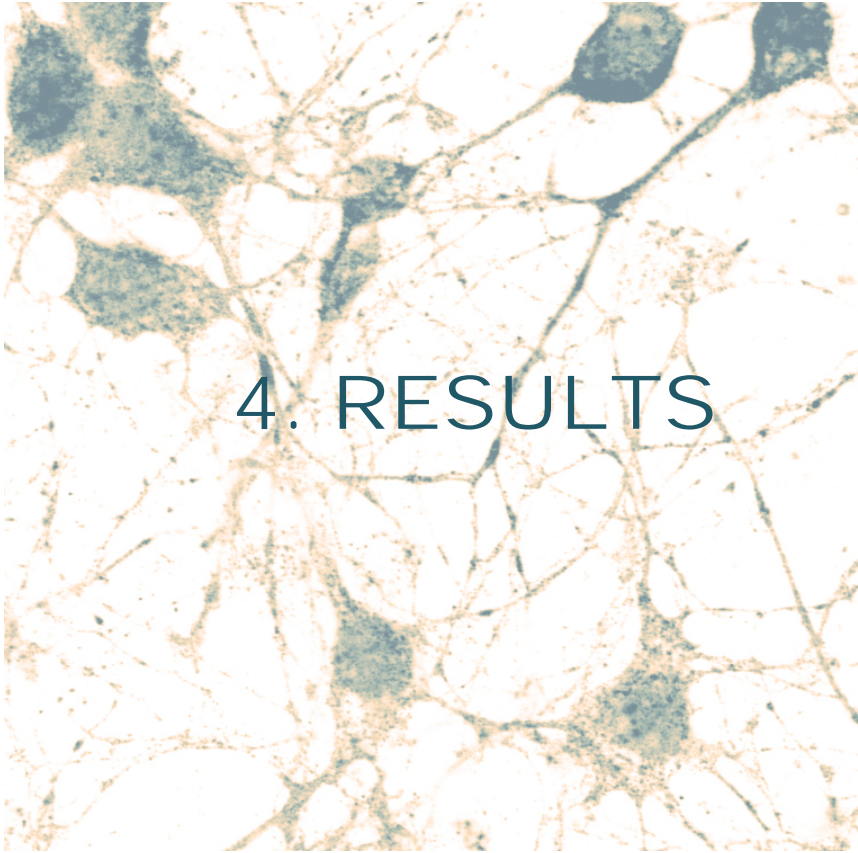
Neurons were grown on glass coverslips. After transfections and treatments they were fixed with 4% paraformaldehyde (v/v) in PBS for 20 min and incubated with DAPI (30 µM; Sigma) for 10 minutes at room temperature. Glass coverslips were then placed on a glass slide using SlowFade® (Molecular Probes, Oregon, USA) in order to avoid fluorescence loss. Confocal microscopy images were obtained using a Leica SP5 microscope (DMI-6000B model; Leica Microsystems GmbH, Wetzlar, Germany) and processed with photoshop cs5 software.

19. STATISTICAL ANALYSIS.

Measurements from individual cultures were always carried out in triplicate. The results are expressed as mean ± S.E.M. (standard error of the mean) values for three different culture preparations. Statistical analysis of the results was performed by one-way

MATERIALS AND METHODS

analysis of variance (ANOVA), followed by the least significant difference multiple range test. In all cases, $P < 0.05$ was considered significant.



4. RESULTS

1. GLYCOLYTIC FLUX INCREASES BY INHIBITING PENTOSE-PHOSPHATE PATHWAY (PPP) OR MITOCHONDRIAL PYRUVATE UPTAKE IN NEURONS.

In order to ascertain whether glucose metabolism is dynamic in neurons, we first set up a new protocol aimed to investigate glucose metabolizing pathways in intact, cultured primary neurons. The rate of glucose metabolized through glycolysis was measured by determining the rate of $^3\text{H}_2\text{O}$ production from $[3\text{-}^3\text{H}]\text{glucose}$, a process that occurs at aldolase, i.e. the glycolytic step that immediately follows the rate-limiting, PFK1-catalyzed reaction. Using this approach, we estimated that neurons, under resting conditions, metabolized glucose through glycolysis at a rate of ~ 1.2 nmol/min \times mg protein (Fig. 1). Incubation of neurons with dehydroepiandrosterone (DHEA; $1 \mu\text{M}$), a well-known inhibitor of G6PD –the rate-limiting step of PPP–, acutely increased $\sim 100\%$ the rate of glycolysis (Fig. 1). Incubation of neurons with 4-hydroxy- α -cyanocinnamate (HCN; 0.1 mM), a compound that, at the concentration used selectively inhibits mitochondrial uptake of pyruvate, also acutely increased $\sim 150\%$ the rate of glycolysis (Fig. 1). Thus, the flux of glucose metabolism through glycolysis in neurons is a process amenable to regulation. Moreover, these results suggest that a considerable proportion ($\sim 50\%$) of glucose entering neurons is metabolized through the PPP.

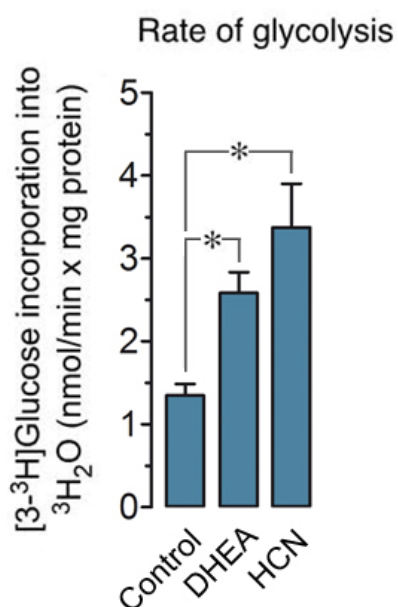


Figure 1. Glycolytic rate is significantly increased upon DHEA and HCN treatments. Neurons at day 6 in culture were incubated in experimental buffer containing $5 \mu\text{Ci/ml}$ of $D\text{-}[3\text{-}^3\text{H}]\text{glucose}$ plus either $1 \mu\text{M}$ DHEA or 0.1 mM HCN. Glycolytic rate was assessed by the determination of $[3\text{-}^3\text{H}]\text{glucose}$ incorporation into $^3\text{H}_2\text{O}$ during the 90 minutes incubation of the experiment. $*P < 0.05$ (ANOVA)($n=3$).

2. THE RATE OF GLUCOSE OXIDIZED THROUGH THE PPP IS INHIBITED BY DHEA AND NOT BY HCN.

At the light of the previous results, we next aimed to directly determine the rate of glucose oxidized through the PPP in neurons. To do so, intact primary neurons in culture were incubated either in the presence of [1-¹⁴C]glucose or [6-¹⁴C]glucose, and the ¹⁴CO₂ released was quantitatively trapped and measured. ¹⁴CO₂ released from [1-¹⁴C]glucose reflects 6PG decarboxylation at 6-phosphogluconate dehydrogenase (6PGD) plus acetyl-CoA decarboxylation at isocitrate dehydrogenase and α-ketogluratae dehydrogenase of the TCA. However, ¹⁴CO₂ released from [6-¹⁴C] glucose exclusively reflects acetyl-CoA decarboxylation at isocitrate dehydrogenase and α-ketogluratae dehydrogenase of the TCA. Thus, the difference between ¹⁴CO₂ released from [1-¹⁴C]glucose and that of [6-¹⁴C]glucose is often used as an estimation of glucose oxidized through the PPP. As shown in Fig. 2a, the rate of glucose oxidized through the PPP was estimated to be ~0.2 nmol/min x mg protein; furthermore, incubation of neurons with DHEA inhibited by 50% the estimated rate of PPP (Fig. 2a). As expected, the rate of PPP was unaffected by HCN (Fig. 2a). When examined ¹⁴CO₂ collected from [1-¹⁴C]glucose and [6-¹⁴C]glucose independently we observed that ¹⁴CO₂ collected from [1-¹⁴C]glucose was unchanged by either treatment (Fig. 2b), whereas ¹⁴CO₂ collected from [6-¹⁴C]glucose dramatically decreased by HCN but was unchanged by DHEA (Fig. 2c). These results indicate that ¹⁴CO₂ collection from [6-¹⁴C]glucose is an excellent estimation of glucose that, being converted into acetyl-CoA, is oxidized at the TCA. Furthermore, the lack of effect of DHEA on ¹⁴CO₂ released from [1-¹⁴C]glucose (Figs. 2b,c) suggests that this value may be underestimated. Indeed, according to the results shown in Fig. 1, DHEA increased glycolysis by ~1.2 nmol/min x mg protein, whereas it decreased PPP by only ~0.1 nm/min x mg protein (Fig. 2a). These results indicate that the extent of PPP activity determined in neurons using this approach appears to be largely underestimated.

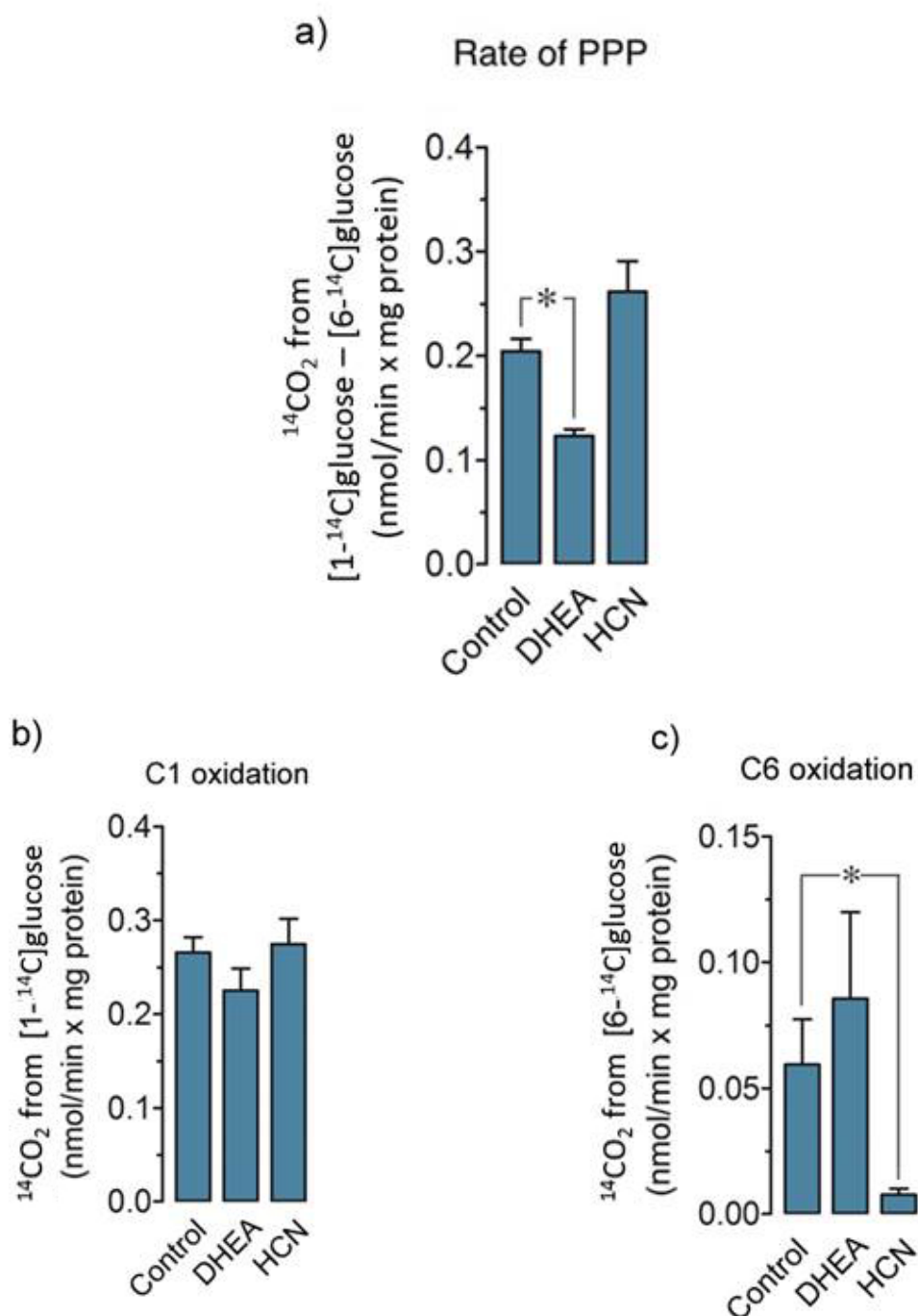


Figure 2. a) PPP rate is significantly decreased upon DHEA treatment. Neurons at day 6 in culture were incubated in experimental buffer containing 0.5 $\mu\text{Ci/ml}$ of either D-[1- ^{14}C]glucose or D-[6- ^{14}C] for 90 minutes and PPP rate was assessed by the determination of the difference between $^{14}\text{CO}_2$ produced by [1- ^{14}C]glucose and that of [6- ^{14}C]glucose. b) $^{14}\text{CO}_2$ produced by [1- ^{14}C]glucose remains unchanged. c) $^{14}\text{CO}_2$ produced by [6- ^{14}C]glucose is almost absent in HCN treated neurons, which accounts for the

effectiveness of HCN in pyruvate transport to the mitochondria blockade. $*P < 0.05$ (ANOVA)($n=3$).

3. PHOSPHOGLUCOSE ISOMERASE (PGI) IS A HIGHLY ACTIVE ENZYME IN NEURONS.

As an attempt to understand the low $^{14}\text{CO}_2$ collection from $[1-^{14}\text{C}]$ glucose in neurons, we reasoned that, after decarboxylation of the only radiolabelled carbon of G6P (C_1) at 6PGD, F6P regenerated from the non-oxidative branch of the PPP is non-radioactive. Thus, provided that F6P is converted back into G6P at the expense of PGI, the radioactive G6P pool would be dramatically reduced. In view that ascertaining the specific radioactivity of intracellular G6P in neurons incubated with $[1-^{14}\text{C}]$ glucose is, technically, rather difficult, we measured the specific activity of PGI. As shown in Fig. 3, PGI specific activity was as high as that of PFK-1. However, the flux of F6P through PFK-1 is limited in neurons by the synthesis of its positive effector, fructose-2,6-bisphosphate (F2,6P_2), whereas PGI is a near-equilibrium enzyme. Thus, the direction of PGI activity exclusively relies on the relative concentrations of G6P and F6P. Accordingly, it is feasible that a large proportion of F6P returning from the PPP would be converted back into G6P, thus contributing to G6P isotopic dilution resulting in an apparently low $^{14}\text{CO}_2$ released from $[1-^{14}\text{C}]$ glucose.

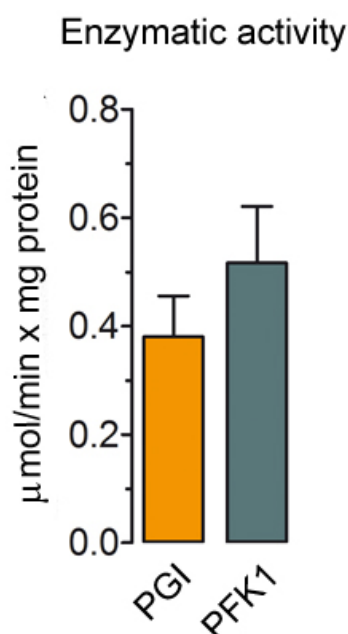


Figure3. PGI presents a similar activity to that observed for PFK-1 in neurons. Neurons at 6 days in culture were re-suspended and lysated with 3 cycles of freezing/thawing. The extract was then used for PGI and PFK-1 activities determination.

4. KNOCK-DOWN OF PGI INCREASES PPP ACTIVITY

We next aimed to more directly test whether PGI activity, acting on its reversal mode (i.e., F6P to G6P), would maintain a high PPP activity in neurons despite not being accounted for the low $^{14}\text{CO}_2$ released from $[1\text{-}^{14}\text{C}]\text{glucose}$. To do so, and in view that there is no known selective inhibitor of PGI activity, we implemented a RNA interfering (RNAi) strategy to knock-down PGI in primary neurons. At day 3 in vitro, cells were transfected with a small interfering RNA (siRNA) targeted against PGI (siPGI), which was previously validated as shown in Fig. 4a. Three days later, when PGI protein abundance decreased by ~70%, neurons were used to assess the rate of $^{14}\text{CO}_2$ release from either $[1\text{-}^{14}\text{C}]\text{glucose}$ and $[6\text{-}^{14}\text{C}]\text{glucose}$. As observed in Fig. 4b, the rate of PPP, as assessed by the difference between the rates of $^{14}\text{CO}_2$ collected from both radiolabelled glucoses, increased significantly by siPGI. This result is compatible with the notion that $[1\text{-}^{14}\text{C}]\text{G6P}$ specific radioactivity is considerably diluted by the return of “cold” (i.e., non-radioactive) F6P into the G6P pool, thus explaining the underestimation of the actual rate of PPP activity. Furthermore, it indicates that the PPP in neurons actively uses PGI activity to recycle G6P. It should be mentioned that siPGI caused no net increase in the rate of $^{14}\text{CO}_2$ released from $[1\text{-}^{14}\text{C}]\text{glucose}$ by siPGI (Fig. 4c) while $^{14}\text{CO}_2$ released from $[6\text{-}^{14}\text{C}]\text{glucose}$ significantly decreased (Fig. 4d) indicating inhibition of G6P flux through glycolysis. In fact, due to the near-equilibrium nature of PGI, inhibition of PGI activity by siPGI would not only affect F6P conversion into G6P, but also vice-versa. Together, these data strongly suggest that glucose entering neurons is actively oxidized through the PPP at the expense of G6P re-cycled from PPP-derived F6P. However, due to isotopic dilution of G6P, the actual value of the glucose proportion entering the PPP is, so far, impossible to be directly determined, at least using this approach.

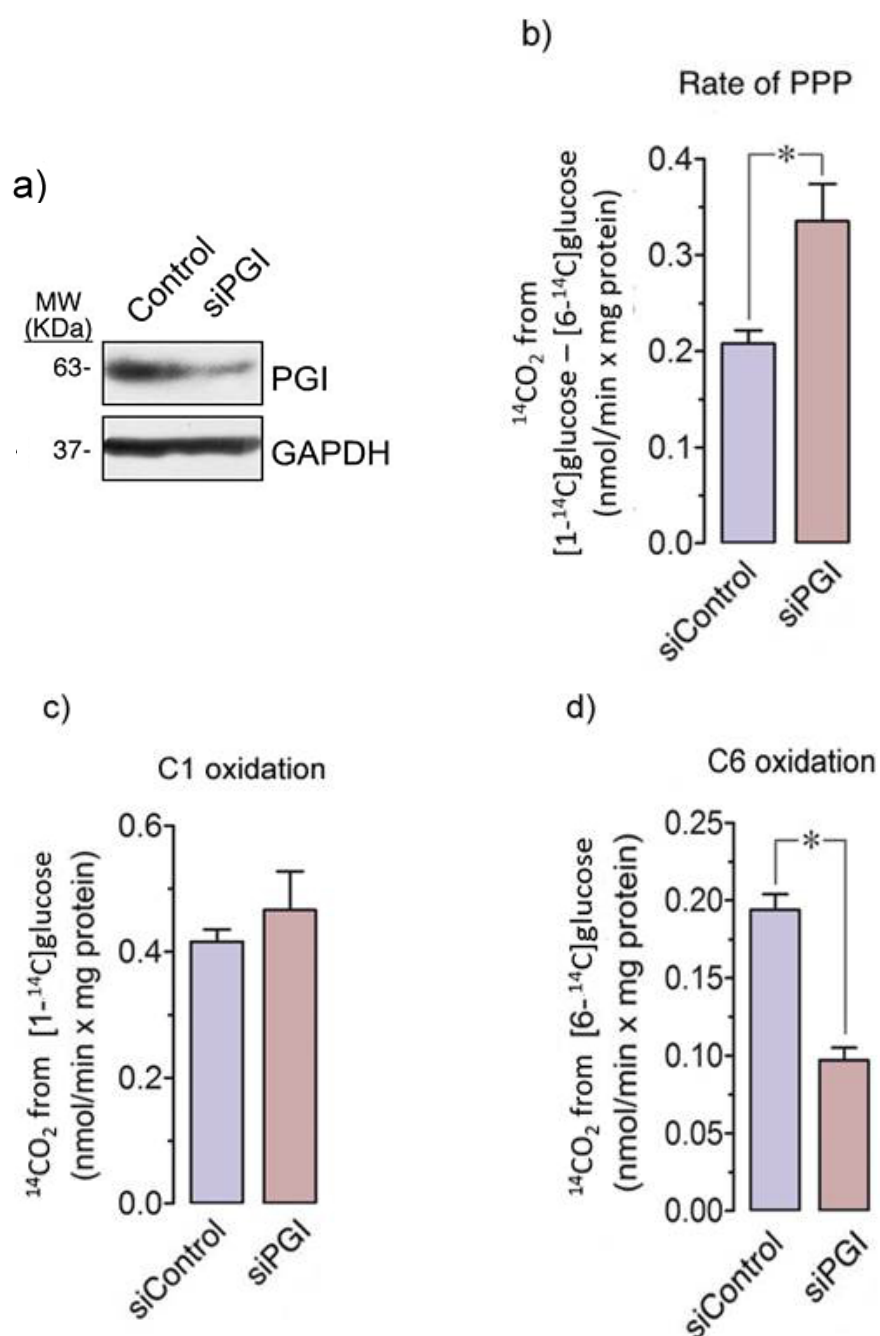


Figure 4. a) siRNA against PGI efficiently knocks down PGI in neurons. Neurons at day 3 in culture were transfected with 100 nM siControl or siPGI, 72 hours later cells were lysed in RIPA buffer and subjected to western blot in order to test the efficiency of PGI knock down. b) PPP rate significantly increases upon PGI silencing. Neurons at day 6 in culture were incubated in experimental buffer containing 0.5 $\mu\text{Ci/ml}$ of either D-[1- ^{14}C]glucose or D-[6- ^{14}C] for 90 minutes, and the PPP assessed by the determination of the difference between $^{14}\text{CO}_2$ produced by [1- ^{14}C]glucose and that of [6- ^{14}C]glucose. c) PGI silencing does not affect $^{14}\text{CO}_2$ produced by [1- ^{14}C]glucose. d) $^{14}\text{CO}_2$ produced by

[6-¹⁴C]glucose C6 oxidation is significantly decreased upon PGI silencing * $P < 0.05$ (ANOVA)($n=3$).

5. EFFECT OF DHEA AND HCN ON GLUCOSE-6-PHOSPHATE CONCENTRATION

To further understand how the PPP is dynamically coupled with glycolysis in neurons, we next investigated the effects of inhibition of PPP and mitochondrial pyruvate uptake on the concentrations of G6P. As shown in Fig. 5, G6P accumulated by ~3.5-fold upon DHEA-mediated inhibition of the PPP rate-limiting enzyme, G6PD. This result strongly suggests a highly active flux of G6P into the PPP in neurons. In contrast, HCN-mediated inhibition of glucose-derived pyruvate oxidation at the TCA by HCN did not affect G6P concentrations (Fig. 5).

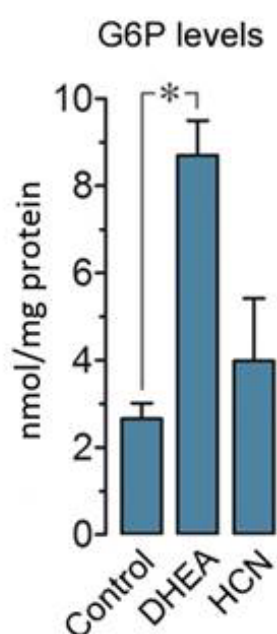


Figure 5. G6P is highly accumulated upon DHEA-mediated inhibition of G6PD, but is unaffected by HCN. Neurons at 6 days in culture were incubated with 1 μ M DHEA or 0.1 mM HCN for 90 minutes. Cells were then lysed in 0.6M NaOH and the resulting extract deproteinized with the same volume of 1% w/v ZnSO₄ and used for G6P quantification. * $P < 0.05$ (ANOVA)($n=3$).

6. EFFECT OF DHEA AND HCN ON EXTRACELLULAR AND INTRACELLULAR LACTATE CONCENTRATIONS

To further understand the impact of PPP inhibition on the intermediary metabolism of neurons, we investigated both intracellular and extracellular lactate concentrations. Inhibition of PPP activity by the G6PD inhibitor DHEA did not affect lactate concentrations, either extracellular (Fig. 6a) or intracellular (Fig. 6b); however, as shown

RESULTS

above, DHEA significantly increased the rate of glycolysis (Fig. 1a) and the rate of [6-¹⁴C]glucose oxidation at the TCA (Fig. 2b), thus indicating that the putative increase in pyruvate by PPP inhibition does not accumulate, but is consumed through the TCA activity (Fig. 2b) and, possibly, converted into alanine. In fact, inhibition of pyruvate uptake into mitochondria by HCN increased the release of lactate (Fig. 6a), thus resulting in unchanged intracellular lactate (Fig. 6b).

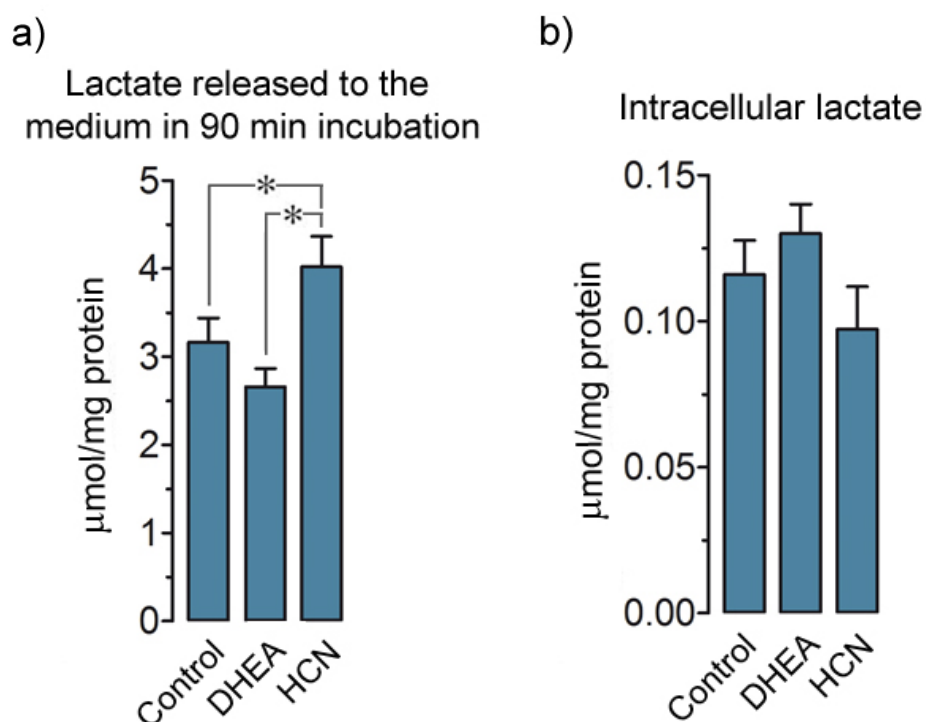


Figure 6. a) Lactate released to the medium is increased upon HCN treatment, indicating that part of the pyruvate that cannot enter the mitochondria is being derived to lactate. Neurons at 6 days in culture were incubated with 1 μM DHEA or 0.1 mM HCN for 90 minutes after which an aliquot of the experimental buffer was obtained for extracellular lactate measurement. b) Intracellular lactate levels remain constant, what suggests that most part of the excess lactate generated upon HCN treatment is being released to the medium. Neurons at 6 days in culture were incubated with 1 μM DHEA or 0.1 mM HCN for 90 minutes. Neurons were then lysed in 0.6M NaOH and the resulting extract deproteinized with the same volume of 1% w/v ZnSO₄ for intracellular lactate measurement. * $P < 0.05$ (ANOVA)($n=3$).

7. CORTICAL PRIMARY NEURONS RESPOND TO GLUTAMATE RECEPTORS ACTIVATION BY INCREASING INTRACELLULAR Ca^{2+} LEVELS.

Altogether, our results therefore indicate that glucose metabolism in neurons is a highly dynamic process that can be easily manipulated and detected in cultured intact primary neurons. Moreover, our data also indicate that, besides glycolysis, a considerable proportion of glucose entering neurons is oxidized through the PPP. However, the current method to directly assess the PPP activity is intrinsically misleading, which leads to a strong underestimation of the actual values of the rate of PPP in neurons. Nevertheless, in view that at the light of our data glycolysis and PPP are highly dynamic in neurons, we next aimed to investigate whether these glucose-metabolizing pathways can be endogenously modulated by physiological neurotransmitter-mediated stimuli.

To do so, we focused on glutamate receptor-mediated stimuli, since rat cortical neurons in culture are known to be predominantly glutamatergic. To ascertain whether neurons at 6 days *in vitro* expressed functional glutamate receptors, the changes in intracellular Ca^{2+} levels using the fluorescent Ca^{2+} -probe, Fura-2, were registered. This method determines Fura-2-dependent fluorescence emitted at 510 nm obtained after excitation at 335/363 nm (F335/F363 ratio), a signal that is directly proportional to intracellular Ca^{2+} levels. As shown in Fig. 7a, incubation of neurons with glutamate (100 μM) immediately increased Fura-2 fluorescence, suggesting Ca^{2+} entry into neurons through the ionotropic glutamate receptors; this effect was maintained for at least 1 minute, although we observed that the increased Fura-2 fluorescence was maintained for several hours (not shown). The increase in Fura-2 fluorescence was partially prevented by the well-known N-methyl-D-aspartate (NMDA) receptor (NMDAR) antagonist, MK-801 (1 μM). This indicates that a considerable proportion (~60%) of glutamate-mediated Ca^{2+} entry was due to NMDA receptor activation. As expected, incubation of neurons with glutamate in the presence of the Ca^{2+} -free experimental buffer, which contains the Ca^{2+} quelator ethylene glycol tetraacetic acid (1 mM EGTA), abolished the changes in 510 nm emissions (Fig. 7a). To further test that these neurons expressed functional NMDAR, Fura-2 fluorescence was also registered in the presence of NMDA. As shown in Fig. 7b, NMDA triggered an increase in the intracellular Ca^{2+} -mediated signal to a similar level of that observed with glutamate. Moreover, this effect was prevented by ~90% with MK-801 (Fig. 7b), and fully abolished by EGTA (Fig. 7b). Thus, the rat cortical neurons used in

RESULTS

this study express functional NMDA subtype of glutamate receptors, therefore being suitable to investigate the metabolic effects of this neurotransmitter.

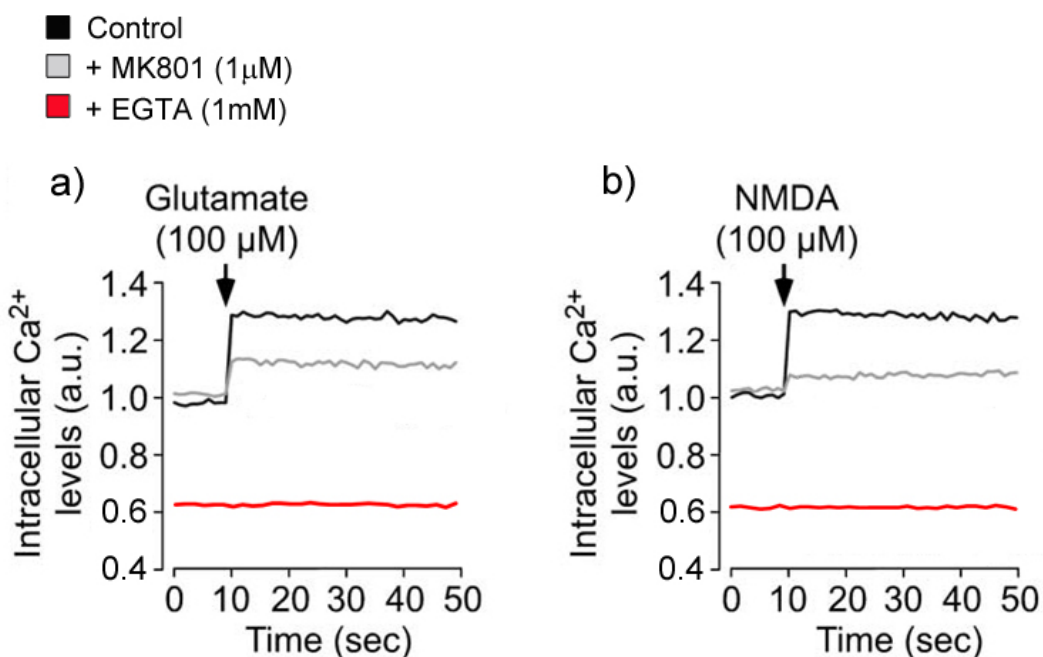


Figure 7. Incubation of rat primary cortical neurons at day 6 in culture with glutamate (a) or NMDA (b) increased the ratio of Fura-2-dependent fluorescence (at 510 nm) obtained after excitation at 335/363 nm (F_{335}/F_{363}), indicating an increase in intracellular Ca^{2+} . MK801 (10 μM) partially prevented glutamate-induced changes in F_{335}/F_{363} ratio and most of NMDA-dependent F_{335}/F_{363} ratio changes. Ca^{2+} -free experimental buffer containing 1 mM EGTA, fully prevented the changes in 510 nm emissions both in NMDA and glutamate-treated neurons.

8. NMDAR STIMULATION PROMOTES PROTEIN STABILIZATION OF THE GLYCOLYTIC-PROMOTING ENZYME PFKFB3 IN NEURONS.

Previous results from our laboratories demonstrated that NMDAR stimulation activates cyclin-dependent kinase 5 (Cdk5) through a Ca^{2+} -calpain-p25-mediated mechanism. In turn, Cdk5 hyperphosphorylates Cdh1, the anaphase-promoting complex/cyclosome (APC/C) co-activator causing the release of Cdh1 from the complex, thus inhibiting its E3 ubiquitylating activity. In view that we had also shown that the key glycolytic-promoting enzyme, PFKFB3, is an APC/C-Cdh1 substrate, we reasoned that NMDAR stimulation, through inhibition of APC/C-Cdh1, should stabilize PFKFB3. To test this hypothesis, we incubated neurons with glutamate (100 μM) to stimulate NMDAR for 15 minutes, cells were washed and further incubated in culture medium; in these, we analyzed Cdh1 phosphorylated status and protein levels of PFKFB3 were analyzed at different time points by western blotting. To test Cdh1 phosphorylation, Cdh1 was immunoprecipitated from neuronal protein lysates 6 h after glutamate treatment, and the immunoprecipitate subjected to western blotting against an anti-phosphoserine antibody. As shown in Fig. 8a, glutamate treatment triggered, as expected, an increase in phosphorylated Cdh1, an effect that was fully prevented by MK801. This indicates that under these conditions, NMDAR stimulation inhibits APC/C-Cdh1 activity according to our previous observations. Analysis of PFKFB3 protein by western blotting revealed that glutamate treatment triggered a time-dependent increase in PFKFB3, an effect that was maximal (~2.1-fold higher) after 6 h (Fig. 8b). To test whether this effect was mediated by NMDAR, neurons were incubated with NMDA (100 μM for 15 min), and PFKFB3 protein levels analyzed 6 h later. As depicted in Figure 8c, NMDA mimicked glutamate at increasing PFKFB3; moreover, incubation of neurons with MK801 prevented glutamate-mediated increase in PFKFB3 after 6 hours (Figure 8d). Together, these data indicate that NMDAR stimulation inhibits APC/C-Cdh1 activity leading to PFKFB3 protein stabilization in primary neurons.

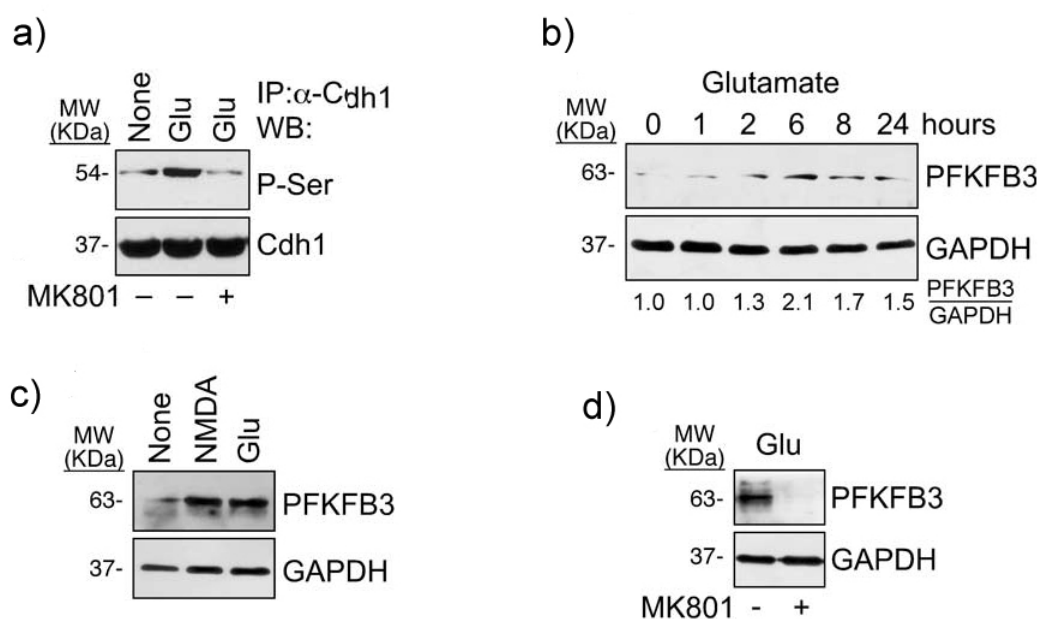


Figure 8. a) *Cdh1* is phosphorylated 6 h after glutamate treatment (100 μ M/15 min), an effect that was prevented by MK801 (10 μ M). b) Incubation of neurons with glutamate (100 μ M/15 min) triggered time-dependent increase in PFKFB3 protein, which was maximal after 6 h. c) NMDA (100 μ M/15 min) mimicked glutamate at increasing PFKFB3. d) NMDA receptor antagonist, MK801 (10 μ M), prevented glutamate-mediated increase in PFKFB3.

9. NMDAR STIMULATION DOES NOT ALTER THE PFKFB3 mRNA LEVELS IN NEURONS.

To elucidate whether the increase in PFKFB3 protein abundance could be due to any transcriptional effect, the PFKFB3 mRNA levels were analyzed by reverse transcription-PCR after 2 and 6 hours of glutamate (100 μ M/15 min) treatment of neurons at 6 days in culture. As shown in Fig. 9, the PFKFB3 mRNA levels remained unchanged after NMDAR stimulation, suggesting that PFKFB3 protein accumulation was not a consequence of increased *PFKFB3* gene transcription or PFKFB3 mRNA stabilization. Rather, our data strongly suggest that the increase in PFKFB protein abundance by NMDAR stimulation was due to protein stabilization.

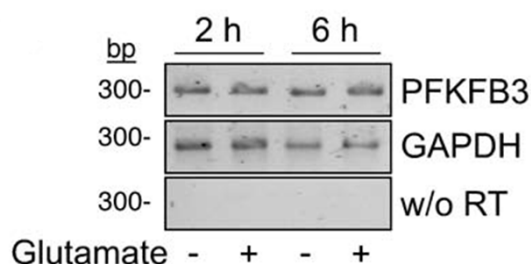


Figure 9. Glutamate (100 μ M/15 min) did not change PFKFB3 mRNA levels, as revealed by the unaltered intensity of the predicted 300 bp band after reverse-transcription of total RNA samples, followed by polymerase chain reaction (RT-PCR) using specific oligonucleotides for PFKFB3; GAPDH (279 bp band) was used as loading control; the black/white inverted images of the agarose gels are shown; w/o RT, RT-PCR for PFKFB3 without reverse transcriptase.

10. NMDAR STIMULATION TRIGGERS NUCLEUS-TO-CYTOSOL PFKFB3 TRANSLOCATION

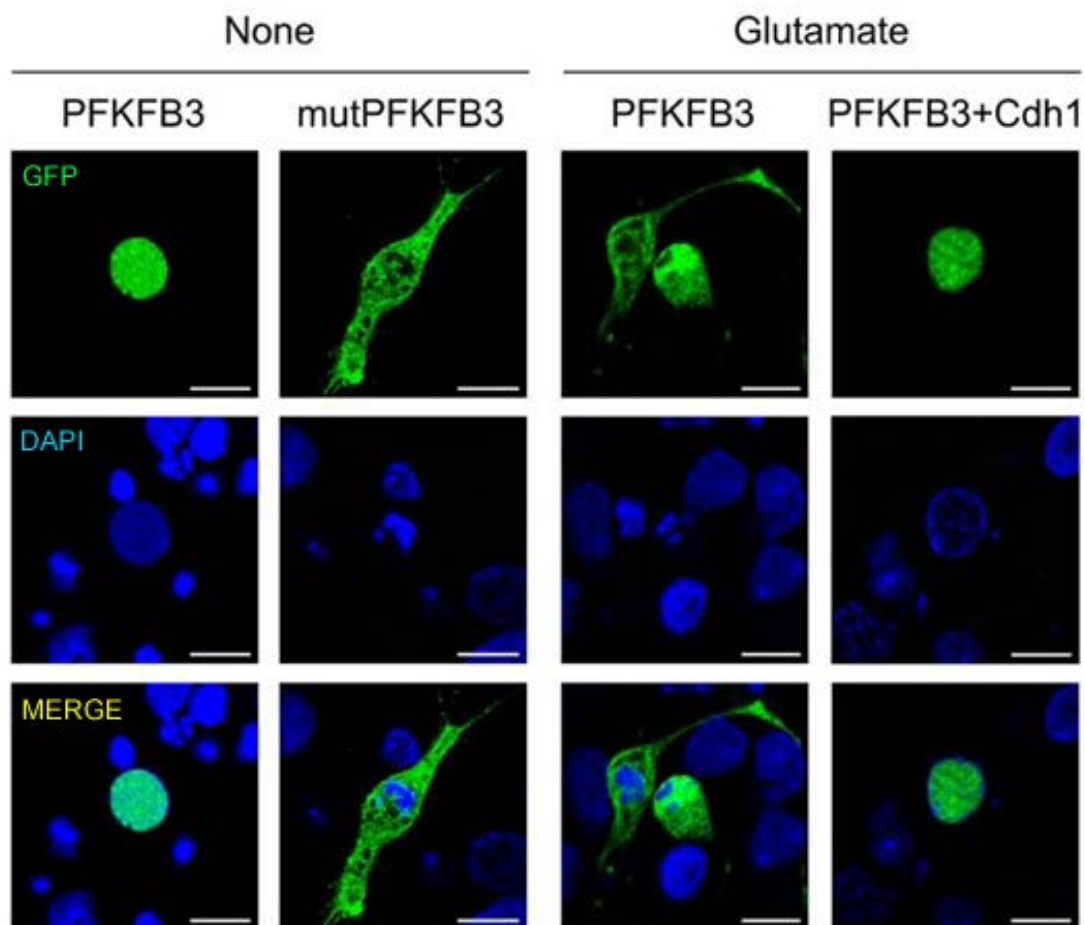
In view that our data indicate that PFKFB3 protein is continuously degraded by APC/C-Cdh1 activity, and that active APC/C-Cdh1 is thought to be confined in the nucleus, we next aimed to investigate the intracellular localization of PFKFB3 protein. We first tried to ascertain this issue using the endogenous accumulation of PFKFB3 after NMDAR stimulation. Unfortunately, the results were not conclusive in view that i) the antibody against PFKFB3 is not useful for immunocytochemistry, and ii) the low abundance of endogenous PFKFB3 in neurons makes it to be hardly detectable (not shown). To circumvent this drawback, we decided to register changes in PFKFB3 localization using expressed green fluorescent protein (GFP)-PFKFB3 fusion protein. To do so, we designed and constructed two versions of GFP-PFKFB3 fusion cDNAs, namely i) the wild type one (PFKFB3), and ii) a mutant form in which the motif responsible for PFKFB3 destabilization (¹⁴²Lys-Glu-Asn or KEN box), was replaced by ¹⁴²Ala-Ala-Ala (AAA) (mutPFKFB3). Thus, the mutant form of PFKFB3 would not be expected to be recognized by Cdh1 for APC/C-Cdh1 ubiquitylation, hence being constitutively stable.

Neurons were, thus, transfected with low amounts (0.16 μ g per well) of either GFP-fusion plasmid DNA vectors (PFKFB3 or mutPFKFB3), and the intracellular localization of the

RESULTS

expressed proteins analyzed by confocal microscopy. As shown in Fig. 10a, expression of wild type PFKFB3 cDNA confined PFKFB3 protein to the nucleus, as judged by the co-localization of GFP fluorescence with nuclear staining with DAPI. However, expression of the mutant form of PFKFB3 insensitive to APC/C-Cdh1 yielded a spread PFKFB3 protein localization, indicating the presence of PFKFB3 protein outside the nucleus (Fig. 10a). Quantification of these observations revealed the preferential nuclear localization of wild type PFKFB3 protein, and the preferential cytoplasmic expression of mutPFKFB3 (Fig, 10b). Treatment of neurons with glutamate (100 μ M / 15 min) led PFKFB3, after 6 h, to spread throughout the cytoplasm (Fig. 10a, b); interestingly, this spread localization of PFKFB3 was prevented by Cdh1 over-expression (Fig. 10a,b), confining PFKFB3 to the nucleus. Together, these results indicate that PFKFB3 protein is localized in the nucleus, where is it targeted for degradation by APC/C-Cdh1; however, glutamate treatment, by inhibiting APC/C-Cdh1 activity, stabilizes PFKFB3, which leaves the nucleus. Whether these changes in PFKFB3 stability and subcellular localization are able to alter the flux of glucose through glycolysis, were our next objective.

a)



b)

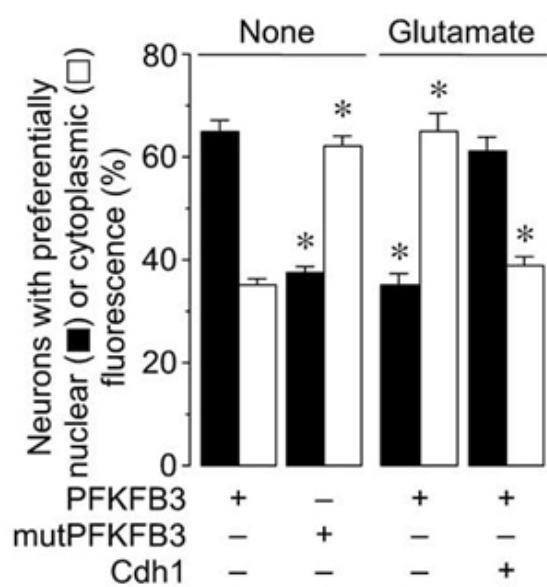


*Figure 10. a) Confocal microscopy images of neurons transfected with GFP-PFKFB3 reveals its nuclear localization. Glutamate promotes PFKFB3 accumulation, as revealed by its spread (nuclear plus cytosolic) localization; Cdh1 overexpression prevented this effect. GFP-PFKFB3, mutated on its KEN box (KEN-AAA; mut-PFKFB3) showed the spread-like localization, regardless of glutamate treatment. b) Percentage of neurons showing nuclear or spread GFP-PFKFB3 localization; these data were obtained by analyzing ~30 neurons per condition per neuronal preparation (n=4). *P<0.05 versus the corresponding (nuclear or cytoplasmic) PFKFB3-none condition (ANOVA).*

11. NMDAR STIMULATION INCREASES THE RATE OF GLYCOLYSIS AND DECREASES THE RATE OF PPP THROUGH PFKFB3.

PFKFB3 activity, by synthesizing F26BP, is known to promote glycolysis in neurons. In view that NMDAR triggered PFKFB3 protein stabilization, we next aimed to elucidate whether this effect exerted functional consequences. To do so, the rate of glycolysis was determined in neurons 6 h after NMDAR stimulation using the conversion of [3-³H]glucose into ³H₂O. As shown in Fig. 11a, NMDAR stimulation led neurons to an increase in the rate of glycolysis; furthermore, to ensure that this effect was due to PFKFB3 stabilization, we designed a siRNA targeted against PFKFB3 (siPFKFB3), which efficiency was first tested by western blotting. To do so, the GFP-PFKFB3 construct was expressed in neurons, which resulted in PFKFB3 accumulation as judged by the band intensity using an anti-GFP antibody (Fig 11b); however, transfection of neurons with the siPFKFB3 decreased PFKFB3 abundance (Fig. 11b). Furthermore, glutamate treatment triggered an increase in the GFP-PFKFB3 band intensity, suggesting PFKFB3 stabilization, an effect that was also prevented by siPFKFB3 (Fig 11b). These results indicate the efficacy of the siPFKFB3 strategy. As shown in Fig. 11a, the increase in the rate of glycolysis triggered by glutamate was prevented in neurons previously transfected with the siPFKFB3, indicating that PFKFB3 stabilization was responsible for the increase in the rate of glycolysis. Furthermore, in view that our previous results showed that glycolysis and PPP are dynamically coupled in neurons (see Figs. 1 and 2), we also investigated whether NMDAR-mediated increase in the rate of glycolysis affected the rate of PPP. As shown in Fig. 11c, neurons treated with glutamate (100 μ M / 15 min) showed, 6 h later, a significant reduction in the rate of glucose oxidation through the PPP, an effect that was wholly prevented by siPFKFB3.

Thus, our results indicate that NMDAR stimulation in neurons triggers a Ca^{2+} -mediated inhibition of APC/C-Cdh1 activity leading to PFKFB3 stabilization in the cytosol leading to a shift of glucose metabolism consisting of glycolysis activation and PPP inhibition.

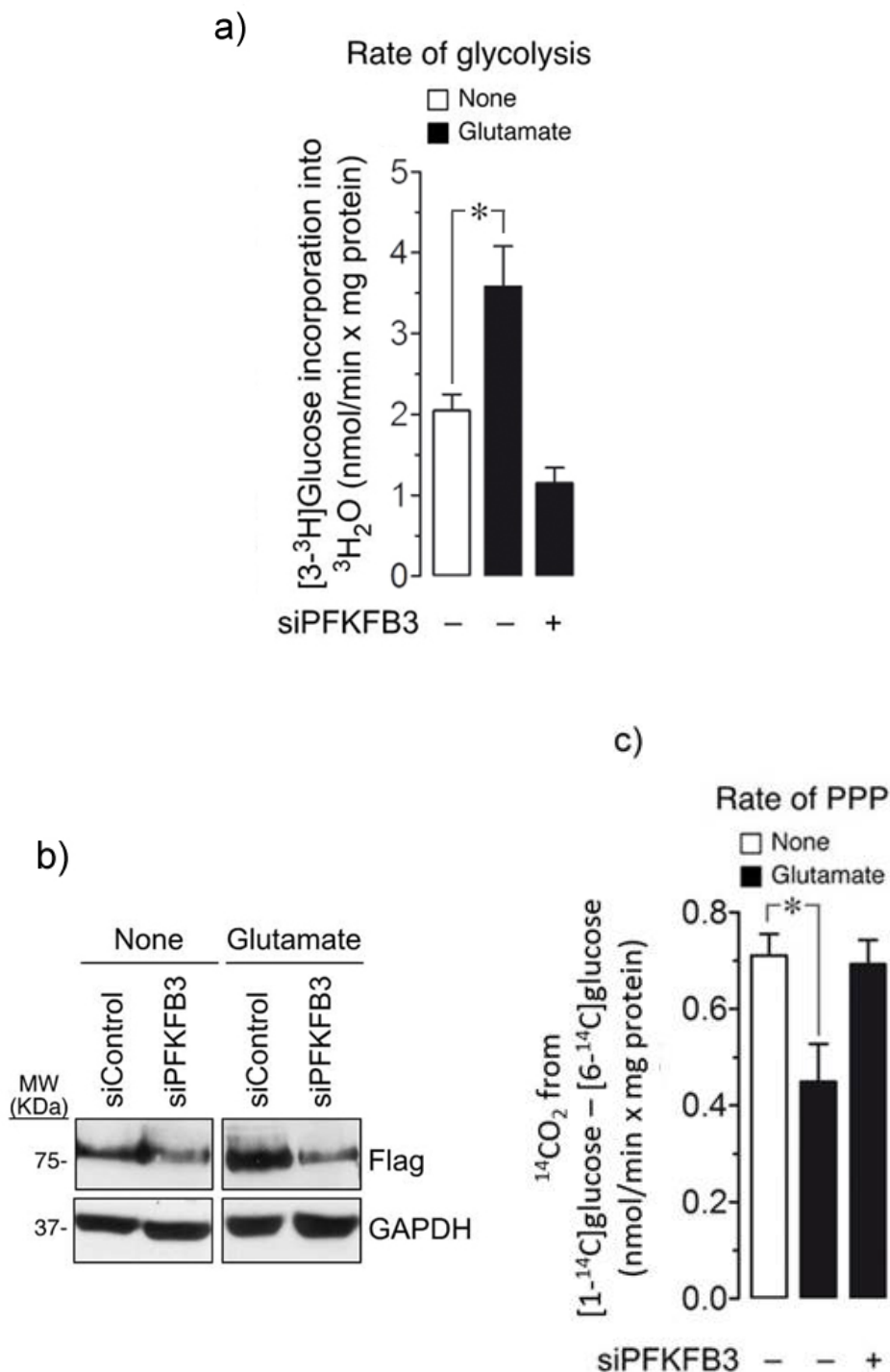


Figure 11. a) Incubation of neurons with glutamate ($100\ \mu\text{M}/15\ \text{min}$) increased, after 6 h, the rate of glycolysis, as assessed by the determination of [$3\text{-}^3\text{H}$]glucose incorporation into $^3\text{H}_2\text{O}$; this effect was abolished by preventing PFKFB3 accumulation in neurons

RESULTS

previously transfected with siPFKFB3. b) Incubation of GFP-PFKFB3-expressing neurons with glutamate (100 μ M/15 min) induced, 6 h after treatment, PFKFB3 accumulation in siRNAControl (100nM) treated neurons, as revealed by an anti-GFP (Flag) antibody; transfection of neurons with an siPFKFB3 (100nM) efficiently reduced PFKFB3 protein and prevented glutamate-induced PFKFB3 accumulation. c) Glutamate treatment decreased, after 6 h, the rate of the PPP, as assessed by the determination of the difference between $^{14}\text{CO}_2$ produced by [1- ^{14}C]glucose and that of [6- ^{14}C]glucose; this effect was abolished by siPFKFB3. * $P < 0.05$ (ANOVA)($n=3$).

12. NMDAR STIMULATION LEADS TO IMPAIRMENT OF GLUTATHIONE REGENERATION THAT IS MEDIATED BY PFKFB3 STABILIZATION.

Glucose oxidation through the PPP regenerates NADPH(H^+), a cofactor of several important enzymes including glutathione reductase. Glutathione reductase requires continuous supply of NADPH(H^+) to regenerate glutathione (GSH) from its oxidized form, glutathione disulfide (GSSG). Accordingly, in view that NMDAR stimulation led to an increase in glycolysis leading to reduced PPP activity, we reasoned whether the decreased PPP activity would result in the impairment in the ability of neurons to regenerate GSH from GSSG. To do so, we analyzed total (GSx) and oxidized (GSSG) glutathione in neurons 6 h after NMDAR stimulation. As shown in Fig. 12, glutamate treatment did not alter total glutathione concentration, but significantly increased its oxidized form; this caused an increase in the oxidized versus total oxidized glutathione (GSSG/GSx) ratio, a well-known index of the oxidized glutathione redox status. All these changes were partially prevented by siPFKFB3, indicating that they were, at least in part, caused by PFKFB3 stabilization after NMDAR stimulation.

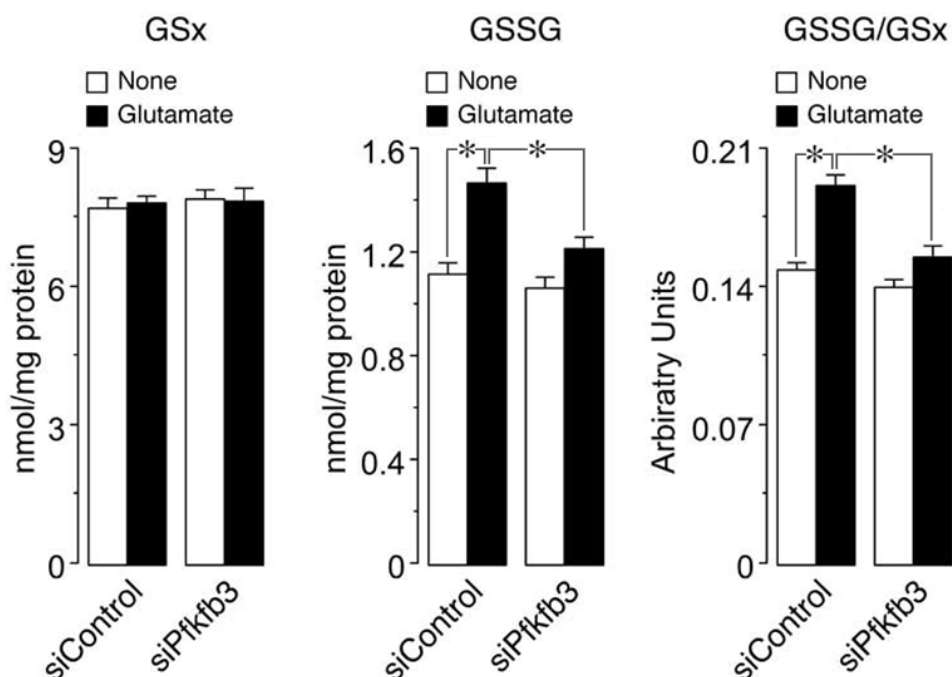


Figure 12. Glutamate treatment did not change GSx (left panel), but it increased GSSG (middle panel) and the oxidized glutathione redox status (GSSG/GSx; right panel); these effects were partially prevented by siPFKFB3. Neurons at day 3 in culture were transfected either with siControl or siPFKFB3 (100 nM). At day 6 they were treated with glutamate (100 μ M/15 min) and the cell extracts used for glutathione determination. * $P < 0.05$ (ANOVA) ($n=3$).

13. THE PPP TO GLYCOLYSIS SHIFT CAUSED BY NMDAR STIMULATION TRIGGERS OXIDATIVE STRESS

In view that reduced glutathione is known to be essential in the detoxification of mitochondrial reactive oxygen species (ROS), we reasoned that the NMDAR-mediated increase in oxidized glutathione would result in oxidative stress. To assess this issue, we analyzed the abundance of mitochondrial ROS using the specific probe, MitoSox, which determines mitochondrial superoxide anion abundance ($O_2^{\cdot-}$). As shown in Fig. 13a, treatment of neurons with glutamate (100 μ M / 15 min) triggered, after 16 h, a significant increase in mitochondrial superoxide, suggesting oxidative stress. Furthermore, this effect was mostly prevented by knocking down PGI with siPGI (Fig. 13a), a treatment that, on our hands, was able to increase the rate of PPP as shown in Fig. 4b. Furthermore, to test if this effect was a consequence of increased glycolysis, we knocked down PFKFB3 and, thereafter, treated neurons with glutamate. As shown in Fig, 13a,

RESULTS

siPFKFB3 mostly prevented the increase in mitochondrial superoxide. To further support the notion that NMDAR-mediated oxidative stress was, at least in part, a consequence of the inhibition of PPP activity, we next aimed to investigate if this effect was counteracted by overexpressing G6PD, i.e. the rate-limiting enzyme of the PPP. As shown in Fig. 13b, expression of the full-length cDNA coding G6PD led to a significant increase in G6PD protein, and this effect was sufficient to fully rescue the increase in mitochondrial superoxide caused by NMDAR (Fig. 13a). Finally, we tested that the observed effect on mitochondrial superoxide was a wholly consequence of NMDAR stimulation, as judged by the full protection triggered by the NMDA antagonist, MK801 (Fig. 13b).

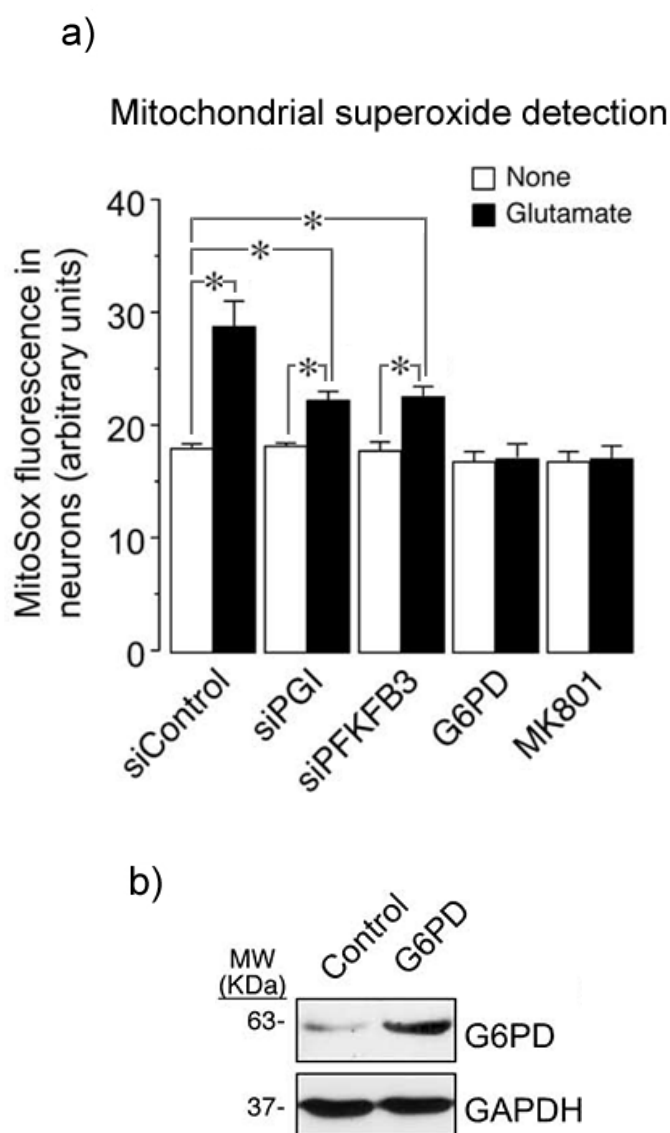


Figure 13. (a) Glutamate treatment (100 μ M/15 min) increased mitochondrial superoxide levels in neurons, as assessed by flow cytometry measurement of MitoSox fluorescence; this effect was prevented by knocking down PGI (siPGI) or PFKFB3 (siPFKFB3),

overexpressing G6PD, or blocking NMDAR with MK801 (10 μ M). b) Transfection of neurons with the full-length DNA encoding G6PD (1.6 μ g/ml) efficiently increased G6PD protein abundance. * P <0.05. (ANOVA)(n =3).

14. NMDAR ACTIVATION TRIGGERS APOPTOTIC DEATH BY SWITCHING PPP TO GLYCOLYSIS.

Given that NMDAR stimulation led to oxidative stress as a consequence of PPP shift to glycolysis, and that oxidative stress is known to cause neuronal death, we next aimed to investigate if the metabolic switch by NMDAR targeted neurons to apoptotic death. To do so, neurons treated with glutamate (100 μ M / 15 min) were incubated, 16 h later, with anti-annexin V and 7AAD, to assess neurons targeted to apoptosis by flow cytometry. As shown in Fig. 14, the proportion of annexin V⁺/7AAD⁻ neurons increased significantly by glutamate treatment, an effect that was partially prevented by PGI or PFKFB3 knock down, as well as by overexpressing G6PD or blocking NMDAR with MK801. Thus, NMDAR stimulation promotes apoptotic death of neurons as a consequence of the shift of PPP to glycolysis.

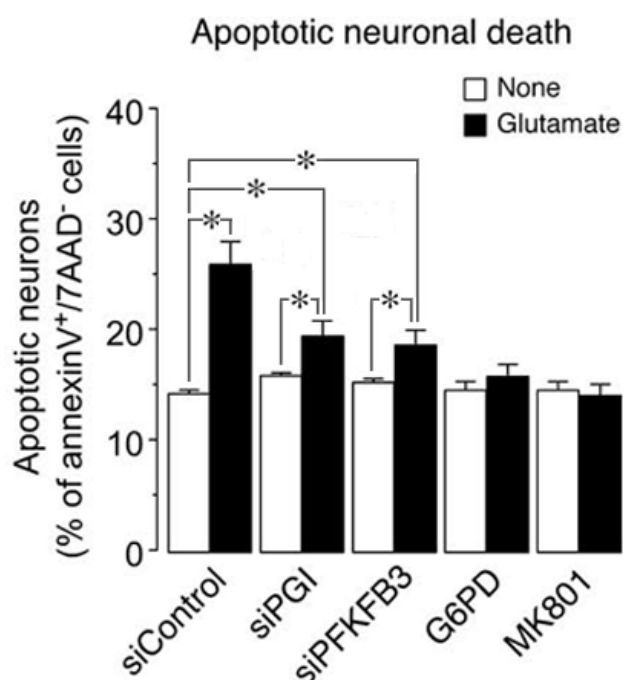


Figure 14. Glutamate treatment increased apoptotic neuronal death, as assessed by determining annexin V⁺/7AAD⁻ neurons fluorescence by flow cytometry; this effect was prevented by silencing PGI (siPGI, 100nM) or PFKFB3 (siPFKFB3, 100nM), overexpressing G6PD (1.6 μ g/ml) or blocking NMDAR with MK801 (10 μ M). * P <0.05. (ANOVA)(n =3).

15. EXPRESSION OF A MUTANT FORM OF PFKFB3 INSENSITIVE TO APC/C-Cdh1 MIMICS NMDAR AT CAUSING OXIDATIVE STRESS AND NEURONAL DEATH.

To further support the notion that PFKFB3 stabilization after APC/C-Cdh1 inhibition is responsible for the metabolic shift, oxidative stress and apoptosis, we next aimed to investigate whether this phenotype could be mimicked by expressing the mutant form of PFKFB3 insensitive to APC/C-Cdh1. As shown in Fig. 15a, incubation of PFKFB3-expressing neurons with glutamate (100 μ M / 15 min) increased mitochondrial superoxide abundance. Interestingly, expression of the APC/C-Cdh1-insensitive form of PFKFB3 (mutPFKFB3) yielded neurons with a similar level of mitochondrial superoxide, an effect that was not further increased by glutamate (Fig. 15a). Analysis of apoptotic neurons under these conditions yielded identical results (Fig. 15b). Together, these results indicate that, after NMDAR stimulation leading to APC/C-Cdh1 inhibition, PFKFB3 is stabilized causing increased glycolysis and reduced PPP activity, which triggers glutathione oxidation and apoptotic death. Thus, PFKFB3 should be considered as an interesting therapeutic target in the treatment of disorders of the central nervous system in which excessive glutamatergic neurotransmission (excitotoxicity) has been documented, such as stroke.

a)

b)

Mitochondrial superoxide detection

Apoptotic neuronal death

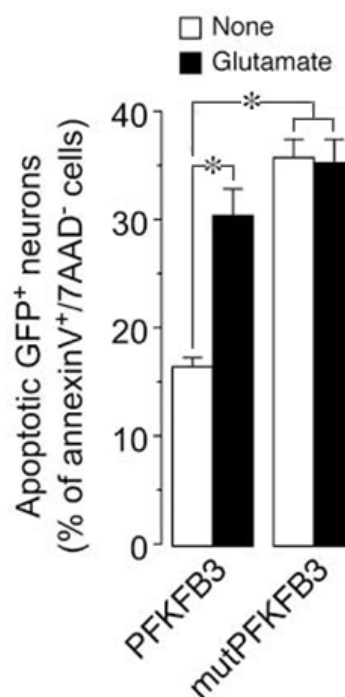
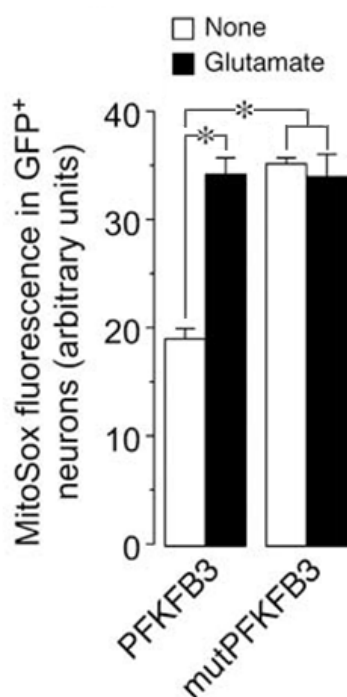


Figure 15. a) Glutamate treatment (100 μ M/15 min) increased mitochondrial superoxide levels in neurons transfected with low levels of wild-type PFKFB3 cDNA (0.16 μ g/ml); transfection of neurons with identical cDNA amounts of the KEN box-mut-PFKFB3 increased superoxide to similar levels to those triggered by glutamate; glutamate did not further enhance superoxide in neurons expressing mut-PFKFB3. b) Glutamate increased apoptotic death of neurons transfected with low levels of PFKFB3 cDNA; transfection of neurons with identical cDNA amounts of mut-PFKFB3 increased apoptotic death to similar levels to those triggered by glutamate; glutamate did not further enhance apoptotic death in neurons expressing mut-PFKFB3. * $P < 0.05$ (ANOVA)($n=3$).

16. THE FRUCTOSE-2,6-BISPHOSPHATASE TIGAR PROTEIN IS EXPRESSED IN NEURONS

Recently, it was discovered a Tp53-inducible glycolysis and apoptotic regulator (TIGAR) that has fructose-2,6-bisphosphatase activity. In view that TIGAR would exert the opposite metabolic effect to PFKFB3, we wondered whether the regulation of glycolysis in neurons would be a function of both TIGAR and PFKFB3. To the best of our knowledge, the expression of TIGAR in brain cells has not been reported. Accordingly, we first aimed to investigate its protein expression in rat cortical neurons and astrocytes in primary culture, by western blotting. As observed in Fig. 16, TIGAR protein is expressed in both cell types, being slightly higher in neurons.

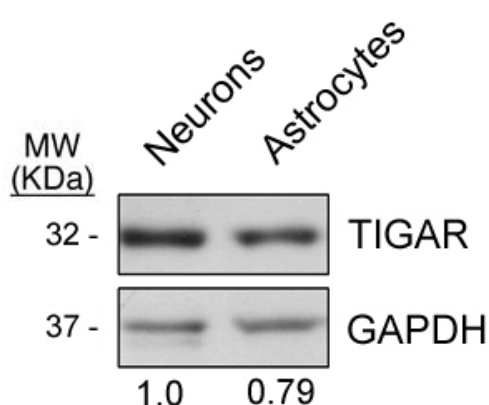


Figure 16. TIGAR is present in both neurons and astrocytes and neurons express higher levels of the protein. Neurons at 6 days in culture and astrocytes at day 15 were lysed in RIPA buffer and subjected to western blot analysis of the levels of TIGAR.

17. ASSESSMENT OF APOPTOSIS AND SUPEROXIDE LEVELS IN PRIMARY NEURONS FROM TIGAR KNOCKOUT MICE

Since TIGAR exerts the opposite metabolic effect of PFKFB3, and we previously observed that PFKFB3 over-expression triggers oxidative stress and apoptotic death, we next aimed to investigate whether the lack of TIGAR mimicked PFKFB3 over-expression. To do so, we first used the knockout approach in view that TIGAR knockout mice were available at the Dr. Karen Vousden's group (Beatson Institute for Cancer Research, Glasgow, UK). Thus, cortical primary neurons from TIGAR knockout mice were performed and superoxide and apoptotic death were investigated. As observed in Fig. 17a and b, neither mitochondrial superoxide abundance nor apoptotic death was significantly increased in TIGAR knockout neurons. However, we reasoned the possibility that glucose metabolism in the TIGAR knockout mice might be compensated thus avoiding the observation of a strong phenotype. Accordingly, we next aimed to modulate TIGAR expression acutely using both over-expression and a knockdown approaches.

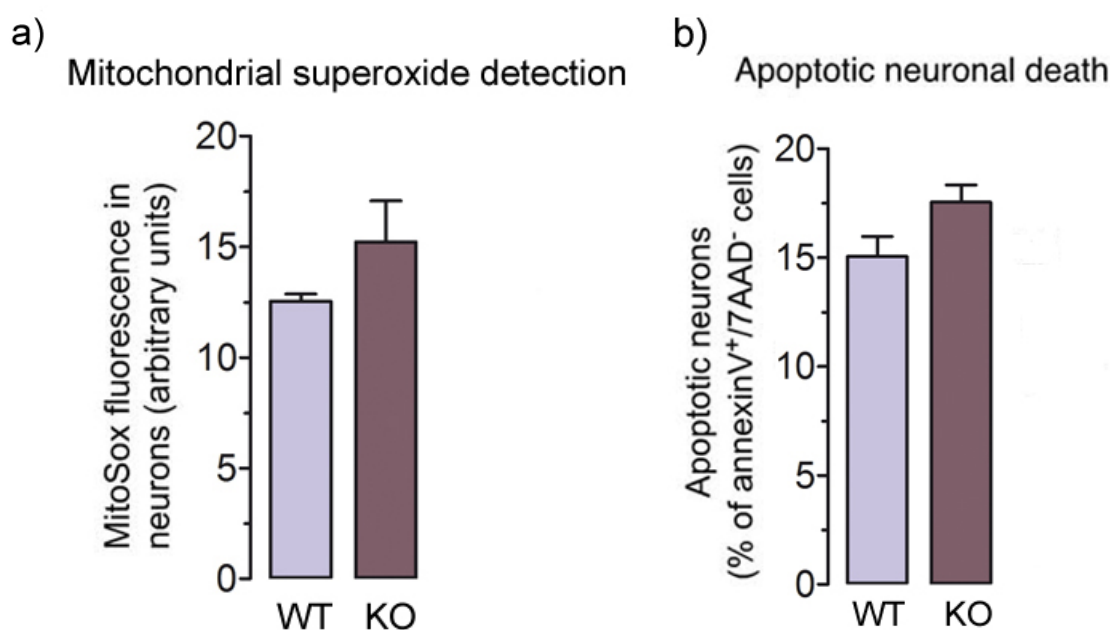


Figure 17. Mitochondrial superoxide levels detection and apoptotic neuronal death in TIGAR WT vs KO mice neurons at 6 days in culture. a) TIGAR KO mice exhibit superoxide levels similar to the WT, as assessed by flow cytometric analysis of MitoSox-RedTM fluorescence. b) TIGAR KO neurons don't show significant increase in apoptosis levels, as assessed by annexin V⁺/7AAD⁻ fluorescence by flow cytometry. (ANOVA).

18. OVER-EXPRESSION OF THE FULL-LENGTH TIGAR cDNA DECREASES FRUCTOSE-2,6-BISPHOSPHATE CONCENTRATION

We first obtained the full-length cDNA coding for TIGAR, which was generously donated by Prof. R. Bartrons (University of Barcelona) and inserted it into peGFP-C1 plasmid vector, which express the GFP-TIGAR fusion protein under the control of the cytomegalovirus promoter. Expression of this plasmid in human embryonic kidney cells (HEK293T) caused a significant decrease in the concentrations of fructose-2,6-bisphosphate when compared with cells transfected with the empty vector (control) (Fig 18). Thus, the peGFP-C1 TIGAR construct is functional.

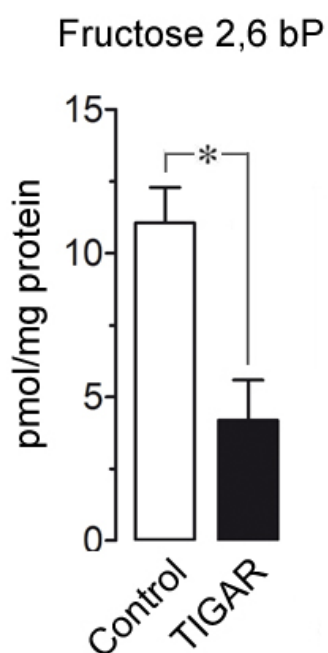


Figure 18. *peGFP-C1 TIGAR expression in HEK293T successfully decreases fructose-2,6-bisphosphate levels. HEK293T cells were transfected with either peGFP-C1 TIGAR plasmid construction or empty vector (1.6 $\mu\text{g/ml}$) and fructose 2,6 bisphosphate concentrations were measured 24 hours post-transfection. * $P < 0.05$ (ANOVA)($n=3$).*

19. TIGAR PREVENTS PFKFB3-INDUCED INCREASE IN MITOCHONDRIAL SUPEROXIDE AND NEURONAL DEATH

We next decided to investigate whether the TIGAR-PFKFB3 axis, by their ability to inversely regulate glycolysis, controls superoxide abundance and neuronal survival. To do so, the APC/C-Cdh1-insensitive form of PFKFB3 (mutPFKFB3) was expressed, at a very low concentrations (0.16 $\mu\text{g/ml}$) in rat cortical primary neurons, which –as previously shown– triggered significant increases in mitochondrial superoxide and apoptotic neuronal death (Figs. 19a,b), as assessed by flow cytometry. Interestingly, co-expression of TIGAR at high concentration (1.6 $\mu\text{g/ml}$) fully rescued these effects (Figs. 19a,b). Thus, oxidative stress and apoptotic neuronal death appears to be controlled by the TIGAR-PFKFB3 axis, at least at the light of over-expression experiments.

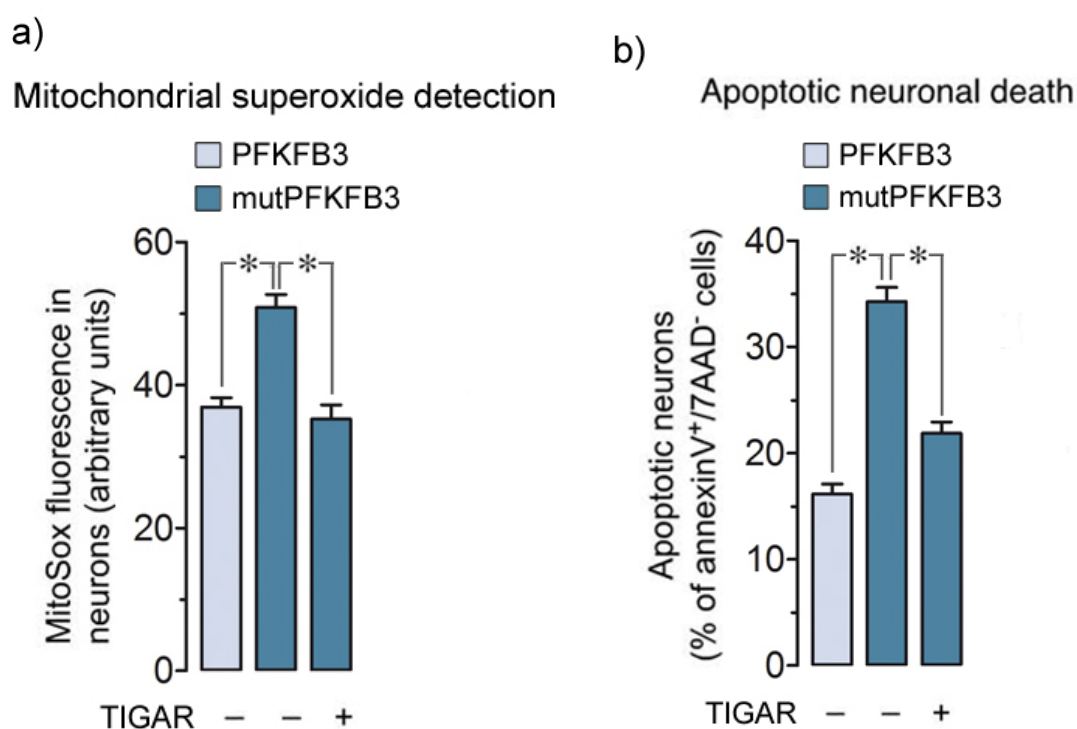


Figure 19 a) Transfection of neurons with low levels of mutPFKFB3 (0.16 $\mu\text{g/ml}$) increases mitochondrial superoxide when compared with the same levels of PFKFB3, as assessed by flow cytometric analysis of MitoSox-RedTM fluorescence. The increase in mitochondrial superoxide is prevented by overexpressing TIGAR (1.6 $\mu\text{g/ml}$). b) Transfection of neurons with low levels of mutPFKFB3 leads to apoptotic cell death that is prevented by overexpressing TIGAR, as assessed by annexin V⁺/7AAD⁻ fluorescence by flow cytometry. * $P < 0.05$ (ANOVA)($n=3$).

20. KNOCKDOWN OF TIGAR IS NOT SUFFICIENT TO INCREASE THE RATE OF GLYCOLYSIS IN PRIMARY NEURONS

In view that we were unable to show more vulnerable neurons to oxidative stress and apoptotic death in TIGAR knockout mice, we decided to acutely knockdown it in mice primary neurons. To do so, we designed a small interfering RNA (siRNA) sequence targeted against *Mus musculus* TIGAR (siTIGAR). Transfection of primary neurons with siTIGAR resulted in a considerable –albeit not full– decrease in TIGAR protein after 3 days (Fig. 20a). However, we were unable to detect any statistically significant increase in the rate of glycolysis in siTIGAR-transfected neurons when compared with siControl-transfected cells (Fig. 20b).

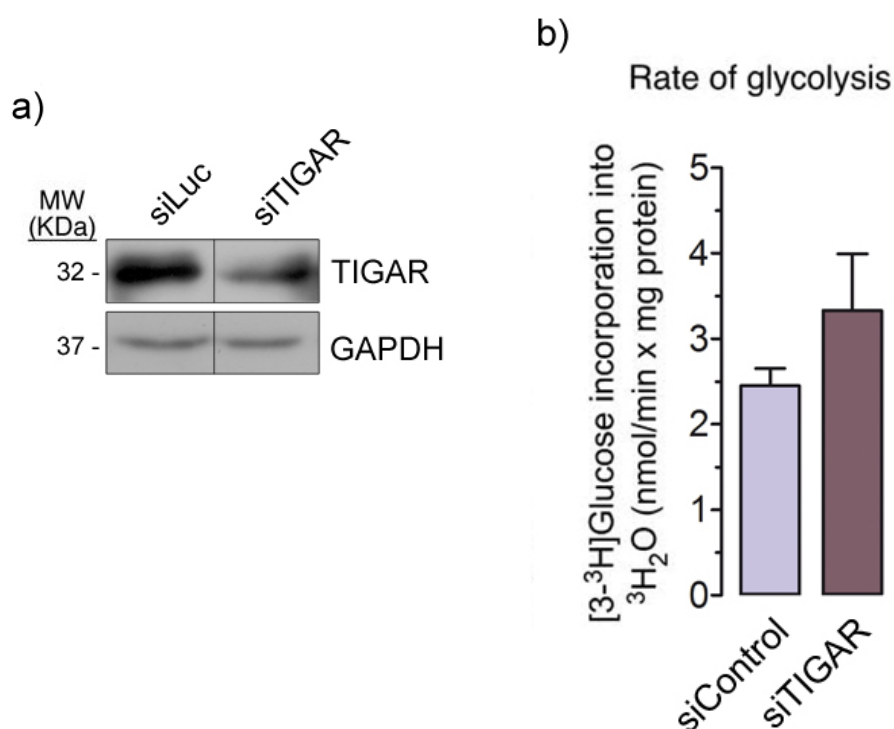


Figure 20. a) TIGAR siRNA efficiently knocks down protein levels in neurons 3 days after transfection. Neurons at day 3 in culture were transfected either with siControl or siTIGAR (20 nM). At day 6 in culture cells were lysed and the protein levels analyzed by western blot. b) Glycolytic rate does not significantly increase upon TIGAR silencing in neurons. Neurons at day 3 in culture were transfected either with siControl or siTIGAR (20 nM) at day 6 in culture glycolytic rate was assessed by the determination of [3-³H]glucose incorporation into ³H₂O. (ANOVA)(n=3).

21. KNOCKDOWN OF TIGAR INCREASES APOPTOTIC NEURONAL DEATH WITHOUT INCREASING SUPEROXIDE

In view that the results on superoxide and survival obtained by over-expressing TIGAR (Fig. 19) were apparently inconsistent with those on glycolysis obtained by knocking down TIGAR (Fig. 20), we decided to investigate superoxide and neuronal survival in TIGAR knockdown neurons. Thus, mice primary neurons were transfected with siTIGAR to knockdown it, followed by incubation in the absence or presence of glutamate (100 μ M / 15 min) to stimulate the NMDAR. As shown in Fig. 21a, siTIGAR did not increase mitochondrial superoxide abundance. However, glutamate treatment did increase superoxide, although this was not potentiated by siTIGAR (Fig. 21a). Interestingly, siTIGAR, as did glutamate, increased apoptotic neuronal death (Fig. 21b); furthermore, siTIGAR potentiated glutamate-induced neuronal death (Fig. 21b). Altogether, our data suggest that, besides its possible control on fructose-2,6-bisphosphate concentrations and glycolysis, TIGAR may play a yet not deciphered role on neuronal survival that is independent on the glycolytic-PPP shift that PFKFB3 exerts.

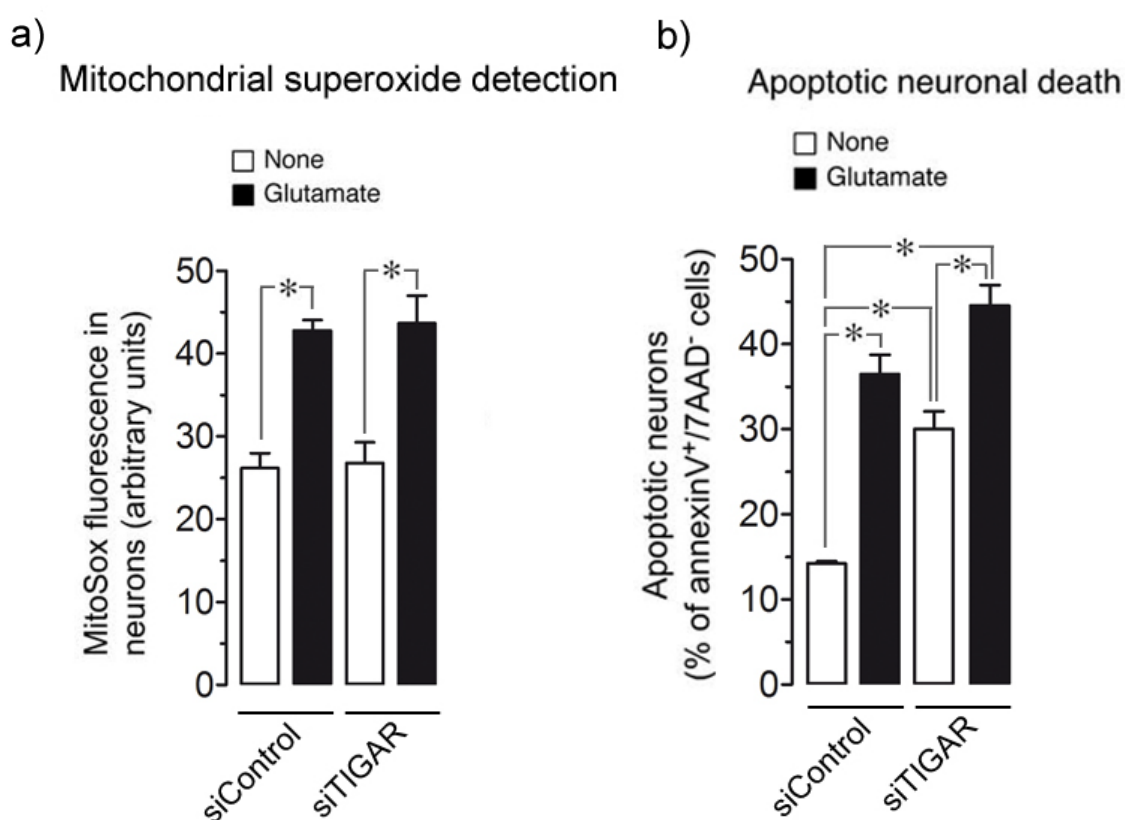


Figure 21. a) Mitochondrial superoxide detection increases by glutamate treatment, but not by siRNA TIGAR, as assessed by flow cytometric analysis of MitoSox-Red™ fluorescence. b) Apoptotic neuronal death increases by siTIGAR in neurons, as assessed by annexin V⁺/7AAD⁻ fluorescence by flow cytometry. * $P < 0.05$ (ANOVA)($n=3$).

22. CONFOCAL ANALYSIS REVEALS NUCLEAR LOCALIZATION OF TIGAR IN NEURONS, BUT NOT IN ASTROCYTES

As an attempt to obtain any clue to explain the metabolic-independent control of neuronal survival by TIGAR, we decided to investigate its subcellular localization. To do so, we performed primary cultures of neurons and mixed neurons-astrocytes from the E16 mice brain cortex. Endogenous TIGAR was then analyzed by immunofluorescence in a confocal microscope. As shown in Fig. 22, endogenous TIGAR expression was spread in neurons, including in the nucleus as judged by its co-localization with the nuclear-specific marker TOPRO-3. In contrast, we observed that TIGAR was exclusively present in the cytosol, not in the nucleus, of astrocytes (Fig. 22). These results suggest that, at least in neurons, TIGAR might exert a yet unknown cytoprotective function in the nucleus that remains to be elucidated.

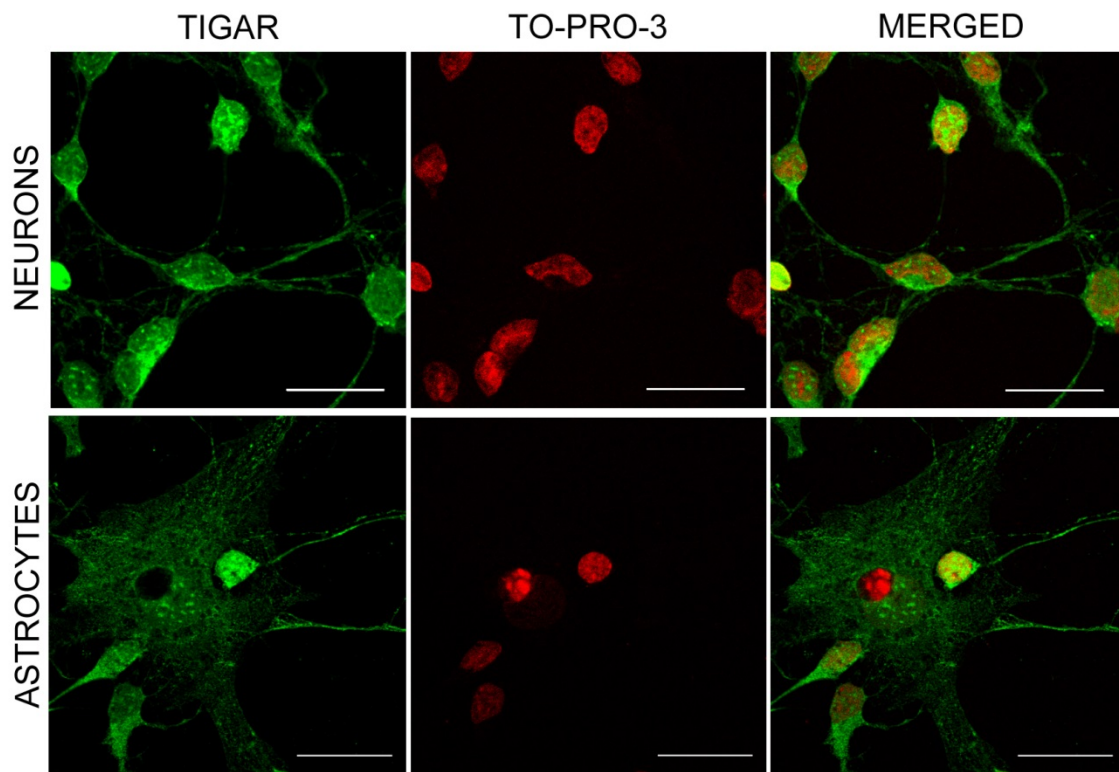
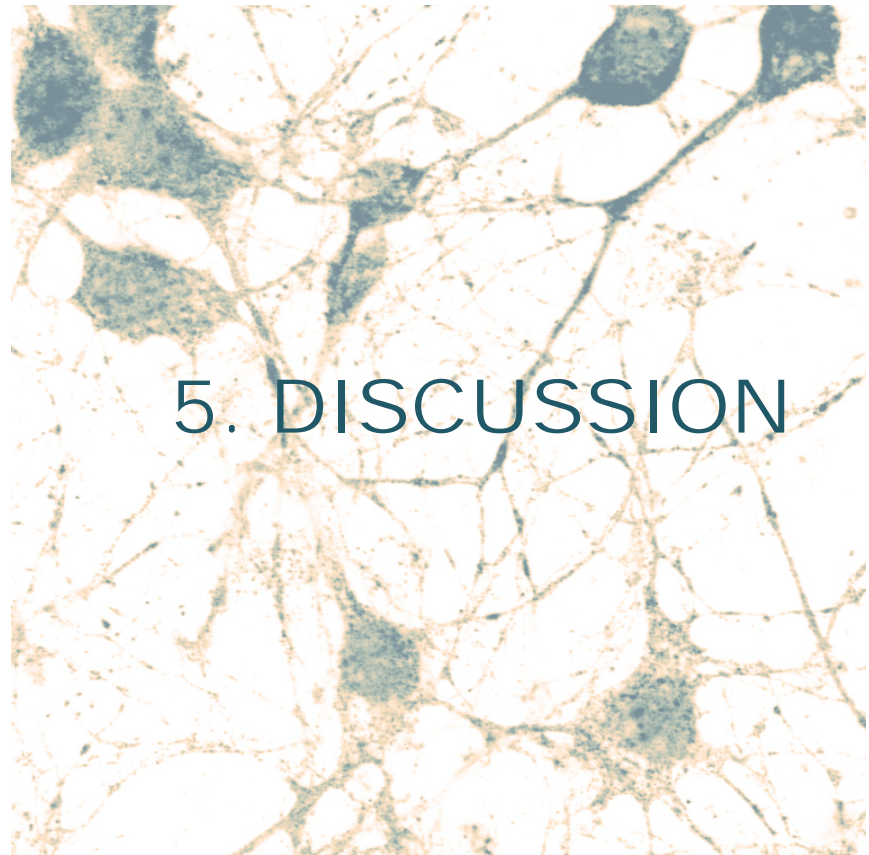


Figure 22. Immunofluorescence analysis of endogenous TIGAR shows a nuclear plus cytoplasmic localization of the protein in neurons, but an exclusive cytoplasmic localization in astrocytes. Cells were grown on glass coverslips and after the immunostaining, images were obtained in a confocal Leica SP5 microscope. Scale bar: 20 μm .



5. DISCUSSION

1. GLYCOLYSIS AND PPP ARE DYNAMIC PROCESSES IN INTACT NEURONS

The differential regulation of the activity of enzymes of glucose metabolism, as well as the complex interplay between cellular metabolic pathways, makes difficult the issue of accurately determining specific glucose-metabolizing fluxes. A common methodology to address this issue consists of determining the metabolites enrichments in ^{13}C , ^{14}C , ^1H or ^3H after incubating cells with appropriately labeled glucoses. The use of ^1H - and ^{13}C -glucose reveals the labeling pattern of intermediary metabolites after magnetic resonance spectroscopy (MRS) or mass spectrometry (MS) analyses, which provides indexes of cellular metabolic activity (Bouzier-Sore et al. 2006, Bak et al. 2006, Brekke *et al.* 2012). However, due to rapid equilibration of substrates through the different pathways, it is hard to discriminate the origin of the metabolic route and its flux.

We have previously used a method suitable to determine the glycolytic and PPP fluxes in detached neurons (Herrero-Mendez et al. 2009). To determine the glycolytic flux, we measured the rate of $[3\text{-}^3\text{H}]\text{glucose}$ incorporation into $^3\text{H}_2\text{O}$, that is produced in the reaction catalyzed by aldolase, thus specifically assessing the flux of glucose through PFK1-catalyzed reaction. $[3\text{-}^3\text{H}]\text{Glucose}$ conversion into $^3\text{H}_2\text{O}$ gives a more accurate index of the glycolytic flux than that of $[5\text{-}^3\text{H}]\text{glucose}$, a method chosen for other authors, since in the latter, $^3\text{H}_2\text{O}$ is produced at enolase, i.e. a reaction that operates after glyceraldehyde-3-phosphate that can be generated through the PPP; this would easily lead to an overestimation of the glycolytic flux, as has been previously described (Goodwin *et al.* 2001). We therefore used, in this work, the rate of conversion of $[3\text{-}^3\text{H}]\text{glucose}$ into $^3\text{H}_2\text{O}$. Moreover, to overcome the possible drawback of using detached cells, we developed a technique to determine the rate of glycolysis in intact, attached neurons, thus maintaining the integrity of axons and dendrites. Using this method, we report that the rate of the glycolytic flux in rat cortical neurons is ~ 1.2 nmol/min x mg protein; this value is slightly lower than that previously reported by our group in detached neurons (~ 2 nmol/min x mg protein). Possibly, detaching neurons from the plate might have caused some undetermined type of stress that affected glucose metabolism.

In view that glycolysis and PPP are interconnected pathways, we aimed to measure the rate of glucose oxidation through the PPP. We decided to use the method that calculates the difference of $^{14}\text{CO}_2$ produced from $[1\text{-}^{14}\text{C}]\text{glucose}$ and that produced from $[6\text{-}^{14}\text{C}]\text{glucose}$. The former is produced at 6-phosphogluconate dehydrogenase (6PGD)-

DISCUSSION

catalyzed reaction in the PPP and at the tricarboxylic acid (TCA) cycle; however, the latter is produced only at the TCA cycle. Using this approach, we report that attached, intact cortical primary neurons oxidize glucose through the PPP at a rate of ~ 0.2 nmol/min x mg protein, a value that is lower than that obtained in our own previous determinations in detached neurons (~ 0.7 nmol/min x mg protein). As for glycolysis, we therefore admit that detaching neurons might induce stress affecting glucose metabolism. Accordingly, the attached intact system that we herein set up is advantageous.

Assuming that most glucose consumption in neurons takes place through glycolysis and PPP, we therefore estimate that approximately 14% of glucose consumption in neurons is oxidized at the PPP. This value contrasts with the reported by other groups who estimated PPP values of $\sim 6\%$ of glucose consumption (Brekke et al. 2012). However, activation of glycolysis by over-expressing PFKFB3 dramatically reduces the rate of PPP (Herrero-Mendez et al. 2009) leading to oxidative stress and neuronal death, as did specific inhibition of G6PD with DHEA (Vaughn & Deshmukh 2008). Thus, the fraction of glucose entering the PPP appears to be highly relevant for neuronal survival, which questions that it would be wholly accounted by such a low proportion (6-14%) of glucose metabolized. We therefore hypothesized that the actual rate values of PPP obtained are underestimated.

To indirectly assess the fraction of glucose entering PPP, we first incubated neurons with DHEA to inhibit G6PD, the rate-limiting enzyme of the PPP, and measured the rate of glycolysis. We observed that the rate of glucose oxidized through the glycolytic flux increased by $\sim 100\%$ in the presence of DHEA; this result suggests that at least $\sim 50\%$ of glucose entering neurons is metabolized through the PPP. As expected, DHEA triggered a large increase in G6P concentrations; however, the flux through PPP was only inhibited by $\sim 50\%$. Thus, the increase of glycolysis caused by DHEA (from 1.2 to 2.4 nmol/min x mg) was produced at the expense of a reduction in PPP from 0.2 to 0.1 nmol/min x mg. Together, these results indicate that the flux of glucose through PPP is largely underestimated in neurons. Furthermore, according to the extent in the increase in glycolysis, and the degree of inhibition in PPP caused by DHEA (approximately a 50%), we estimate that the actual rate of PPP in neurons is around 2.4 nmol/min x mg, i.e. about double than the rate of glycolysis. Unfortunately, this value could not be directly demonstrated.

Since the rates of PPP are underestimated, we sought to find an explanation. We noticed that F6P derived from the non-oxidative branch of the PPP can be converted back to G6P, a fact that is usually ignored when estimating metabolic fluxes (Brekke et al. 2012). This reaction is catalyzed by phosphoglucose isomerase (PGI), which is a near-equilibrium enzyme therefore allowing the F6P-to-G6P reaction. This issue is critically important in the context of PPP activity determinations, because the decarboxylation of C-1 of [1-¹⁴C]glucose yields unlabeled PPP end-point intermediates, F6P and GAP. Unlabeled F6P, by converting back into G6P, would reduce the specific radioactivity of intracellular [1-¹⁴C]G6P that would result in an underestimation of ¹⁴CO₂ collected. To assess this possibility, we measured PGI activity in primary neurons, which was as high as PFK1. Since PGI is a near-equilibrium enzyme and, therefore, its activity depends on the relative concentrations of F6P and G6P, whereas PFK1 activity in neurons is highly dependent on F2,6P₂ levels that are very low in neurons (Herrero-Mendez *et al.* 2009), it is not unlikely that a large fraction of F6P would indeed be converted into G6P. To test this hypothesis more directly, we next knocked-down PGI in neurons, and determined the rate of PPP. We found that PGI knockdown had a ~90% higher flux through PPP, which strongly supports the notion of the [1-¹⁴C]G6P isotopic dilution as a determinant factor in the underestimation of the actual value of the rate of PPP in these cells.

Besides the above-mentioned methodological limitation, both approaches to assess the glycolytic and PPP fluxes appear to be specific, as demonstrated by the consistent results obtained by, not only DHEA, but also HCN. Thus, HCN treatment triggered a ~150% increase in glycolytic rate, indicating that metabolism of glucose through glycolysis is tightly controlled in neurons. The increase of glycolytic rate observed by HCN is possibly due to an attempt to compensate for the lack of pyruvate oxidation for TCA cycle and oxidative phosphorylation. It should be mentioned that the inhibition of ATP synthesis would increase the AMP:ATP ratio that, in turn, activates AMPK to phosphorylate –and activate– PFKFB3 (Almeida *et al.* 2004, Marsin *et al.* 2002), as well as to promote GLUT3 translocation to the plasma membrane (Cidad *et al.* 2004, Weisova *et al.* 2009). In view that the observed increase in glycolysis is not accompanied by a concomitant decrease in PPP, our results also suggest that HCN triggered an increase in glucose uptake in neurons.

Altogether, our results therefore indicate that glucose metabolism in neurons is a highly dynamic process that can be easily manipulated and detected in cultured intact primary neurons. Moreover, our data also indicate that, besides glycolysis, a considerable

proportion of glucose entering neurons is oxidized through the PPP. In view that glycolysis and PPP are highly dynamic in neurons, we next aimed to investigate whether these glucose-metabolizing pathways can be endogenously modulated by physiological neurotransmitter-mediated stimuli.

2. GLYCOLYSIS AND PPP CAN BE MODULATED BY ENDOGENOUS STIMULI WITH PATHOPHYSIOLOGICAL CONSEQUENCES

We have previously shown that, in contrast to astrocytes, neurons continuously degrade the glycolytic-promoting enzyme PFKFB3 (Herrero-Mendez et al. 2009). This occurs by APC^{Cdh1}-mediated PFKFB3 ubiquitylation followed by proteasomal degradation, and is responsible for keeping glucose oxidized through the PPP (Herrero-Mendez et al. 2009). Here, now we show that short-term activation of glutamate receptors triggers a delayed, time-dependent accumulation of PFKFB3 protein. This effect depends on NMDAR, which are known to promote a cascade of events leading to APC^{Cdh1} inhibition (Maestre et al. 2008). Thus, through a Ca²⁺-calpain dependent mechanism, NMDAR promotes p35 cleavage to p25 leading to cyclin-dependent kinase 5 (Cdk5) activation; in turn, active Cdk5 phosphorylates Cdh1, which is released from the APC complex leading to APC^{Cdh1} inhibition (Maestre et al. 2008). Accordingly, we hypothesized that the stabilization of PFKFB3 that we observed could be a consequence of the known NMDAR-mediated APC^{Cdh1} inhibition. As expected, Cdh1 was phosphorylated by glutamate treatment, thus under our conditions, APC^{Cdh1} resulted inhibited. Furthermore, in agreement with the presence of a nuclear-targeting motif in PFKFB3 (Yalcin *et al.* 2009), we found that PFKFB3 was localized in the nucleus, where neurons actively degraded it. Thus, we hypothesized that, upon glutamate stimulation, PFKFB3 would spread from the nucleus to the cytosol. In fact, we found that such a spread took place in a Cdh1-inhibitable process, since the PFKFB3 mutant form lacking the Cdh1-recognizing KEN motif spontaneously accumulated in the cytosol. Together, these results indicate that PFKFB3 nuclear stabilization followed by cytosolic spread is the consequence of APC^{Cdh1} inhibition. The mechanism whereby PFKFB3 is released from the nucleus remains unclear, although it seems to be specifically dependent on Cdh1. These results are likely of physiological significance in view of the cytoplasmic localization of the PFKFB3 target, PFK1. In fact, we found that NMDAR-mediated PFKFB3 protein stabilization and translocation to the cytosol led to increased glycolytic rate in neurons.

It should be noted that PFKFB3 stabilization takes place several hours (~6 h) after glutamate treatment, thus explaining the absence of measurable short-term glycolytic stimulation in cortical neurons in a previous study (Almeida & Bolanos 2001). Accordingly, the delayed increase in glycolysis that we observe does not appear to be a neuronal attempt to rapidly compensate for the mitochondrial energy dysfunction, which occurs immediately after NMDAR stimulation (Dugan *et al.* 1995). Instead, the delayed glycolysis activation reflects a long-term metabolic adaptation of neurons by an excitotoxic insult, which is in agreement with previous findings indicating that, to be fully active, calpains must be activated by relatively high cytosolic Ca^{2+} concentrations (Baki *et al.* 1996, Tompa *et al.* 1996, Brustovetsky *et al.* 2010). Such an adaptation concurs with concomitant decrease in the rate of glucose oxidation through the PPP. Importantly, this shift (the increase in glycolysis and the decrease in PPP) could be fully abolished by siPFKFB3, indicating that both metabolic pathways are highly dependent on PFKFB3 activity.

Furthermore, the metabolic PPP to glycolysis shift triggered by NMDAR stimulation was accompanied by oxidative stress, as revealed both by an increase in the oxidized glutathione redox status and the increased mitochondrial superoxide detection, as well as apoptotic neuronal death. Either silencing PFKFB3 or G6PD overexpression prevented such a metabolic shift and the concomitant ROS production by NMDAR stimulation. Moreover, silencing PGI, which is able to both inhibit glycolysis (Herrero-Mendez *et al.* 2009) and stimulate PPP (this work), was also sufficient to prevent NMDAR-mediated increase in ROS production. In conclusion, our results show that following PFKFB3 stabilization by NMDAR stimulation, neurons undergo oxidative stress and apoptotic cell death, highlighting the essential role of PPP at regulating neuronal apoptosis (Vaughn & Deshmukh 2008). Furthermore, we show that the loss of PPP activity by APC^{Cdh1} inhibition should be considered a novel and important player in excitotoxicity, hence suggesting that selective inhibition of PFKFB3 in neurons might be considered as a novel therapeutic target against neurodegeneration.

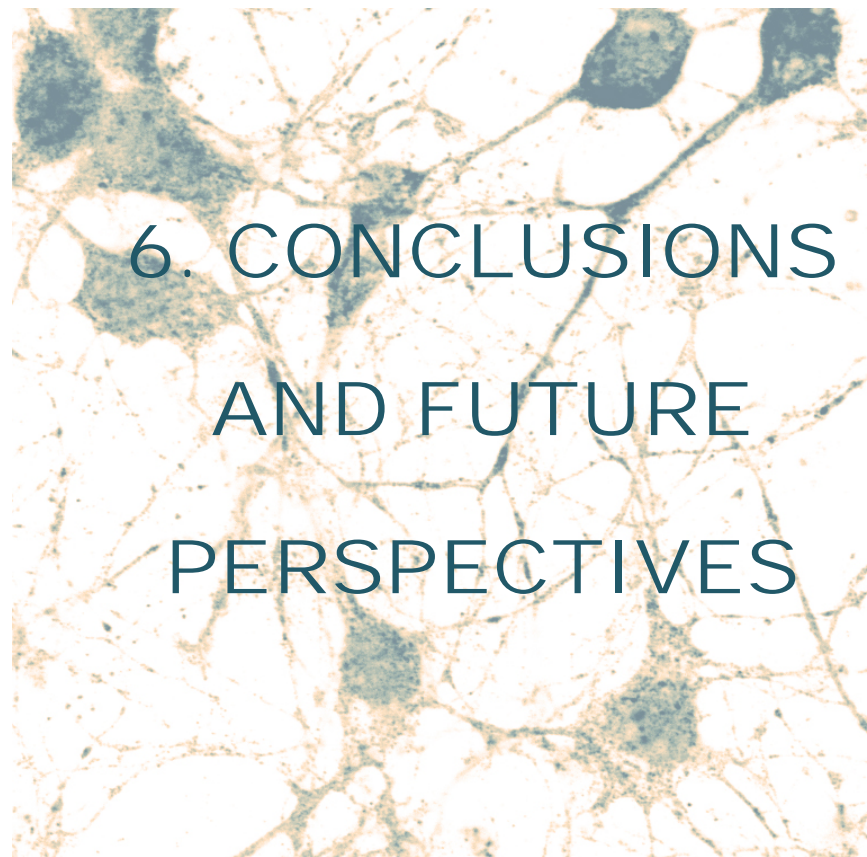
3. TIGAR: A NEW PLAYER IN NEURONAL GLUCOSE METABOLISM AND BEYOND

In view that, at the light of our results, the levels of the PFKFB3 product, F2,6P₂, control glucose metabolism and survival of neurons, we next aimed to elucidate whether TIGAR, a recently uncovered fructose-2,6-bisphosphatase enzyme (Bensaad *et al.* 2006), takes

DISCUSSION

a role in this function. First, we identified TIGAR protein in neurons and in astrocytes in primary culture, which has not been reported so far. Since TIGAR exerts the opposite metabolic effect of PFKFB3 (Bensaad *et al.* 2006, 2009), we next aimed to elucidate whether the lack of TIGAR mimicked PFKFB3 over-expression at modulating ROS and apoptosis. To do so, we first used TIGAR knockout mice, available at Prof. Karen Vousden's group (Beatson Institute for Cancer Research, Glasgow, UK). Surprisingly, neither mitochondrial superoxide abundance nor apoptotic death was significantly increased in TIGAR knockout neurons. This is not unexpected in view that this knockout mice is not inducible, which might have up-regulated compensatory mechanisms. Accordingly, we next aimed to investigate the role of TIGAR by either over-expressing it, or knocking it down, both in rat and in mice neurons in primary culture.

Interestingly, co-expression of TIGAR with the mutant form of PFKFB3 that is insensitive to APC^{Cdh1} –hence stable in neurons– (mutPFKFB3), fully rescued the mutPFKFB3-mediated increase in mitochondrial superoxide and apoptotic death. Next, we designed a siRNA against mouse TIGAR; knocking TIGAR down (siTIGAR) did not induce an increase in the glycolytic rate in neurons, which is not unexpected in view that neurons already express very low F2,6P₂ levels (Almeida *et al.* 2004). However, siTIGAR was accompanied by an increase in apoptotic cell death that was independent of increased superoxide anion. In this context, it should be noticed that, besides its function as a bisphosphatase, very recently it has been reported that TIGAR can be present in mitochondria, where it links hexokinase-II to the outer membrane (Cheung *et al.* 2012). Moreover, it has also been shown that TIGAR can be present in the nucleus, where it may control cell cycle progression (Madan *et al.* 2012). We therefore hypothesized that the increase in apoptosis by siTIGAR under our conditions may be due to an alternative function of TIGAR besides its glycolysis regulatory ability. In fact, the immunofluorescence images of endogenous TIGAR in neurons and in astrocytes reveal its presence both in the nucleus and cytosol in neurons, but not in astrocytes where TIGAR could only be found in cytosol. Together, these results suggest that TIGAR may play a yet unknown function that requires its presence in the nucleus of neurons. Whether this is linked to neuronal differentiation and survival remains to be elucidated.



6. CONCLUSIONS
AND FUTURE
PERSPECTIVES

1. CONCLUSIONS

At the light of the results presented in this work, we have obtained the following conclusions:

1- The radiometric assays based on [3-³H]glucose incorporation into ³H₂O, and on the difference in [1-¹⁴C] glucose and [6-¹⁴C] glucose incorporations into ¹⁴CO₂, are specific for determining the rates of glycolysis and PPP, respectively, in attached, intact primary neurons. However, phosphoglucose isomerase in neurons works at near-equilibrium, causing [¹⁴C] glucose isotopic dilution due to the return of [¹⁴C]-free fructose-6-phosphate into glucose-6-phosphate. Thus, the rates of PPP activity reported values are largely underestimated.

2- Neurons metabolize, approximately, double of glucose-6-phosphate through the PPP and the rest through glycolysis in resting conditions; however, this ratio is amenable to regulation to adapt neurons to a wide range of different stress conditions.

3- Over-stimulation of glutamate receptors, mainly of the NMDA-subtypes, is sufficient to cause PFKFB3 protein stabilization leading to a PPP to glycolysis metabolic shift. Consequently, the redox status of glutathione changes leading to oxidative stress and apoptotic neuronal death. These results identify PFKFB3 as a novel therapeutic target against excitotoxicity.

4- The recently discovered fructose-2,6-bisphosphatase enzyme, TIGAR, is expressed in neurons, where it contributes to the regulation of neuronal glycolysis. Thus, overexpression of TIGAR prevents PFKFB3-induced, superoxide-dependent apoptotic neuronal death. In contrast, TIGAR knockdown increases apoptotic neuronal death through a superoxide-independent manner. This, together with the intriguing nuclear localization of TIGAR in neurons, suggests a distinct, yet to be defined, function of this protein.

2. FUTURE PERSPECTIVES

Here, we developed a sensitive and specific method for the determination of glucose metabolizing fluxes through pentose-phosphate pathway and glycolysis in neurons. A key feature of this novel method is that glucose metabolism can be studied in the attached neurons, i.e. still maintaining intact their axons and dendrites. This differs with previous protocols in which these studies were performed in detached, suspended neurons hence lacking these important processes. Accordingly, this method will be useful to assess how these metabolic pathways are finely tuned during neurotransmission upon different kinds of physiological stimuli.

Our results also highlight that the unbalance in glucose metabolism has profound implications in neuronal redox status and survival. Thus, here we identified a novel molecular mechanism that can account for neuronal death during excitotoxicity, i.e. during excessive and long term activation of glutamate receptors. Excitotoxicity is a well-known phenomenon associated with several neurodegenerative diseases and stroke. Accordingly, our work will open a new research opportunity to investigate different therapeutic approaches to those already in use. For instance, the development of potent specific inhibitors of PFKFB3 –which is responsible for the metabolic shift leading to neuronal death in excitotoxicity– is an interesting idea worth to pursue in the future.

Finally, we have shown that the recently discovered protein TIGAR is expressed in neurons and in astrocytes. Furthermore, according to our data, in neurons TIGAR plays a key role in neuronal survival, although this might be associated to its nuclear localization, rather than to its metabolic effect at degrading fructose-2,6-bisphosphate and, hence, glycolysis. Studying the yet unknown regulatory mechanisms of TIGAR in neuronal survival and/or differentiation appears to be an attractive field worth to investigate in the near future.



7. RESÚMEN EN
ESPAÑOL

INTRODUCCIÓN

1. Metabolismo glucídico en el cerebro.

A pesar de que el cerebro únicamente representa un 2% del peso total corporal, es responsable de más del 20% del consumo total de O_2 y glucosa (Sokoloff 1992). Defectos en el metabolismo cerebral de glucosa se han relacionado con la aparición de enfermedades neurodegenerativas, como la enfermedad de Alzheimer (Piert et al. 1996), PD (Aviles-Olmos et al. 2013) o Huntington (Ciarmiello et al. 2006).

Las principales vías de metabolización de glucosa son la glucólisis y la vía de las pentosas fosfato, a pesar de que los astrocitos también son capaces de almacenar glucógeno (Wiesinger et al. 1997) y constituyen un reservorio importante de glucosa en condiciones en las que existe un déficit en el aporte de glucosa al cerebro (Choi et al. 2003). De hecho, el glucógeno almacenado por los astrocitos es fundamental para mantener la actividad sináptica y para la supervivencia neuronal en hipoglucemia (Swanson & Choi 1993, Suh et al. 2007). La actividad glucolítica es mucho más baja (aproximadamente 4 veces menor) en neuronas que en astrocitos (Herrero-Mendez et al. 2009), una observación que va acompañada por una menor oxidación de la glucosa en el ciclo de los ácidos tricarbóxicos en neuronas (Garcia-Nogales et al. 2003). En astrocitos, en cambio, la glucosa se utiliza predominantemente por vía glucolítica y en concreto, transforman una gran parte de la glucosa en lactato (Leo et al. 1993). De acuerdo con la hipótesis de la lanzadera de lactato astrocitos-neuronas, el lactato producido por los astrocitos se utiliza como fuente de energía por las neuronas (Bouzier-Sore et al. 2003, Zielke et al. 2007, Boumezbeur et al. 2010, Pellerin et al. 2007).

La causa de la baja actividad glucolítica en neuronas es que presentan, a diferencia de los astrocitos, niveles muy bajos de fosfofructo-2-kinasa/fructosa-2,6-bisfosfatasa (PFKFB), en concreto, de la isoforma 3 (PFKFB3), que es la más abundante en cerebro (Herrero-Mendez et al. 2009). La PFKFB3 es una enzima bifuncional que presenta un dominio kinasa, que sintetiza fructosa-2,6-bisfosfato ($F2,6P_2$), y un dominio bisfosfatasa, que desfosforila $F2,6P_2$ para obtener fructosa-6-fosfato.

PFKFB3 en concreto, es la isoforma que presenta la relación kinasa/bisfosfatasa más alta (~700:1) (Ventura et al. 1991), de manera que su función es prácticamente kinasa, por tanto sintetiza $F2,6P_2$. La $F2,6P_2$ es el principal efector alostérico positivo de la 6-

fosfofructo-1-kinasa (PFK1), una enzima clave en la regulación de la glucólisis, de modo que PFKFB3 se puede considerar una enzima pro-glucolítica.

Los bajos niveles de PFKFB3 en neuronas se deben a que esta isoforma es la única que presenta una secuencia Lys-Glu-Asn (KEN), que es un motivo de reconocimiento por Cdh1, una proteína adaptadora de la E3 ubiquitina ligasa APC/C (anaphase-promoting complex/cyclosome), que ubiquitina proteínas diana, marcándolas para su degradación por el proteasoma. A diferencia de los actrocitos, APC/C-Cdh1 es muy activo en neuronas y es el responsable de los bajos niveles de PFKFB3 en estas células. Este estricto control de los niveles de PFKFB3 es esencial para la supervivencia neuronal, puesto que de este modo las neuronas metabolizan parte de la glucosa por la vía de las pentosas-fosfato, que es esencial para generar NADPH(H⁺) y por tanto para la regeneración de glutatión, su principal sistema antioxidante (Herrero-Mendez *et al.* 2009).

Recientemente, se ha descubierto otra proteína que regula los niveles de F2,6P₂ en la célula. TIGAR (TP53-induced glycolysis and apoptosis regulator), es una fructosa-2,6-bisfosfatasa que en células tumorales promueve la defensa frente a estrés oxidativo promoviendo la actividad de la vía de las pentosas-fosfato (Bensaad *et al.* 2006, 2009). Además de sus funciones como bisfosfatasa, TIGAR puede translocarse a la mitocondria formando un complejo con la hexokinasa II, aumentando su actividad (Cheung *et al.* 2012) y también tiene efectos en regulación del ciclo celular en el núcleo (Madan *et al.* 2012). Hasta el momento no se conoce nada relacionado con la expresión o funciones de TIGAR en cerebro.

2. Neurotransmisión glutamatérgica y excitotoxicidad

El glutamato es el principal neurotransmisor excitador en el sistema nervioso central (Butcher & Hamberger 1987), y está relacionado con el procesamiento de información y la plasticidad sináptica. Este neurotransmisor activa tres tipos principales de receptores ionotrópicos, acoplados a canales iónicos (AMPA, KAINATO y NMDA), y varios tipos de receptores metabotrópicos, que están acoplados a proteínas-G (mGLU1 - mGLU8) (Dong et al. 2009).

En concreto, los receptores NMDA (N-metil-D-Aspartato), son canales permeables a Na^+ , K^+ , y Ca^{2+} . Cuando estos receptores son sobre-activados, tiene lugar un proceso patológico conocido como excitotoxicidad que está relacionado con el desarrollo de múltiples enfermedades neurodegenerativas, como la de Huntington (Lievens *et al.* 2001, Estrada-Sanchez *et al.* 2009), PD (Broadstock *et al.* 2012), Esclerosis Lateral Amiotrófica (Kruman *et al.* 1999, Rothstein *et al.* 1995, Howland *et al.* 2002) o Alzheimer (Mattson *et al.* 1992).

La sobre-estimulación de receptores NMDA provoca una entrada masiva de Ca^{2+} en la célula que produce, entre otros efectos, disfunción mitocondrial que conlleva una bajada en los niveles de ATP, estrés oxidativo (Wang *et al.* 1994, Khodorov *et al.* 1996), liberación de citocromo c (Urushitani *et al.* 2001, Luetjens *et al.* 2000) o activación de calpaínas, una familia de cisteína proteasas dependientes de Ca^{2+} (Brustovetsky *et al.* 2010). Entre otros efectos, las calpaínas transforman p35 en p25. Cuando Cdk5 se une a p25 se activa (Lee *et al.* 2000) y a su vez fosforila Cdh1, inactivándolo y por tanto inhibiendo la actividad de APC/C-Cdh1, promoviendo la acumulación de sus sustratos (Jaquenoud *et al.* 2002, Maestre *et al.* 2008).

HIPÓTESIS Y OBJETIVOS

1. Hipótesis

En vista de los antecedentes descritos, nuestra hipótesis es que el metabolismo glucídico en neuronas en condiciones normales está dirigido principalmente hacia la PPP con el fin de generar poder reductor en forma de NADPH(H⁺). Cuando se produce un exceso de activación de receptores NMDA, la inactivación del complejo APC/C-Cdh1 podría conllevar una estabilización de PFKFB3. En estas circunstancias podría tener lugar una modificación en el metabolismo neuronal que disminuyera la utilización de glucosa por la PPP y que por tanto pudiera contribuir al estrés oxidativo y a la muerte neuronal en excitotoxicidad. Además, TIGAR, cuya expresión y función en neuronas se desconoce, podría jugar un papel importante en este eje de regulación del metabolismo y la supervivencia neuronal debido a su actividad como fructosa-2,6-bisfosfatasa.

2. Objetivos

Con el fin de demostrar si estas hipótesis son ciertas, nos planteamos los siguientes objetivos:

- 1- Establecer un método sensible y específico para la determinación del flujo glucolítico y de la actividad de la PPP en neuronas en cultivo adheridas a la placa.
- 2- Cuantificar la actividad glucolítica y de PPP que presentan las neuronas en cultivo en condiciones basales.
- 3- Determinar si la activación de receptores NMDA por glutamato conlleva una estabilización de PFKFB3 en neuronas, así como sus posibles consecuencias sobre el estado redox y la supervivencia neuronal.
- 4- Analizar si TIGAR está presente en neuronas y, en ese caso, su implicación en la regulación del metabolismo y sus efectos sobre la supervivencia neuronal.

RESULTADOS Y DISCUSIÓN

1. La actividad glucolítica en neuronas aumenta tanto al inhibir la vía de las pentosas fosfato como la captación mitocondrial de piruvato.

Con el fin de estudiar el metabolismo glucídico en neuronas, pusimos a punto un nuevo protocolo para determinar la actividad glucolítica y de la vía de las pentosas fosfato en neuronas adheridas a la placa. El flujo de glucosa metabolizada por vía glucolítica se determinó como la velocidad de producción de $^3\text{H}_2\text{O}$ a partir de $[3\text{-}^3\text{H}]$ glucosa, un proceso que tiene lugar en la reacción catalizada por la aldolasa. De este modo, pudimos determinar que las neuronas en condiciones basales tienen una actividad glucolítica aproximada de 1.2 nmol/min x mg de proteína (Fig. 1). Las neuronas incubadas con dehidroepiandrosterona (DHEA; 1 μM), un inhibidor de la G6PD, la enzima limitante del flujo a través de la PPP, incrementaron su actividad glucolítica al doble de su actividad basal (Fig. 1), lo que nos sugiere que una proporción considerable de glucosa (aproximadamente el 50%) se está metabolizando en la PPP. El tratamiento con 4-hidroxi- α -cianocinamato (HCN), un compuesto que a la concentración utilizada inhibe selectivamente la captación de piruvato por la mitocondria, incrementó ~125% la actividad glucolítica, lo que podría deberse a un intento por parte de las neuronas de compensar la falta de piruvato que entra en la mitocondria y por tanto la posible bajada en los niveles de ATP.

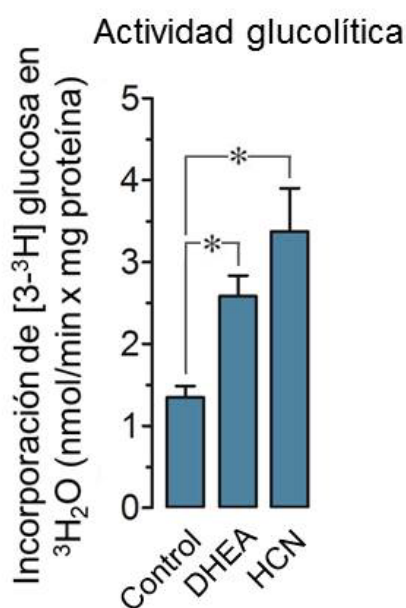


Figura 1. La actividad glucolítica se incrementa significativamente con DHEA e HCN. Neuronas a 6 días de cultivo fueron incubadas en el medio de experimentación que contenía 5 $\mu\text{Ci/ml}$ de D- $[3\text{-}^3\text{H}]$ glucosa más DHEA 1 μM o HCN 0.1mM. La velocidad glucolítica fue determinada mediante la medida de la incorporación de $[3\text{-}^3\text{H}]$ glucosa en $^3\text{H}_2\text{O}$ durante los 90 minutos de incubación del experimento. * $P < 0.05$ (ANOVA)($n=3$).

2. La velocidad de oxidación de glucosa por la PPP se inhibe con DHEA.

En vista de los resultados obtenidos previamente, decidimos determinar la actividad de la PPP en neuronas. Para ello, las neuronas se incubaron en presencia de $[1-^{14}\text{C}]$ glucosa o de $[6-^{14}\text{C}]$ glucosa y se midió el $^{14}\text{CO}_2$ liberado. La $[1-^{14}\text{C}]$ glucosa se descarboxila en la reacción catalizada por la 6-fosfogluconato deshidrogenasa y en la descarboxilación de la acetil-CoA en las reacciones catalizadas por la isocitrato deshidrogenasa y la α -cetoglutarato deshidrogenasa en el ciclo de los ácidos tricarbóxicos. En cambio, la $[6-^{14}\text{C}]$ glucosa únicamente se descarboxila en el TCA. De este modo, la diferencia entre el $^{14}\text{CO}_2$ liberado a partir de la $[1-^{14}\text{C}]$ glucosa y el liberado a partir de la $[6-^{14}\text{C}]$ glucosa se utiliza como una estimación de la glucosa metabolizada por la PPP. Como se muestra en la figura 2, la velocidad de oxidación de la glucosa en la PPP fue de aproximadamente 0.2 nmol/min x mg proteína y la incubación con DHEA disminuyó un 50% la actividad de la vía. De acuerdo con estos resultados, el tratamiento con DHEA incrementó la actividad glucolítica 1.2 nmol/min x mg proteína pero únicamente disminuyó la de la PPP 0.1 nmol/min x mg proteína, lo que nos indica que la determinación de la actividad de la PPP utilizando esta metodología podría estar altamente infraestimada.

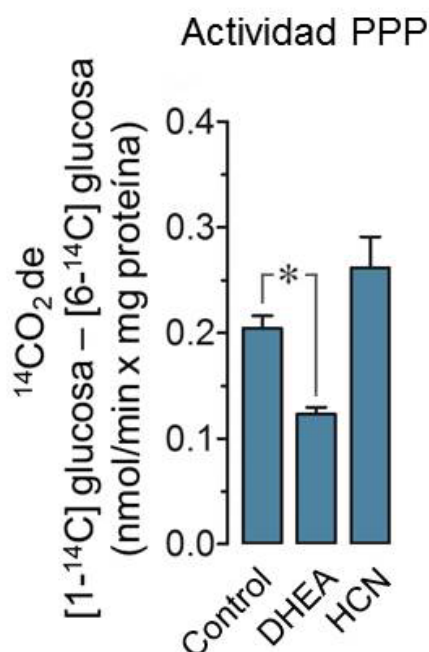


Figura 2. La velocidad de la PPP disminuye significativamente en las neuronas tratadas con DHEA. Neuronas a 6 días de cultivo fueron incubadas en medio de experimentación que contenía 0.5 $\mu\text{Ci/ml}$ de D- $[1-^{14}\text{C}]$ glucosa o D- $[6-^{14}\text{C}]$ glucosa durante 90 minutos y la velocidad de la PPP fue determinada como la diferencia entre el $^{14}\text{CO}_2$ proveniente de la descarboxilación de $[1-^{14}\text{C}]$ glucosa y el proveniente de la descarboxilación de $[6-^{14}\text{C}]$ glucosa. * $P < 0.05$ (ANOVA)($n=3$).

3. La fosfoglucosa isomerasa (PGI) presenta una actividad elevada en neuronas.

En vista de los bajos niveles de $^{14}\text{CO}_2$ provenientes de la $[1-^{14}\text{C}]$ glucosa detectados, nos planteamos la posibilidad de que la F6P regenerada a partir de la fase no oxidativa de la PPP, que ya no es radiactiva, pudiera estar siendo convertida de nuevo en G6P por la PGI. En este caso, la radiactividad de la reserva de G6P podría verse altamente disminuida, pudiendo ser la causa de la infraestimación de la actividad de la PPP observada. Con el objeto de esclarecer si esta podría ser la causa, medimos la actividad específica de la PGI. Como se muestra en la figura 3, la actividad de la PGI resultó ser tan alta como la de la PFK1. Sin embargo, el flujo de F6P a través de la PFK1 está limitado en neuronas como consecuencia de la baja síntesis de su efector alostérico positivo, la fructosa-2,6-bisfosfato, mientras que la PGI es una enzima cercana al equilibrio y la dirección de la actividad de esta enzima depende exclusivamente de las concentraciones relativas de F6P y G6P. Debido a esto, es posible que una gran proporción de F6P proveniente de la PPP se esté reconvirtiendo en G6P y por tanto contribuyendo a la dilución isotópica de la G6P, resultando en una aparentemente baja liberación de $^{14}\text{CO}_2$ a partir de $[1-^{14}\text{C}]$ glucosa.

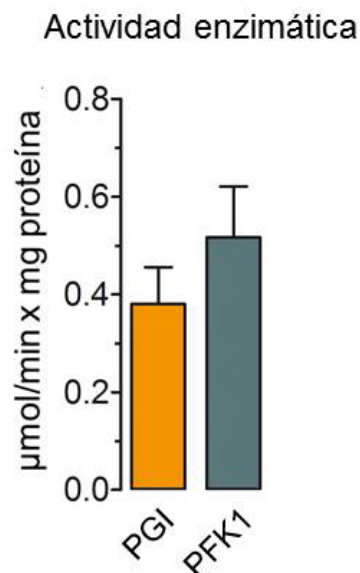


Figura3. La PGI presenta una actividad similar a la PFK-1 en neuronas. Neuronas a 6 días de cultivo fueron lisadas con 3 ciclos de congelación/descongelación. El extracto así obtenido se utilizó para medir la actividad de la PGI y PFK-1.

4. El silenciamiento de la PGI conlleva un incremento en la actividad de la PPP.

Seguidamente, nos propusimos comprobar de manera más directa nuestra hipótesis. Para ello, diseñamos un siRNA dirigido contra la PGI (siPGI). A los 3 días de cultivo, las neuronas primarias se transfectaron con siPGI, que como se muestra en la figura 4a disminuyó con éxito los niveles de proteína (~70%) después de 72 horas, y se utilizaron para determinar la actividad de la PPP. Como se observa en la figura 4b, la actividad de la PPP detectada se incrementó significativamente en las neuronas transfectadas con siPGI. Este resultado es compatible con que la radiactividad específica de la [1-¹⁴C] G6P se vea diluida por la entrada de G6P no radiactiva proveniente de F6P, es más, indica que la PGI en neuronas recicla G6P activamente.

En conjunto, estos datos sugieren que la glucosa que entra en las neuronas se oxida activamente por la PPP junto con G6P reciclada a partir de F6P proveniente de la fase no oxidativa de la PPP. Sin embargo, debido a la dilución isotópica de la G6P, el valor real de la proporción de glucosa que se incorpora a la PPP no se puede determinar, al menos utilizando esta metodología.

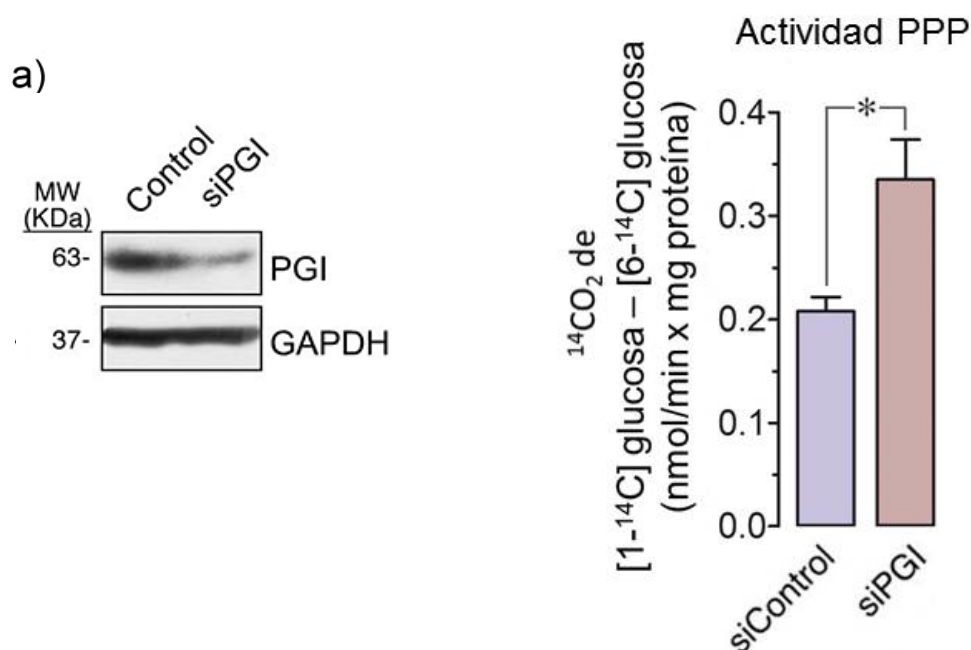


Figura 4. a) El siRNA dirigido contra la PGI silencia eficazmente la proteína en neuronas. Neuronas a 3 días de cultivo se transfectaron con siControl o siPGI 100 nM. 72 horas después las células se lisaron en RIPA y se sometieron a una transferencia de western blot para comprobar el silenciamiento de la PGI. b) La velocidad de la PPP se incrementa significativamente al silenciar la PGI. Neuronas a 6 días de cultivo se incubaron en tampón de experimentación que contenía 0.5 $\mu\text{Ci/ml}$ de D-[1- ^{14}C] glucosa o D-[6- ^{14}C] glucosa durante 90 minutos y la velocidad de la vía se determinó calculando la diferencia entre el $^{14}\text{CO}_2$ producido por [1- ^{14}C] glucosa y el producido por [6- ^{14}C] glucosa. * $P < 0.05$ (ANOVA)($n=3$).

5. Efecto de DHEA e HCN sobre la concentración de G6P

Finalmente, para ver cómo la PPP está dinámicamente acoplada con la glucólisis en neuronas, investigamos los efectos de la inhibición de la PPP y de la capacidad de piruvato por la mitocondria sobre las concentraciones de G6P. Como se muestra en la figura 5, la G6P se acumuló en las neuronas tratadas con DHEA. Este resultado sugiere de manera convincente que existe un alto flujo de G6P hacia la PPP en neuronas. En cambio, el tratamiento con HCN no afectó a la concentración de G6P.

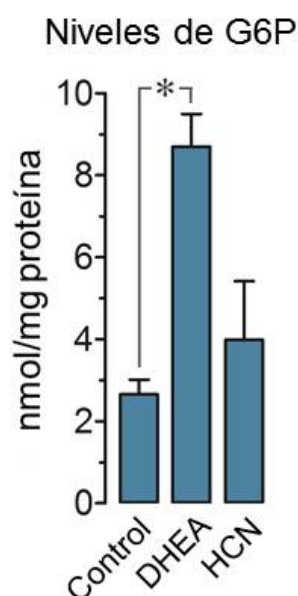


Figura 5. La G6P se acumula en las neuronas tratadas con DHEA, pero no se ve afectada por HCN. Neuronas a 6 días de cultivo se incubaron con DHEA 1 μM DHEA o HCN 0.1 mM durante 90 minutos. Posteriormente las células se lisaron en NaOH 0.6 M. El extracto resultante se desproteinizó con el mismo volumen de ZnSO_4 al 1% w/v y se utilizó para determinar la concentración de G6P. * $P < 0.05$ (ANOVA)($n=3$).

6. Las neuronas corticales en cultivo primario responden a la activación de los receptores de glutamato incrementando los niveles de Ca^{2+} intracelular.

Seguidamente, en vista de que nuestros datos indican que tanto la glucólisis como la PPP son procesos altamente dinámicos en neuronas, nos propusimos investigar si estas vías de metabolización de glucosa se pueden modular de manera endógena por estímulos fisiológicos de neurotransmisión. En primer lugar quisimos determinar si las neuronas a 6 días de cultivos expresan receptores funcionales de glutamato. Para ello, medimos los cambios en los niveles de Ca^{2+} intracelular utilizando Fura-2, una sonda que emite fluorescencia a 510 nm, pero cuya longitud de onda de excitación varía de 363 nm (libre) a 335 nm (unida a Ca^{2+}). De este modo, la relación F335/F363 es directamente proporcional a los niveles de Ca^{2+} intracelular. Como se muestra en la figura 6a, la incubación de neuronas con glutamato (100 μM , 15 min) incrementó inmediatamente la fluorescencia de Fura-2, lo que sugiere una entrada de Ca^{2+} en las neuronas por medio de receptores ionotrópicos de glutamato. Este incremento en la entrada de Ca^{2+} se previno parcialmente con MK801 (1 μM), un inhibidor selectivo de los receptores NMDA, indicando que una proporción elevada (~60%) del Ca^{2+} que entraba en la célula estaba mediada por la activación de estos receptores. Es más, la incubación de neuronas con NMDA incrementó los niveles de Ca^{2+} intracelular de manera similar al glutamato y una vez más este efecto se previno con MK801 (~90%). Como era de esperar, la incubación de neuronas con NMDA o glutamato en la presencia de un tampón al que se le añadió EGTA, un quelante de calcio, no produjo ningún cambio en la emisión a 510 nm.

En conclusión, las neuronas corticales de rata a 6 días de cultivo expresan receptores NMDA funcionales, lo que nos permite investigar los efectos metabólicos de este neurotransmisor.

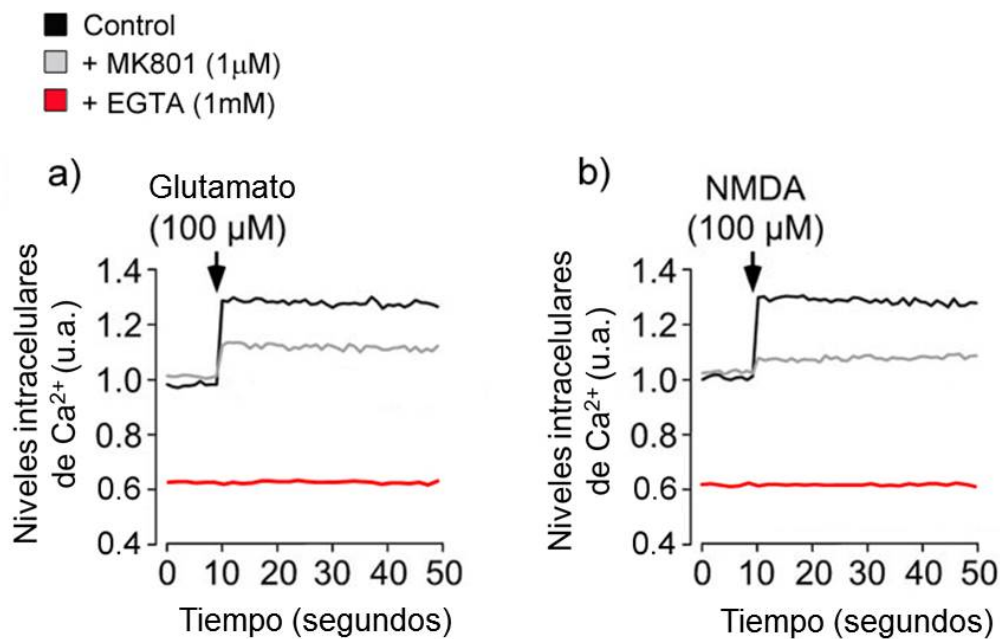


Figura 6. La incubación de neuronas corticales de rata a 6 días de cultivo con glutamato (panel izquierdo) o NMDA (panel derecho), incrementaron la relación F335/F363 de Fura-2, indicando un incremento en los niveles intracelulares de Ca^{2+} . La incubación con MK801 (10 μ M) previno parcialmente tanto el efecto del glutamato como el del NMDA. La utilización de un tampón libre de Ca^{2+} , conteniendo EGTA 1 mM, previno completamente los cambios de emisión a 510 nm en ambas condiciones.

7. La activación de receptores NMDA promueve la estabilización de la enzima pro-glucolítica PFKFB3 en neuronas.

Resultados previos en nuestro laboratorio demostraron que la estimulación de receptores NMDA activa la ciclina dependiente de kinasa 5 (Cdk5) por un mecanismo dependiente de Ca^{2+} y calpaina (Herrero-Mendez *et al.* 2009). A su vez, Cdk5 hiperfosforila Cdh1, que es un co-activador del complejo promotor de la anafase/ciclosoma (APC/C). Cdh1 hiperfosforilado, se separa del complejo, por tanto inhibiendo su actividad como E3 ubiquitina-ligasa (Maestre *et al.* 2008).

En vista de que también hemos demostrado que la PFKFB3 es un sustrato de APC/C-Cdh1 (Herrero-Mendez *et al.* 2009), razonamos que la estimulación de receptores NMDA, mediante la inactivación de APC/C-Cdh1 podría conllevar una estabilización de PFKFB3. Con el fin de comprobar esta hipótesis, incubamos neuronas con glutamato

(100 μ M, 15 min) y analizamos tanto los niveles de PFKFB3 como el estado de fosforilación de Cdh1 a distintos tiempos mediante western blot. Para determinar el estado de fosforilación de Cdh1, la proteína se inmunoprecipitó a partir de lisados obtenidos a las 6 horas post-tratamiento, se sometió a una transferencia de western blot y se incubó con un anticuerpo anti fosfo serina. Como se muestra en la figura 7a, el tratamiento con glutamato ocasionó un aumento en la fosforilación de Cdh1, efecto que se previno por completo con la utilización de MK801. Esto indica que en estas condiciones, la estimulación de receptores NMDA inhibe el complejo APC/C-Cdh1, de acuerdo con nuestras observaciones previas. El análisis de los niveles de PFKFB3 mediante western mostró que el tratamiento con glutamato producía una acumulación tiempo dependiente de la proteína, efecto que fue máximo a las 6 horas (Figura 7b). Este efecto fue mimetizado por neuronas estimuladas con NMDA (Figura 7c), lo que demuestra la implicación de estos receptores. Es más, como se muestra en la figura 7d, la incubación de las neuronas con MK801 previno la acumulación de PFKFB3. En conjunto estos datos indican que la estimulación de los receptores NMDA inhibe la actividad del complejo APC/C-Cdh1, lo que conlleva la acumulación de PFKFB3 en neuronas primarias.

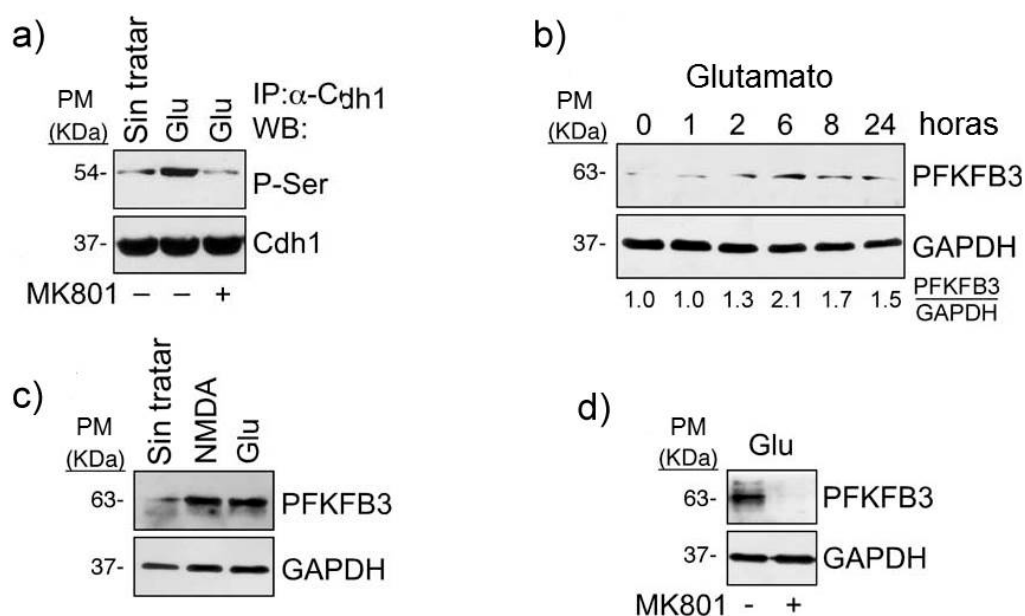


Figura 7. a) Cdh1 se encuentra fosforilado 6 horas después del tratamiento con glutamato (100 μ M/15 min), un efecto que se previene con MK801 (10 μ M). b) La incubación de neuronas con glutamato (100 μ M/15 min) produce una acumulación de PFKFB3 tiempo-dependiente, cuyo máximo efecto se observa a las 6 horas de tratamiento. c) NMDA (100 μ M/15 min) produce el mismo efecto de acumulación de PFKFB3 que le glutamato. d) El antagonista de los receptores NMDA MK801 (10 μ M), previene el incremento de PFKFB3 mediado por glutamato.

8. La estimulación de receptores NMDA produce la translocación del núcleo al citosol de la PFKFB3.

En vista que nuestros resultados indican que la proteína PFKFB3 está siendo continuamente degradada por APC/C-Cdh1 y que APC/C-Cdh1 es activa en el núcleo, nos propusimos investigar la localización subcelular de PFKFB3. Para ello expresamos tanto PFKFB3 silvestre como una construcción constitutivamente estable en la que la KEN box, responsable de su degradación, fue mutada a AAA (denominada mutPFKFB3), ambas fusionadas con GFP, y analizamos los cambios en su localización subcelular. Las neuronas se transfectaron con cantidades pequeñas (0.16 μ g/ml) de cada uno de estos plásmidos y su localización se analizó por microscopía confocal. Como se muestra en la figura 8, PFKFB3 silvestre está localizada en el núcleo, mientras que la mutante mostraba también una localización citosólica. El tratamiento de las neuronas con glutamato (100 μ M / 15 min) produjo un cambio de PFKFB3 hacia el citoplasma, efecto que se previno al sobreexpresar Cdh1. En conjunto, estos resultados indican que la proteína PFKFB3 está localizada en el núcleo, donde es marcada para su degradación por APC/C-Cdh1; sin embargo, el tratamiento con glutamato, al inhibir la actividad del complejo, estabiliza PFKFB3, que a su vez sale del núcleo. Nuestro siguiente objetivo fue ver si los cambios en la estabilidad de PFKFB3, así como sus cambios en localización subcelular, tenían algún efecto sobre el flujo de la glucosa a través de la vía glucolítica.

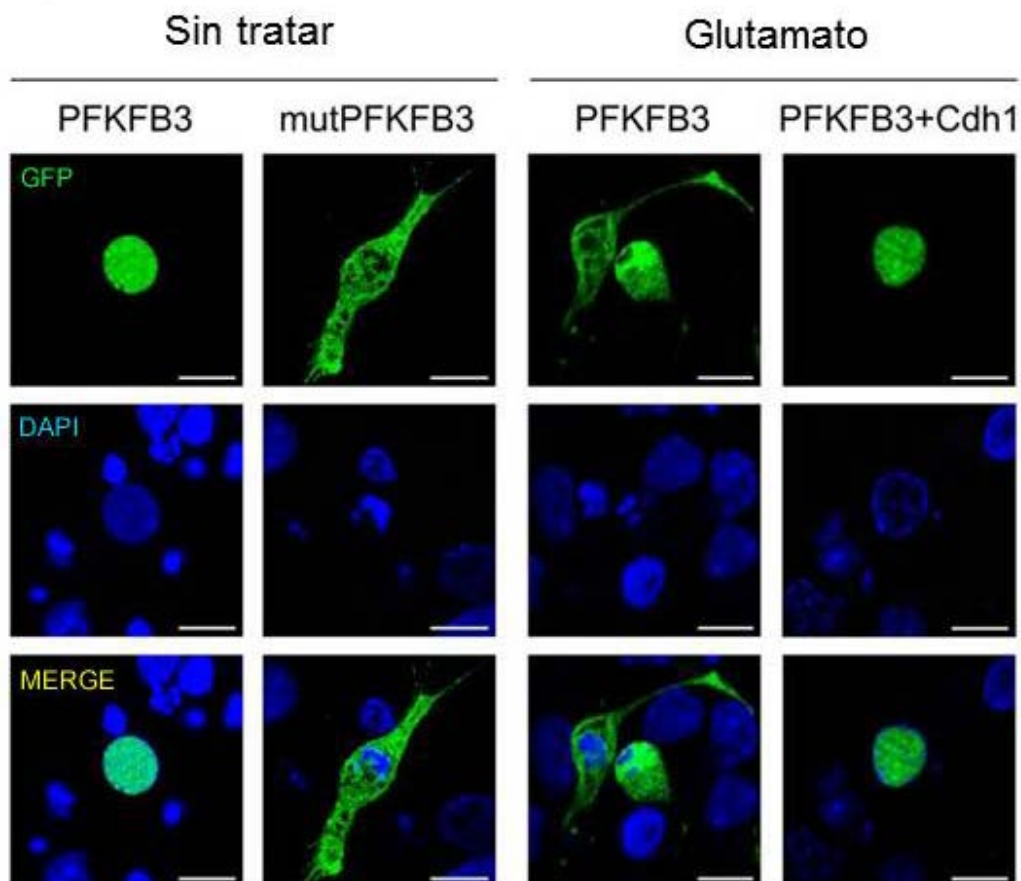


Figura 8. Imágenes de microscopía confocal de neuronas transfectadas con GFP-PFKFB3. El tratamiento con glutamato promueve la acumulación y localización de PFKFB3 tanto en el núcleo como el en citosol celular, efecto que se previene con la sobreexpresión de Cdh1. GFP-PFKFB3, mutado en su caja KEN (KEN-AAA; mut-PFKFB3) muestra esa misma localización independientemente del tratamiento con glutamato.

9. La estabilización de PFKFB3 mediada por receptores NMDA aumenta la actividad glucolítica y disminuye la de PPP

Es sabido que la PFKFB3, mediante la síntesis de F2,6P₂, promueve la glucólisis en neuronas. En vista que la estimulación de receptores NMDA produce una estabilización de PFKFB3, nos propusimos investigar sus posibles consecuencias funcionales. Para ello, después de 6 horas post estimulación de los receptores NMDA, se midió la actividad glucolítica en neuronas determinando la producción de ³H₂O a partir de [3-³H] glucosa. Como se muestra en la figura 9a, la estimulación de los receptores NMDA produjo un incremento en la velocidad glucolítica en neuronas. Con el fin de comprobar que ese efecto era debido a una acumulación de PFKFB3, diseñamos un siRNA contra la proteína, cuya eficiencia fue comprobada por western blot. Para ello, la construcción GFP-PFKFB3 se expresó en neuronas, lo que produjo una acumulación de la PFKFB3 a juzgar por la intensidad de la banda obtenida con un anticuerpo anti-GFP (Figura 9b), sin embargo, la transfección de las neuronas con siPFKFB3, disminuyó la abundancia de la proteína, es más, el tratamiento con glutamato produjo un incremento en la intensidad de la banda GFP-PFKFB3, sugiriendo una estabilización de la PFKFB3, efecto que también se previno con siPFKFB3. Como se muestra en la figura 9a, el incremento en la velocidad glucolítica producido por glutamato se previno en neuronas previamente transfectadas con siPFKFB3, lo que indica que la estabilización de esta proteína era la responsable del incremento en velocidad glucolítica observado. Es más, en vista de que nuestros resultados previos muestran que la glucólisis y PPP son vías dinámicamente relacionadas en neuronas, también investigamos si el incremento en glucólisis afectaba a la actividad de la PPP. Como se muestra en la figura 9c, las neuronas tratadas con glutamato también mostraron, a las 6 horas, una reducción de la velocidad de oxidación de la glucosa por la PPP, un efecto que se previno completamente en las neuronas previamente transfectadas con siPFKFB3. Por tanto, nuestros resultados indican que la estimulación de receptores NMDA en neuronas produce una inhibición, mediada por Ca²⁺ de la actividad de APC/C-Cdh1, que a su vez origina una estabilización de PFKFB3 en el citosol, produciendo una desviación del metabolismo de la glucosa hacia glucólisis, disminuyendo la PPP.

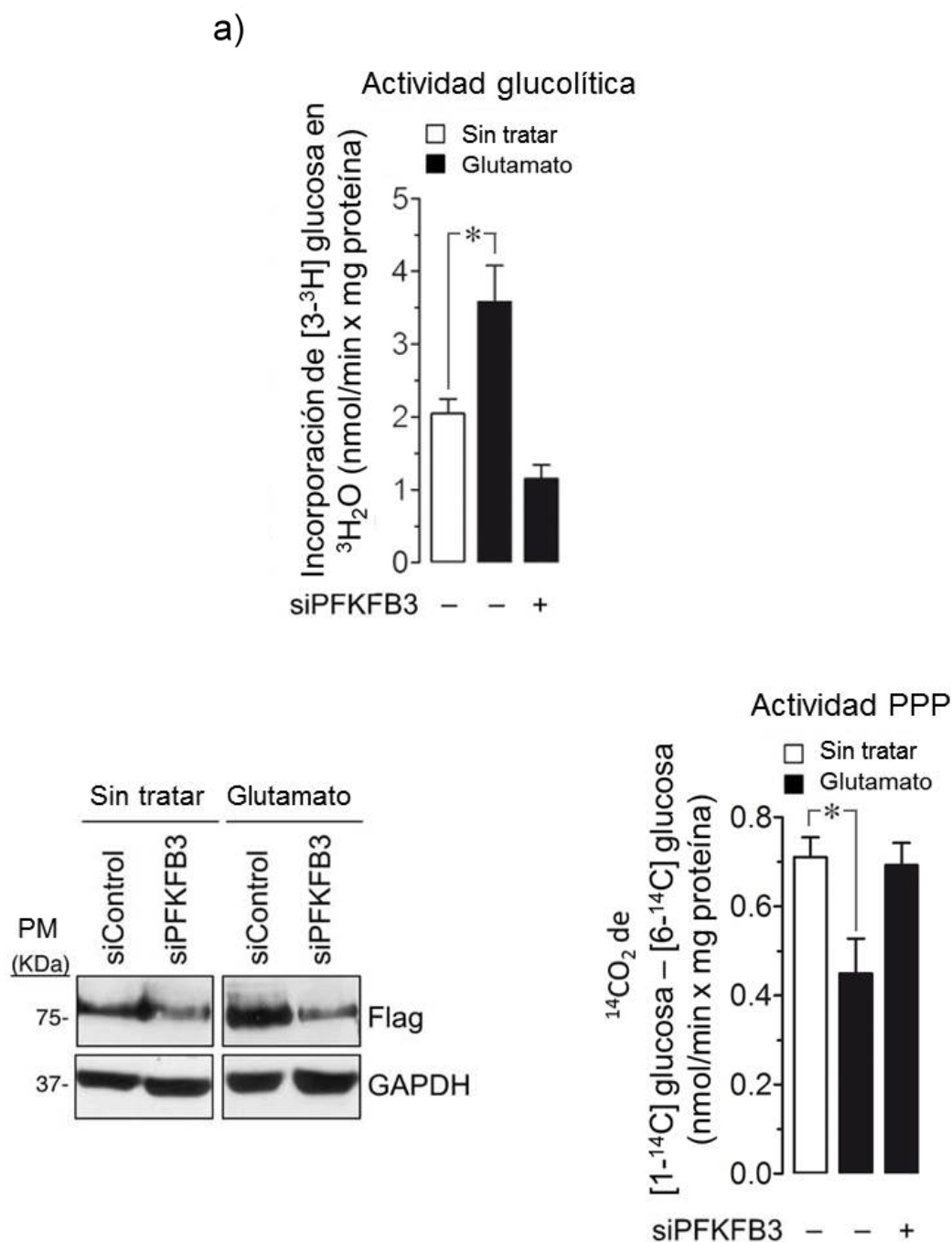


Figura 9. a) La incubación de neuronas con glutamato (100 μ M/15 min) produjo un incremento a las 6 horas de la velocidad glucolítica, determinada mediante la producción de $^3\text{H}_2\text{O}$ a partir de [$3\text{-}^3\text{H}$] glucosa; este efecto se previno evitando la acumulación de PFKFB3 mediante una transfección previa de las neuronas con siPFKFB3. b) La incubación de neuronas expresando GFP-PFKFB3 con glutamato (100 μ M/15 min), indujo, a las 6 horas post tratamiento, la acumulación de la proteína, efecto que se

previno en las neuronas previamente transfectadas con siPFKFB3 (100 nM). c) El tratamiento con glutamato disminuyó, a las 6 horas post tratamiento, la velocidad de la PPP, determinada mediante el cálculo de la diferencia entre el $^{14}\text{CO}_2$ producido a partir de $[1\text{-}^{14}\text{C}]$ glucosa y el producido a partir de $[6\text{-}^{14}\text{C}]$ glucosa; este efecto se previno en las neuronas previamente transfectadas con siPFKFB3. $*P < 0.05$ (ANOVA)($n=3$).

10. La estimulación de receptores NMDA produce un defecto en la regeneración de glutatión mediada por la estabilización de PFKFB3

La oxidación de glucosa en la PPP genera NADPH(H^+), un cofactor de múltiples enzimas entre las que se encuentra la glutatión reductasa. La glutatión reductasa necesita un aporte continuo de NADPH(H^+) para regenerar glutatión (GSH) a partir de su forma oxidada, GSSG. En vista de que la estimulación de receptores NMDA conlleva un incremento en glucólisis y una disminución en la actividad de la PPP, quisimos saber si esa disminución en la actividad de la PPP produce un desbalance en la capacidad de las neuronas de regenerar glutatión. Para ello analizamos los niveles de glutatión total (GSx) y oxidado (GSSG) en neuronas a las 6 horas de estimulación de los receptores NMDA. Como se muestra en la figura 10, el tratamiento con glutamato no modificó la concentración total de glutatión, pero incrementó significativamente su forma oxidada. Todos estos efectos se previnieron parcialmente con siPFKFB3, indicando que fueron, al menos en parte, mediados por la estabilización de PFKFB3 producida por la estimulación de los receptores NMDA.

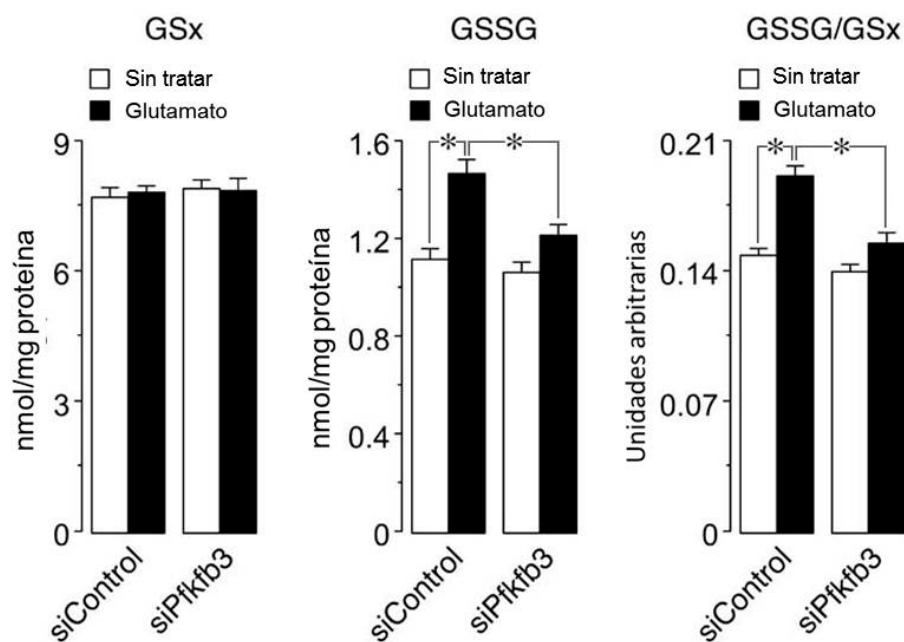


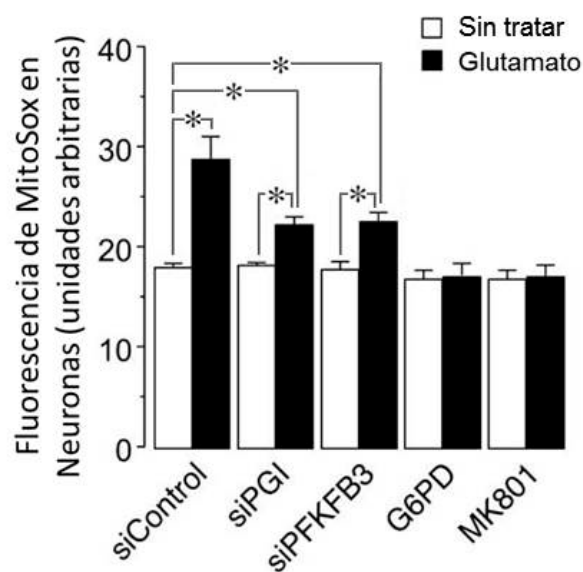
Figura 10. El tratamiento con glutamato no modificó la concentración de GSx (panel izquierdo), pero incrementó la de GSSG (panel intermedio) y por tanto el estado redox general del glutatión (GSSG/GSx; panel derecho); estos efectos se previnieron parcialmente con siPFKFB3. Neuronas a 3 días de cultivo fueron transfectadas con siControl o siPFKFB3 (100 nM). Al sexto día se trataron con glutamato (100 μ M/15 min) y los extractos celulares obtenidos a las 6 horas post tratamiento se utilizaron para la determinación de glutatión. * $P < 0.05$ (ANOVA)($n=3$).

11. La desviación del metabolismo de la glucosa de la PPP a glucolisis como consecuencia de la estimulación de receptores NMDA produce estrés oxidativo

En vista de que el glutatión reducido es esencial para la detoxificación de las especies reactivas de oxígeno mitocondriales, nos planteamos que el incremento en glutatión oxidado mediado por NMDAR podría originar estrés oxidativo. Para comprobar esta hipótesis, analizamos la abundancia de anión superóxido en la mitocondria, utilizando la sonda MitoSox-Red. Como se muestra en la figura 11a, el tratamiento de las neuronas con glutamato produjo, a las 16 horas, un incremento significativo en los niveles mitocondriales de anión superóxido, sugiriendo estrés oxidativo. Este efecto se previno silenciando la PGI, un tratamiento que, según nuestros resultados previos, es capaz de

incrementar la actividad de la PPP (figura 4b). Para comprobar si este efecto era consecuencia de un incremento en la glucólisis, silenciamos PFKFB3 previamente al tratamiento con glutamato. Como se muestra en la figura 11a, siPFKFB3 previno casi totalmente el incremento en superóxido. Para apoyar la hipótesis de que el estrés oxidativo mediado por la activación de receptores NMDA es debido, al menos en parte, a una inhibición de la actividad de la PPP, nos propusimos investigar si este efecto se prevenía al sobreexpresar la G6PD, la enzima limitante de la PPP. Como se muestra en la figura 11b, la expresión del cDNA codificante para la proteína conllevó un aumento significativo de los niveles de G6PD y este efecto fue suficiente para rescatar completamente el incremento en superóxido mitocondrial causado por NMDA (Figura 11a). Finalmente, comprobamos que el efecto observado sobre los niveles mitocondriales de superóxido era exclusivamente dependiente de la activación de NMDA, a juzgar por la completa protección brindada por su antagonista, MK801 (figura 11h)

a) Detección de superóxido mitocondrial



b)

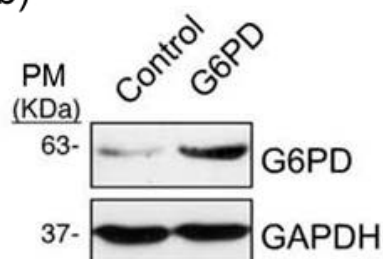


*Figura 11. a) El tratamiento con glutamato (100 μ M/15 min) incrementó los niveles de anión superóxido en neuronas, medido mediante la detección de fluorescencia de MitoSox-Red por citometría de flujo; este efecto se previno silenciando PGI (siPGI) o PFKFB3 (siPFKFB3), sobreexpresando G6PD o bloqueando los receptores NMDA con MK801 (10 μ M). b) la transfección de neuronas con el cDNA completo codificante para G6PD (1.6 μ g/m) incrementó eficientemente la abundancia de la proteína. * $P < 0.05$. (ANOVA)($n=3$).*

12. La activación de receptores NMDA induce muerte neuronal por apoptosis como consecuencia de la desviación del metabolismo glucídico de la PPP a glucolisis

Como la estimulación de receptores NMDA produce estrés oxidativo como consecuencia de la desviación del metabolismo de la glucosa hacia glucolisis, y dado que el estrés oxidativo puede desencadenar la muerte neuronal, a continuación quisimos investigar si esta modificación en el metabolismo producía muerte neuronal por apoptosis. Para ello, las neuronas se trataron con glutamato (100 μ M / 15 min) y 16 horas después se incubaron con anti anexina V y 7AAD con el fin de determinar mediante citometría de flujo las neuronas que estaban sufriendo apoptosis. Como se muestra en la figura 12, la proporción de neuronas anexina V⁺/7AAD⁻ se incrementó significativamente en las neuronas tratadas con glutamato. Este efecto se previno parcialmente silenciando la PGI o la PFKFB3, sobre expresando la G6PD o bloqueando los receptores NMDA con MK801. Por tanto, la estimulación de receptores NMDA induce la muerte neuronal por apoptosis como consecuencia del cambio en el metabolismo de la glucosa de PPP a glucolisis.

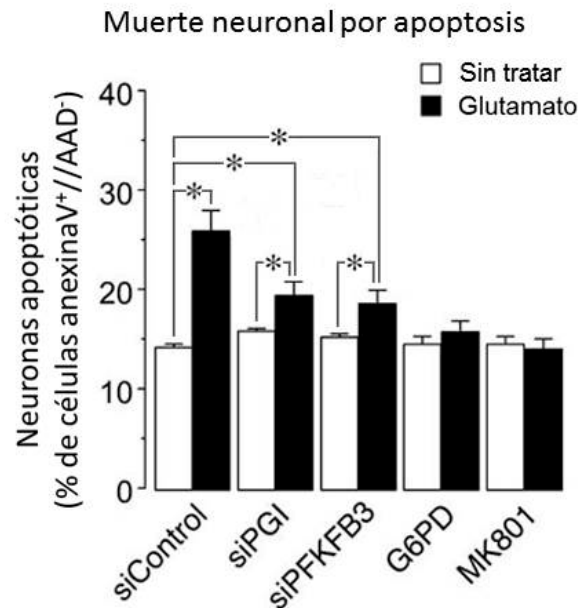


Figura 12. El tratamiento con glutamato incrementó la muerte neuronal por apoptosis, como se pudo observar mediante el análisis por citometría de flujo de la relación de células anexina V⁺/AAD⁻; este efecto se previno silenciando PGI (siPGL, 100 nM) o PFKFB3 (siPFKFB3, 100 nM), sobre expresando G6PD (1.6 µg/ml) o bloqueando los receptores NMDA con MK801 (10 µM). *P<0.05.(ANOVA)(n=3).

13. La expresión de una forma mutada de PFKFB3 no detectable por APC/C-Cdh1 produce un efecto similar a la activación de receptores NMDA

Para apoyar los resultados que indican que la estabilización de PFKFB3 producida por la inhibición de APC/C-Cdh1 es la responsable del estrés oxidativo y apoptosis, nos propusimos investigar si este fenotipo podría ser reproducido mediante la expresión de una forma mutada de la PFKFB3 que no puede ser reconocida por APC/C-Cdh1. Como se muestra en la figura 13a, la incubación de neuronas expresando PFKFB3 silvestre con glutamato, incrementó los niveles de superóxido en la mitocondria de forma similar a las neuronas que expresaban la forma mutada (mutPFKFB3). La determinación de las neuronas que estaban sufriendo un proceso de apoptosis produjo resultados idénticos (figura 13b). En conjunto, estos resultados indican que la inhibición de APC/C-Cdh1 mediada por la estimulación de receptores NMDA produce una estabilización de PFKFB3 que hace que aumenten los niveles de glutatión oxidado y finalmente origina la

muerte neuronal por apoptosis. Por tanto, PFKFB3 podría ser considerada una diana terapéutica interesante en el tratamiento de desórdenes en el sistema nervioso central en los que se haya descrito un exceso de neurotransmisión glutamatérgica (excitotoxicidad).

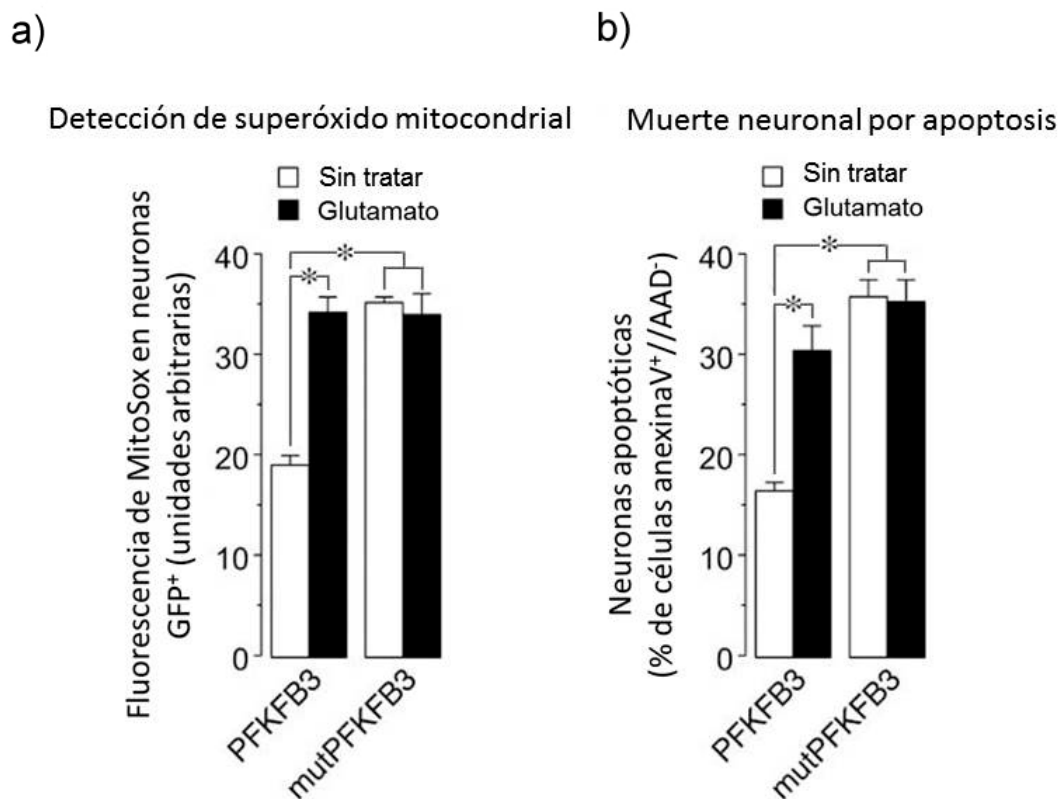


Figura 13. a) El tratamiento con glutamato ($100 \mu\text{M}/15 \text{ min}$) incrementó los niveles de superóxido en neuronas transfectadas con concentraciones pequeñas de PFKFB3 silvestre ($0.16 \mu\text{g/ml}$); la transfección de neuronas con las mismas cantidades de cDNA de mutPFKFB3 incrementó los niveles de superóxido de manera similar al tratamiento con glutamato; sin embargo, el glutamato no incrementó más los niveles de superóxido en neuronas expresando mutPFKFB3. b) El tratamiento con glutamato incrementó la muerte por apoptosis en neuronas transfectadas con niveles bajos de cDNA de PFKFB3 silvestre; la transfección con cantidades idénticas de cDNA de mutPFKFB3 incrementó la muerte por apoptosis de forma similar al glutamato; sin embargo, el glutamato no incrementó aún más la apoptosis en las neuronas expresando mutPFKFB3. * $P < 0.05$ (ANOVA)($n=3$).

14. La proteína TIGAR, con función fructosa-2,6-bisfosfatasa, se encuentra expresada en neuronas

TIGAR (Tp53-inducible glycolysis and apoptotic regulator) es una proteína con actividad fructosa-2,6-bisfosfatasa que ha sido recientemente descubierta. En vista de que TIGAR podría tener efectos metabólicos opuestos a PFKFB3, nos preguntamos si la regulación de la actividad glucolítica en neuronas podría estar regulada tanto por TIGAR como por PFKFB3. Para ello, en primer lugar quisimos investigar si esta proteína está expresada en neuronas corticales de rata y en astrocitos en cultivo primario, mediante western blot. Como se muestra en la figura 14, TIGAR está expresada en ambos tipos celulares, siendo su expresión algo mayor en neuronas.

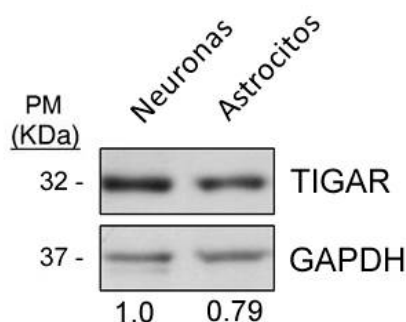


Figura 14. TIGAR está presente tanto en neuronas como astrocitos y las neuronas presentan niveles ligeramente mayores de la proteína. Neuronas a 6 días de cultivo y astrocitos a día 15 se lisaron en tampón RIPA y se sometieron a una transferencia de western blot con el fin de analizar los niveles de TIGAR en ambos tipos celulares.

15. Determinación de apoptosis y niveles de superóxido en neuronas procedentes de ratones KO de TIGAR

Dado que TIGAR presenta una actividad opuesta a la PFKFB3 y que previamente hemos observado que la acumulación de PFKFB3 produce estrés oxidativo y muerte neuronal por apoptosis, nos propusimos investigar si la deficiencia de TIGAR producía efectos similares a la sobreexpresión de PFKFB3. Para ello en primer lugar utilizamos ratones KO para TIGAR disponibles en el grupo de la doctora Karen Vousden (Beatson Institute for Cancer Research, Glasgow, Reino Unido) y realizamos cultivos primarios de neuronas corticales para medir los niveles de superóxido y la muerte por apoptosis. Como se observa en las figuras 15a y 15b, ni los niveles mitocondriales de superóxido ni la muerte por apoptosis se vieron incrementados en las neuronas procedentes de estos animales. Sin embargo, razonamos que puesto que estos ratones no son inducibles, el

metabolismo glucolítico podría estar sufriendo algún proceso de compensación que impidiera observar un fenotipo claro. Por ello decidimos realizar nuevos experimentos modulando los niveles de TIGAR tanto por sobreexpresión como por silenciamiento.

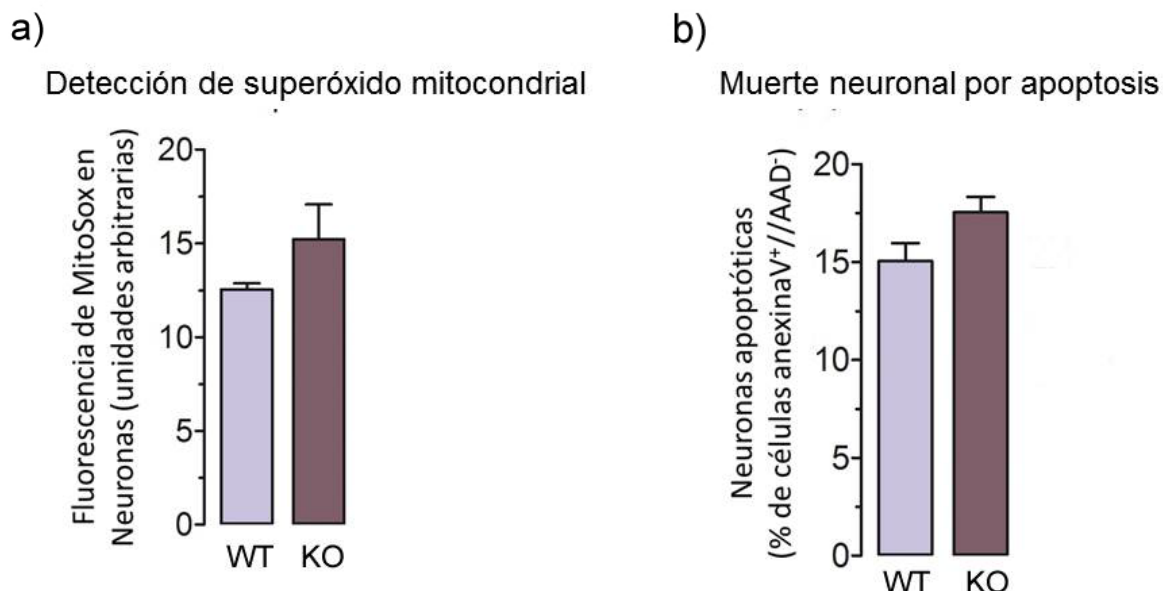


Figura 15. Detección de los niveles de anión superóxido mitocondriales y la muerte neuronal por apoptosis en neuronas de ratones silvestres y KO para TIGAR a 6 días de cultivo. a) Las neuronas procedentes del ratón KO para TIGAR presentan niveles de superóxido similares a los del silvestre, determinados mediante el análisis de fluorescencia de MitoSox-Red por citometría de flujo. b) Las neuronas procedentes del ratón KO para TIGAR no muestran un incremento significativo en los niveles de apoptosis respecto al control, determinados mediante la relación de neuronas anexina V⁺/AAD⁻ por citometría de flujo. (ANOVA).

16. TIGAR previene el incremento en superóxido mitocondrial y en apoptosis mediado por PFKFB3.

Seguidamente, decidimos investigar si el eje TIGAR-PFKFB3, mediante su capacidad para regular la glucólisis, podría regular los niveles de superóxido y la supervivencia neuronal. Para ello se expresó la forma mutPFKFB3 en concentraciones muy bajas (0.16 µg/ml) en neuronas corticales de rata en cultivo primario que, como se ha mostrado previamente, produce incrementos significativos en los niveles de superóxido mitocondriales y en la muerte por apoptosis. La co-expresión de TIGAR a altas concentraciones (1.6 µg/ml) previno completamente estos efectos (figuras 16a y 16b).

En conclusión, tanto el estrés oxidativo como la muerte neuronal por apoptosis parecen estar regulados por el eje TIGAR-PFKFB3.

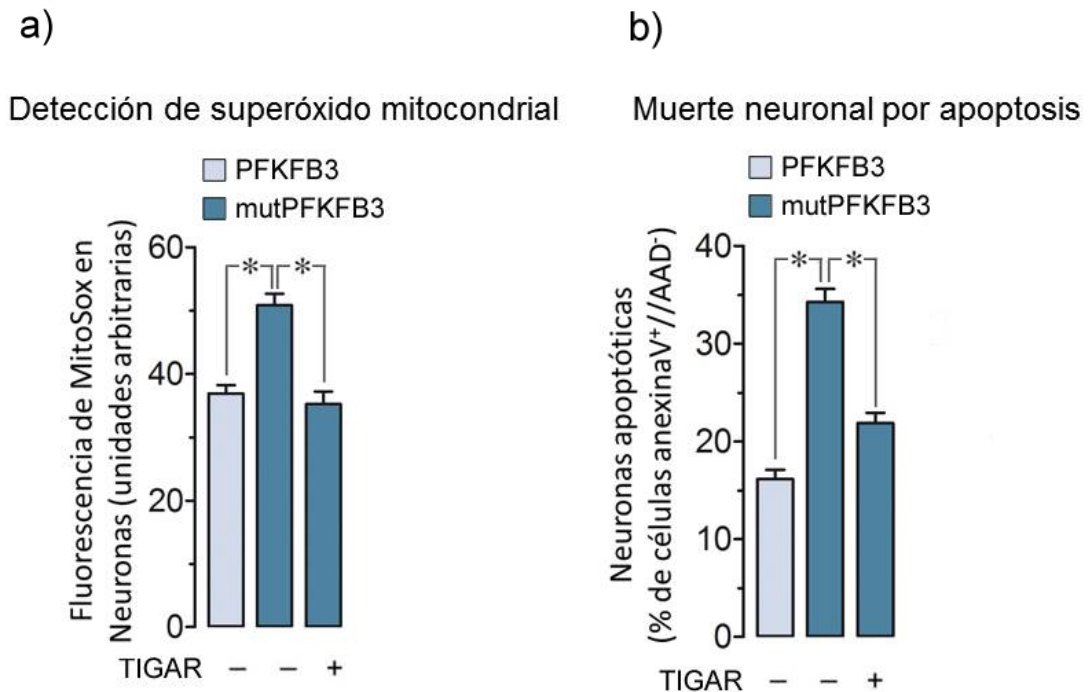


Figura 16 a) Las neuronas que expresan mutPFKFB3 (0.16 $\mu\text{g/ml}$) presentan un incremento en los niveles de anión superóxido mitocondrial, determinado mediante el análisis, por citometría de flujo, de la fluorescencia de MitoSox-Red, en comparación con las neuronas que expresan niveles idénticos de PFKFB3 silvestre. El incremento en superóxido se previene sobreexpresando TIGAR (1.6 $\mu\text{g/ml}$). b) Las neuronas que expresan niveles bajos de mutPFKFB3 presentan un incremento en la muerte por apoptosis, determinada mediante la medida por citometría de flujo de la proporción de células anexina V⁺/AAD⁻, que también se previene sobreexpresando TIGAR. * $P < 0.05$ (ANOVA)($n=3$).

17. El silenciamiento de TIGAR no es suficiente para incrementar la velocidad glucolítica en neuronas primarias

Seguidamente, silenciamos TIGAR en neuronas primarias de ratón. Para ello, diseñamos un siRNA contra TIGAR de *Mus musculus*. La transfección de neuronas con siTIGAR produjo un considerable (aunque no completo) descenso en los niveles de TIGAR después de 3 días (figura 17a). Sin embargo, no detectamos ningún incremento

significativo en la actividad glucolítica en neuronas transfectadas con siTIGAR respecto a las transfectadas con siControl (figura 17b).

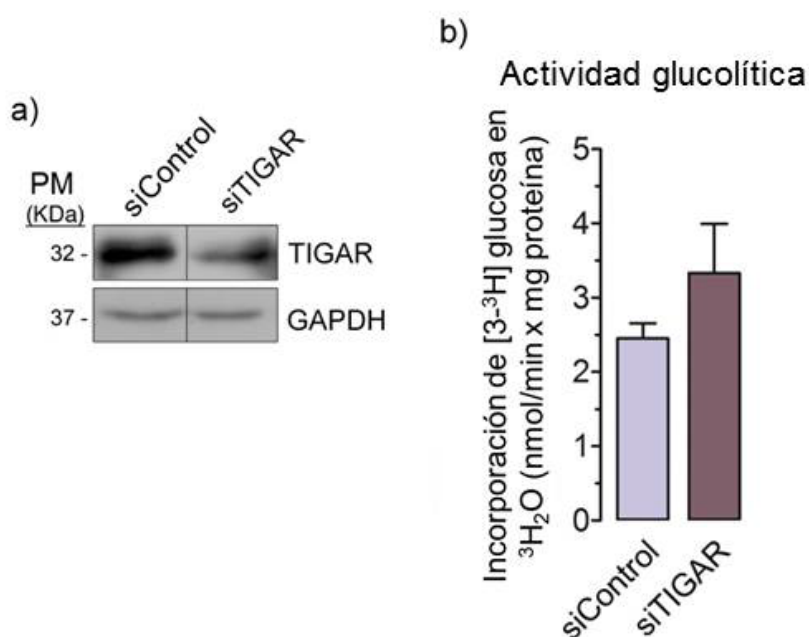


Figura 17. a) El siRNA de TIGAR silencia eficientemente los niveles de proteína en neuronas a los 3 días de transfección. Neuronas a 3 días de cultivo fueron transfectadas con siControl o siTIGAR (20 nM) a los 6 días de cultivo, las células se lisaron y se analizaron los niveles de proteína mediante western blot. b) La velocidad glucolítica, determinada mediante la producción de ³H₂O a partir de [3-³H] glucosa no aumenta significativamente en las neuronas transfectadas con siTIGAR.(ANOVA).

18. El silenciamiento de TIGAR en neuronas incrementa la muerte por apoptosis sin afectar a los niveles de superóxido

En vista que los resultados obtenidos sobre los niveles de superóxido y apoptosis mediante la sobreexpresión de TIGAR eran aparentemente inconsistentes con los obtenidos con el ratón KO, decidimos investigar esos efectos en neuronas en las que previamente silenciamos TIGAR. Para ello las neuronas corticales primarias de ratón se transfectaron con siTIGAR y posteriormente se trataron con glutamato, con el fin de estimular los receptores NMDA. Como se muestra en la figura 18a, siTIGAR no incrementó los niveles de superóxido, sin embargo, sí incrementó la muerte neuronal por apoptosis, es más, las neuronas transfectadas con siTIGAR vieron potenciado el efecto del glutamato sobre la muerte neuronal (figura 18b). En conjunto, nuestros resultados sugieren que, independientemente de un posible control de la concentración

de fructosa-2,6-bisfosfato y de la glucólisis, TIGAR podría presentar otras funciones sobre la supervivencia neuronal.

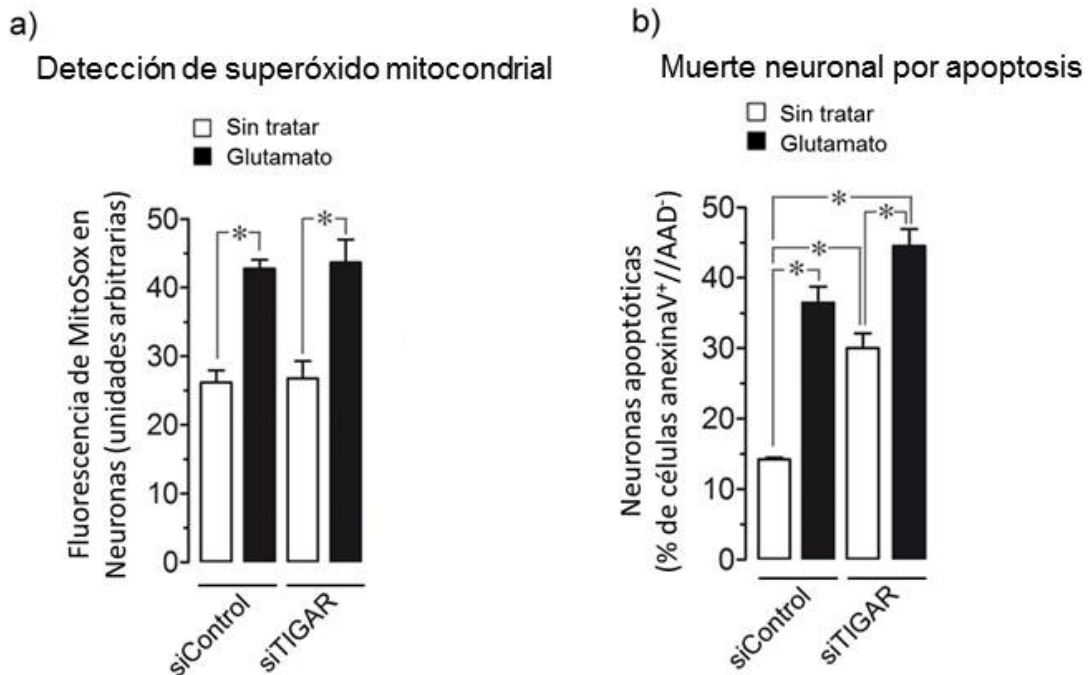


Figura 18. a) Los niveles de superóxido mitocondrial aumentan en las células tratadas con glutamato, pero no en las que han sido transfectadas con siTIGAR. b) La muerte neuronal por apoptosis se ve incrementada en neuronas transfectadas con siTIGAR y potencia el efecto del glutamato. * $P < 0.05$ (ANOVA)($n=3$).

19. TIGAR presenta una localización nuclear en neuronas

Con el objetivo de intentar esclarecer el control sobre supervivencia neuronal (independiente de la regulación metabólica) de TIGAR, decidimos investigar su localización subcelular. Para ello, llevamos a cabo cultivos primarios de neuronas y mixtos de neuronas y astrocitos a partir de embriones de ratón de 16 días de gestación. La localización endógena de TIGAR se analizó por inmunofluorescencia en un microscopio confocal. Como se muestra en la figura 19, TIGAR presenta una localización tanto citosólica como nuclear en neuronas, a juzgar por su co-localización con el marcador nuclear TOPRO-3. Sin embargo, TIGAR no está presente en el núcleo en astrocitos. Estos resultados sugieren que, al menos en neuronas, TIGAR podría presentar una función citoprotectora, aún desconocida, en el núcleo.

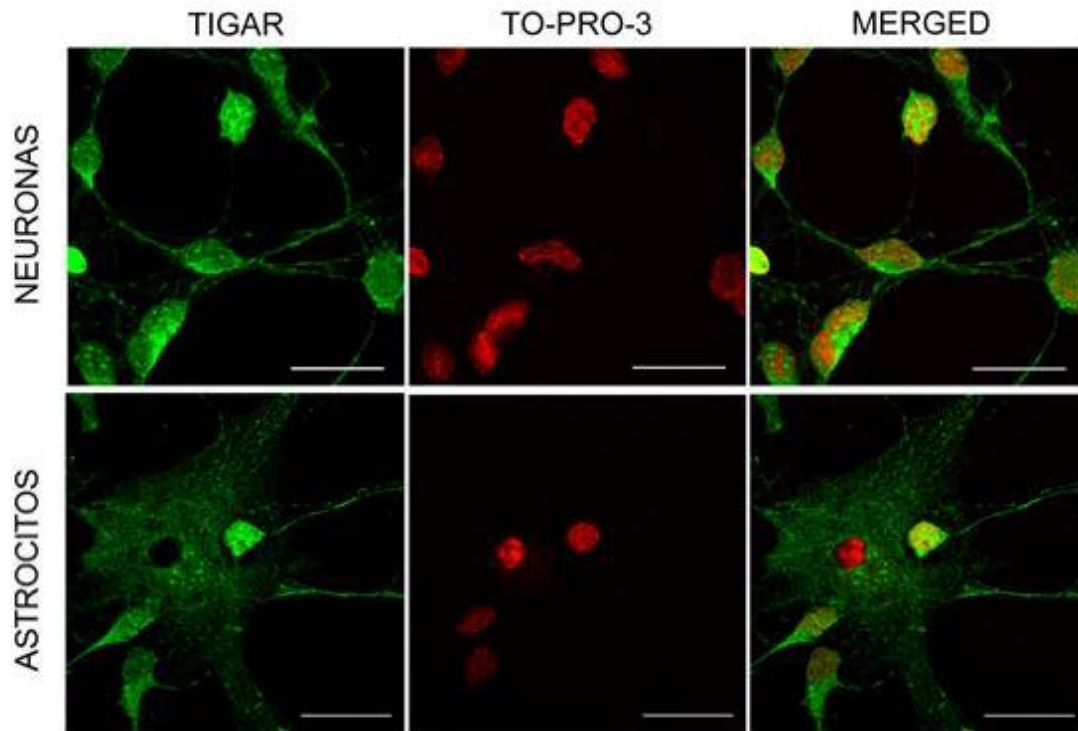


Figura 19. El análisis por inmunofluorescencia de la localización endógena de TIGAR muestra una localización citoplasmática y nuclear en neuronas. En astrocitos, sin embargo, la localización es únicamente citoplasmática Barra de escala: 20 μ m.

CONCLUSIONES

A la vista de los resultados presentados en este trabajo, hemos obtenido las siguientes conclusiones:

1- Los ensayos radiométricos basados en la medida de la incorporación de [3-³H] glucosa en ³H₂O, y en la diferencia de la incorporación de [1-¹⁴C] glucosa y [6-¹⁴C] glucosa en ¹⁴CO₂, son específicos para determinar las velocidades glucolítica y de la PPP, respectivamente, en neuronas en placa. Sin embargo, la fosfoglucosa isomerasa en neuronas funciona cercana al equilibrio, lo que origina la dilución isotópica de [¹⁴C] glucosa debido al reciclaje de fructosa-6-fosfato no marcada en glucosa-6-fosfato. Debido a esto, la velocidad de la PPP medida está ampliamente infraestimada.

2- Las neuronas metabolizan, aproximadamente, el doble de la glucosa-6-fosfato por la vía de las pentosas-fosfato y el resto por glucolisis en condiciones de reposo; sin embargo, esta relación está sujeta a regulación para adaptarse a diferentes condiciones de estrés.

3- La sobre estimulación de los receptores de glutamato, en concreto el subtipo NMDA, es suficiente para producir la estabilización de PFKFB3, ocasionando una modificación del metabolismo de la glucosa de PPP a glucolisis. En consecuencia, el estado redox del glutatión cambia, produciendo estrés oxidativo y muerte neuronal por apoptosis. Estos resultados identifican PFKFB3 como una nueva diana terapéutica contra la excitotoxicidad.

4- La reciente descubierta fructose-2.6-bisfosfatasa TIGAR está expresada en neuronas, donde contribuye a la regulación de la glucolisis neuronal. De este modo, la sobre expresión de TIGAR previene de la muerte neuronal por apoptosis producida por PFKFB3. En cambio, el silenciamiento de TIGAR produce un incremento en la muerte neuronal por apoptosis que es independiente de los niveles de superóxido. Estos resultados, junto con la presencia de TIGAR en el núcleo, sugieren una función, aún por determinar de esta proteína en neuronas.



8. REFERENCES

REFERENCES

Aarts, M., Liu, Y., Liu, L., Besshoh, S., Arundine, M., Gurd, J. W., Wang, Y. T., Salter, M. W. and Tymianski, M. (2002) Treatment of ischemic brain damage by perturbing NMDA receptor- PSD-95 protein interactions. *Science*, 298, 846-850.

Almeida, A., Almeida, J., Bolanos, J. P. and Moncada, S. (2001) Different responses of astrocytes and neurons to nitric oxide: the role of glycolytically generated ATP in astrocyte protection. *Proc Natl Acad Sci U S A*, 98, 15294-15299.

Almeida, A. and Bolanos, J. P. (2001) A transient inhibition of mitochondrial ATP synthesis by nitric oxide synthase activation triggered apoptosis in primary cortical neurons. *J Neurochem*, 77, 676-690.

Almeida, A., Bolanos, J. P. and Moncada, S. (2010) E3 ubiquitin ligase APC/C-Cdh1 accounts for the Warburg effect by linking glycolysis to cell proliferation. *Proc Natl Acad Sci U S A*, 107, 738-741.

Almeida, A., Bolanos, J. P. and Moreno, S. (2005) Cdh1/Hct1-APC is essential for the survival of postmitotic neurons. *J Neurosci*, 25, 8115-8121.

Almeida, A., Heales, S. J., Bolanos, J. P. and Medina, J. M. (1998) Glutamate neurotoxicity is associated with nitric oxide-mediated mitochondrial dysfunction and glutathione depletion. *Brain Res*, 790, 209-216.

Almeida, A., Moncada, S. and Bolanos, J. P. (2004) Nitric oxide switches on glycolysis through the AMP protein kinase and 6-phosphofructo-2-kinase pathway. *Nat Cell Biol*, 6, 45-51.

Alvarez, G., Ramos, M., Ruiz, F., Satrustegui, J. and Bogonez, E. (2003) Pyruvate protection against beta-amyloid-induced neuronal death: role of mitochondrial redox state. *J Neurosci Res*, 73, 260-269.

Ames, A., 3rd (2000) CNS energy metabolism as related to function. *Brain Res Brain Res Rev*, 34, 42-68.

Ando, M., Uehara, I., Kogure, K., Asano, Y., Nakajima, W., Abe, Y., Kawauchi, K. and Tanaka, N. (2010) Interleukin 6 enhances glycolysis through expression of the glycolytic enzymes hexokinase 2 and 6-phosphofructo-2-kinase/fructose-2,6-bisphosphatase-3. *J Nippon Med Sch*, 77, 97-105.

Araujo, I. M., Carreira, B. P., Pereira, T. et al. (2007) Changes in calcium dynamics following the reversal of the sodium-calcium exchanger have a key role in AMPA receptor-mediated neurodegeneration via calpain activation in hippocampal neurons. *Cell Death Differ*, 14, 1635-1646.

Attwell, D. and Laughlin, S. B. (2001) An energy budget for signaling in the grey matter of the brain. *J Cereb Blood Flow Metab*, 21, 1133-1145.

Aviles-Olmos, I., Limousin, P., Lees, A. and Foltynie, T. (2013) Parkinson's disease, insulin resistance and novel agents of neuroprotection. *Brain*, 136, 374-384.

REFERENCES

- Bak, L. K., Obel, L. F., Walls, A. B., Schousboe, A., Faek, S. A., Jajo, F. S. and Waagepetersen, H. S.** (2012) Novel model of neuronal bioenergetics: postsynaptic utilization of glucose but not lactate correlates positively with Ca²⁺ signalling in cultured mouse glutamatergic neurons. *ASN Neuro*, 4.
- Bak, L. K., Schousboe, A., Sonnewald, U. and Waagepetersen, H. S.** (2006) Glucose is necessary to maintain neurotransmitter homeostasis during synaptic activity in cultured glutamatergic neurons. *J Cereb Blood Flow Metab*, 26, 1285-1297.
- Bak, L. K., Walls, A. B., Schousboe, A., Ring, A., Sonnewald, U. and Waagepetersen, H. S.** (2009) Neuronal glucose but not lactate utilization is positively correlated with NMDA-induced neurotransmission and fluctuations in cytosolic Ca²⁺ levels. *J Neurochem*, 109 Suppl 1, 87-93.
- Baki, A., Tompa, P., Alexa, A., Molnar, O. and Friedrich, P.** (1996) Autolysis parallels activation of mu-calpain. *Biochem J*, 318 (Pt 3), 897-901.
- Bano, D., Young, K. W., Guerin, C. J., Lefevre, R., Rothwell, N. J., Naldini, L., Rizzuto, R., Carafoli, E. and Nicotera, P.** (2005) Cleavage of the plasma membrane Na⁺/Ca²⁺ exchanger in excitotoxicity. *Cell*, 120, 275-285.
- Baquer, N. Z., Hothersall, J. S. and McLean, P.** (1988) Function and regulation of the pentose phosphate pathway in brain. *Curr Top Cell Regul*, 29, 265-289.
- Barford, D.** (2011) Structural insights into anaphase-promoting complex function and mechanism. *Philos Trans R Soc Lond B Biol Sci*, 366, 3605-3624.
- Bartrons, R. and Caro, J.** (2007) Hypoxia, glucose metabolism and the Warburg's effect. *J Bioenerg Biomembr*, 39, 223-229.
- Ben-Yoseph, O., Boxer, P. A. and Ross, B. D.** (1994) Oxidative stress in the central nervous system: monitoring the metabolic response using the pentose phosphate pathway. *Dev Neurosci*, 16, 328-336.
- Bensaad, K., Cheung, E. C. and Vousden, K. H.** (2009) Modulation of intracellular ROS levels by TIGAR controls autophagy. *EMBO J*, 28, 3015-3026.
- Bensaad, K., Tsuruta, A., Selak, M. A., Vidal, M. N., Nakano, K., Bartrons, R., Gottlieb, E. and Vousden, K. H.** (2006) TIGAR, a p53-inducible regulator of glycolysis and apoptosis. *Cell*, 126, 107-120.
- Bergmeyer, H. U., Bernt, E., Schmidt, F. and Stork, H.** (1974) Determination with hexokinase and glucoses-phosphate dehydrogenase. In: *Methods of Enzymatic Analysis* pp. 1196-1201. Verlag Chemie GmbH, Weinheim.
- Biagiotti, E., Guidi, L., Del Grande, P. and Ninfali, P.** (2003) Glucose-6-phosphate dehydrogenase expression associated with NADPH-dependent reactions in cerebellar neurons. *Cerebellum*, 2, 178-183.
- Blazquez, C., Woods, A., de Ceballos, M. L., Carling, D. and Guzman, M.** (1999) The AMP-activated protein kinase is involved in the regulation of ketone body production by astrocytes. *J Neurochem*, 73, 1674-1682.
- Bolanos, J. P.** (2013) Adapting glycolysis to cancer cell proliferation: the MAPK pathway focuses on PFKFB3. *Biochem J*, 452, e7-9.

- Bolanos, J. P., Peuchen, S., Heales, S. J., Land, J. M. and Clark, J. B.** (1994) Nitric oxide-mediated inhibition of the mitochondrial respiratory chain in cultured astrocytes. *J Neurochem*, 63, 910-916.
- Boumezbeur, F., Petersen, K. F., Cline, G. W., Mason, G. F., Behar, K. L., Shulman, G. I. and Rothman, D. L.** (2010) The contribution of blood lactate to brain energy metabolism in humans measured by dynamic ¹³C nuclear magnetic resonance spectroscopy. *J Neurosci*, 30, 13983-13991.
- Bouzier-Sore, A. K., Voisin, P., Bouchaud, V., Bezancon, E., Franconi, J. M. and Pellerin, L.** (2006) Competition between glucose and lactate as oxidative energy substrates in both neurons and astrocytes: a comparative NMR study. *Eur J Neurosci*, 24, 1687-1694.
- Bouzier-Sore, A. K., Voisin, P., Canioni, P., Magistretti, P. J. and Pellerin, L.** (2003) Lactate is a preferential oxidative energy substrate over glucose for neurons in culture. *J Cereb Blood Flow Metab*, 23, 1298-1306.
- Brand, M. D.** (2011) The sites and topology of mitochondrial superoxide production. *Exp Gerontol*, 45, 466-472.
- Brekke, E. M., Walls, A. B., Schousboe, A., Waagepetersen, H. S. and Sonnewald, U.** (2012) Quantitative importance of the pentose phosphate pathway determined by incorporation of ¹³C from [2-¹³C]- and [3-¹³C]glucose into TCA cycle intermediates and neurotransmitter amino acids in functionally intact neurons. *J Cereb Blood Flow Metab*, 32, 1788-1799.
- Broadstock, M., Austin, P. J., Betts, M. J. and Duty, S.** (2012) Antiparkinsonian potential of targeting group III metabotropic glutamate receptor subtypes in the rodent substantia nigra pars reticulata. *Br J Pharmacol*, 165, 1034-1045.
- Bruno, V., Battaglia, G., Kingston, A., O'Neill, M. J., Catania, M. V., Di Grezia, R. and Nicoletti, F.** (1999) Neuroprotective activity of the potent and selective mGlu1a metabotropic glutamate receptor antagonist, (+)-2-methyl-4 carboxyphenylglycine (LY367385): comparison with LY357366, a broader spectrum antagonist with equal affinity for mGlu1a and mGlu5 receptors. *Neuropharmacology*, 38, 199-207.
- Brustovetsky, T., Bolshakov, A. and Brustovetsky, N.** (2010) Calpain activation and Na⁺/Ca²⁺ exchanger degradation occur downstream of calcium deregulation in hippocampal neurons exposed to excitotoxic glutamate. *J Neurosci Res*, 88, 1317-1328.
- Butcher, S. P. and Hamberger, A.** (1987) In vivo studies on the extracellular, and veratrine-releasable, pools of endogenous amino acids in the rat striatum: effects of corticostriatal deafferentation and kainic acid lesion. *J Neurochem*, 48, 713-721.
- Carbonell, J., Feliu, J. E., Marco, R. and Sols, A.** (1973) Pyruvate kinase. Classes of regulatory isoenzymes in mammalian tissues. *Eur J Biochem*, 37, 148-156.
- Carvalho, C., Cardoso, S., Correia, S. C., Santos, R. X., Santos, M. S., Baldeiras, I., Oliveira, C. R. and Moreira, P. I.** (2012) Metabolic alterations induced by sucrose intake and Alzheimer's disease promote similar brain mitochondrial abnormalities. *Diabetes*, 61, 1234-1242.
- Castellano, C., Cestari, V. and Ciamei, A.** (2001) NMDA receptors and learning and memory processes. *Curr Drug Targets*, 2, 273-283.

REFERENCES

- Cataldo, A. M. and Broadwell, R. D.** (1986) Cytochemical identification of cerebral glycogen and glucose-6-phosphatase activity under normal and experimental conditions. II. Choroid plexus and ependymal epithelia, endothelia and pericytes. *J Neurocytol*, 15, 511-524.
- Ciarmiello, A., Cannella, M., Lastoria, S., Simonelli, M., Frati, L., Rubinsztein, D. C. and Squitieri, F.** (2006) Brain white-matter volume loss and glucose hypometabolism precede the clinical symptoms of Huntington's disease. *J Nucl Med*, 47, 215-222.
- Cidad, P., Almeida, A. and Bolanos, J. P.** (2004) Inhibition of mitochondrial respiration by nitric oxide rapidly stimulates cytoprotective GLUT3-mediated glucose uptake through 5'-AMP-activated protein kinase. *Biochem J*, 384, 629-636.
- Collins, G. H., Cowden, R. R. and Nevis, A. H.** (1968) Myoclonus epilepsy with Lafora bodies. An ultrastructural and cytochemical study. *Arch Pathol*, 86, 239-254.
- Collins, M. O., Husi, H., Yu, L., Brandon, J. M., Anderson, C. N., Blackstock, W. P., Choudhary, J. S. and Grant, S. G.** (2006) Molecular characterization and comparison of the components and multiprotein complexes in the postsynaptic proteome. *J Neurochem*, 97 Suppl 1, 16-23.
- Cunnane, S., Nugent, S., Roy, M. et al.** (2011) Brain fuel metabolism, aging, and Alzheimer's disease. *Nutrition*, 27, 3-20.
- Cheng, K. and Ip, N. Y.** (2003) Cdk5: a new player at synapses. *Neurosignals*, 12, 180-190.
- Cheung, E. C., Athineos, D., Lee, P. et al.** (2013) TIGAR Is Required for Efficient Intestinal Regeneration and Tumorigenesis. *Dev Cell*.
- Cheung, E. C., Ludwig, R. L. and Vousden, K. H.** (2012) Mitochondrial localization of TIGAR under hypoxia stimulates HK2 and lowers ROS and cell death. *Proc Natl Acad Sci U S A*, 109, 20491-20496.
- Chittajallu, R., Vignes, M., Dev, K. K., Barnes, J. M., Collingridge, G. L. and Henley, J. M.** (1996) Regulation of glutamate release by presynaptic kainate receptors in the hippocampus. *Nature*, 379, 78-81.
- Choi, D. W.** (1987) Ionic dependence of glutamate neurotoxicity. *J Neurosci*, 7, 369-379.
- Choi, I. Y., Seaquist, E. R. and Gruetter, R.** (2003) Effect of hypoglycemia on brain glycogen metabolism in vivo. *J Neurosci Res*, 72, 25-32.
- Choo, A. M., Geddes-Klein, D. M., Hockenberry, A., Scarsella, D., Mesfin, M. N., Singh, P., Patel, T. P. and Meaney, D. F.** (2012) NR2A and NR2B subunits differentially mediate MAP kinase signaling and mitochondrial morphology following excitotoxic insult. *Neurochem Int*, 60, 506-516.
- Chuquet, J., Quilichini, P., Nimchinsky, E. A. and Buzsaki, G.** (2010) Predominant enhancement of glucose uptake in astrocytes versus neurons during activation of the somatosensory cortex. *J Neurosci*, 30, 15298-15303.
- Delgado-Esteban, M., Almeida, A. and Bolanos, J. P.** (2000) D-Glucose prevents glutathione oxidation and mitochondrial damage after glutamate receptor stimulation in rat cortical primary neurons. *J Neurochem*, 75, 1618-1624.

- Dong, X. X., Wang, Y. and Qin, Z. H.** (2009) Molecular mechanisms of excitotoxicity and their relevance to pathogenesis of neurodegenerative diseases. *Acta Pharmacol Sin*, 30, 379-387.
- Dringen, R.** (2000) Metabolism and functions of glutathione in brain. *Prog Neurobiol*, 62, 649-671.
- Dringen, R., Gebhardt, R. and Hamprecht, B.** (1993) Glycogen in astrocytes: possible function as lactate supply for neighboring cells. *Brain Res*, 623, 208-214.
- Dringen, R., Gutterer, J. M., Gros, C. and Hirrlinger, J.** (2001) Aminopeptidase N mediates the utilization of the GSH precursor CysGly by cultured neurons. *J Neurosci Res*, 66, 1003-1008.
- Dugan, L. L., Sensi, S. L., Canzoniero, L. M., Handran, S. D., Rothman, S. M., Lin, T. S., Goldberg, M. P. and Choi, D. W.** (1995) Mitochondrial production of reactive oxygen species in cortical neurons following exposure to N-methyl-D-aspartate. *J Neurosci*, 15, 6377-6388.
- Dunaway, G. A., Kasten, T. P., Sebo, T. and Trapp, R.** (1988) Analysis of the phosphofructokinase subunits and isoenzymes in human tissues. *Biochem J*, 251, 677-683.
- Emile, L., Mercken, L., Apiou, F., Pradier, L., Bock, M. D., Menager, J., Clot, J., Doble, A. and Blanchard, J. C.** (1996) Molecular cloning, functional expression, pharmacological characterization and chromosomal localization of the human metabotropic glutamate receptor type 3. *Neuropharmacology*, 35, 523-530.
- Estrada-Sanchez, A. M., Montiel, T., Segovia, J. and Massieu, L.** (2009) Glutamate toxicity in the striatum of the R6/2 Huntington's disease transgenic mice is age-dependent and correlates with decreased levels of glutamate transporters. *Neurobiol Dis*, 34, 78-86.
- Farrar, G. and Farrar, W. W.** (1995) Purification and properties of the pyruvate kinase isozyme M1 from the pig brain. *Int J Biochem Cell Biol*, 27, 1145-1151.
- Ferreira, J. M., Burnett, A. L. and Rameau, G. A.** (2011) Activity-dependent regulation of surface glucose transporter-3. *J Neurosci*, 31, 1991-1999.
- Filomeni, G., Cardaci, S., Da Costa Ferreira, A. M., Rotilio, G. and Ciriolo, M. R.** (2011) Metabolic oxidative stress elicited by the copper(II) complex [Cu(isaepy)₂] triggers apoptosis in SH-SY5Y cells through the induction of the AMP-activated protein kinase/p38MAPK/p53 signalling axis: evidence for a combined use with 3-bromopyruvate in neuroblastoma treatment. *Biochem J*, 437, 443-453.
- Flohe, L., Gunzler, W., Jung, G., Schaich, E. and Schneider, F.** (1971) [Glutathione peroxidase. II. Substrate specificity and inhibitory effects of substrate analogues]. *Hoppe Seylers Z Physiol Chem*, 352, 159-169.
- Flohe, L., Toppo, S., Cozza, G. and Ursini, F.** (2011) A comparison of thiol peroxidase mechanisms. *Antioxid Redox Signal*, 15, 763-780.

REFERENCES

- Frolova, A. I., O'Neill, K. and Moley, K. H.** (2011) Dehydroepiandrosterone inhibits glucose flux through the pentose phosphate pathway in human and mouse endometrial stromal cells, preventing decidualization and implantation. *Mol Endocrinol*, 25, 1444-1455.
- Fukui, H. and Moraes, C. T.** (2008) The mitochondrial impairment, oxidative stress and neurodegeneration connection: reality or just an attractive hypothesis? *Trends Neurosci*, 31, 251-256.
- Garcia-Nogales, P., Almeida, A. and Bolanos, J. P.** (2003) Peroxynitrite protects neurons against nitric oxide-mediated apoptosis. A key role for glucose-6-phosphate dehydrogenase activity in neuroprotection. *The Journal of biological chemistry*, 278, 864-874.
- Gimenez-Cassina, A., Lim, F., Cerrato, T., Palomo, G. M. and Diaz-Nido, J.** (2009) Mitochondrial hexokinase II promotes neuronal survival and acts downstream of glycogen synthase kinase-3. *J Biol Chem*, 284, 3001-3011.
- Glodzik, L., King, K. G., Gonen, O., Liu, S., De Santi, S. and de Leon, M. J.** (2008) Memantine decreases hippocampal glutamate levels: a magnetic resonance spectroscopy study. *Prog Neuropsychopharmacol Biol Psychiatry*, 32, 1005-1012.
- Goodwin, G. W., Cohen, D. M. and Taegtmeyer, H.** (2001) [5-3H]glucose overestimates glycolytic flux in isolated working rat heart: role of the pentose phosphate pathway. *Am J Physiol Endocrinol Metab*, 280, E502-508.
- Grueter, B. A. and Winder, D. G.** (2005) Group II and III metabotropic glutamate receptors suppress excitatory synaptic transmission in the dorsolateral bed nucleus of the stria terminalis. *Neuropsychopharmacology*, 30, 1302-1311.
- Gunter, K. K. and Gunter, T. E.** (1994) Transport of calcium by mitochondria. *J Bioenerg Biomembr*, 26, 471-485.
- Gunter, T. E. and Gunter, K. K.** (2001) Uptake of calcium by mitochondria: transport and possible function. *IUBMB Life*, 52, 197-204.
- Gutmann, I. and Wahlefeld, A. W.** (1974) *Methods of Enzymatic Analysis* (ed. Bergmeyer, H. U.) pp. 1464-1468. Weinheim.
- Guzman, M. and Blazquez, C.** (2004) Ketone body synthesis in the brain: possible neuroprotective effects. *Prostaglandins Leukot Essent Fatty Acids*, 70, 287-292.
- Halim, N. D., McFate, T., Mohyeldin, A. et al.** (2010) Phosphorylation status of pyruvate dehydrogenase distinguishes metabolic phenotypes of cultured rat brain astrocytes and neurons. *Glia*, 58, 1168-1176.
- Halliwell, B.** (2011) Free radicals and antioxidants - quo vadis? *Trends Pharmacol Sci*, 32, 125-130.
- Hardingham, G. E. and Bading, H.** (2010) Synaptic versus extrasynaptic NMDA receptor signalling: implications for neurodegenerative disorders. *Nat Rev Neurosci*, 11, 682-696.

- Hardingham, G. E., Fukunaga, Y. and Bading, H.** (2002) Extrasynaptic NMDARs oppose synaptic NMDARs by triggering CREB shut-off and cell death pathways. *Nat Neurosci*, 5, 405-414.
- Heales, S. J., Bolanos, J. P., Land, J. M. and Clark, J. B.** (1994) Trolox protects mitochondrial complex IV from nitric oxide-mediated damage in astrocytes. *Brain Res*, 668, 243-245.
- Heine, M., Thoumine, O., Mondin, M., Tessier, B., Giannone, G. and Choquet, D.** (2008) Activity-independent and subunit-specific recruitment of functional AMPA receptors at neurexin/neuroigin contacts. *Proc Natl Acad Sci U S A*, 105, 20947-20952.
- Hekimi, S., Lapointe, J. and Wen, Y.** (2011) Taking a "good" look at free radicals in the aging process. *Trends Cell Biol*, 21, 569-576.
- Herrero-Mendez, A., Almeida, A., Fernandez, E., Maestre, C., Moncada, S. and Bolanos, J. P.** (2009) The bioenergetic and antioxidant status of neurons is controlled by continuous degradation of a key glycolytic enzyme by APC/C-Cdh1. *Nat Cell Biol*, 11, 747-752.
- Hirrlinger, J., Schulz, J. B. and Dringen, R.** (2002) Glutathione release from cultured brain cells: multidrug resistance protein 1 mediates the release of GSH from rat astroglial cells. *J Neurosci Res*, 69, 318-326.
- Howland, D. S., Liu, J., She, Y. et al.** (2002) Focal loss of the glutamate transporter EAAT2 in a transgenic rat model of SOD1 mutant-mediated amyotrophic lateral sclerosis (ALS). *Proc Natl Acad Sci U S A*, 99, 1604-1609.
- Hsieh, M. H., Ho, S. C., Yeh, K. Y., Pawlak, C. R., Chang, H. M., Ho, Y. J., Lai, T. J. and Wu, F. Y.** (2012) Blockade of metabotropic glutamate receptors inhibits cognition and neurodegeneration in an MPTP-induced Parkinson's disease rat model. *Pharmacol Biochem Behav*, 102, 64-71.
- Hue, L. and Rider, M. H.** (1987) Role of fructose 2,6-bisphosphate in the control of glycolysis in mammalian tissues. *Biochem J*, 245, 313-324.
- Jaquenoud, M., van Drogen, F. and Peter, M.** (2002) Cell cycle-dependent nuclear export of Cdh1p may contribute to the inactivation of APC/C(Cdh1). *EMBO J*, 21, 6515-6526.
- Johnson, K. A., Jones, C. K., Tantawy, M. N., Bubser, M., Marvanova, M., Ansari, M. S., Baldwin, R. M., Conn, P. J. and Niswender, C. M.** (2013) The metabotropic glutamate receptor 8 agonist (S)-3,4-DCEPG reverses motor deficits in prolonged but not acute models of Parkinson's disease. *Neuropharmacology*, 66, 187-195.
- Joly, C., Gomeza, J., Brabet, I., Curry, K., Bockaert, J. and Pin, J. P.** (1995) Molecular, functional, and pharmacological characterization of the metabotropic glutamate receptor type 5 splice variants: comparison with mGluR1. *J Neurosci*, 15, 3970-3981.
- Kanai, Y. and Hediger, M. A.** (1992) Primary structure and functional characterization of a high-affinity glutamate transporter. *Nature*, 360, 467-471.
- Kasischke, K. A., Vishwasrao, H. D., Fisher, P. J., Zipfel, W. R. and Webb, W. W.** (2004) Neural activity triggers neuronal oxidative metabolism followed by astrocytic glycolysis. *Science*, 305, 99-103.

REFERENCES

- Kaufman, A. M., Milnerwood, A. J., Sepers, M. D. et al.** (2012) Opposing roles of synaptic and extrasynaptic NMDA receptor signaling in cocultured striatal and cortical neurons. *J Neurosci*, 32, 3992-4003.
- Khodorov, B., Pinelis, V., Vergun, O., Storzhevykh, T. and Vinskaya, N.** (1996) Mitochondrial deenergization underlies neuronal calcium overload following a prolonged glutamate challenge. *FEBS Lett*, 397, 230-234.
- Klepper, J. and Voit, T.** (2002) Facilitated glucose transporter protein type 1 (GLUT1) deficiency syndrome: impaired glucose transport into brain-- a review. *Eur J Pediatr*, 161, 295-304.
- Knott, A. B., Perkins, G., Schwarzenbacher, R. and Bossy-Wetzell, E.** (2008) Mitochondrial fragmentation in neurodegeneration. *Nat Rev Neurosci*, 9, 505-518.
- Kruman, II, Pedersen, W. A., Springer, J. E. and Mattson, M. P.** (1999) ALS-linked Cu/Zn-SOD mutation increases vulnerability of motor neurons to excitotoxicity by a mechanism involving increased oxidative stress and perturbed calcium homeostasis. *Exp Neurol*, 160, 28-39.
- Laloux, M., Van Schaftingen, E., Francois, J. and Hers, H. G.** (1985) Phosphate dependency of phosphofructokinase 2. *Eur J Biochem*, 148, 155-159.
- Le, W. D., Colom, L. V., Xie, W. J., Smith, R. G., Alexianu, M. and Appel, S. H.** (1995) Cell death induced by beta-amyloid 1-40 in MES 23.5 hybrid clone: the role of nitric oxide and NMDA-gated channel activation leading to apoptosis. *Brain Res*, 686, 49-60.
- Lee, M. S., Kwon, Y. T., Li, M., Peng, J., Friedlander, R. M. and Tsai, L. H.** (2000) Neurotoxicity induces cleavage of p35 to p25 by calpain. *Nature*, 405, 360-364.
- Leo, G. C., Driscoll, B. F., Shank, R. P. and Kaufman, E.** (1993) Analysis of [1-13C]D-glucose metabolism in cultured astrocytes and neurons using nuclear magnetic resonance spectroscopy. *Dev Neurosci*, 15, 282-288.
- Li, H. and Jogl, G.** (2009) Structural and biochemical studies of TIGAR (TP53-induced glycolysis and apoptosis regulator). *J Biol Chem*, 284, 1748-1754.
- Lievens, J. C., Woodman, B., Mahal, A., Spasic-Boscovic, O., Samuel, D., Kerkerian-Le Goff, L. and Bates, G. P.** (2001) Impaired glutamate uptake in the R6 Huntington's disease transgenic mice. *Neurobiol Dis*, 8, 807-821.
- Lipton, S. A.** (2004) Failures and successes of NMDA receptor antagonists: molecular basis for the use of open-channel blockers like memantine in the treatment of acute and chronic neurologic insults. *NeuroRx*, 1, 101-110.
- Loaiza, A., Porras, O. H. and Barros, L. F.** (2003) Glutamate triggers rapid glucose transport stimulation in astrocytes as evidenced by real-time confocal microscopy. *J Neurosci*, 23, 7337-7342.
- Luetjens, C. M., Bui, N. T., Sengpiel, B., Munstermann, G., Poppe, M., Krohn, A. J., Bauerbach, E., Krieglstein, J. and Prehn, J. H.** (2000) Delayed mitochondrial dysfunction in excitotoxic neuron death: cytochrome c release and a secondary increase in superoxide production. *J Neurosci*, 20, 5715-5723.

- Madan, E., Gogna, R., Kuppusamy, P., Bhatt, M., Pati, U. and Mahdi, A. A.** (2012) TIGAR induces p53-mediated cell-cycle arrest by regulation of RB-E2F1 complex. *Br J Cancer*, 107, 516-526.
- Maestre, C., Delgado-Esteban, M., Gomez-Sanchez, J. C., Bolanos, J. P. and Almeida, A.** (2008) Cdk5 phosphorylates Cdh1 and modulates cyclin B1 stability in excitotoxicity. *EMBO J*, 27, 2736-2745.
- Mari, M., Morales, A., Colell, A., Garcia-Ruiz, C. and Fernandez-Checa, J. C.** (2009) Mitochondrial glutathione, a key survival antioxidant. *Antioxid Redox Signal*, 11, 2685-2700.
- Marsin, A. S., Bouzin, C., Bertrand, L. and Hue, L.** (2002) The stimulation of glycolysis by hypoxia in activated monocytes is mediated by AMP-activated protein kinase and inducible 6-phosphofructo-2-kinase. *J Biol Chem*, 277, 30778-30783.
- Mateo, Z. and Porter, J. T.** (2007) Group II metabotropic glutamate receptors inhibit glutamate release at thalamocortical synapses in the developing somatosensory cortex. *Neuroscience*, 146, 1062-1072.
- Matsuda, K., Fletcher, M., Kamiya, Y. and Yuzaki, M.** (2003) Specific assembly with the NMDA receptor 3B subunit controls surface expression and calcium permeability of NMDA receptors. *J Neurosci*, 23, 10064-10073.
- Mattson, M. P., Cheng, B., Davis, D., Bryant, K., Lieberburg, I. and Rydel, R. E.** (1992) beta-Amyloid peptides destabilize calcium homeostasis and render human cortical neurons vulnerable to excitotoxicity. *J Neurosci*, 12, 376-389.
- McDonald, J. W. and Johnston, M. V.** (1990) Physiological and pathophysiological roles of excitatory amino acids during central nervous system development. *Brain Res Brain Res Rev*, 15, 41-70.
- Minchenko, A., Leshchinsky, I., Opentanova, I., Sang, N., Srinivas, V., Armstead, V. and Caro, J.** (2002) Hypoxia-inducible factor-1-mediated expression of the 6-phosphofructo-2-kinase/fructose-2,6-bisphosphatase-3 (PFKFB3) gene. Its possible role in the Warburg effect. *J Biol Chem*, 277, 6183-6187.
- Mosconi, L., Pupi, A. and De Leon, M. J.** (2008) Brain glucose hypometabolism and oxidative stress in preclinical Alzheimer's disease. *Ann N Y Acad Sci*, 1147, 180-195.
- Murphy, M. P. (2009) How mitochondria produce reactive oxygen species. *Biochem J*, 417, 1-13.
- Nelson, D. L. and Cox, M. M.** (2001) Lehninger, principles of biochemistry third edition.
- Nguyen, D., Alavi, M. V., Kim, K. Y. et al.** (2011) A new vicious cycle involving glutamate excitotoxicity, oxidative stress and mitochondrial dynamics. *Cell Death Dis*, 2, e240.
- Novellademunt, L., Bultot, L., Manzano, A., Ventura, F., Rosa, J. L., Vertommen, D., Rider, M. H., Navarro-Sabate, A. and Bartrons, R.** (2013) PFKFB3 activation in cancer cells by the p38/MK2 pathway in response to stress stimuli. *Biochem J*, 452, 531-543.

REFERENCES

- Novellademunt, L., Obach, M., Millan-Arino, L., Manzano, A., Ventura, F., Rosa, J. L., Jordan, A., Navarro-Sabate, A. and Bartrons, R.** (2012) Progesterins activate 6-phosphofructo-2-kinase/fructose-2,6-bisphosphatase 3 (PFKFB3) in breast cancer cells. *Biochem J*, 442, 345-356.
- Obach, M., Navarro-Sabate, A., Caro, J. et al.** (2004) 6-Phosphofructo-2-kinase (pfkfb3) gene promoter contains hypoxia-inducible factor-1 binding sites necessary for transactivation in response to hypoxia. *J Biol Chem*, 279, 53562-53570.
- Okar, D. A., Manzano, A., Navarro-Sabate, A., Riera, L., Bartrons, R. and Lange, A. J.** (2001) PFK-2/FBPase-2: maker and breaker of the essential biofactor fructose-2,6-bisphosphate. *Trends in biochemical sciences*, 26, 30-35.
- Paoletti, P. and Neyton, J.** (2007) NMDA receptor subunits: function and pharmacology. *Curr Opin Pharmacol*, 7, 39-47.
- Paul, S. and Connor, J. A.** (2010) NR2B-NMDA receptor-mediated increases in intracellular Ca²⁺ concentration regulate the tyrosine phosphatase, STEP, and ERK MAP kinase signaling. *J Neurochem*, 114, 1107-1118.
- Payne, V. A., Arden, C., Wu, C., Lange, A. J. and Agius, L.** (2005) Dual role of phosphofructokinase-2/fructose bisphosphatase-2 in regulating the compartmentation and expression of glucokinase in hepatocytes. *Diabetes*, 54, 1949-1957.
- Pellerin, L., Bouzier-Sore, A. K., Aubert, A., Serres, S., Merle, M., Costalat, R. and Magistretti, P. J.** (2007) Activity-dependent regulation of energy metabolism by astrocytes: an update. *Glia*, 55, 1251-1262.
- Pellerin, L. and Magistretti, P. J.** (1994) Glutamate uptake into astrocytes stimulates aerobic glycolysis: a mechanism coupling neuronal activity to glucose utilization. *Proc Natl Acad Sci U S A*, 91, 10625-10629.
- Pellerin, L., Pellegrini, G., Bittar, P. G., Charnay, Y., Bouras, C., Martin, J. L., Stella, N. and Magistretti, P. J.** (1998) Evidence supporting the existence of an activity-dependent astrocyte-neuron lactate shuttle. *Dev Neurosci*, 20, 291-299.
- Pierre, K. and Pellerin, L.** (2005) Monocarboxylate transporters in the central nervous system: distribution, regulation and function. *J Neurochem*, 94, 1-14.
- Piert, M., Koeppe, R. A., Giordani, B., Berent, S. and Kuhl, D. E.** (1996) Diminished glucose transport and phosphorylation in Alzheimer's disease determined by dynamic FDG-PET. *J Nucl Med*, 37, 201-208.
- Pines, G., Danbolt, N. C., Bjonas, M. et al.** (1992) Cloning and expression of a rat brain L-glutamate transporter. *Nature*, 360, 464-467.
- Porras, O. H., Loaiza, A. and Barros, L. F.** (2004) Glutamate mediates acute glucose transport inhibition in hippocampal neurons. *J Neurosci*, 24, 9669-9673.
- Porras, O. H., Ruminot, I., Loaiza, A. and Barros, L. F.** (2008) Na⁽⁺⁾-Ca⁽²⁺⁾ cosignaling in the stimulation of the glucose transporter GLUT1 in cultured astrocytes. *Glia*, 56, 59-68.
- Poyton, R. O., Ball, K. A. and Castello, P. R.** (2009) Mitochondrial generation of free radicals and hypoxic signaling. *Trends Endocrinol Metab*, 20, 332-340.

- Puddifoot, C., Martel, M. A., Soriano, F. X., Camacho, A., Vidal-Puig, A., Wyllie, D. J. and Hardingham, G. E.** (2012) PGC-1alpha negatively regulates extrasynaptic NMDAR activity and excitotoxicity. *J Neurosci*, 32, 6995-7000.
- Rebrin, I. and Sohal, R. S.** (2008) Pro-oxidant shift in glutathione redox state during aging. *Adv Drug Deliv Rev*, 60, 1545-1552.
- Reynolds, A., Leake, D., Boese, Q., Scaringe, S., Marshall, W. S. and Khvorova, A.** (2004) Rational siRNA design for RNA interference. *Nat Biotechnol*, 22, 326-330.
- Riera, L., Manzano, A., Navarro-Sabate, A., Perales, J. C. and Bartrons, R.** (2002) Insulin induces PFKFB3 gene expression in HT29 human colon adenocarcinoma cells. *Biochim Biophys Acta*, 1589, 89-92.
- Rose, I. A. and Warms, J. V.** (1967) Mitochondrial hexokinase. Release, rebinding, and location. *J Biol Chem*, 242, 1635-1645.
- Rothstein, J. D., Dykes-Hoberg, M., Pardo, C. A. et al.** (1996) Knockout of glutamate transporters reveals a major role for astroglial transport in excitotoxicity and clearance of glutamate. *Neuron*, 16, 675-686.
- Rothstein, J. D., Van Kammen, M., Levey, A. I., Martin, L. J. and Kuncl, R. W.** (1995) Selective loss of glial glutamate transporter GLT-1 in amyotrophic lateral sclerosis. *Ann Neurol*, 38, 73-84.
- Ruiz-Garcia, A., Monsalve, E., Novellademunt, L. et al.** (2011) Cooperation of adenosine with macrophage Toll-4 receptor agonists leads to increased glycolytic flux through the enhanced expression of PFKFB3 gene. *J Biol Chem*, 286, 19247-19258.
- Samhan-Arias, A. K., Tyurina, Y. Y. and Kagan, V. E.** (2011) Lipid antioxidants: free radical scavenging versus regulation of enzymatic lipid peroxidation. *J Clin Biochem Nutr*, 48, 91-95.
- Sanchez-Alvarez, R., Taberner, A. and Medina, J. M.** (2004) Endothelin-1 stimulates the translocation and upregulation of both glucose transporter and hexokinase in astrocytes: relationship with gap junctional communication. *J Neurochem*, 89, 703-714.
- Saraiva, L. M., Seixas da Silva, G. S., Galina, A., da-Silva, W. S., Klein, W. L., Ferreira, S. T. and De Felice, F. G.** (2010) Amyloid-beta triggers the release of neuronal hexokinase 1 from mitochondria. *PLoS One*, 5, e15230.
- Schioth, H. B., Craft, S., Brooks, S. J., Frey, W. H., 2nd and Benedict, C.** (2012) Brain insulin signaling and Alzheimer's disease: current evidence and future directions. *Mol Neurobiol*, 46, 4-10.
- Shah, K., Desilva, S. and Abbruscato, T.** (2012) The Role of Glucose Transporters in Brain Disease: Diabetes and Alzheimer's Disease. *Int J Mol Sci*, 13, 12629-12655.
- Shimizu, N., Matsunami, T. and Onishi, S.** (1960) Histochemical demonstration of ascorbic acid in the locus coeruleus of the mammalian brain. *Nature*, 186, 479-480.
- Sokoloff, L.** (1992) The brain as a chemical machine. *Prog Brain Res*, 94, 19-33.

REFERENCES

- Sokoloff, L., Wechsler, R. L., Balls, K. and Kety, S.** (1950) The relation of the cerebral O₂ consumption to the total body metabolism in hyperthyroidism. *J Clin Invest*, 29, 847.
- Sotelo-Hitschfeld, T., Fernandez-Moncada, I. and Barros, L. F.** (2012) Acute feedback control of astrocytic glycolysis by lactate. *Glia*, 60, 674-680.
- Starling, A. J., Andre, V. M., Cepeda, C., de Lima, M., Chandler, S. H. and Levine, M. S.** (2005) Alterations in N-methyl-D-aspartate receptor sensitivity and magnesium blockade occur early in development in the R6/2 mouse model of Huntington's disease. *J Neurosci Res*, 82, 377-386.
- Suh, S. W., Bergher, J. P., Anderson, C. M., Treadway, J. L., Fosgerau, K. and Swanson, R. A.** (2007) Astrocyte glycogen sustains neuronal activity during hypoglycemia: studies with the glycogen phosphorylase inhibitor CP-316,819 ([R-R*,S*]-5-chloro-N-[2-hydroxy-3-(methoxymethylamino)-3-oxo-1-(phenylmethyl)propyl]-1H-indole-2-carboxamide). *J Pharmacol Exp Ther*, 321, 45-50.
- Swanson, R. A. and Choi, D. W.** (1993) Glial glycogen stores affect neuronal survival during glucose deprivation in vitro. *J Cereb Blood Flow Metab*, 13, 162-169.
- Swanson, R. A., Morton, M. M., Sagar, S. M. and Sharp, F. R.** (1992) Sensory stimulation induces local cerebral glycogenolysis: demonstration by autoradiography. *Neuroscience*, 51, 451-461.
- Szutowicz, A., Bielarczyk, H., Jankowska-Kulawy, A., Pawelczyk, T. and Ronowska, A.** (2013) Acetyl-CoA the Key Factor for Survival or Death of Cholinergic Neurons in Course of Neurodegenerative Diseases. *Neurochem Res*.
- Tanabe, Y., Masu, M., Ishii, T., Shigemoto, R. and Nakanishi, S.** (1992) A family of metabotropic glutamate receptors. *Neuron*, 8, 169-179.
- Temple, M. D., Perrone, G. G. and Dawes, I. W.** (2005) Complex cellular responses to reactive oxygen species. *Trends Cell Biol*, 15, 319-326.
- Thornton, B. R. and Toczyski, D. P.** (2006) Precise destruction: an emerging picture of the APC. *Genes Dev*, 20, 3069-3078.
- Tietze, F.** (1969) Enzymic method for quantitative determination of nanogram amounts of total and oxidized glutathione: applications to mammalian blood and other tissues. *Anal Biochem*, 27, 502-522.
- Tominaga, N., Tsujikawa, T., Minami, Y., Wu, R. F., Watanabe, F., Sakakibara, R. and Uyeda, K.** (1997) Effect of replacement of the amino and the carboxyl termini of rat testis fructose 6-phosphate, 2-kinase:fructose 2,6-bisphosphatase with those of the liver and heart isozymes. *Arch Biochem Biophys*, 347, 275-281.
- Tompa, P., Baki, A., Schad, E. and Friedrich, P.** (1996) The calpain cascade. Mu-calpain activates m-calpain. *J Biol Chem*, 271, 33161-33164.
- Ui-Tei, K., Naito, Y., Takahashi, F., Haraguchi, T., Ohki-Hamazaki, H., Juni, A., Ueda, R. and Saigo, K.** (2004) Guidelines for the selection of highly effective siRNA sequences for mammalian and chick RNA interference. *Nucleic Acids Res*, 32, 936-948.

- Urushitani, M., Nakamizo, T., Inoue, R., Sawada, H., Kihara, T., Honda, K., Akaike, A. and Shimohama, S.** (2001) N-methyl-D-aspartate receptor-mediated mitochondrial Ca(2+) overload in acute excitotoxic motor neuron death: a mechanism distinct from chronic neurotoxicity after Ca(2+) influx. *J Neurosci Res*, 63, 377-387.
- Uyeda, K.** (1979) Phosphofructokinase. *Adv Enzymol Relat Areas Mol Biol*, 48, 193-244.
- Van Schaftingen, E., Lederer, B., Bartrons, R. and Hers, H. G.** (1982) A kinetic study of pyrophosphate: fructose-6-phosphate phosphotransferase from potato tubers. Application to a microassay of fructose 2,6-bisphosphate. *Eur J Biochem*, 129, 191-195.
- Vaughn, A. E. and Deshmukh, M.** (2008) Glucose metabolism inhibits apoptosis in neurons and cancer cells by redox inactivation of cytochrome c. *Nat Cell Biol*, 10, 1477-1483.
- Ventura, F., Rosa, J. L., Ambrosio, S., Gil, J. and Bartrons, R.** (1991) 6-phosphofructo-2-kinase/fructose-2,6-bisphosphatase in rat brain. *Biochem J*, 276 (Pt 2), 455-460.
- Vera, G. and Tapia, R.** (2012) Activation of group III metabotropic glutamate receptors by endogenous glutamate protects against glutamate-mediated excitotoxicity in the hippocampus in vivo. *J Neurosci Res*, 90, 1055-1066.
- Vidaurre, O. G., Gascon, S., Deogracias, R., Sobrado, M., Cuadrado, E., Montaner, J., Rodriguez-Pena, A. and Diaz-Guerra, M.** (2012) Imbalance of neurotrophin receptor isoforms TrkB-FL/TrkB-T1 induces neuronal death in excitotoxicity. *Cell Death Dis*, 3, e256.
- Vignes, M. and Collingridge, G. L.** (1997) The synaptic activation of kainate receptors. *Nature*, 388, 179-182.
- Vilchez, D., Ros, S., Cifuentes, D. et al.** (2007) Mechanism suppressing glycogen synthesis in neurons and its demise in progressive myoclonus epilepsy. *Nat Neurosci*, 10, 1407-1413.
- Vincent, I., Jicha, G., Rosado, M. and Dickson, D. W.** (1997) Aberrant expression of mitotic cdc2/cyclin B1 kinase in degenerating neurons of Alzheimer's disease brain. *J Neurosci*, 17, 3588-3598.
- Visintin, R., Prinz, S. and Amon, A.** (1997) CDC20 and CDH1: a family of substrate-specific activators of APC-dependent proteolysis. *Science*, 278, 460-463.
- Wamelink, M. M., Struys, E. A. and Jakobs, C.** (2008) The biochemistry, metabolism and inherited defects of the pentose phosphate pathway: a review. *J Inher Metab Dis*, 31, 703-717.
- Wang, G. J., Randall, R. D. and Thayer, S. A.** (1994) Glutamate-induced intracellular acidification of cultured hippocampal neurons demonstrates altered energy metabolism resulting from Ca²⁺ loads. *J Neurophysiol*, 72, 2563-2569.
- Wang, Z., Gardiner, N. J. and Fernyhough, P.** (2008) Blockade of hexokinase activity and binding to mitochondria inhibits neurite outgrowth in cultured adult rat sensory neurons. *Neurosci Lett*, 434, 6-11.

REFERENCES

- Watanabe, F. and Furuya, E.** (1999) Tissue-specific alternative splicing of rat brain fructose 6-phosphate 2-kinase/fructose 2,6-bisphosphatase. *FEBS Lett*, 458, 304-308.
- Watanabe, H. and Passonneau, J. V.** (1973) Factors affecting the turnover of cerebral glycogen and limit dextrin in vivo. *J Neurochem*, 20, 1543-1554.
- Waxman, E. A. and Lynch, D. R.** (2005) N-methyl-D-aspartate receptor subtypes: multiple roles in excitotoxicity and neurological disease. *Neuroscientist*, 11, 37-49.
- Weisova, P., Concannon, C. G., Devocelle, M., Prehn, J. H. and Ward, M. W.** (2009) Regulation of glucose transporter 3 surface expression by the AMP-activated protein kinase mediates tolerance to glutamate excitation in neurons. *J Neurosci*, 29, 2997-3008.
- Weiss, J. H., Pike, C. J. and Cotman, C. W.** (1994) Ca²⁺ channel blockers attenuate beta-amyloid peptide toxicity to cortical neurons in culture. *J Neurochem*, 62, 372-375.
- Wen, Y., Yang, S., Liu, R., Brun-Zinkernagel, A. M., Koulen, P. and Simpkins, J. W.** (2004) Transient cerebral ischemia induces aberrant neuronal cell cycle re-entry and Alzheimer's disease-like tauopathy in female rats. *J Biol Chem*, 279, 22684-22692.
- White, R. J. and Reynolds, I. J.** (1997) Mitochondria accumulate Ca²⁺ following intense glutamate stimulation of cultured rat forebrain neurones. *J Physiol*, 498 (Pt 1), 31-47.
- Wiesinger, H., Hamprecht, B. and Dringen, R.** (1997) Metabolic pathways for glucose in astrocytes. *Glia*, 21, 22-34.
- Wilson, J. E.** (2003) Isozymes of mammalian hexokinase: structure, subcellular localization and metabolic function. *J Exp Biol*, 206, 2049-2057.
- Wroge, C. M., Hogins, J., Eisenman, L. and Mennerick, S.** (2012) Synaptic NMDA receptors mediate hypoxic excitotoxic death. *J Neurosci*, 32, 6732-6742.
- Yalcin, A., Clem, B. F., Simmons, A. et al.** (2009) Nuclear targeting of 6-phosphofructo-2-kinase (PFKFB3) increases proliferation via cyclin-dependent kinases. *J Biol Chem*, 284, 24223-24232.
- Yu, A. C., Drejer, J., Hertz, L. and Schousboe, A.** (1983) Pyruvate carboxylase activity in primary cultures of astrocytes and neurons. *J Neurochem*, 41, 1484-1487.
- Zala, D., Hinckelmann, M. V., Yu, H., Lyra da Cunha, M. M., Liot, G., Cordelieres, F. P., Marco, S. and Saudou, F.** (2013) Vesicular glycolysis provides on-board energy for fast axonal transport. *Cell*, 152, 479-491.
- Zielke, H. R., Zielke, C. L. and Baab, P. J.** (2007) Oxidation of (14)C-labeled compounds perfused by microdialysis in the brains of free-moving rats. *J Neurosci Res*, 85, 3145-3149.

Excitotoxic stimulus stabilizes PFKFB3 causing pentose-phosphate pathway to glycolysis switch and neurodegeneration

P Rodriguez-Rodriguez¹, E Fernandez¹, A Almeida^{1,2} and JP Bolaños^{*1}

6-Phosphofructo-2-kinase/fructose-2,6-bisphosphatase-3 (PFKFB3) is a master regulator of glycolysis by its ability to synthesize fructose-2,6-bisphosphate, a potent allosteric activator of 6-phosphofructo-1-kinase. Being a substrate of the E3 ubiquitin ligase anaphase-promoting complex-Cdh1 (APC^{Cdh1}), PFKFB3 is targeted to proteasomal degradation in neurons. Here, we show that activation of N-methyl-D-aspartate subtype of glutamate receptors (NMDAR) stabilized PFKFB3 protein in cortical neurons. Expressed PFKFB3 was found to be mainly localized in the nucleus, where it is subjected to degradation; however, expression of PFKFB3 lacking the APC^{Cdh1}-targeting KEN motif, or following NMDAR stimulation, promoted accumulation of PFKFB3 and its release from the nucleus to the cytosol through an excess Cdh1-inhibitable process. NMDAR-mediated increase in PFKFB3 yielded neurons having a higher glycolysis and lower pentose-phosphate pathway (PPP); this led to oxidative stress and apoptotic neuronal death that was counteracted by overexpressing glucose-6-phosphate dehydrogenase, the rate-limiting enzyme of the PPP. Furthermore, expression of the mutant form of PFKFB3 lacking the KEN motif was sufficient to trigger oxidative stress and apoptotic death of neurons. These results reveal that, by inhibition of APC^{Cdh1}, glutamate receptors activation stabilizes PFKFB3 thus switching neuronal metabolism leading to oxidative damage and neurodegeneration.

Cell Death and Differentiation (2012) 19, 1582–1589; doi:10.1038/cdd.2012.33; published online 16 March 2012

In contrast to the neuroprotective actions of mild glutamatergic synaptic activity,¹ persistent activation of the N-methyl-D-aspartate subtype of glutamate receptors (NMDAR) – including the extra-synaptic ones² – is known to underlie the pathogenesis of a number of neurological disorders, including Alzheimer's disease, amyotrophic lateral sclerosis or stroke.³ This phenomenon, known as excitotoxicity, causes neuronal apoptotic death through a not yet fully understood mechanism, but it is thought to involve an increase in intracellular Ca²⁺ through NMDAR, followed by plasma membrane depolarization and, hence, opening of voltage-gated Ca²⁺ channels, release from intracellular stores and reversal of the plasma membrane Na⁺/Ca²⁺ exchanger.⁴ This process eventually triggers the accumulation of mitochondrial Ca²⁺, leading to increased reactive oxygen species (ROS) formation, mitochondrial energy dysfunction, permeability transition pore opening and cytochrome *c* release.⁵ Besides mitochondria, it has also been recently shown that cytoplasmic NADPH oxidase has a key role in ROS production upon NMDAR stimulation.⁶ Thus, Ca²⁺ influx activates protein kinase C, which in turn phosphorylates and activates p47^{phox}; p47^{phox} coordinates NADPH oxidase subunit organization, leading

to enzyme activation.⁶ Regardless the origin of ROS, it is thought that neurons are highly vulnerable to mitochondrial stress, likely because of their inability to sufficiently activate glycolysis and, hence, to transiently compensate energy deficiency.^{7,8} In contrast to neurons, astrocytes and other proliferative cells readily invoke glycolysis as a cytoprotective mechanism.^{8–11}

Glycolysis is controlled by the activity of 6-phosphofructo-1-kinase, the activity of which is highly dependent on its potent allosteric activator, fructose-2,6-bisphosphate (F2,6P₂); in the brain, F2,6P₂ biosynthesis almost exclusively relies on 6-phosphofructo-2-kinase/fructose-2,6-bisphosphatase-3 (PFKFB3) activity.^{12,13} Previously, we reported that the inability of neurons to promote cytoprotective glycolysis is because of the virtual absence of PFKFB3.¹⁴ Furthermore, we recently found that PFKFB3, through its KEN motif, is a substrate of the E3 ubiquitin ligase, anaphase-promoting complex (APC)-Cdh1 (APC^{Cdh1}),¹⁵ which accounts for the high instability of PFKFB3 and low glycolytic rate in neurons.¹⁵

Inhibition of APC^{Cdh1} in postmitotic neurons triggers an accumulation of its substrate, cyclin B1, which mediates apoptotic death.¹⁶ Moreover, cyclin B1 accumulation can also

¹Departamento de Bioquímica y Biología Molecular, Instituto de Neurociencias de Castilla y León, Universidad de Salamanca, Edificio Departamental, Salamanca, Spain and ²Unidad de Investigación, Instituto de Estudios de Ciencias de la Salud de Castilla y León, Hospital Universitario de Salamanca, Salamanca, Spain

*Corresponding author: JP Bolaños, Department of Biochemistry and Molecular Biology, University of Salamanca, Edificio Departamental, Lab. 122, Salamanca 37007, Spain. Tel: +34 923 294 781; Fax: +34 923 294 579; E-mail: jbolanos@usal.es

Keywords: oxidative stress; neurons; Cdh1; APC; glutamate

Abbreviations: ANOVA, analysis of variance; APC, anaphase-promoting complex; Cdk5, cyclin-dependent kinase-5; cDNA, complementary DNA; DMSO, dimethyl sulphoxide; EDTA, ethylene diamine tetraacetic acid; EGTA, ethylene glycol tetraacetic acid; G6PD, glucose-6-phosphate dehydrogenase; GFP, green fluorescent protein; GSH, reduced glutathione; GSSG, oxidized glutathione; GSx, total glutathione; NMDA, N-methyl-D-aspartic acid; NMDAR, N-methyl-D-aspartic acid receptor; PFKFB3, 6-phosphofructo-2-kinase/fructose-2,6-bisphosphatase-3; PGI, phosphoglucose isomerase; PPP, pentose-phosphate pathway; ROS, reactive oxygen species; SDS, sodium dodecyl sulfate; siRNA, small interfering RNA; TIGAR, Tp53-inducible glycolysis and apoptosis factor

Received 07.10.11; revised 08.2.12; accepted 21.2.12; Edited by M Deshmukh; published online 16.3.12

be recapitulated by NMDAR stimulation, which activates cyclin-dependent kinase 5 (Cdk5)-mediated Cdh1 phosphorylation, leading to APC^{Cdh1} inhibition.¹⁷ In view of the control that APC^{Cdh1} exerts over PFKFB3 stability,¹⁵ here we hypothesized whether NMDAR stimulation, *via* APC^{Cdh1} inhibition,¹⁷ regulates PFKFB3 protein levels in neurons. We show that NMDAR activation, through inhibition of APC^{Cdh1} caused PFKFB3 stabilization leading to increased glycolysis and reduced activity of the pentose-phosphate pathway (PPP). This metabolic alteration triggered oxidative damage and excitotoxic neuronal death, thus suggesting that modulators of neuronal energy metabolism should be considered as targets in therapeutic strategies against neurodegenerative diseases.

Results

In order to test whether rat primary cortical neurons in culture responded to glutamate receptor activation, we first monitored the changes in Fura-2 fluorescence. As shown in Figure 1a, Fura-2 F335/F363 ratio – an index of intracellular Ca²⁺ levels – increased by ~1.3-fold immediately after the addition of glutamate (100 μM) or N-methyl-D-aspartate (NMDA; 100 μM). Furthermore, pre-incubation of neurons

with the NMDAR antagonist, MK801 (10 μM), prevented by ~60% glutamate-mediated increase in F335/F363 ratio (Figure 1a, left panel); MK801 almost abolished (by ~90%) NMDA-mediated increase in F335/F363 ratio (Figure 1a, right panel). These results suggest that, under our experimental conditions – cells grown in serum-based medium – cortical neurons express functional NMDAR and, hence, are useful for the study of excitotoxic-mediated metabolic changes. To investigate whether glutamate receptor activation controls PFKFB3 stability, we then incubated neurons with glutamate (100 μM/15 min), and the levels of PFKFB3 protein were analyzed by western blotting. As shown in Figure 1b, glutamate triggered a time-dependent increase in PFKFB3, an effect that was maximal (by ~2.1-fold) after 6 h. To see whether this effect was mediated by NMDAR, neurons were incubated with NMDA (100 μM/15 min), and PFKFB3 protein levels analyzed 6 h later. As depicted in Figure 1c, NMDA mimicked glutamate at increasing PFKFB3. Moreover, incubation of neurons with MK801 prevented glutamate-mediated increase in PFKFB3 (Figure 1d). Glutamate did not alter PFKFB3 mRNA levels (Figure 1e). These results suggest that activation of NMDAR stabilizes PFKFB3 protein in neurons.

Next, we investigated the involvement of APC^{Cdh1} activity in determining PFKFB3 stabilization by NMDAR. In view that NMDAR activation promotes APC^{Cdh1} inhibition by Cdk5-mediated phosphorylation of Cdh1,¹⁷ we tested whether this observation could be confirmed in our conditions. As shown in Figure 2a, glutamate (100 μM/15 min) promoted, after 4 h, H1 phosphorylation in neuronal samples immunoprecipitated with anti-Cdk5; furthermore, this effect was prevented by MK801, suggesting NMDAR-mediated activation of Cdk5 activity. In addition, Cdh1 was phosphorylated – suggesting APC^{Cdh1} inhibition – 6 h after glutamate treatment, an effect that was also prevented by MK801 (Figure 2b). To further investigate if APC^{Cdh1} activity regulated PFKFB3 stability upon glutamate receptor stimulation, neurons were transfected with a green fluorescent protein (GFP)-PFKFB3 construct to visualize PFKFB3 subcellular localization by confocal microscopy. PFKFB3 was mainly localized in the nucleus of neurons, but glutamate treatment promoted its accumulation, as revealed by the spread (nuclear plus cytosolic) localization (Figures 2c and d). Interestingly, Cdh1 overexpression prevented this effect, suggesting that deficiency in active Cdh1 was responsible for glutamate-mediated PFKFB3 spreading (Figures 2c and d). Furthermore, expression of a GFP-PFKFB3 form with its KEN box mutated to AAA (mut-PFKFB3), hence, insensitive to APC^{Cdh1} activity,¹⁵ showed the spread-like localization, regardless of glutamate treatment (Figures 2c and d). Thus, glutamate-mediated PFKFB3 stabilization occurs *via* APC^{Cdh1} inhibition.

To elucidate whether NMDAR-mediated PFKFB3 protein stabilization had functional consequences for neuronal metabolism, we assessed the rates of glycolysis and PPP, as well as the glutathione redox status. The efficacy of a small interfering RNA against PFKFB3 (siPFKFB3) to prevent PFKFB3 protein accumulation was first tested. To do so, primary neurons were transfected with the GFP-PFKFB3 complementary DNA (cDNA) construct, and PFKFB3 protein was determined using an anti-flag (anti-GFP) antibody. As shown in Figure 3a, PFKFB3 was accumulated 6 h after

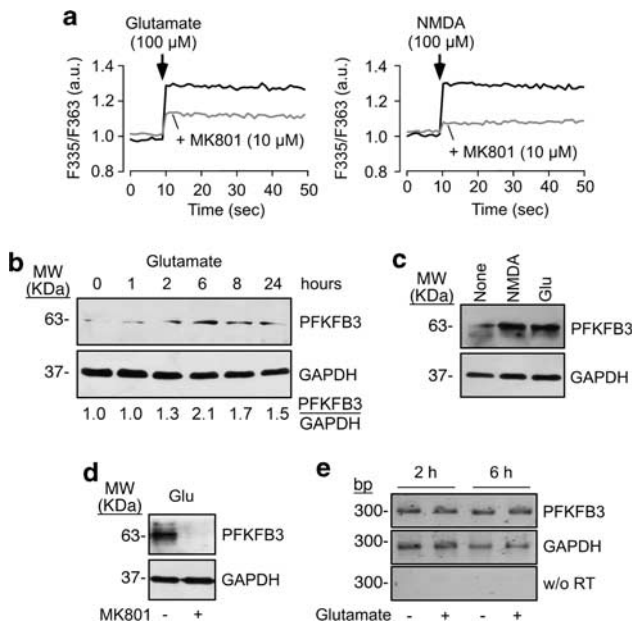


Figure 1 Activation of NMDAR stabilizes PFKFB3 protein in neurons. (a) Incubation of rat primary cortical neurons with glutamate (left panel) or NMDA (right panel) increased the ratio of Fura-2-dependent fluorescence (at 510 nm) obtained after excitation at 335/363 nm (F335/F363), indicating an increase in intracellular Ca²⁺. MK801 (10 μM) partially prevented glutamate-induced changes in F335/F363 ratio and most of NMDA-dependent F335/F363 ratio changes. (b) Incubation of neurons with glutamate (100 μM/15 min) triggered time-dependent increase in PFKFB3 protein, which was maximal after 6 h. (c) NMDA (100 μM/15 min) mimicked glutamate at increasing PFKFB3. (d) NMDA receptor antagonist, MK801 (10 μM), prevented glutamate-mediated increase in PFKFB3. (e) Glutamate (100 μM/15 min) did not change PFKFB3 mRNA levels, as revealed by the unaltered intensity of the predicted 300 bp band after reverse-transcription of total RNA samples, followed by polymerase chain reaction (RT-PCR) using specific oligonucleotides for PFKFB3; GAPDH (279 bp band) was used as loading control; the black/white inverted images of the agarose gels are shown; w/o RT, RT-PCR for PFKFB3 without reverse transcriptase

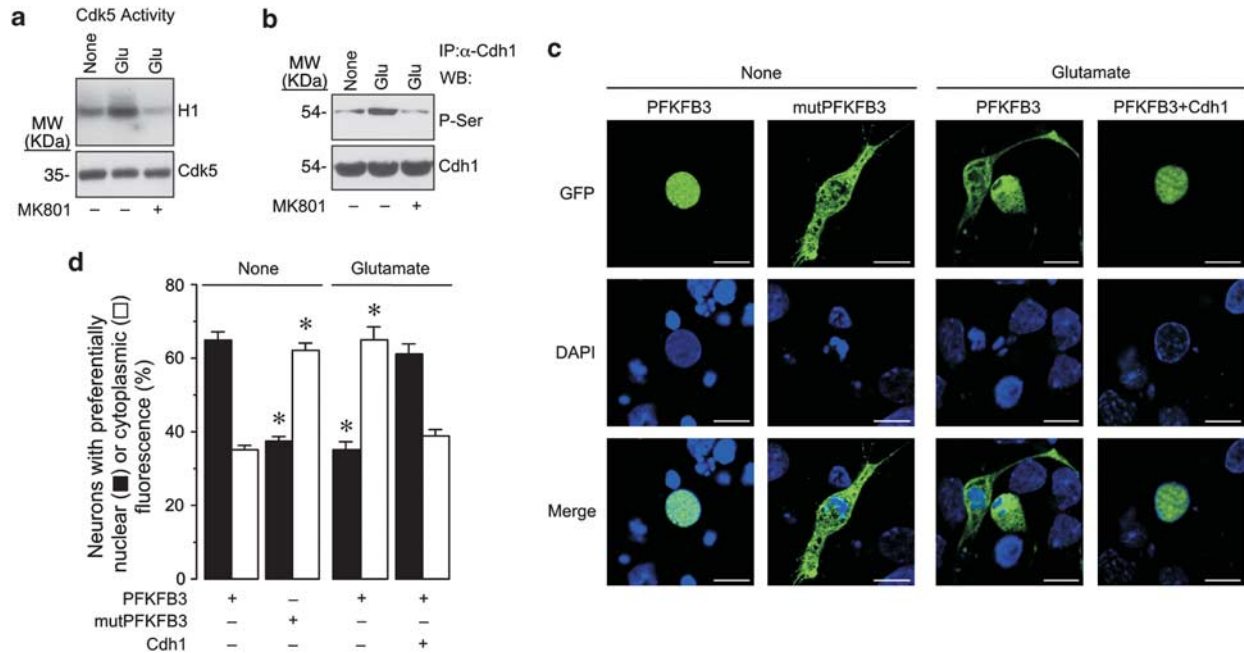


Figure 2 Glutamate-mediated PFKFB3 stabilization occurs via Cdk5-mediated inhibition of APC^{Cdh1} activity. (a) Glutamate treatment (100 μ M/15 min) increased, after 1 h, Cdk5-mediated H1 phosphorylation in rat primary cortical neurons; this effect was fully abolished by MK801 (10 μ M). (b) Cdh1 is phosphorylated 6 h after glutamate treatment (100 μ M/15 min), an effect that was prevented by MK801 (10 μ M). (c) Confocal microscopy images of neurons transfected with GFP-PFKFB3 reveals its nuclear localization. Glutamate promotes PFKFB3 accumulation, as revealed by its spread (nuclear plus cytosolic) localization; Cdh1 overexpression prevented this effect. GFP-PFKFB3 mutated on its KEN box (KEN \rightarrow AAA; mut-PFKFB3) showed the spread-like localization, regardless of glutamate treatment. (d) Percentage of neurons showing nuclear or spread GFP-PFKFB3 localization in the experiments shown in c; these data were obtained by analyzing \sim 30 neurons per condition per neuronal preparation ($n = 4$). * $P < 0.05$ versus the corresponding (nuclear or cytoplasmic) PFKFB3-none condition (ANOVA)

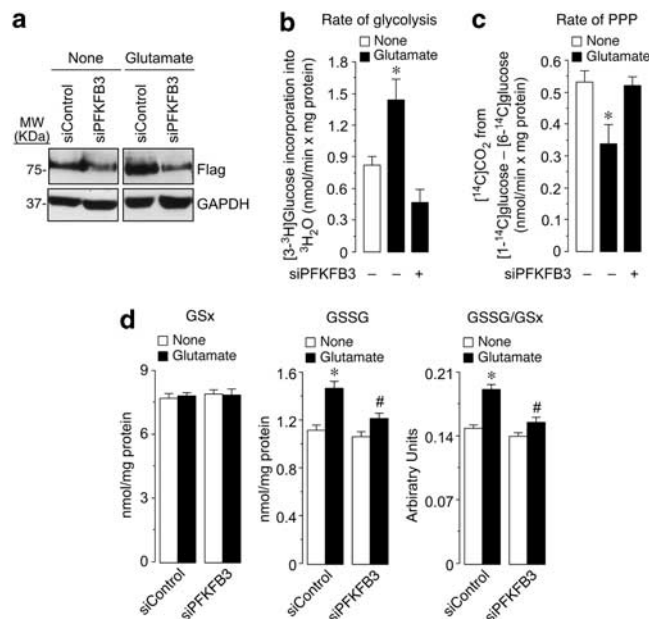


Figure 3 Glutamate stimulates PFKFB3-dependent increase in glycolysis, a decrease in PPP and promotes glutathione oxidation in neurons. (a) Incubation of GFP-PFKFB3-expressing neurons with glutamate (100 μ M/15 min) induced, 6 h after treatment, PFKFB3 accumulation in control, siRNA-treated neurons (siControl), as revealed by an anti-GFP (Flag) antibody; transfection of neurons with an siPFKFB3 efficiently reduced PFKFB3 protein and prevented glutamate-induced PFKFB3 accumulation. (b) Incubation of neurons with glutamate (100 μ M/15 min) increased, after 6 h, the rate of glycolysis, as assessed by the determination of [3-³H]glucose incorporation into ³H₂O; this effect was abolished by preventing PFKFB3 accumulation in neurons previously transfected with siPFKFB3. (c) Glutamate treatment decreased, after 6 h, the rate of the PPP, as assessed by the determination of the difference between ¹⁴C₂ produced by [1-¹⁴C]glucose and that of [6-¹⁴C]glucose; this effect was abolished by siPFKFB3. (d) Glutamate treatment did not change GSx (left panel), but it increased GSSG (middle panel) and the oxidized glutathione redox status (GSSG/GSx; right panel); these effects were partially prevented by siPFKFB3. * $P < 0.05$ versus none; # $P < 0.05$ versus the corresponding siControl (ANOVA)

glutamate (100 μ M/15 min) incubation in control neurons (siControl); however, transfection of neurons with an siPFKFB3 decreased PFKFB3 protein abundance in control neurons and prevented glutamate-mediated PFKFB3 accumulation. We then assessed the rate of glycolysis, and we found it to be significantly enhanced, after 6 h, by glutamate treatment (Figure 3b); moreover, this was abolished by preventing PFKFB3 accumulation using the siPFKFB3 (Figure 3b). In view that glycolysis and PPP are two interconnected metabolic pathways, we then assessed whether the increase in glycolysis altered glucose utilization through the PPP. We found that glutamate treatment decreased, after 6 h, the rate of PPP, an effect that was abolished by siPFKFB3 (Figure 3c). Thus, glutamate triggers a PFKFB3-dependent increase in glycolysis and decrease in the PPP.

It has been previously shown that glucose metabolism through the PPP is neuroprotective^{15,18,19} because of its NADPH-regenerating function. Thus, NADPH is an essential cofactor for glutathione regeneration, hence, the PPP becomes necessary to prevent neuronal death by oxidative stress.¹⁸ Thus, we next aimed to elucidate whether the metabolic PPP/glycolytic shift triggered by glutamate treatment induced oxidative stress. As shown in Figure 3d, total glutathione (GSx) was unaltered, but its oxidized form (GSSG) and the glutathione oxidized status (GSSG/GSx ratio) significantly increased 6 h after glutamate treatment, and these effects were prevented by siPFKFB3. To further support evidence for oxidative stress, we next evaluated whether a putative increased ROS production by glutamate could be rescued by either knocking down a key glycolytic enzyme, phosphoglucose isomerase (PGI), or by overexpressing glucose-6-phosphate dehydrogenase (G6PD), the rate-limiting enzyme of the PPP that we have previously shown to be efficient in neurons.^{15,18} The efficacy of these tools were first tested by western blotting (Figure 4a); thus, transfection of neurons with the siRNA against PGI efficiently knocked down PGI protein, whereas overexpression of the cDNA encoding G6PD increased neuronal G6PD abundance. Glutamate treatment (100 μ M/15 min) increased, after 6 h, neuronal ROS, an effect that was prevented by knocking down PGI or PFKFB3, as it was by overexpressing G6PD, or by blocking NMDAR with MK801 (Figure 4b). To assess neuronal vulnerability to oxidative stress in this paradigm, we then analyzed the proportion of annexin V⁺/7AAD⁻ neurons (indicating neurons that had been targeted to apoptosis) after glutamate treatment. We found that glutamate increased, though modestly, apoptotic neuronal death via a mechanism that could be prevented by silencing PGI or PFKFB3, as well as by overexpressing G6PD or blocking NMDAR (Figure 4c). Together, these results indicate that NMDAR activation triggers oxidative stress and targets neurons for apoptotic death by shifting PPP to glycolysis.

Finally, we sought to elucidate whether APC^{Cdh1} activity was responsible for PFKFB3-mediated oxidative stress and neurodegeneration in excitotoxicity. As shown in Figure 5a, glutamate increased ROS in neurons transfected with low levels of wild-type PFKFB3 cDNA. However, transfection of neurons with identical cDNA amounts of the KEN box-mutant form of PFKFB3 (mut-PFKFB3) increased ROS to levels

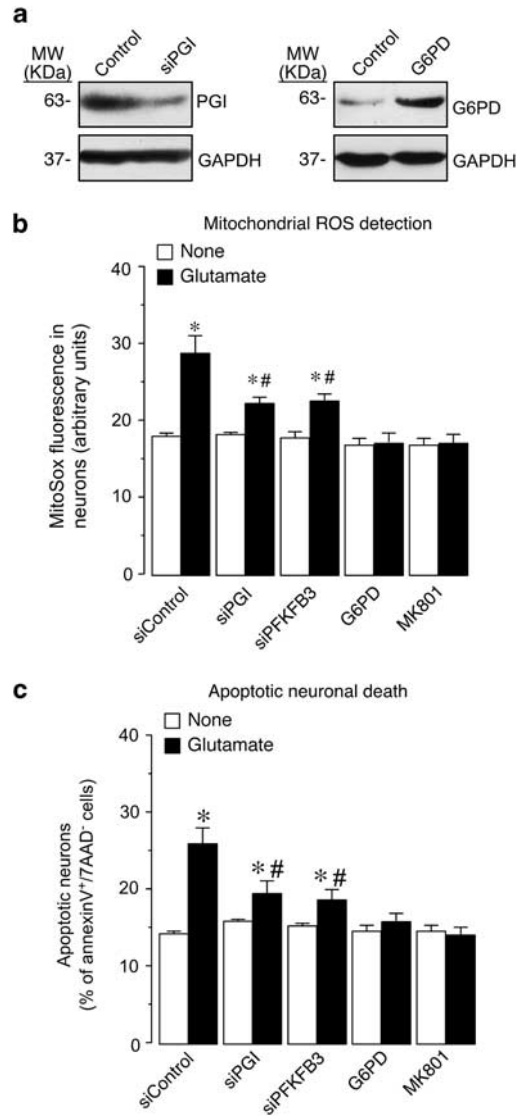


Figure 4 NMDAR activation triggers oxidative stress and apoptotic death by switching PPP to glycolysis. (a) Transfection of neurons with an siRNA against PGI (siPGI), efficiently knocked down PGI protein abundance (left panel). Transfection of neurons with the full-length DNA encoding G6PD efficiently increased G6PD protein abundance (right panel). (b) Glutamate treatment (100 μ M/15 min) increased ROS in neurons, as assessed by MitoSox fluorescence by flow cytometry; this effect was prevented by knocking down PGI (siPGI) or PFKFB3 (siPFKFB3), overexpressing G6PD, or blocking NMDAR with MK801 (10 μ M). (c) Glutamate treatment increased apoptotic neuronal death, as assessed by annexin V⁺/7-AAD⁻ fluorescence by flow cytometry; this effect was prevented by silencing PGI (siPGI) or PFKFB3 (siPFKFB3), overexpressing G6PD or blocking NMDAR with MK801. **P* < 0.05 versus none; #*P* < 0.05 versus siControl (glutamate); 5 × 10⁴ events were acquired in triplicate; results mean ± S.E.M. from three independent neuronal preparations, *n* = 3; ANOVA)

similar to those triggered by glutamate; moreover, glutamate did not further enhance ROS in neurons expressing mut-PFKFB3 (Figure 5a). Interestingly, apoptotic death triggered by glutamate in neurons transfected with PFKFB3 was mimicked by mut-PFKFB3 (Figure 5b). Thus, expression of APC^{Cdh1}-insensitive PFKFB3 mimics glutamate at causing oxidative stress and neuronal death.

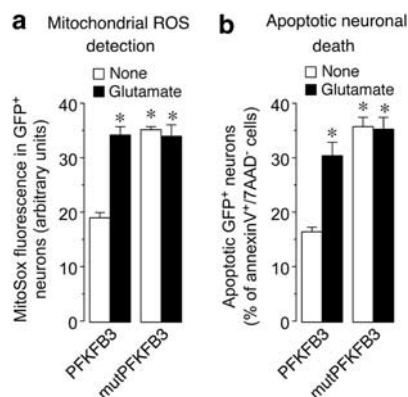


Figure 5 Expression of APC^{Cdh1}-insensitive PFKFB3 mimics glutamate at causing oxidative stress and neuronal death. (a) Glutamate treatment (100 μ M/15 min) increased ROS in neurons transfected with low levels of wild-type PFKFB3 cDNA; transfection of neurons with identical cDNA amounts of the KEN box-mut-PFKFB3 increased ROS to similar levels to those triggered by glutamate; glutamate did not further enhance ROS in neurons expressing mut-PFKFB3. (b) Glutamate increased apoptotic death of neurons transfected with low levels of PFKFB3 cDNA; transfection of neurons with identical cDNA amounts of mut-PFKFB3 increased apoptotic death to similar levels to those triggered by glutamate; glutamate did not further enhance apoptotic death in neurons expressing mut-PFKFB3. * $P < 0.05$ versus none (PFKFB3; 3×10^4 events were acquired in triplicate; results mean \pm S.E.M. from three independent neuronal preparations, $n = 3$; ANOVA)

Discussion

Neurons continuously degrade the glycolytic-promoting enzyme PFKFB3 by APC^{Cdh1} activity, and this allows a considerable proportion of glucose to be oxidized via the PPP, which functions as an antioxidant and survival metabolic pathway.¹⁵ Here, we show that a short-term activation of glutamate receptors in cortical neurons triggers delayed, time-dependent PFKFB3 protein accumulation; the lack of change in the PFKFB3 mRNA abundance ruled out a transcriptional effect. Moreover, NMDA mimicked glutamate, and NMDAR antagonist MK801 prevented PFKFB3 accumulation, indicating the direct involvement of NMDAR stimulation in PFKFB3 stabilization. Previously, it was reported that NMDAR stimulation in cortical neurons promotes, in a Ca²⁺-dependent manner, p35 cleavage to p25 by calpain leading to Cdk5 activation.²⁰ Here, we show that, under our experimental culture conditions, rat primary cortical neurons efficiently responded to NMDAR stimulation, as judged by the MK801-inhibitable increased intracellular Ca²⁺ levels. Moreover, we show that glutamate induced Cdk5 activation in a process that was antagonized by MK801, indicating the involvement of NMDAR. Given that NMDAR-mediated activation of Cdk5 phosphorylates Cdh1 leading to APC^{Cdh1} inhibition,¹⁷ we hypothesized that the stabilization of PFKFB3 could be consequence of NMDAR-mediated APC^{Cdh1} inhibition. In good agreement with the presence of a nuclear-targeting motif in PFKFB3,²¹ we found that expressed PFKFB3 was localized in the nucleus, where neurons actively degraded it. In addition, we show that Cdh1 was phosphorylated by glutamate treatment, and that this was accompanied by cellular spread of PFKFB3 from the nucleus to cytosol in a Cdh1-inhibitable process; interestingly, the PFKFB3 mutant form lacking the Cdh1-recognizing KEN motif spontaneously

accumulated. Together, these results indicate that PFKFB3 nuclear stabilization followed by cytosolic spread is the consequence of APC^{Cdh1} inhibition. The mechanism whereby PFKFB3 is released from the nucleus remains unclear, although the physiological significance is likely in view of the cytoplasmic localization of the PFKFB3 target, 6-phospho-fructo-1-kinase.

NMDAR-mediated PFKFB3 protein stabilization led to increased PFKFB3 activity and efficiently upregulated the rate of glycolysis in neurons. In previous studies, neurons failed to upregulate glycolysis immediately after the bioenergetic stress caused by mitochondrial inhibitors^{8,22} or NMDAR activation.¹⁴ However, it should be noted that PFKFB3 stabilization takes place several hours after glutamate treatment, thus explaining the absence of measurable short-term glycolytic stimulation in cortical neurons in the previous studies.^{8,14,22} Accordingly, the delayed increase in glycolysis that we observe does not appear to be a neuronal attempt to rapidly compensate for the mitochondrial energy dysfunction, which occurs immediately after NMDAR stimulation.⁷ Instead, the delayed glycolysis activation reflects a long-term metabolic adaptation of neurons by excitotoxic insult; however, such an adaptation concurs with concomitant decrease in the rate of glucose oxidation through the PPP, hence, triggering oxidative stress and neurotoxicity. Intriguingly, although the stimulation of glycolysis is cytotoxic in neurons, it is cytoprotective in astrocytes.⁸ This different outcome shown by neurons and astrocytes is consistent with the expression of a robust antioxidant system in astrocytes that is not present in neurons.²³ Upon inhibition of mitochondrial respiration, astrocytes switch on glycolysis, via the 5'-AMP-activated protein kinase-PFKFB3 pathway,¹⁴ to compensate for the ATP deficiency without affecting their antioxidant status.²⁴ However, shifting glucose utilization from PPP to glycolysis in neurons compromises the efficacy of the critical antioxidant NADPH-glutathione regenerating system, hence causing delayed neurotoxicity. Importantly, both the increase in glycolysis and the decrease in PPP could be fully abolished by siPFKFB3, indicating that both metabolic pathways are wholly controlled by PFKFB3. In this context, it should be mentioned that Tp53-inducible glycolysis and apoptosis regulator (TIGAR), by catalyzing F2,6P₂ degradation inhibits glycolysis and stimulates PPP.²⁵ Thus, the control over F2,6P₂ concentrations by either PFKFB3 – with a main fructose-6-phosphate-2-kinase activity^{12,13} – or TIGAR – with fructose-2,6-bisphosphatase activity²⁵ – appears to determine the fate of glucose metabolism. However, no evidence for NMDAR-mediated p53 upregulation is currently available, hence, remaining elusive whether TIGAR induction has a determinant role in neuronal metabolic change upon NMDAR stimulation.

The metabolic PPP to glycolysis shift triggered by NMDAR stimulation was accompanied by oxidative stress, as revealed both by an increase in the oxidized glutathione redox status and by the increased mitochondrial ROS, as well as apoptotic neuronal death. These data contrast with those reporting that NMDAR-mediated increase in neuronal ROS could be blocked with 6-aminonicotinamide, an inhibitor of PPP that produces NADPH required for NADPH oxidase activity.⁶ Whether the different neuronal settings (defined *versus*

serum-based media) or the types of tools used (pharmacological *versus* genetic approaches to modulate glycolysis and PPP) are responsible for this apparent controversy remains elusive. However, in our hands, silencing PFKFB3 or PGI, which effectively inhibited glycolysis,¹⁵ or G6PD overexpression, a potent activator of the PPP,¹⁸ prevented such a metabolic switch and the concomitant ROS production by NMDAR stimulation. In fact, PPP activity produces reduced equivalents in the form of NADPH,²⁶ which is also a necessary cofactor for antioxidant glutathione regeneration.¹⁸ Thus, PFKFB3 silencing significantly prevented the increase in oxidized glutathione status caused by NMDAR stimulation and this was critical at determining neuronal survival. Interestingly, it has been shown that, when oxidized, cytochrome *c* is released from mitochondria, hence promoting apoptotic neuronal death, and that PPP activity is essential at maintaining cytochrome *c* reduced.²⁷ Our results, showing oxidative stress and neurodegeneration following PFKFB3 stabilization by NMDAR stimulation, confirm the critical role of PPP at regulating neuronal apoptosis. Furthermore, they show that the loss of PPP activity by APC^{Cdh1} inhibition is a novel and important player in excitotoxicity. Together, these findings highlight the importance of metabolic modulation in excitotoxicity and neurodegeneration and emphasize that metabolic targets should be considered when designing therapeutic strategies.

Materials and Methods

Plasmid constructions and site-directed mutagenesis. The rat PFKFB3 full-length cDNA (splice variant K6; 1563 bp; accession number BAA21754) was obtained, by reverse-transcriptase polymerase chain reaction (RT-PCR), at our laboratory.¹⁵ PFKFB3 cDNA was fused, at its 5'-terminus, with the full-length cDNA encoding the GFP and subcloned in pCDNA3.0 vector. This GFP-PFKFB3 cDNA fusion construct was then subjected to site-directed mutagenesis of its KEN-box to AAA using the QuikChange XL site-directed mutagenesis kit (Stratagene, La Jolla, CA, USA) using the following forward and reverse primers, respectively: 5'-ATCCTTCATTTGCCGACGAGCTGACTTCAA GGC-3' and 5'-ATGCCCTTGAAGTCAGCTGCTCGGCAAAATGAAGG-3' (mutated nucleotides underlined). Human full-length Cdh1 cDNA (accession number NM_016263) was a generous gift of Dr. J Pines (Gurdon Institute, University of Cambridge, UK).

RNA interference. To knockdown PGI (accession number NM_207192), we used the following sequence for siRNA: 5'-CCTTACCAGACGTAGTGT-3' (nt 1248–1266). To knockdown PFKFB3 we used the sequence 5'-AAAGCCTC GCATCAACAGC-3' (nt 1908–1926). Both siRNAs were previously validated at our laboratory for efficacy.^{14,15} An siRNA against luciferase (5'-CTGACGCGAATAC TTGATT-3') was used as control.

RT-PCR analysis. Total RNA was purified from neurons using a commercially available kit (Sigma, Saint Louis, MO, USA). PFKFB3 mRNA expression was analyzed by 4.5% agarose electrophoresis after RT-PCR using the following forward and reverse oligonucleotides, respectively: 5'-CCAGCCTTGGACCCT GATAAATG-3' and 5'-TCCACACGCGGAGGTCCTTCAGAT-3' for PFKFB3, and 5'-CTGGCGTCTTACCACCAT-3' and 5'-AGGGGCCATCCACAGTCTT-3' for GAPDH. Reverse transcription was performed at 48 °C for 50 min, and PCR conditions were 10 min at 95 °C, 35 cycles of 1 min at 95 °C, 1 min at 58 °C and 30 s at 68 °C. Final extension was carried out for 10 min at 72 °C. In no case was a band detected by PCR without reverse transcription.

Antibodies. An anti-PFKFB3 (K3-K6 splice variants) antibody was generated, by rabbit immunization with the synthetic peptide⁵⁰⁸MRSRSPRSGAESSQKH⁵²¹-C, at our laboratory as previously described.¹⁵ A commercial anti-PFKFB3 antibody raised against a C-terminal region of the human PFKFB3 (protein accession

Q16875; catalog number H00005209-M08, Novus Biologicals, Cambridge, UK) was also used; this antibody cross-reacts with human and rat PFKFB3, thus recognizing a region that is shared by all translational products of the rat K1 to K8 PFKFB3 mRNA splice variants. Anti-Cdh1 (AR38) was a generous gift from J Gannon (Clare Hall Laboratories, Cancer Research, UK). Anti-Cdk5 (C-8) and anti-PGI (K-16) were from Santa Cruz Biotechnology (Heidelberg, Germany). Anti-GFP was purchased from Abcam (Cambridge Science Park, Cambridge, UK). Anti-G6PD and anti-GAPDH were purchased from Sigma, and anti-phosphoserine from Zymed (Invitrogen, Groningen, The Netherlands).

Cell cultures. Cortical neurons in primary culture were prepared from fetal (E16) Wistar rats. Cells were seeded (2.5×10^5 cells/cm²) in DMEM (Sigma) supplemented with 10% (v/v) fetal calf serum (Roche Diagnostics, Heidelberg, Germany) and incubated at 37 °C in a humidified 5% CO₂-containing atmosphere. After 48 h of plating, the medium was replaced with DMEM supplemented with 5% horse serum (Sigma) and with 20 mM D-glucose. On day 4, cytosine arabinoside (10 μM) was added in order to prevent non-neuronal proliferation. Cells were used by day 6, when enrichment was ~99% (neurofilament; data not shown).

Cell treatments. Transfection of cells with plasmid vectors was carried out using 0.16–1.6 μg/ml of the plasmids, as indicated in the figure legends. All transfections were performed using lipofectamine 2000 (Invitrogen) following the manufacturer's instructions, at day 5 *in vitro*. After 6 h, the medium was removed and cells were further incubated overnight in the presence of culture medium. For RNA interference experiments, siRNAs (purchased from Thermo Fisher Scientific, Lafayette, CO, USA; sequences described above) were used. In dose-response preliminary settings, primary neurons were transfected, using Lipofectamine 2000 with 20–100 nM of the siRNAs, which showed a dose-dependent effect; only the results using 100 nM are shown. siRNA transfections were performed at day 3 *in vitro* and experiments were performed at day 6, when an efficient knockdown of the target proteins was obtained. For NMDAR activation, neurons at 6 days *in vitro* were incubated with 100 μM glutamate (plus 10 μM glycine) or 100 μM NMDA (plus 10 μM glycine) in buffered Hanks' solution (pH 7.4) for 15 min.⁷ When indicated, incubations were performed in the presence of MK-801 (10 μM; Sigma). Neurons were then washed and further incubated in culture medium for the indicated time period.

Flow cytometric analysis of apoptotic cell death. APC/C-conjugated annexin-V and 7-aminoactinomycin D (7-AAD) (Becton Dickinson Biosciences, San Jose, CA, USA) were used to determine quantitatively the percentage of apoptotic neurons by flow cytometry. Cells were stained with annexin V-APC and 7-AAD, following the manufacturer's instructions, and were analyzed on a FACScalibur flow cytometer (15 mW argon ion laser tuned at 488 nm) using the CellQuest software (BDB). Both GFP⁺ and GFP⁻ cells were analyzed separately and the annexin V-APC-stained cells that were 7-AAD-negative were considered to be apoptotic.¹⁵

Detection of ROS. This was carried out using MitoSox-Red (Invitrogen). Neurons were incubated with 2 μM MitoSox-Red for 30 min, washed with PBS and the fluorescence assessed by flow cytometry.¹⁵

Measurement of the glycolytic and PPP fluxes. Suspensions of known amounts of cells ($4\text{--}5 \times 10^5$ cells) obtained by smooth detaching from the cultures 6 h after glutamate treatments, were incubated in sealed vials containing a central well, which was used for ¹⁴CO₂ or ³H₂O trapping. Cells were incubated in the presence of 1 μCi of either D-[1-¹⁴C] glucose or D-[6-¹⁴C] glucose for PPP determinations, whereas 5 μCi of D-[3-³H] glucose were used for glycolytic flux determinations, both in a Krebs–Henseleit buffer (11 mM Na₂HPO₄, 122 mM NaCl, 3.1 mM KCl, 0.4 mM KH₂PO₄, 1.2 mM MgSO₄, 1.3 mM CaCl₂; pH 7.4) containing 5 mM D-glucose at 37 °C. In order to ensure an adequate O₂ supply for oxidative metabolism by the cells throughout the 90 min incubation period, the gas phase in the vials containing the cells was supplied with extra O₂ before the vials were sealed. The glycolytic flux was measured by assaying the rate of ³H₂O production from [3-³H]glucose, as detailed previously.¹⁵ The PPP flux was measured by assessing the difference between ¹⁴CO₂ production from [1-¹⁴C]glucose – which decarboxylates via the 6-phosphogluconate dehydrogenase-catalyzed reaction – and that of [6-¹⁴C]glucose – which decarboxylates via the tricarboxylic acid cycle.^{18,28}

Glutathione measurements. For glutathione determinations, neurons were treated with 1% (w/v) sulfosalicylic acid and centrifuged at $13\,000 \times g$ for 5 min

at 4 °C. GSx (the amount of reduced glutathione (GSH), plus two times the amount of oxidized glutathione (GSSG)) and GSSG concentrations were measured in the supernatants using the enzymatic method of Tietze.²⁹ GSSG was quantified after derivatization of GSH in the samples with 2-vinylpyridine. Data were extrapolated to those obtained with GSSG standards (0–5 μM for GSSG; 0–50 μM for GSx). The glutathione redox status was expressed as the GSSG/GSx ratio, as previously described.^{18,30}

Fura-2 fluorescence measurements. To estimate the intracellular Ca²⁺-dependent changes by NMDAR stimulation in cortical neurons we used the fluorescent probe Fura-2 (acetoxymethyl-derivative; Life Technologies, Eugene, OR, USA), as previously described.³¹ Essentially, neurons at 6 days *in vitro*, seeded in 96-well plates (Nunc), were incubated with Fura-2 (2 μM; dissolved in dimethyl sulphoxide (DMSO)) for 40 min in DMEM at 37 °C. Then, cells were washed and further incubated with standard buffer (140 mM NaCl, 2.5 mM KCl, 15 mM Tris-HCl, 5 mM D-glucose, 1.2 mM Na₂HPO₄, 1 mM MgSO₄ and 1 mM CaCl₂, pH 7.4) for 30 min and 37 °C. Finally, the standard buffer was removed and experimental buffer (140 mM NaCl, 2.5 mM KCl, 15 mM Tris-HCl, D-glucose, 1.2 mM Na₂HPO₄, and 2 mM CaCl₂, pH 7.4), either in the absence or in the presence of MK801 (10 μM), was added. Emissions at 510 nm, after excitations at 335 and 363 nm, respectively, were recorded at 1 s intervals in a Varioskan Flash (Thermo Fischer, Vantaa, Finland) spectrofluorometer at 32 °C. After ~10 s, glutamate (100 μM) or NMDA (100 μM) (plus 10 μM glycine) was injected and emissions were further recorded for 50 s. Ca²⁺-dependent fluorescence changes were estimated by representing the ratio of fluorescence emitted at 510 nm obtained after excitation at 335 nm divided by that at 363 nm (F335/F363). Background subtraction was accomplished from emission values obtained in Fura-2-lacking (DMSO-containing) neurons. In preliminary experiments, the Ca²⁺ specificity of the measurements was tested in Ca²⁺-free experimental buffer containing 1 mM ethylene glycol tetraacetic acid (EGTA), which fully prevented the changes in 510 nm emissions (data not shown). At least, six wells were recorded per condition in each experiment (*n* = 4 experiments) and the averaged values are shown.

Western blot analysis. After transfections and treatments, neurons were lysed in RIPA buffer (2% sodium dodecylsulphate, 2 mM ethylene diamine tetraacetic acid (EDTA), 2 mM EGTA, 50 mM Tris; pH 7.5), supplemented with phosphatase inhibitors (1 mM Na₃VO₄, 50 mM NaF) and protease inhibitors (100 μM phenylmethylsulfonyl fluoride, 50 μg/ml anti-papain, 50 μg/ml pepstatin, 50 μg/ml amastatin, 50 μg/ml leupeptin, 50 μg/ml bestatin and 50 μg/ml soybean trypsin inhibitor) and boiled for 5 min. Aliquots of cell extracts were subjected to sodium dodecyl sulfate (SDS) polyacrylamide gel (MiniProtein, Bio-Rad, Hercules, CA, USA) and blotted with antibodies overnight at 4 °C. Signal detection was performed with an enhanced chemiluminescence kit (Pierce, Thermo Scientific, Waltham, MA, USA).

Immunoprecipitation and Cdk5 kinase activity. Neurons were lysed in ice-cold buffer containing 50 mM Tris-HCl (pH 7.5), 150 mM NaCl, 10 mM EDTA, 2 mM EGTA, 1% NP-40, supplemented with the phosphatase and protease inhibitors cited above. Cell extracts were clarified by centrifugation and supernatants (50 μg of protein for immunoprecipitation experiments, 500 μg for Cdk5 kinase assays) were incubated with anti-Cdh1 or anti-Cdk5, overnight at 4 °C, followed by the addition of 15–30 μl of protein A-sepharose (GE Healthcare Life Sciences, Uppsala, Sweden) for 1–2 h at 4 °C. Immunoprecipitates were extensively washed with lysis buffer and either detected by western blot analysis against anti-phosphoserine or resuspended in kinase buffer (20 mM Tris-HCl pH 7.6, 20 mM MgCl₂, 2 mM MnCl₂, 1 mM EDTA, 1 mM EGTA, 0.1 mM dithiothreitol) containing 20 μM ATP, 10 μCi of [γ-³²P]ATP and histone-H1 (50 μg/ml; Sigma) for SDS-polyacrylamide gel (12%) electrophoresis; transferred proteins were visualized by autoradiography and anti-Cdk5 blotting.³²

Protein determinations. Protein concentrations were determined in the cell suspensions, lysates or in parallel cell culture incubations after solubilization with 0.1 M NaOH. Protein concentrations were determined as described³³ using bovine serum albumin as a standard.

Confocal microscopy. Neurons were grown on glass coverslips. After transfections and treatments they were fixed with 4% (v/v) in PBS) paraformaldehyde for 20 min and incubated with DAPI (30 μM; Sigma). Confocal microscopy images were obtained with a Leica SP5 microscope (DMI-6000B model; Leica Microsystems GmbH, Wetzlar, Germany).

Statistical analysis. Measurements from individual cultures were always carried out in triplicate. The results are expressed as mean ± S.E.M. values for three different culture preparations. Statistical analysis of the results was performed by one-way analysis of variance (ANOVA), followed by the least significant difference multiple range test. In all cases, *P* < 0.05 was considered significant.

Conflict of Interest

The authors declare no conflict of interest.

Acknowledgements. The technical assistance of Monica Resch is gratefully acknowledged. This work was funded by the Spanish Ministerio de Ciencia e Innovación (Consolider-Ingenio CSD2007-00020; SAF2010-20008), Instituto de Salud Carlos III (PS09/0366), FEDER (European regional development fund) and the Junta de Castilla y León (GREX206). PR-R is a recipient of a predoctoral FPU fellowship from the Ministerio de Ciencia e Innovación.

- Papadia S, Soriano FX, Leveille F, Martel MA, Dakin KA, Hansen HH *et al*. Synaptic NMDA receptor activity boosts intrinsic antioxidant defenses. *Nat Neurosci* 2008; **11**: 476–487.
- Hardingham GE, Bading H. Synaptic versus extrasynaptic NMDA receptor signalling: implications for neurodegenerative disorders. *Nat Rev Neurosci* 2010; **11**: 682–696.
- Bossy-Wetzel E, Schwarzenbacher R, Lipton SA. Molecular pathways to neurodegeneration. *Nat Med* 2004; **10**: S2–S9.
- Bano D, Young KW, Guerin CJ, Lefevre R, Rothwell NJ, Naldini L *et al*. Cleavage of the plasma membrane Na⁺/Ca²⁺ exchanger in excitotoxicity. *Cell* 2005; **120**: 275–285.
- Celsi F, Pizzo P, Brini M, Leo S, Fotino C, Pinton P *et al*. Mitochondria, calcium and cell death: a deadly triad in neurodegeneration. *Biochim Biophys Acta* 2009; **1787**: 335–344.
- Brennan AM, Suh SW, Won SJ, Narasimhan P, Kauppinen TM, Lee H *et al*. NADPH oxidase is the primary source of superoxide induced by NMDA receptor activation. *Nat Neurosci* 2009; **12**: 857–863.
- Almeida A, Bolaños JP. A transient inhibition of mitochondrial ATP synthesis by nitric oxide synthase activation triggered apoptosis in primary cortical neurons. *J Neurochem* 2001; **77**: 676–690.
- Almeida A, Almeida J, Bolaños JP, Moncada S. Different responses of astrocytes and neurons to nitric oxide: the role of glycolytically-generated ATP in astrocyte protection. *Proc Natl Acad Sci USA* 2001; **98**: 15294–15299.
- Bolaños JP, Almeida A, Moncada S. Glycolysis: a bioenergetic or a survival pathway? *Trends Biochem Sci* 2010; **35**: 145–149.
- Allaman I, Belanger M, Magistretti PJ. Astrocyte-neuron metabolic relationships: for better and for worse. *Trends Neurosci* 2011; **34**: 76–87.
- Pellerin L. Food for thought: the importance of glucose and other energy substrates for sustaining brain function under varying levels of activity. *Diabetes Metab* 2010; **36** (Suppl 3): S59–S63.
- Manzano A, Rosa JL, Ventura F, Perez JX, Nadal M, Estivill X *et al*. Molecular cloning, expression, and chromosomal localization of a ubiquitously expressed human 6-phosphofructo-2-kinase/fructose-2,6-bisphosphatase gene (PFKFB3). *Cytogenet Cell Genet* 1998; **83**: 214–217.
- Hirata T, Kato M, Okamura N, Fukasawa M, Sakakibara R. Expression of human placental-type 6-phosphofructo-2-kinase/fructose 2,6-bisphosphatase in various cells and cell lines. *Biochem Biophys Res Commun* 1998; **242**: 680–684.
- Almeida A, Moncada S, Bolaños JP. Nitric oxide switches on glycolysis through the AMP protein kinase and 6-phosphofructo-2-kinase pathway. *Nat Cell Biol* 2004; **6**: 45–51.
- Herrero-Mendez A, Almeida A, Fernandez E, Maestre C, Moncada S, Bolaños JP. The bioenergetic and antioxidant status of neurons is controlled by continuous degradation of a key glycolytic enzyme by APC/C-Cdh1. *Nat Cell Biol* 2009; **11**: 747–752.
- Almeida A, Bolaños JP, Moreno S. Cdh1/Hct1-APC is essential for the survival of postmitotic neurons. *J Neurosci* 2005; **25**: 8115–8121.
- Maestre C, Delgado-Esteban M, Gomez-Sanchez JC, Bolaños JP, Almeida A. Cdk5 phosphorylates Cdh1 and modulates cyclin B1 stability in excitotoxicity. *Embo J* 2008; **27**: 2736–2745.
- García-Nogales P, Almeida A, Bolaños JP. Peroxynitrite protects neurons against nitric oxide-mediated apoptosis. A key role for glucose-6-phosphate dehydrogenase activity in neuroprotection. *J Biol Chem* 2003; **278**: 864–874.
- Delgado-Esteban M, Almeida A, Bolaños JP. D-Glucose prevents glutathione oxidation and mitochondrial damage after glutamate receptor stimulation in rat cortical primary neurons. *J Neurochem* 2000; **75**: 1618–1624.
- Lee MS, Kwon YT, Li M, Peng J, Friedlander RM, Tsai LH. Neurotoxicity induces cleavage of p35 to p25 by calpain. *Nature* 2000; **405**: 360–364.
- Yalcin A, Clem BF, Simmons A, Lane A, Nelson K, Clem AL *et al*. Nuclear targeting of 6-phosphofructo-2-kinase (PFKFB3) increases proliferation via cyclin-dependent kinases. *J Biol Chem* 2009; **284**: 24223–24232.